In vitro and *in vivo* properties of GLP-1 producing neurons: the brain actions of a gut hormone

Marie Kragelund Bachmann Holt

Presented for a UCL Doctorate of Philosophy (PhD) in Neuroscience

October 2017

Department of Neuroscience, Physiology and Pharmacology

UCL

Declaration of Originality

I, Marie Kragelund Bachmann Holt confirm that the work presented in this thesis is my own. Where information has been derived from other sources, I confirm that this has been indicated in the thesis.

Abstract

Glucagon-like peptide-1 (GLP-1) is an incretin and neuropeptide primarily known for its role in glucose homeostasis. GLP-1 also has potent anti-obesogenic potential, and is known to inhibit food intake, food reward, and diet-induced obesity. In addition, brain GLP-1 increases heart rate and mediates effects of acute stress. Within the brain, GLP-1 is produced by preproglucagon (PPG) neurons in the caudal brainstem.

Although the potential role of GLP-1 has been studied through pharmacological activation of brain GLP-1 receptors, little is known about the cellular properties and physiological role(s) of PPG neurons.

In this thesis, a complementary array of *in vitro* and *in vivo* techniques was used to study the physiological roles of PPG neurons. *In vitro* Ca^{2+} imaging revealed that PPG neuron activity is modulated by a range of compounds relaying signals of energy balance, satiety, and visceral illness. *In vivo,* I selectively manipulated PPG neurons in mice using chemogenetic tools. Activation of PPG neurons dramatically reduced feeding, supporting a role for brain-derived GLP-1 in appetite control. Although selective inactivation of PPG neurons had no effect on *ad libitum* feeding, large meal- or stress-induced reductions in food intake were abolished when PPG neurons were silenced.

In freely-behaving mice, systemic GLP-1 receptor activation had no effect on arterial blood pressure, but increased heart rate via stimulation of the sympathetic nervous system. Although permanent ablation of PPG neurons had no effect on heart rate and blood pressure, selective activation of PPG neurons using chemogenetic tools increased heart rate.

These results provide the first evidence of the physiological role played by the GLP-1 producing neurons in the caudal brainstem. Activity of these neurons is modulated by diverse neural and humoral signals. They are critically important in the prevention of overeating as well as stress-induced hypophagia and may contribute to central nervous mechanisms of cardiovascular control.

1. Introduction

2. Materials and Methods

3. Characterisation of PPG neurons *in vitro* using a genetically encoded calcium indicator

4. The physiological role of PPG neurons in food intake

5. The role of PPG neurons in cardiovascular control

6. Summary and Perspectives

Acknowledgements

First and foremost, I would like to acknowledge my primary supervisor and mentor Stefan Trapp for giving me this opportunity and for supporting me and my development as a scientist throughout. Stefan has always been approachable, thorough, and ready with advice, and I have truly appreciated his passion for research and his never failing good mood. I want to thank Alex Gourine for reading my thesis and for always asking the right questions. I want to thank everyone in the Centre for Cardiovascular and Metabolic Neuroscience: Alla, Patrick, Neph, Svet, and Izzy for always being ready with a helping hand or a chat. I want to acknowledge the UCL graduate research scholarship and MRC UK for funding my PhD and UCL for providing an excellent neuroscience community, which never fails to inspire. A big thank you to Andy Ramage for letting me have so many of his drugs. I want to acknowledge the fantastic work by UCL Biological Services, in particular Mike, Jayne, Kirsty, and Sinead, who are always happy to help.

Thank you to everyone who helped me at Florida State University. Diana Williams for taking me in, Nicole for teaching me, and Calyn and Sarah for letting me 'take advantage of the nice Americans'.

I have been lucky enough to have fantastic teachers along the way. Marina Romero-Ramos and Vanesa Sanchez-Guajardo gave me my first taste of experimental neuroscience; Richard Ang taught me cardiovascular techniques in mice; and Dan Brierley gave me (much needed) statistics lectures towards the end. I cannot stress enough how grateful I am to James Richards for listening, guiding, and motivating me. James taught me almost everything I know, including a whole load of (essential) English slang.

I want to thank the friends who supported me throughout. Thank you to Stine, Lara, Alice, and Emma for the laughs and distractions. I have had fantastic encouragement from Vibeke from the beginning of my life in science. I am truly thankful to have had such great fellow PhD students, Anna and Dan Cook, who were constants in this journey. Ian was an ever reliable source of advice. I am very grateful for the moral support, the roof over my head, and all the tea provided by Sue and Mike Corcoran towards the end.

A very special thank you to my brothers, Oliver, Kasper, and Morten, for always believing in me. I am eternally grateful for the endless support and encouragement from my parents, Else and Anders, who have never dictated, but always backed my choices.

Finally, thank you, David, for being by my side through all the tough bits, for challenging and supporting me, questioning and guiding me, and for sharing all the joy in the end.

Neuroanatomical abbreviations

AP	Area postrema
Arc	Arcuate nucleus
BNST	Bed nucleus stria terminalis
CAA	Central autonomic area
CNS	Central nervous system
CVO	Circumventricular organ
dLS	Dorsal lateral septum
DMH	Dorsomedial hypothalamus
IML	Intermediolateral nucleus
IRT	Intermediate reticular nucleus
lDTg	Lateral dorsal tegmental area
LH	Lateral hypothalamus
LS	Lateral septum
NAc	Nucleus accumbens
NTS	Nucleus of the solitary tract
PBN	Parabrachial nucleus
POA	Preoptic area of the hypothalamus
PVN	Paraventricular nucleus of the hypothalamus
PVT	Paraventricular nucleus of the thalamus
VLM	Ventral lateral medulla
vHPF	Ventral hippocampal formation
VMH	Ventromedial hypothalamus
VTA	Ventral tegmental area

Miscellaneous

5-HT	5-hydroxytryptamine, serotonin
AAV	Adeno-associated virus
AChR	Acetylcholine receptor
ACSF	Artificial cerebrospinal fluid
AgRP	Agouti-related peptide
ATP	Adenosine triphosphate
AUC	Area under the curve
bpm	Beats per minute
BSA	Bovine serum albumin
CCK	Cholecystokinin
CGRP	Calcitonin gene-related peptide
CNO	Clozapine *N*-Oxide
Cre	Cre-recombinase
CSF	Cerebrospinal fluid
DPP-IV	Dipeptidylpeptidase-IV
DREADD	Designer Receptor Exclusively Activated by Designer Drugs
DTA	Diphtheria toxin subunit A

EGFP	Enhanced green fluorescent protein
Ex4	Exendin-4
Ex9	Exendin-3(9-39)
FBS	Fetal bovine serum
GLP-1	Glucagon-like peptide-1(7-36)amide
GLP-1R	GLP-1 receptor
GOI	Gene of interest
HFD	High-fat diet
i.c.v.	Intracerebroventricular
IL-6	Interleukin-6
i.p.	Intraperitoneal
i.v.	Intravenous
LepR	Leptin receptor
MAP	Mean arterial blood pressure
ORF	Open reading frame
POMC	Pro-opiomelanocortin
PPG	Preproglucagon
ROI	Region of interest
tdRFP	tandem-dimer red fluorescent protein
VPR	Volume-pressure recording
YFP	Yellow fluorescent protein

1. Introduction

The obesity epidemic is arguable the most severe health challenge of this century. The prevalence of overweight more than doubled between 1980 and 2013, with 2.1 billion people overweight or obese in 2013 (Ng et al. 2014). Obesity increases the risk of diabetes, some types of cancer, and cardiovascular disease (Mokdad et al. 2003; Carreras-Torres et al. 2017), the latter of which was the primary cause of death in the world in 2012 (WHO 2016).

At the heart of obesity lies appetite regulation. Bodyweight is maintained by stringently regulated physiological processes and slight dysregulation of these processes results in significant weight gain. Obesity can in turn trigger the development of metabolic syndrome, the medical term for the combination of obesity, diabetes, and hypertension. Food consumption is regulated by a complex set of hormonal and neural mechanisms (Suzuki et al. 2012). Long-term cues of energy balance as well as short term signals of satiation, reward, and stress all affect appetite, motivation to eat, and energy expenditure.

Glucagon-like peptide-1 (GLP-1) is a potent regulator of food intake within the brain. Initially discovered as an enhancer of insulin secretion (Holst et al. 1987; Wang et al. 1995), its many beneficial effects have been delineated over the last two decades and are now known to include cardioprotection (Bose et al. 2005; Ban et al. 2008; Ussher and Drucker 2012; Basalay et al. 2016), maintenance of blood glucose levels (Alcántara et al. 1997; Toft-Nielsen et al. 1999), decreased drug reward (Egecioglu et al. 2013b; Graham et al. 2013; Skibicka 2013), neuroprotection (Holscher 2013; Hansen et al. 2015), and decreased appetite and bodyweight (Tang-Christensen et al. 1996; Turton et al. 1996; Flint et al. 1998).

As more effort is put into uncovering the therapeutic potential of GLP-1, additional effects are emerging, some of which may be damaging to health. For example, GLP-1 is now known to increase heart rate, a potentially detrimental effect in patients who already have cardiovascular pathology due to obesity (Barragán et al. 1994; Yamamoto et al. 2002; Robinson et al. 2013; Smits et al. 2016; Bremholm et al. 2017). GLP-1 is expressed in the gut and in neurons in the central nervous system (CNS) and many of its effects have been attributed to activation of GLP-1 receptors (GLP-1Rs) within the brain. This thesis presents novel insight into the role of the CNS GLP-1 system in food intake, stress, and cardiovascular control.

1.1 GLP-1 – structure and function

1.1.1 Proglucagon undergoes tissue-specific posttranslational processing

GLP-1 is expressed from the glucagon (*GCG*) gene. From this gene, the preproglucagon (PPG) mRNA is transcribed, which is translated to form the proglucagon prohormone (Holst 2007). Proglucagon undergoes tissue-specific, differential post-translational processing as shown in Fig 1.1 (Mojsov et al. 1986). Glucagon is secreted from α-cells in the endocrine pancreas (Sutherland and De Duve 1948), whereas GLP-1 is produced in enteroendocrine L-cells in the gut (Ørskov et al. 1986), as well as PPG neurons in the CNS (Jin et al. 1988). Full-length GLP-1 is truncated to form the biologically active form, GLP-1(7-36)amide (Holst et al. 1987; Orskov et al. 1988; Wettergren et al. 1993), and GLP-1 is now widely used to denote the biologically active GLP-1(7-36)amide.

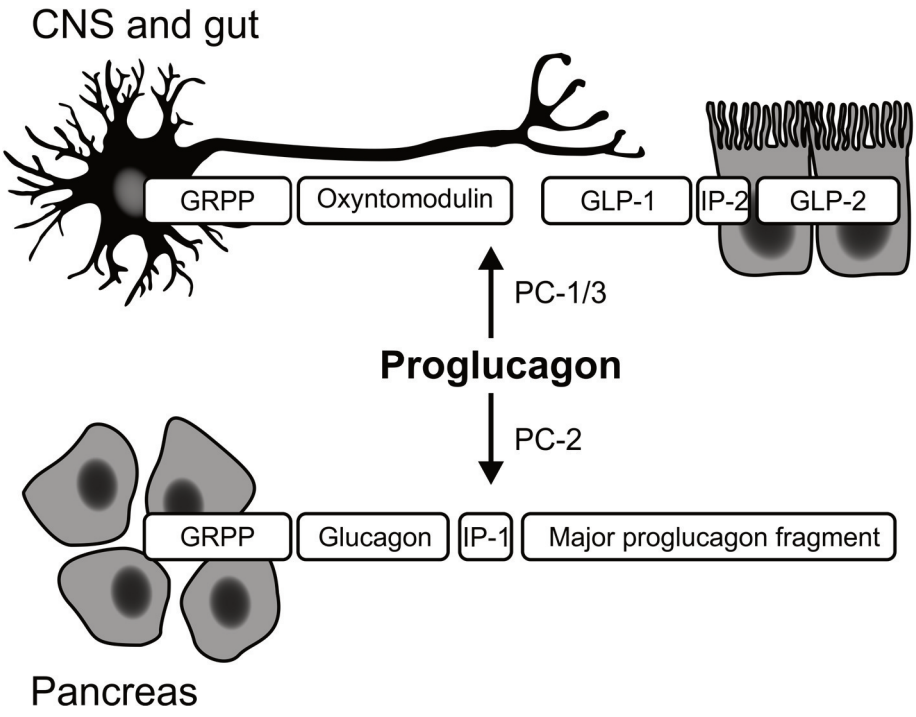

Fig 1.1 Tissue-specific post-translational processing of the proglucagon hormone. In neurons in the CNS and enteroendocrine L-cells in the intestine, proglucagon is processed by prohormone convertase-1/3 (PC-1/3) into glicentin-related pancreatic polypeptide (GRPP), oxyntomodulin, GLP-1, intervening peptide-2 (IP-2), and GLP-2. In pancreatic α-cells, proglucagon is processed by PC-2 into glucagon, IP-1, major proglucagon fragment (MPF), and GRPP.

1.1.2 Peripheral GLP-1 regulates blood glucose levels

Peripherally, GLP-1 is released from L-cells into the bloodstream in response to the presence of macronutrients in the gut (Kreymann et al. 1987; Gribble et al. 2003; Vilsboll et al. 2003; Reimann et al. 2008). From the blood, GLP-1 reaches the pancreas where it acts on β-cells to

enhance the secretion of insulin in response to glucose (Holst et al. 1987; Kreymann et al. 1987; Mojsov et al. 1987; Wang et al. 1995), while inhibiting the release of glucagon from α-cells (Orskov et al. 1988). In addition, GLP-1 increases glucose uptake by peripheral tissues (Alcántara et al. 1997). These potent effects of GLP-1 on glucose homeostasis have led to the use of GLP-1 analogues in the treatment of diabetes. Investigations of the role of GLP-1 have been greatly facilitated by the use of two long-acting GLP-1 analogues, exendin-4 (Ex4) (Thorens et al. 1993) and liraglutide (Larsen et al. 2001), as well as the selective GLP-1R antagonist, exendin-9 (Ex9) (Thorens et al. 1993).

1.1.3 Central actions of GLP-1

Although initially identified as an incretin, it was quickly discovered that GLP-1 dramatically reduces food intake in rodents (Tang-Christensen et al. 1996; Turton et al. 1996; Meeran et al. 1999; Williams et al. 2009) and humans (Flint et al. 1998; Gutzwiller et al. 1999; Astrup et al. 2009). The effect on feeding was largely thought to be mediated by activation of GLP-1Rs in the brain (Turton et al. 1996; Meeran et al. 1999). Central GLP-1, here referring to GLP-1 acting within the CNS, has since been found to affect a range of physiological processes:

1) When injected into the brain, GLP-1 not only decreases food intake, but also induces nausea and *conditioned taste aversion* in rats and mice (Thiele et al. 1997; Lachey et al. 2005). 2) GLP-1 enhances *cognitive function* and memory through neuroprotection (Oka et al. 2000; During et al. 2003; Abbas et al. 2009; Holscher 2013; Hansen et al. 2015). 3) Central GLP-1 increases *thermogenesis* via hypothalamic AMPK (AMP-activated protein kinase) and activation of the sympathetic nervous system (Yamamoto et al. 2002; Lockie et al. 2012; Beiroa et al. 2014). 4) Brain GLP-1R activation increases *heart rate* in rats (Barragán et al. 1994; Yamamoto et al. 2002) and mice (Griffioen et al. 2011). 5) Central GLP-1 attenuates the *rewarding effects* of food (Dickson et al. 2012) and psychostimulant drugs (Egecioglu et al. 2013b; Skibicka 2013; Tuesta et al. 2017). 6) Finally, evidence is emerging for a role of central GLP-1 in the physiological responses to *acute stress* (Kinzig et al. 2003; Maniscalco et al. 2012, 2015; Ghosal et al. 2013, 2017; Holt and Trapp 2016).

1.1.4 The source of central GLP-1

The source of GLP-1 acting within the brain is a much-debated topic. It remains unclear whether peripheral GLP-1 can readily cross the blood-brain barrier (Orskov et al. 1996; Kastin et al. 2002; Kastin and Akerstrom 2003). Kastin et al. (2002) found evidence for the entry into brain tissue of a radio-labelled, stable GLP-1 analogue, ^{125}I-Ala8Ser-GLP-1. However, Orskov et al. (1996) presented convincing evidence that only the circumventricular organs (CVOs), areas in which

the blood-brain barrier is leaky, are accessible to circulating GLP-1. Importantly, GLP-1 is rapidly degraded in the bloodstream by dipeptidylpeptidase-IV (DPP-IV) and has a half-life of two mins with no intact GLP-1 remaining 10 mins after injection (Kieffer et al. 1995). This rapid elimination of biologically active GLP-1 from the bloodstream makes it unlikely that peripherally released GLP-1 reaches the brain in sufficient amounts to activate brain GLP-1Rs. Indeed, it is thought that only 25% of released GLP-1 reaches the liver (Holst and Deacon 2005; Holst 2007), and although GLP-1 was found to increase in the hepatic portal vein after intake of a meal in rats, no GLP-1 was detected in the vena cava (Punjabi et al. 2014), suggesting most of the peptide is degraded before it reaches the brain circulation. Considering these findings, it is likely that GLP-1Rs behind the blood-brain barrier are activated by GLP-1 released from a central source.

1.2 The anatomy of the central GLP-1 system

1.2.1 GLP-1 is produced by cells in the olfactory bulb, brainstem, and spinal cord

Within the brain, GLP-1 is expressed by PPG neurons found in the caudal brainstem, the olfactory bulb, and in the dorsal horn of the spinal cord near the lumbar enlargement (Jin et al. 1988; Larsen et al. 1997a; Merchenthaler et al. 1999; Llewellyn-Smith et al. 2011, 2015; Thiebaud et al. 2016). These cells have been identified through their immunoreactivity to GLP-1 (Jin et al. 1988; Rinaman 1999b; Zheng et al. 2015b); by detecting the PPG mRNA through *in situ* hybridisation (Larsen et al. 1997a; Merchenthaler et al. 1999); and recently via the development of a transgenic mouse expressing yellow fluorescent protein (YFP) under the control of the glucagon promoter (Reimann et al. 2008; Hisadome et al. 2010; Llewellyn-Smith et al. 2011). Because the glucagon promoter drives PPG expression, YFP is selectively produced in PPG cells in the brain (Hisadome et al. 2010; Llewellyn-Smith et al. 2011) and intestine (Reimann et al. 2008), as well as in glucagon-producing α-cells in the pancreas (Reimann et al. 2008). Based on these methods, similar distributions of GLP-1 or PPG expression have been found in mice (Hisadome et al. 2010; Llewellyn-Smith et al. 2011), rats (Merchenthaler et al. 1999; Rinaman 1999b), macaques (Vrang and Grove 2011), and humans (Zheng et al. 2015a), suggesting the central GLP-1 system is conserved within mammals.

PPG neurons in the caudal medulla are arranged in two clusters of cells, with the largest population of neurons in the nucleus of the solitary tract (NTS), situated lateral of the dorsal motor nucleus of the vagus and dorsal of the hypoglossal nucleus. A smaller group of neurons is found in the intermediate reticular nucleus (IRT) extending towards the ventral surface of the medulla (Jin et al. 1988; Merchenthaler et al. 1999; Hisadome et al. 2010; Llewellyn-Smith et al. 2011). In addition, a few cells are located along the midline dorsal of the central canal (Llewellyn-

Smith et al. 2011). PPG neurons in the caudal brainstem are considered to be glutamatergic (Trapp and Cork 2015; Zheng et al. 2015b) and do not express choline acetyl transferase (ChAT) or tyrosine hydroxylase (TH), indicating they are neither cholinergic nor catecholaminergic (Larsen et al. 1997a; Hisadome et al. 2010; Llewellyn-Smith et al. 2013). Along with GLP-1 and glutamate, PPG neurons express the remaining products of tissue-specific posttranslational processing of the proglucagon hormone (Fig 1.1): Oxyntomodulin, GRPP, and GLP-2. Oxyntomodulin inhibits food intake by activating GLP-1Rs in the brain (Dakin et al. 2001; Baggio et al. 2004b), whereas GLP-2 acts on the GLP-2 receptor to inhibit food intake in rats (Tang-Christensen et al. 2000) and mice (Lovshin and Drucker 2013), suggesting PPG neurons, with all their known transmitters, are regulators of feeding.

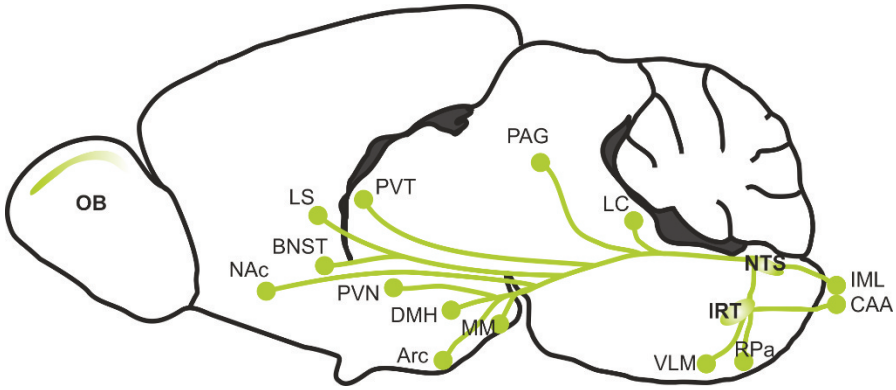

Fig 1.2 The brain GLP-1 system. GLP-1 is expressed by PPG neurons in the nucleus of the solitary tract (**NTS**), the intermediate reticular nucleus (**IRT**), and the olfactory bulb (**OB**). PPG neurons are also found in the deep dorsal horn of the spinal cord (not shown). From the NTS and IRT, PPG neurons project to a range of forebrain and brainstem nuclei as well as areas of the spinal cord. Nucleus Accumbens (NAc), lateral septum (LS), bed nucleus stria terminalis (BNST), paraventricular nucleus of the thalamus (PVT). Paraventricular (PVN), dorsomedial (DMH), arcuate (Arc), and mammillary (MM) hypothalamic nuclei. PAG: Periaqueductal gray area, LC: Locus coeruleus, VLM: Ventrolateral medulla, RPa: Raphé pallidus. IML: Intermediolateral nucleus, CAA: Central autonomic area. Drawing based on (Franklin and Paxinos 2008).

Brainstem PPG neurons project to nuclei throughout the brain, many of which are involved in autonomic control, including the paraventricular nucleus of the hypothalamus (PVN) and the ventrolateral medulla (VLM) (Fig 1.2) (Vrang et al. 2007; Llewellyn-Smith et al. 2011, 2013). Recently, NTS PPG neurons were found to send close appositions to sympathetic preganglionic neurons in the central autonomic area (CAA) and intermediolateral nucleus (IML) of the spinal cord (Llewellyn-Smith et al. 2015). This projection pattern suggests PPG neurons may be important in the control of the activity of the sympathetic nervous system. Notably, olfactory bulb PPG neurons are considered to be interneurons or short-axon cells and are therefore

thought not to contribute to GLP-1 signalling in the rest of the brain (Merchenthaler et al. 1999; Thiebaud et al. 2016).

1.2.2 GLP-1Rs are widely expressed in the brain

GLP-1Rs are found throughout the CNS from the olfactory bulb to lamina 5-10 of the sacral part of the spinal cord (Larsen et al. 1997a; Merchenthaler et al. 1999; Cork et al. 2015). Furthermore, GLP-1Rs are expressed in peripheral vagal afferent cell bodies in the nodose ganglion (Nakagawa et al. 2004; Bucinskaite et al. 2009; Iwasaki et al. 2017) and in vagal afferent terminals in the hepatic portal vein (Vahl et al. 2007). Due to lack of antibodies reliably detecting GLP-1R, the expression pattern has been investigated using GLP-1 binding assays (Goke et al. 1995), *in situ* hybridisation (Merchenthaler et al. 1999), and more recently transgenic mice expressing a fluorescent reporter in GLP-1R-producing neurons (Richards et al. 2014; Cork et al. 2015).

In accordance with the projection pattern of GLP-1 neurons (Fig 1.2), dense expression of GLP-1Rs is found in areas implicated in control of energy balance, including several hypothalamic nuclei: PVN, the arcuate nucleus (Arc), and the dorsomedial hypothalamus (DMH) (Merchenthaler et al. 1999; Cork et al. 2015). In addition, GLP-1Rs are found in the mesolimbic system with high expression in the paraventricular nucleus of the thalamus (PVT), the dorsal lateral septum (dLS), the amygdala, and the bed nucleus stria terminalis (BNST) (Merchenthaler et al. 1999; Cork et al. 2015). In rats, GLP-1Rs are also present in the nucleus accumbens (NAc) and the ventral tegmental area (VTA) (Merchenthaler et al. 1999) and these regions have been found to receive direct input from NTS GLP-1-expressing neurons (Dossat et al. 2011; Alhadeff et al. 2012). Interestingly, only few cells were found in these areas in the mouse (Cork et al. 2015), suggesting species differences may exist.

As well as in nuclei involved in the control of energy balance, GLP-1R expression is found in areas associated with regulation of the sympathetic nervous system and physiological responses to stress, including the PVN, VLM, spinal cord, central amygdala and the dLS (Merchenthaler et al. 1999; Cork et al. 2015). Notably, these areas are also innervated by PPG neurons (Vrang et al. 2007; Llewellyn-Smith et al. 2011, 2013).

Finally, dense GLP-1R expression is present in CVOs: the subfornical organ, the area postrema (AP), and the median eminence, as well as in neurons in the hippocampus (Goke et al. 1995; Merchenthaler et al. 1999; Cork et al. 2015). These areas receive little innervation from PPG neurons (Llewellyn-Smith et al. 2011, 2013), and the endogenous source of GLP-1 acting at these

sites remains unknown. It is possible these GLP-1Rs detect GLP-1 in the bloodstream or cerebrospinal fluid (Orskov et al. 1996; Hsu et al. 2015).

1.3 PPG neurons monitor general homeostasis

With their location in the NTS, PPG neurons are ideally situated to receive and relay signals of changes in the body's internal environment (Grill and Hayes 2012). Homeostasis is a tightly controlled equilibrium, which ensures the optimal working conditions for the organism. Energy balance, core temperature, blood glucose, and blood pressure are stringently monitored and regulated through neural and hormonal mechanism. Dysregulation of those mechanisms can lead to obesity, diabetes, and cardiovascular disease. Interestingly, the body copes well with repeated challenges to homeostasis, including visceral illness, inflammation, and changes in blood glucose in response to food consumption. To counteract these challenges and restore homeostasis, the body initiates a range of physiological and behavioural processes. Following intake of a large meal for example, insulin is released to restore euglycaemia while food intake is suppressed. These processes may rely on recruitment of PPG neurons and central GLP-1.

Two primary methods have been employed to investigate the regulation of PPG neuron activity. Detection of the product of the immediate early gene, *cFOS*, is a common technique for assessing neuronal activity (Sagar et al. 1988). Simultaneous immunostaining for the cFOS protein and GLP-1 has revealed a range of systemic stimuli, which activate PPG neurons *in vivo*. More recently, the development of the PPG-YFP mouse (Reimann et al. 2008) has allowed identification of live PPG neurons in *in vitro* brainstem sections (Hisadome et al. 2010). This has facilitated the use of patch-clamp electrophysiology to investigate the cellular properties of PPG neurons (Hisadome et al. 2010, 2011). Fig 1.3 illustrates the proposed regulation of PPG neuron activity as detailed in the following sections.

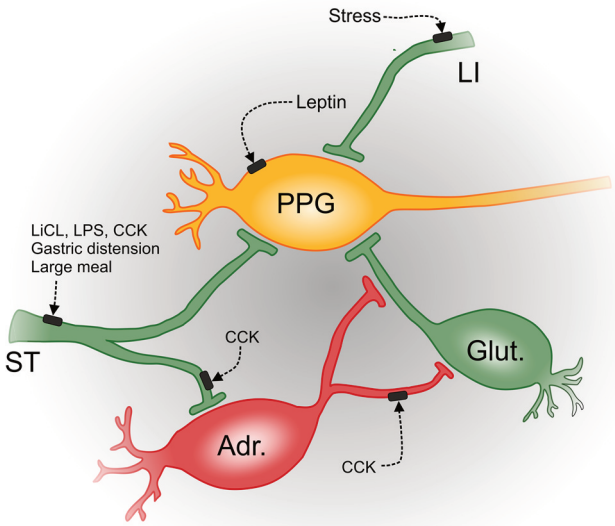

Fig 1.3 Regulation of PPG neuron activity. PPG neurons receive input from the solitary tract (ST), which relays information from the periphery to the NTS, including signals of interoceptive stress. LiCL, LPS, and CCK-8 may activate PPG neurons through this pathway. Similarly, the NTS receives limbic input (LI) with signals of psychogenic stress. Finally, PPG neurons are directly activated by leptin, and CCK-8 activates these cells indirectly by stimulating adrenergic (Adr.) input onto glutamatergic (Glut.) cells resulting in increased firing of PPG neurons. Diagram expanded on from (Hisadome et al. 2011).

Approximately 75% of PPG neurons in the NTS are spontaneously active with regular firing of action potentials at 1.9±0.2 Hz (Hisadome et al. 2010). A smaller population (19%) was found to be burst firing and less than 10% were electrically silent (Hisadome et al. 2010).

In accordance with the role of central GLP-1 in the control of feeding, gastric distension induces cFOS expression in GLP-1-producing neurons in the NTS of rats (Vrang et al. 2003). The satiating effect of gastric distension was later shown to be dependent on hindbrain GLP-1R signalling, suggesting distension of the stomach induces release of GLP-1 centrally (Hayes et al. 2009). Furthermore, patch-clamp electrophysiology of PPG neurons in mice revealed that stimulation of the solitary tract (ST), which conveys afferent sensory information to the NTS, evokes glutamatergic excitatory postsynaptic potentials in PPG neurons. These data suggest gastric distension activates vagal afferents, which relay the signal via the ST to PPG neurons in the NTS (Hisadome et al. 2010) (Fig 1.3). There is no direct evidence for activation of NTS PPG neurons in response to vagal afferent stimulation *in vivo*.

The satiation hormone leptin directly depolarises mouse PPG neurons *in vitro* (Hisadome et al. 2010). The existence of leptin receptors (lepRs) on PPG neurons appears to be species-specific with clear evidence for lepR expression in mice (Goldstone et al. 1997; Hisadome et al. 2010; Garfield et al. 2012), but no expression in rats (Huo et al. 2008). In spite of this, leptin and GLP-1 have been shown to interact to reduce food intake in rats (Goldstone et al. 1997; Williams et al. 2006; Zhao et al. 2012), suggesting the existence of a link between the two systems also in rats. In particular, GLP-1R-mediated satiation disappeared after a 24-hour fast, but could be rescued with continuous infusion of leptin (Williams et al. 2006). Cholecystokinin-8 (CCK-8) also activated a subset of NTS PPG neurons in mice. In contrast to the direct effect of leptin, this

effect was indirect and depended on α1-adrenoceptor signalling and modulation of glutamatergic input, resulting in increased firing rate (Hisadome et al. 2011). Notably, other hunger-regulating hormones had no effect on PPG neuron activity, including peptide-YY, ghrelin, and GLP-1 itself (Hisadome et al. 2010).

There is a noticeable lack of robust evidence for activation of PPG neurons in response to normal feeding. Sweetened milk has been shown to induce cFOS expression in NTS GLP-1-producing neurons (Gaykema et al. 2009). However, Linda Rinaman (1999a) found that even a large meal failed to activate PPG neurons in rats. Later her group did find that activation of PPG neurons is correlated with meal size, but that intake of a very large, unexpected meal is required to robustly activate these cells (Kreisler et al. 2014; Kreisler and Rinaman 2016), similarly to what is required for general neuronal activation in the NTS and AP (Rinaman et al. 1998).

A more vigorous stimulus for PPG neurons appears to be visceral malaise. In rats, approximately 60% of GLP-1-producing neurons expressed cFOS in response to interoceptive stress induced by intraperitoneal (i.p.) injection of LiCl, CCK-8, and lipopolysaccharide (LPS), all of which mimic situations of infection and general malaise (Rinaman 1999b). LiCl-induced cFOS expression in GLP-1-producing neurons was later confirmed in mice (Lachey et al. 2005) and the hypophagic response to LiCl was found to be attenuated by central GLP-1R inhibition in rats (Rinaman 1999a). These data suggest PPG neurons are sensitive to general malaise. Furthermore, not only interoceptive stress, but also acute psychogenic stress in the form of 30 mins of restraint activated cFOS expression in GLP-1-producing neurons in the NTS (Maniscalco et al. 2015).

1.4 GLP-1 regulates food intake through diverse mechanisms

1.4.1 Central GLP-1 regulates food intake

Since its role in food intake was first discovered (Tang-Christensen et al. 1996; Turton et al. 1996), a complex system of GLP-1-mediated hypophagia has been revealed. GLP-1 or its analogues reduce food intake when injected directly into a range of brain regions. Table 1.1 summarises findings using microinjections of GLP-1, Ex4, or Ex9 into different brain areas. The bulk of this evidence is based on studies in rats, with very limited data available on the food intake-suppressive effects of GLP-1R activation in mice.

Three main brain systems are involved in the hypophagic response to GLP-1R stimulation (Table 1.1). 1) Activation of brainstem GLP-1Rs has been shown to reduce chow intake in rats. 2) Several hypothalamic nuclei express GLP-1Rs (Merchenthaler et al. 1999; Cork et al. 2015) and injection of Ex4 or GLP-1 into these areas suppresses feeding in rats. Notably, one study confirmed the

ability of PVN and Arc nucleus GLP-1Rs to decrease food intake in mice. 3) Activation of GLP-1Rs in nuclei, which are part of the mesolimbic system, reduces food intake. Ex4 was found to hyperpolarise and decrease firing of neurons in the PVT. Considering the heavy innervation of this area from PPG neurons and the dense expression of GLP-1Rs in this area, this is a potentially critical nucleus for the control of food intake mediated by central GLP-1.

The hypothalamus is a well-established site for the control of energy balance and brainstem nuclei, in particular the NTS, are emerging as important brain regions in food intake regulation. The hypothalamus and the NTS are both thought to primarily affect homeostatic feeding – that is feeding to meet the caloric needs of the organism. On the other hand, the mesolimbic system is considered a key regulator of hedonic food intake, defined as feeding beyond immediate caloric need or an increased motivation to eat (Skibicka 2013). A role for GLP-1 in reward is currently being cemented with suppressive effects being shown on hedonic food intake (Table 1.1), as well as on the reinforcing effects of psychostimulants, including alcohol (Vallöf et al. 2016), nicotine (Egecioglu et al. 2013a; Tuesta et al. 2017), cocaine (Graham et al. 2013; Sørensen et al. 2015; Schmidt et al. 2016), and amphetamine (Erreger et al. 2012; Egecioglu et al. 2013b).

Microinjection of Ex4 into the ventral hippocampal formation (vHPF) of rats reduces intake of chow or western diet by decreasing average meal size during the dark cycle (Hsu et al. 2015). The effect of Ex4 was in part mediated by a decreased motivation to work for food, as seen by a reduction in the number of times rats were willing to press a lever to receive a sugar pellet (Hsu et al. 2015). The hippocampus is a curious site of GLP-1 action. No innervation from PPG neurons has been detected in this region (Llewellyn-Smith et al. 2011), however there is clear expression of GLP-1Rs (Merchenthaler et al. 1999; Cork et al. 2015) and GLP-1R-expressing neurons respond electrically to GLP-1 (Cork et al. 2015). The source of GLP-1 acting on hippocampal neurons is unknown. It was proposed by Hsu et al. (2015) that GLP-1 is released from PPG neurons into CSF and reaches the vHPF from there. This mode of volume transmission is presumably much slower than traditional synaptic transmission.

	Area	Drugs	Species	Effects on food intake, food reward, and malaise	References
	Brain	i.c.v. GLP-1, Ex9	Rat	GLP-1 dose-dependently decreased chow intake, whereas Ex9 increased intake in satiated, not hungry, rats. Ex4 attenuates food reward without inducing malaise.	(Tang-Christensen et al. 1996; Turton et al. 1996; Dickson et al. 2012)
Brainstem	Hindbrain	4th i.c.v. Ex4	Rat	Hindbrain Ex4 decreases chow intake. This was dependent on PKA and MAPK signalling.	(Hayes et al. 2011a)
	NTS	Ex4, Ex9	Rat	NTS Ex4 preferentially decreases HFD intake. Chow intake is attenuated, when chow is the only source of calories. NTS Ex4 reduces food motivation and reward. GLP-1R inhibition increases chow intake and attenuates hypophagia induced by gastric distension.	(Hayes et al. 2009; Alhadeff et al. 2012; Alhadeff and Grill 2014)
	PBN	Ex4, GLP-1, Ex9	Rat	Intra-PBN Ex4 decreases HFD and chow intake, whereas Ex9 increases both. Ex4 decreases the motivation to work for sucrose pellets.	(Alhadeff et al. 2014; Richard et al. 2014)
	lDTg	Ex4, Ex9	Rat	Intra-lDTg Ex4 decreases meal size (chow) without inducing malaise. Ex9 increases intake.	(Reiner et al. 2017)
Hypothalamus	i.c.v.	3rd i.c.v. GLP-1	Rat	3rd ventricle and lateral ventricle GLP-1 reduce food intake.	(Schick et al. 2003)
	PVN	Ex4, GLP-1, Ex9	Rat, mouse	Ex4 decreases chow intake more potently than GLP-1. GLP-1 does not induce conditioned taste aversion. Ex9 increases chow intake in rats.	(McMahon and Wellman 1998; Sandoval et al. 2008; Katsurada et al. 2014; Burmeister et al. 2017)
	Arc	Ex4, GLP-1, Ex9	Rat, mouse	Intra-Arc Ex4 dose-dependently decreases food intake. Peripheral liraglutide was shown in one study to be dependent on the Arc and in another to work via a different area.	(Secher et al. 2014; Burmeister et al. 2017)
	DMH/VMH	GLP-1	Rat	Intra-DMH and intra-VMH GLP-1 decreases chow intake.	(Schick et al. 2003)
	LH	Ex4, GLP-1, Ex9	Rat	Intra-LH Ex4 decreases chow intake and food motivation, and Ex9 increases both.	(Schick et al. 2003; López-Ferreras et al. 2017)
Mesolimbic	LS	Ex4, Ex9	Rat	Intra-LS Ex4 decreases chow and HFD intake as well as food motivation and reward without inducing malaise. Ex9 increases chow intake and dLS ex9 increases food reward.	(Terrill et al. 2016)
	VTA	Ex4, Ex9	Rat	Intra-VTA Ex4 decreases chow intake and food reward. Intra-VTA Ex9 does not affect food intake.	(Dickson et al. 2012; Mietlicki-Baase et al. 2013)
	NAc	Ex4, GLP-1, Ex9	Rat	Intra-NAc Ex4 and GLP-1 attenuates food reward and intake of palatable, liquid diet. This appears to be specific for the NAc core, but does not induce release of dopamine. Intra-NAc GLP-1 does not induce malaise.	(Dossat et al. 2011, 2013; Dickson et al. 2012; Mietlicki-Baase et al. 2014)
	PVT	Ex4, Ex9	Rat	Intra-PVT Ex4 reduces chow and HFD intake, whereas Ex9 increases chow intake. Ex4 does not induce malaise and suppresses food-seeking behaviour and food reward. Ex4 hyperpolarises and decreases firing of PVT neurons.	(Ong et al. 2017)
	vHPF	Ex4, Ex9	Rat	Ex4 decreases intake of chow and western diet by reducing meal size and food motivation.	(Hsu et al. 2015)

Table 1.1 Effects of GLP-1R stimulation or inhibition in a range of brain regions. Indicated are the areas targeted, drugs used, species investigated, and the outcome of the experiments as well as relevant references. Abbreviations: NTS: Nucleus of the solitary tract, PBN: parabrachial nucleus, lDTg: lateral dorsal tegmental area, PVN: paraventricular nucleus, Arc: Arcuate nucleus, DMH: dorsomedial hypothalamus, VMH: ventromedial hypothalamus, LH: lateral hypothalamus, LS: lateral septum, VTA: ventral tegmental area, NAc: nucleus accumbens, PVT: thalamic paraventricular nucleus, vHPF: ventral hippocampal formation, i.c.v.: intracerebroventricular, HFD: high-fat diet.

1.4.2 Endogenous release of GLP-1 suppresses food intake in rats

With the exception of the vHPF, the regions mentioned above all receive innervation from PPG neurons, suggesting these neurons could regulate both food intake and food reward (Larsen et al. 1997b; Llewellyn-Smith et al. 2011, 2013). In spite of abundant evidence for GLP-1-mediated hypophagia, few studies have addressed the role of centrally produced GLP-1.

In 2011, Barrera et al. knocked down GLP-1 in the NTS of rats using short-hairpin RNA (shRNA). They reported a 50% reduction in GLP-1 levels and elevated food intake and bodyweight. This demonstrated for the first time a role for centrally produced GLP-1 in the regulation of normal feeding, although it is worth noting that the effects on bodyweight appeared to be mainly due to a less severe nadir in weight following stereotaxic surgery (Barrera et al. 2011). In support of the observations by Barrera et al. (2011), direct inhibition of GLP-1Rs in a range of areas increases food intake in rats (Table 1.1), although these results have not yet been reproduced in mice.

In fact, in contrast to evidence from studies in rats, data from mice suggest central, endogenous GLP-1 may not play a major role in regulation of homeostatic food intake and bodyweight. Global genetic knock-out of the *GLP-1R* gene did not affect bodyweight or food intake, whereas glucose homeostasis was disrupted (Scrocchi et al. 1996). Similarly, selective knockdown of brain GLP-1Rs did not affect bodyweight or feeding, although it did attenuate the hypophagic response to systemic liraglutide (Sisley et al. 2014).

In summary, central GLP-1R stimulation suppresses food intake and attenuates the rewarding value of food. However, the role of endogenous GLP-1 in the control of feeding remains elusive with conflicting evidence from rats and mice.

1.4.3 A role for intestinal GLP-1 in control of food intake

The existence of GLP-1-producing cells in both the periphery and brain raises the question whether they make up two functionally, as well as anatomically, distinct systems. There is ample evidence that GLP-1 suppresses food intake when injected i.p. (Abbott et al. 2005; Williams et

al. 2006, 2009, 2011) or directly into the blood stream (Rüttimann et al. 2009; Baumgartner et al. 2010; Zhang and Ritter 2012; Punjabi et al. 2014; Ronveaux et al. 2014). However, the relative contribution of central and peripheral GLP-1Rs is unknown. Williams et al. (2009) presented convincing evidence that peripheral GLP-1 plays a role in satiety in rats. First, peripheral suppression of GLP-1Rs increased food intake during light phase or after a large meal. Second, while the effects of i.p. GLP-1 were abolished by peripherally administered Ex9, inhibition of central GLP-1Rs did not affect the hypophagic effect of i.p. GLP-1, suggesting the effects of i.p. GLP-1 are mediated by peripheral GLP-1Rs.

Experimental evidence now points to a role for vagal transmission in the effects of peripheral GLP-1. GLP-1Rs are expressed in the nodose ganglion (Kakei et al. 2002; Nakagawa et al. 2004; Richards et al. 2014), on vagal afferent terminals in the hepatic portal vein (Vahl et al. 2007), and in the gastric branch of the vagus nerve (Bucinskaite et al. 2009). Furthermore, GLP-1 depolarises (Gaisano et al. 2010) and increases intracellular [Ca^{2+}] (Kakei et al. 2002; Iwasaki et al. 2017) in nodose ganglion neurons *in vitro* and elicits activity in gastric vagal afferents *in vivo* (Bucinskaite et al. 2009). Interestingly, knock-down of nodose ganglion GLP-1Rs increases meal size in rats without affecting daily food intake or bodyweight, suggesting vagal activation by GLP-1 regulates feeding behaviour (Krieger et al. 2015).

1.5 Central GLP-1 mediates physiological responses to stress

The literature on the role of GLP-1 in food intake regulation is extensive. However, the physiological context in which GLP-1-mediated hypophagia becomes important is less well-studied. A reduction in food intake can be indicative of not only decreased caloric need (homeostatic feeding), but also of a change in the emotional state resulting in a decreased motivation to eat. Indeed, psychogenic stress in response to restraint dramatically suppresses feeding (Krahn et al. 1990).

1.5.1 GLP-1 activates neuroendocrine pathways involved in stress regulation

Stress is the collection of physiological and behavioural responses to physical and homeostatic challenges (Sawchenko et al. 2000; Dayas et al. 2001; Ulrich-Lai and Herman 2009). Appropriate stress responses are essential for the survival of the organism by allowing it to overcome aversive and potentially damaging conditions. Neural control of stress is complex and involves recruitment of neuroendocrine pathways resulting in activation of the sympathetic nervous system and the hypothalamus-pituitary-adrenal (HPA) axis (Ulrich-Lai and Herman 2009). Increased sympathetic outflow leads to an increase in heart rate and blood pressure, whereas

activation of the HPA axis increases the blood levels of stress hormones, adrenocorticotropic hormone (ACTH) and corticosterone (rodent equivalent of human cortisol).

Exposing a rat to 5 mins on an elevated platform or 30 mins of restraint robustly activates cFOS expression in GLP-1-producing neurons (Maniscalco et al. 2015). Interestingly, the hypophagic response to acute stress is suppressed by i.c.v. infusion of GLP-1R antagonist, Ex9, indicating the central GLP-1 system is recruited to reduce food intake in response to stress (Maniscalco et al. 2015).

In support of a role for GLP-1 in stress, peripheral administration of GLP-1 activates the HPA axis in rodents and humans, and central delivery of the GLP-1R agonist, Ex4, increases blood corticosterone in rodents (Gil-Lozano et al. 2010). Notably, inhibition of corticosterone-releasing hormone (CRH) prevented the increase in ACTH and corticosterone, suggesting central GLP-1 activates CRH-releasing neurons, most likely in the PVN (Larsen et al. 1997b; Sarkar et al. 2003). Indeed, GLP-1-positive axons innervate CRH-expressing PVN neurons (Sarkar et al. 2003), which are activated by GLP-1 *in vitro* (Katsurada et al. 2014) and *in vivo* (Larsen et al. 1997b). Furthermore, Kinzig et al. (2003) demonstrated that GLP-1R activation directly in the PVN increases blood ACTH and corticosterone levels. Interestingly, injections of GLP-1 directly into the amygdala increased anxiety-like behaviour, including reduced time spent in the open arms of an elevated plus maze (Kinzig et al. 2003).

1.5.2 GLP-1-mediated tachycardia

In addition to its stimulatory effects on the HPA axis, central GLP-1 may increase the activity of the sympathetic nervous system. Infusions of GLP-1 or Ex4 i.c.v. increases heart rate and blood pressure in rats (Barragán et al. 1999; Yamamoto et al. 2002). This cardiovascular response was correlated with activation of autonomic regulatory neurons, neurons in the spinal cord, and cells in the adrenal medulla suggesting recruitment of the sympathetic nervous system (Yamamoto et al. 2003). Unusually for caudal NTS neurons, PPG neurons directly innervate sympathetic preganglionic neurons in the spinal cord, supporting a role for central GLP-1 in autonomic regulation (Llewellyn-Smith et al. 2015).

These data suggest that the central GLP-1 system does not simply decrease food intake in response to changes in energy demand, but rather contributes to the physiological response to interoceptive and psychogenic stress by increasing levels of stress hormones in the blood, increasing heart rate, decreasing food intake, and mobilising glucose (Holt and Trapp 2016).

1.6 Genetic tools to investigate the role of central GLP-1

1.6.1 Cre-Lox technology

The development of genetic tools over the last decade has revolutionised neuroscience research. In particular, the use of Cre-lox technology in combination with chemogenetic tools has elucidated, to name a few, the role of agouti-related peptide (AgRP) (Wu et al. 2012), calcitonin gene-related peptide (CGRP) (Campos et al. 2016), and CCK neurons (D'Agostino et al. 2016) in appetite control; the importance of orexin neurons in the regulation of physical activity (Kosse et al. 2017); and a dorsal raphe nucleus → BNST circuit regulating fear and anxiety (Marcinkiewcz et al. 2016).

Cre-recombinase (Cre) catalyses homologous recombination between short DNA sequences known as loxP sites (Hoess et al. 1982; Hoess and Abremski 1985). This facilitates selective deletion or expression of a gene of interest (GOI) in genetically defined cell populations. Cre expression is usually driven by a promoter, which defines the cell population under investigation. Promoter-driven expression ensures Cre is selectively expressed in the cells of interest. Cre-dependent expression of a GOI is commonly achieved in one of two ways (Fig 1.4):

1) A translational STOP site is inserted in front of the GOI. This translational brake usually consists of one or several polyadenylation sequences as well as stop codons in all reading frames (Luche et al. 2007). The STOP site is flanked by loxP sites. In the absence of Cre, translation is hindered by the presence of the STOP site. In the presence of Cre, homologous recombination leads to excision of the STOP site and translation of the GOI is facilitated (Luche et al. 2007).
2) The GOI is placed in reverse orientation for successful expression of the protein. Flanking the GOI are two antiparallel, heterotypic loxP sites. Two recombination events catalysed by Cre lead to inversion of the GOI allowing for stable expression (Schnutgen et al. 2003; Luche et al. 2007; Atasoy et al. 2008). This is commonly referred to as the FLEX-switch system (Atasoy et al. 2008).

Cre-dependent GOIs can be introduced either at the embryo state or later using viral gene delivery. Adeno-associated viruses and lentiviruses are now widely used to express recombinant proteins in specific brain regions. This offers considerable advantages over Cre-dependent GOIs inserted into the genome. Firstly, it is spatially specific, with GOI expression being limited to the site of viral infection. Secondly, it is temporally specific. Mice can be injected as adults avoiding any compensatory mechanisms during development.

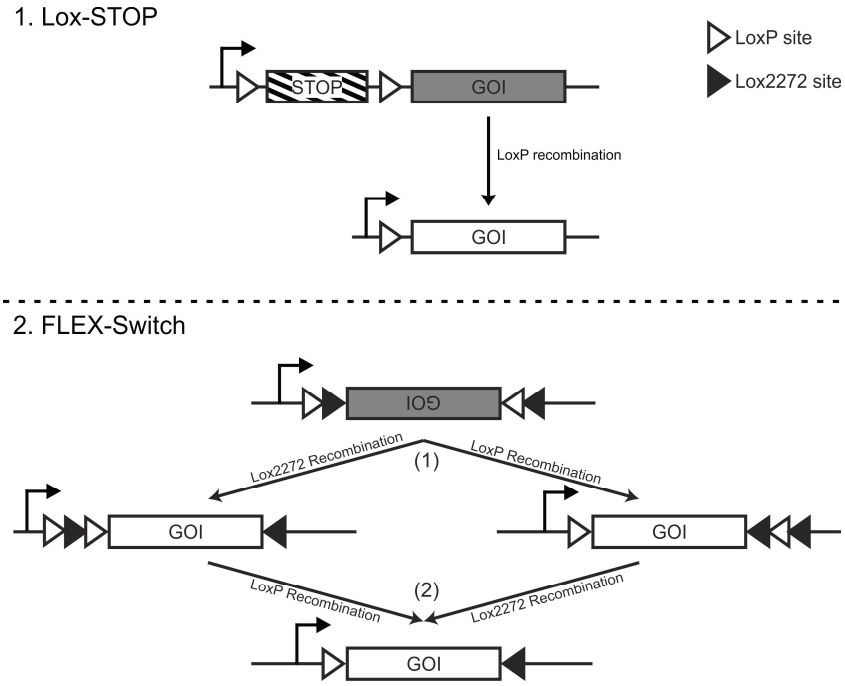

Fig 1.4 Cre-dependent expression systems. In the Lox-STOP model, a translational STOP site hinders the expression of the gene of interest (GOI). Cre recombinase catalyses recombination between the two LoxP DNA recognition sites flanking the STOP site. This disinhibits expression of the GOI. In the FLEX-Switch model (Atasoy et al. 2008), the GOI is inserted in the reverse orientation resulting in no successful expression of the protein. The GOI is flanked by two antiparallel, heterotypic Lox sites, LoxP and Lox2272. Cre induces two steps of recombination between antiparallel lox sites leading to permanent inversion of the GOI and stable expression.

1.6.2 Chemogenetic tools

Cre-lox technology is widely used in combination with opto- and chemogenetics. These techniques rely on the transgenic expression of receptors or channels on the surface of cells, which allows the experimenter to manipulate the activity of the cells. In this thesis, I make use of three constructs to manipulate the activity of PPG neurons. 1) Diphtheria toxin subunit A (DTA) inhibits translation by inactivating eukaryotic elongation factor-2 (eEF-2). This inhibition of protein synthesis ultimately leads to cell death (Wu et al. 2014). 2) HM3Dq (Alexander et al. 2009) and 3) HM4Di (Armbruster et al. 2007) are types of designer receptors exclusively activated by designer drugs (DREADDs), a tool developed to selectively activate or inactivate cell populations using an otherwise inert ligand. HM3Dq and HM4Di are G-protein coupled receptors modified from the human muscarinic acetylcholine receptor (AChR). They no longer respond to acetylcholine. Instead they are activated by clozapine-N-oxide (CNO). HM3Dq is coupled intracellularly to $G_{\alpha q}$, whereas HM4Di is coupled to $G_{\alpha i/o}$. Binding of CNO to the HM3Dq receptor

leads to increased electrical activity of the cells (Alexander et al. 2009), whereas stimulation of HM4Di leads to neuronal silencing (Armbruster et al. 2007).

1.7 Overall hypothesis

The evidence discussed highlights the wide-ranging effects of central GLP-1 and the diverse modulatory inputs to PPG neurons. The proposed role of central GLP-1 in distinct processes such as stress, reward, and homeostatic feeding raises many questions regarding the physiological function of GLP-1 within the brain. While pharmacological studies have addressed the importance of downstream targets of central GLP-1, there is presently little known about the physiological role of PPG neurons in food intake and stress.

Based on this, I put forward the hypothesis that NTS PPG neurons regulate food intake, stress, heart rate, and blood pressure, and that PPG neuron activity is modulated by a range of compounds signalling satiety, energy balance, and visceral illness.

To investigate this, I used genetic and surgical techniques in mice to monitor and manipulate the activity of NTS PPG neurons with the following aims:

1. Further characterise NTS PPG neurons using *in vitro* Ca^{2+} imaging in brainstem slices.
2. Determine the importance of NTS PPG neurons in food intake regulation by manipulating their activity *in vivo.*
3. Elucidate the role of the GLP-1 system in cardiovascular control by using biotelemetry in awake, behaving mice.

2. Materials and Methods

2.1 *In vitro* solutions and reagents

2.1.1 Cloning

Water: All water for cloning was molecular biology grade (Eppendorf)

TRIzol (Life Technologies)

Phusion high-fidelity polymerase (Life Technologies)

Super optimal broth with catabolite repression (SOC) medium: 0.5% Yeast Extract, 2% tryptone, 10 mM NaCl, 2.5 mM KCl, 10 mM $MgCl_2$, 10 mM $MgSO_4$ and 20 mM Glucose

Ampicillin (Sigma)

LB-Broth (Sigma)

Agar (DBH)

Green GoTaq Hot start polymerase master mix (Promega)

Deoxynucleotides (dNTPs, New England Biololabs)

Dithiothretiol (DTT, Invitrogen)

RNaseOUT (Invitrogen)

Superscript III Reverse Transcriptase (Invitrogen)

Phire Hot Start II (Invitrogen)

Maxiprep kit (PureLink, Invitrogen)

Miniprep kit (GenElute, Sigma)

PCR clean-up kit (GenElute, Sigma)

MultiCore restriction buffer (Promega)

Bovine Serum Albumin (BSA, Invitrogen)

Agarose (QualexGold, Hybaid GmbH)

TAE (50x, AppliChem)

Ethidium bromide (0.5 µg/ml, Sigma)

2.1.2 Cell culture

DMEM culture medium (Sigma)

L-glutamine (2mM, Sigma)

FBS, 10x (Sigma)

Non-essential amino acids (M7145, Sigma)

Penicillin (50 units/ml, Sigma)

Streptomycin (50 µg/ml, Sigma)

IMDM culture medium (Gibco)

2.1.3 Virus production

Water: All water was filtered using a 0.22 µM water filtering unit (Millipore) and autoclaved.

$CaCl_2$ (2.5 M, Sigma)

Hepes-buffered saline (50 mM HEPES, 280 mM NaCl, 1.5 mM Na_2HPO_4)

Tris buffer (20 mM)

NaCl in 20 mM Tris buffer: 150 mM, 200 mM, 300 mM, 400 mM, 500 mM, 1M, 2M

Phosphate-buffered saline tablets, PBS, (Gibco)

Sodium deoxycholeate (0.5%, Sigma)

Benzonase nuclease (50 u/ml, E-1014, Sigma)

Heparin columns, HiTrap Heparin HP 1ml (GE Healthcare Life Sciences)

Amicon Ultra centrifugal filter tubes (Millipore)

2.1.4 Immunohistochemistry

Formaldehyde solution (37% with 10-15% methanol, Sigma)

Optimal cutting temperature medium, OCT, (Tissue-Tek, Sakura Finetek)

Phosphate buffer (PB, 0.1 M Na_2PO_4 in water, pH 7.4)

SuperFrost Plus microscope slides (VWR)

Coverslip glasses (VWR)

VectaShield antifade mounting media for fluorescence (Vector Laboratories)

Antigen	Antibody	Origin	Dilution	Source
GCaMP3	Anti-GFP	Chicken	1:500	#AB13970, lot #623923, Abcam
tdRFP/mCherry	Anti-dsRed	Rabbit	1:500	#632496, Clontech
cFOS	Anti-Fos	Rabbit	1:400	#2250S, Cell Signalling Tech
GLP-1	Anti-GLP-1	Rabbit	1:200	#T-4057, Peninsula

Table 2.1. List of primary antibodies.

Antigen	Antibody	Origin	Dilution	Source
Chicken IgG	Anti-chicken IgG	Goat	1:1000	#A-11039, Life Technologies
Rabbit IgG	Anti-rabbit IgG	Sheep	1:1000	#C2306, Sigma

Table 2.2. list of secondary antibodies.

2.1.5 In vitro *imaging and electrophysiology solutions*

ACSF (in mM in dH_2O): 3 KCl, 118 NaCl, 25 $NaHCO_3$, 10 Glucose, 1 $MgCl_2$, 2 $CaCl_2$; pH 7.4

Recovery solution (in mM in water): 3 KCl, 118 NaCl, 25 $NaHCO_3$, 1.2 NaH_2PO_4, 2.5 Glucose, 7 $MgCl_2$, 0.5 $CaCl_2$; pH 7.4

High-Mg^{2+}/low-Ca^{2+} ACSF (in mM in water): 2.5 KCl, 200 sucrose, 28 $NaHCO_3$, 1.25 NaH_2PO_4, 7 Glucose, 7 $MgCl_2$, 0.5 $CaCl_2$; pH 7.4

Low-Cl^- intracellular solution (in mM in water): 120 K-gluconate, 1 NaOH, 5 BAPTA, 1 $MgCl_2$, 1 $CaCl_2$, 5 Hepes, 2 K_2-ATP; pH 7.3

2.2 Drugs

2.2.1 In vitro *Ca^{2+} imaging and patch-clamp electrophysiology*

All drugs were dissolved in dH_2O as stocks, except for DNQX, which was dissolved in DMSO; TTX, which was dissolved at 1 mM in sodium-citrate buffer; and CNO, which was dissolved in saline. The final working concentration, indicated below, was made up in ACSF.

(2R)-amino-5-phosphonovaleric acid (APV, 25 µM, Tocris)
5-hydroxytryptamine hydrochloride (5-HT, 20 µM, Sigma)
6,7-dinitroquinoxaline-2,3-dione (DNQX, 20 µM, Tocris)
Adenosine triphosphate (ATP, 1 mM, Sigma)
Carbachol (100 µM, Sigma)
Cholecystokinin octapeptide (CCK-8, 100 nM, Tocris)
Clozapine-N-oxide (CNO, 1 µM, Hello Bio)
Glutamate (100 µM, Sigma)
Granisetron (5 µM, Tocris)
Interleukin-6 (IL-6, 2 nM, Preprotech)
Ketanserin (1 µM, Tocris)
Leptin (1 nM, gift from Novo Nordisk)
Phenylbiguanide (PBG, 1 and 10 µM, Tocris)
Tetrodotoxin (TTX, 0.5 µM, Cayman Chemical)

2.2.2 In vivo *food intake and biotelemetry*

All drugs for *in vivo* experiments were dissolved in saline (0.9% w/v NaCl).

Atenolol (i.p., 2 mg/kg in 1 ml/kg saline, Sigma)
CNO (i.p., 2 mg/kg in 5 ml/kg saline, Hello Bio)
Ex4 (i.p., 10 µg/kg in 100 µl saline, Tocris)
Ex9 (intra-dLS, 10 µg in 500 nl saline, American Peptides)
GLP-1 (i.p., 100 µg/kg in 100 µl saline, Tocris)

2.2.3 Surgery

Ketamine (Vetalar, 50 µg/kg intramuscular, Zoetis)
Medetomidine (Domitor, 1 mg/kg intramuscular, Orion Pharma)
Atipamezol hydrochloride (Antisedan, 2.5 mg/kg intramuscular, Zoetis)
Buprenorphine (0.5 mg/kg, subcutaneously)
Carprofen (Rimadyl, 5 mg/kg, subcutaneously, Zoetis)

2.3 Cre-dependent viruses

The following Cre-dependent recombinant adeno-associated viruses (rAAVs) were used to manipulate NTS PPG neurons and image GLP-1R-expressing neurons in the dLS.

Name	Protein encoded	Application	Source
AAV8-mCherry-Flex-DTA	mCherry or DTA	Ablation	UNC vectorcore
AAV2-FLEX-HM3Dq:mCherry	HM3Dq:mCherry	Activation	UNC vectorcore
AAV8-FLEX-HM3Dq:mCherry	HM3Dq:mCherry	Activation	VVF, ZNZ, Zurich
AAV2-FLEX-HM4Di:mCherry	HM4Di:mCherry	Inhibition	UNC vectorcore
AAV8-FLEX-EGFP	EGFP	Control	VVF, ZNZ, Zurich
AAV1/2-FLEX-Perceval	Perceval	Control	Made in house
AAV1/2-FLEX-GCaMP3	GCaMP3	Ca^{2+} imaging	Made in house

Table 2.3. Cre-dependent viruses.

2.4 Virus production

2.4.1 AAV Plasmid amplification and purification

Plasmids amplified routinely for AAV1/2 production were:

- pH21, containing AAV1 Rev and Cap sequences
- pRV1, containing AAV2 Rev and Cap sequences
- pFΔ6, the adeno-virus helper plasmid

Additionally, two AAV plasmids were amplified:

- pAAV-CBA-FLEX-GCaMP3, containing a Cre-dependent ORF for the calcium indicator, GCaMP3 (Tian et al. 2009).
- pAAV-CBA-FLEX-Perceval, containing a Cre-dependent ORF for the ATP indicator, Perceval (Berg et al. 2009), here used as a control construct.

pAAV-CBA-FLEX-GCaMP3 was subcloned as described in section 2.4.3 and pAAV-CBA-FLEX-Perceval was subcloned in the same way by James E. Richards. The Perceval ORF was a kind gift from Professor Guy Rutter, Imperial College London.

Plasmids were defrosted on ice along with 100 µl XL-1 cells. Plasmid (100-200 ng) was added directly to bacteria. Ten mins later, the cells were heat-shocked at 42°C for 45 s to facilitate uptake of the plasmid and then returned to ice for two mins. SOC medium (250 µl) was added to the transformed bacteria, which were incubated at 37°C shaking at 225 rpm for one hour. Next, 30 µl of the bacterial solution was spread onto ampicillin-containing agar plates and left to incubate at 37°C overnight. As an exception, transformed bacteria containing the AAV helper plasmid pFΔ6 were not spread onto plates, but added directly into 600 ml growth medium, LB-Broth, containing ampicillin (100 µg/ml). Following overnight incubation, bacterial colonies were

transferred to flasks containing 300 ml LB-Broth with ampicillin (100 µg/ml) and incubated for 16-20 hours at 37°C shaking at 225 rpm. Following culture growth, plasmids were purified using a Maxiprep kit. Bacterial cells were pelleted by centrifugation at 1500 x *g*, resuspended, and lysed. Lysates were filtered and loaded onto an anion-exchange column. After washing, column-bound DNA was eluted and then precipitated using isopropanol. DNA was pelleted at 4,500 x *g* for one hour, washed in 5 ml 70% ethanol, and resuspended in water.

2.4.2 Plasmid digestion and electrophoresis

For verification of correct plasmid amplification, purified DNA was digested. Reactions (20 µl) in water were set up containing 1 x MultiCore buffer, 0.5 unit of each restriction enzyme (Table 2.4), 0.5 mg/ml BSA and 1 µg plasmid DNA. Reactions were incubated at 37°C for one hour and fragments were separated on a 1% agarose gel containing 0.5 µg/ml ethidium bromide. The gel was run at 60 V for one hour and fragments were visualised using UV light.

Plasmid	Enzymes	Fragment sizes
pH21	EcoRI	4.5 kb, 2.8 kb, and 0.2 kb
pRV1	XbaI	7.5 kb and 3.8 kb
pFΔ6	HindIII	5.5 kb, 3 kb, 3 kb, 2.3 kb, and 1.5 kb
pAAV-CBA-FLEX-GCaMP3	EcoRI+EcoRV	5.6 kb, 1.4 kb
pAAV-CBA-FLEX-Perceval	EcoRI+EcoRV	5.6 kb, 2.5 kb

Table 2.4. Digestions of plasmids using restriction enzymes.

2.4.3 Subcloning of pAAV-CBA-FLEX-GCaMP3

2.4.3.1 RNA EXTRACTION

Live brainstem slices containing the NTS from a PPG-Cre/GCaMP3 transgenic mouse were prepared as described in section 2.7.1 and homogenised in TRIzol using a glass tissue homogeniser. To extract RNA, tissue homogenate was separated into lipid, protein, DNA, and RNA phases using 0.2 ml chloroform per 1 ml of homogenate. The sample was centrifuged for 15 mins at 12,000 x *g* at 4°C after which three distinct phases were seen. The upper aqueous phase containing the RNA was precipitated using 0.5 ml isopropanol per ml of TRIzol. Precipitated RNA was pelleted at 12,000 x *g* at 4°C for 10 mins and resuspended in 1 ml 75% ethanol to wash. RNA was pelleted at 7,500 x *g* for 5 mins at 4°C and the supernatant carefully removed. The pellet was airdried, resuspended in RNase-free water, and stored at -80°C.

2.4.3.2 GCaMP3 OPEN READING FRAME GENERATION

GCaMP3 cDNA was generated from isolated mRNA by mixing 0.5 µM RT primer (Table 2.5), 500 µM dNTPs, and 4 µl RNA (section 2.4.3.1) in nuclease-free water (total volume 13 µl). The sample

was incubated at 65°C for five mins followed by five mins on ice and then centrifuged briefly at 7,500 x *g.* To the sample was added: 1 x First-Strand buffer, 50 mM DTT, 1 unit RNaseOUT and 1 unit Superscript III (final volume 20 µl) and GCaMP3 cDNA was synthesised according to the following protocol:

- 25°C 5 mins
- 50°C 60 mins
- 70°C 15 mins

The GCaMP3 ORF was amplified by PCR using Phusion high-fidelity polymerase (primers in Table 2.5). Primers were designed to contain restriction enzyme sites recognized by EcoRI and EcoRV, respectively (underlined in Table 2.5). GCaMP3 cDNA (2 µl) was added to 25 µl aqueous solution containing 1 x Phusion buffer, 1% DMSO, 0.5 µM forward and reverse primers, 200 µM dNTPs, and 1 unit Phusion HF polymerase. A PCR reaction was run:

- Initial denaturation of DNA 98°C for 30 s
- DNA denaturation 98°C for 10 s
- Primer annealing 61°C for 30 s
- Elongation 72°C for 45 s

  ] 35 cycles
- Final elongation 72°C for 5 mins

The amplicon size was determined using agarose gel electrophoresis as described in section 2.4.2. The amplicon was purified using the GenElute PCR Clean-Up kit and stored at -20°C.

2.4.3.3 SUBCLONING

The GCaMP3 ORF and pAAV-FLEX backbone (pAAV-CBA-FLEX, kind gift from William Wisden) (Atasoy et al. 2008; Murray et al. 2011) were digested using EcoRI and EcoRV as described in section 2.4.2. Restriction reactions were incubated at 37°C for two hours and purified using the GenElute PCR Clean-Up kit. To ligate the ORF and backbone, 10 µl reactions were set up containing 1 x T4 ligase buffer, 1 unit T4 DNA ligase, and ORF and backbone DNA in a 3:1 molar ratio. A control ligation with no ORF was set up simultaneously. Ligation reactions were left at 4°C overnight. Competent XL-1 cells were transformed with 1 µl of the ligated construct, pAAV-CBA-FLEX-GCaMP3, as described in section 2.4.1 and spread onto ampicillin-containing agar plates. Colony PCR was performed the following day using primers listed in Table 2.5. Reactions were set up in water containing 1 x Phire Hot Start II buffer, 200 µM dNTPs, 0.5 µM forward and reverse primers and 1 unit Phire Hot Start II polymerase (20 µl total volume). P10 pipette tips were used to collect ten colonies from the agar plate. They were then submerged briefly into Phire reaction buffer and then dropped into 5-7 ml LB-Broth containing ampicillin (100 µg/ml). The PCR was run while waiting for the starter cultures to grow:

- Initial denaturation of DNA 98°C for 30 s
- DNA denaturation 98°C for 5 s
- Primer annealing 62°C for 5 s
- Elongation 72°C for 20 s

(30 cycles)

- Final elongation 72°C for 1 min

Resulting amplicons were resolved on a 1% agarose gel as described in section 2.4.2. Starter cultures were inoculated overnight at 37°C shaking at 225 rpm and DNA was isolated using a Miniprep kit. One clone was picked for further processing. LB-Broth (300 ml) containing ampicillin (100 µg/ml) was inoculated with 100 µl starter culture and left to grow at 37°C overnight. DNA was purified using a Maxiprep kit as described in section 2.4.1. The purified construct was digested (Table 2.4) and fragments separated using agarose gel electrophoresis (section 2.4.2). Finally, the correct orientation of the insert was confirmed by sequencing using primers designed to recognize sequences flanking the insert (Table 2.5).

Application	Binding	Sequence
First strand synthesis	3’	5’–TAACGCAACGTACCTTCG–3’
ORF amplification	5’	5’–GGTTCCAAGATATCATGGGTTCTCATCATCATCA–3’
ORF amplification	3’	5’–CCGGTTAAGAATTCTTACTTCGCTGTCATCATTTG–3’
Colony PCR/Sequence	5’	5’–GCTGTTAAAGCTTGAACCTC–3’
Colony PCR/Sequence	3’	5’–ACGTGCTGGTTATTGTGCTG–3’

Table 2.5. Primer sequences for subcloning. Restriction enzyme recognition sites are underlined.

2.4.4 Cell culture

Human embryonic kidney cells, AD293T cells (Stratagene, UK) were routinely cultured in Dulbecco’s modified Eagle’s medium (DMEM) containing 10% heat-inactivated fetal bovine serum (FBS), 2 mM L-glutamine, 50 units/ml penicillin and 50 µg/ml streptomycin. Cells were passaged every three days and replaced when number of passages reached 30.

2.4.5 Virus particle generation

The rAAV production protocol was adapted from McClure et al. (2011). Two confluent T-75 flasks of AD293T cells were seeded in five 15 cm dishes. When the cells covered 70-80% of the dish the medium was changed to Iscove’s Modified Dulbecco’s Medium containing 5% FBS. Three hours later, cells were co-transfected with either pAAV-FLEX-Perceval or pAAV-FLEX-GCaMP3 and helper plasmids pH21, pRV1, and pFΔ6 using $CaPO_4$. 1650 µl 2.5 M $CaCl_2$ was added to 12 ml H_2O. 62.5 µg AAV plasmid, 125 µg pFΔ6, 31.25 µg pRV1 and 31.25 µg pH21 were added to the $CaCl_2$ solution and filtered through a 0.2 µm filter. HBS (2x, 13 ml) was added dropwise while vigorously agitating the DNA-$CaCl_2$ solution. $CaPO_4$-DNA complexes were allowed to form for 2 mins and added dropwise to the cells. The next day, 16 hours after transfection, the medium

was changed to DMEM. Two days later, 64 hours after transfection, cells were dissociated and pelleted by centrifugation at 800 x *g*. Cells were resuspended in 20 mM Tris and 150 mM NaCl and digested in 0.5% sodium deoxycholeate and 50 u/ml benzonase nuclease to release rAAV particles. Cell debris was removed by centrifugation at 3000 x *g* for 15 mins and the supernatant was passed through a 0.45 µm filter unit (Millipore, UK).

2.4.6 Virus purification and concentration

rAAV particles were bound to pre-equilibrated 1 ml heparin columns using a peristaltic pump at a flow rate of 0.5 ml/min. Viral particles were eluted by gradually increasing the concentration of NaCl in 20mM Tris (In the following way: 200 mM, 300 mM, 400 mM, 500 mM, 1 M, and 2 M NaCl). rAAV particles were concentrated using Amicon Ultra centrifugal filter tubes (Millipore) by centrifuging repeatedly at 2000 x *g* for 15 min. Concentrated virus was washed twice in 3.5 ml phosphate-buffered saline (PBS) by centrifuging repeatedly at 2000 x *g* for 15 mins until virus volume reached 100-200 µl. Concentrated AAVs were stored as 5 µl aliquots at -80°C.

2.5 Animals

Wild-type male C57BL/6 mice were obtained from Harlan UK/US. Experiments were conducted in the UCL Biological Services Unit. The involvement of dLS GLP-1Rs in acute stress (Section 4.2.8) was studied at Florida State University, FL, USA, in collaboration with Dr Diana Williams. Mice were handled several times a week and kept on a 12h light/12h dark cycle with *ad libitum* access to water and food unless otherwise noted. They were fed normal chow (Teklad) or high-fat diet (HFD, 60% energy from fat, 15% from protein, custom made, TestDiet) as indicated and were group-housed when not subjected to biotelemetry or food intake measurements.

2.5.1 Transgenic strains

Transgenic mice were bred in-house. Transgenic mouse strains were kindly provided by Dr Frank Reimann and Professor Fiona M. Gribble:

- Glu-Cre/Rosa26-GCaMP3/tdRFP heterozygous transgenic mice with GCaMP3 on one allele and tdRFP on the other were obtained by Dr Frank Reimann by crossing mice expressing Cre under the control of the glucagon promoter (Glu12-Cre (Parker et al. 2012)) with a commercially available ROSA26-lox-stop-lox-GCaMP3 reporter strain (Jax strain 014538) (Zariwala et al. 2012). To optimise GCaMP3 expression levels this strain was selectively bred by me to produce two independent strains: Glu-Cre/Rosa26-GCaMP3 (**PPG-Cre/GCaMP3**) or Glu-Cre/Rosa26-tdRFP (**PPG-Cre/tdRFP**).

- GLP-1R-Cre/Rosa26-tdRFP (**GLP-1R-Cre/tdRFP**) (Richards et al. 2014; Cork et al. 2015). This strain expresses Cre under the control of the GLP-1R promoter and tdRFP in a Cre-dependent manner, resulting in Cre and tdRFP expression in GLP-1R neurons.

2.5.2 Animal genotyping

Mice were genotyped for breeding purposes. A small tissue biopsy was taken from the ear and digested using Proteinase K at 55°C for one hour. The presence of three transgenes as well as a tissue control β-catenin was verified using GoTaq mastermix (primer pairs in Table 2.6).

Application	Binding	Sequence
GCaMP3	5’	5’–CTTCAAGATCCGCCACAAC–3’
GCaMP3	3’	5’–TTGAAGAAGATGGTGCGCT–3’
Cre	5’	5’–AATTGAGCTCATTTGGACTGCC–3’
Cre	3’	5’–GTAGTCCCTCACATCCTCAGG–3’
tdRFP	5’	5’–CTACAGGAACAGGTGGTGG –3’
tdRFP	3’	5’–CTGTTCCTGGGGCATGGC–3’
β-catenin	5’	5’–AAGGTAGAGTGATGAAAGTTGTT–3’
β-catenin	3’	5’–CACCATGTCCTCTGTCTATTC–3’

Table 2.6. Primer sequences for genotyping.

Reactions (25 µl) contained 12.5 µl GoTaq Green mastermix, 0.5 µM forward and reverse primer and 3 µl digested tissue sample. Double reactions were run (β-catenin and tdRFP in one and Cre and GCaMP3 in the other) under the following conditions:

- Initial denaturation of DNA — 95°C for 2 mins
- DNA denaturation — 95°C for 1 min
- Primer annealing — 58°C for 1 min
- Elongation — 72°C for 1 min

(40 cycles)

- Final elongation — 72°C for 5 mins

Amplicons were separated and visualised on a 1% agarose gel as described in section 2.4.2.

2.6 Immunohistochemistry

2.6.1 Transcardial perfusion and tissue preparation

Mice were anaesthetised using 1.4 g/kg urethane. The diaphragm was pierced and the heart exposed. A needle was inserted into the left ventricle and an incision was made into the right atrium to introduce an outlet for the perfusion solution. Using 50 ml syringes, the mouse was perfused with 50 ml of ice-cold 0.1 M phosphate buffer (PB) followed by 50 ml of ice-cold 4% formaldehyde/1% methanol in 0.1 M PB. The brain was extracted and post-fixed in 4% formaldehyde/1% methanol in 0.1 M PB at 4°C. The following day, the brain was transferred to 30% sucrose in 0.1 M PB for cryoprotection. After infiltration of sucrose it was blocked without

the use of a brain matrix. The brain was mounted onto a pedestal using OCT and sectioned on a cryostat (Bright Instruments, UK) into five series of 30 µm coronal sections, which were kept in 0.1 M PB at 4°C for later use.

2.6.2 Immunostaining procedure

To prevent unspecific binding, sections were blocked for one hour in 0.1 M PB containing 1% BSA, 0.1% Triton X-100 and 10% serum from the origin species of the secondary antibody (Table 2.2). The primary antibody (Table 2.1) was added to the blocking solution and sections were incubated overnight at 4°C gently agitated at 150 rpm. The next day, sections were washed 5 x 5 mins in 0.1 M PB at room temperature, followed by incubation with the secondary antibody (Table 2.2) in blocking solution for two hours at room temperature gently agitated at 150 rpm. Sections were washed 5 x 5 mins in 0.1 M PB at room temperature and mounted onto positively charged microscope slides. A drop of VectaShield Antifade mounting media was added and the sections were covered with glass coverslips.

Immunofluorescence was visualised on an upright widefield microscope (Leica) equipped with GFP (Chroma 49002, Excitation: 470±20 nm, Emission: 525±25 nm, dichroic mirror: 495 nm) and RFP (Chroma 49008, Excitation: 560±20 nm, Emission: 630±37 nm, dichroic mirror: 585 nm) filter cubes. Images were captured using a colour camera (Retiga 3000, QImaging) and the Q-Capture Pro 7 software (QImaging) and montages containing several frames were created using Image Composite Editor (Microsoft). Brightness and contrast were adjusted using Fiji image analysis software (Schindelin et al. 2012).

2.7 *In vitro* imaging and electrophysiology

2.7.1 Sample preparation

Mice were deeply anaesthetised with isofluorane and decapitated. The brainstem or forebrain was removed and placed in ice-cold high-Mg^{2+}/low-Ca^{2+} ACSF. Coronal sections (200 µm thick) were cut on a vibratome (Campden Instruments) and left in recovery solution at 34°C. After 45 mins, sections were transferred to ACSF and left to adjust for a minimum of 30 mins. To maintain pH 7.4 and sufficient oxygenation, solutions were constantly bubbled with 95% O_2/5% CO_2.

2.7.2 Ca^{2+} imaging

Ca^{2+} imaging was performed in one of two configurations:

1. On a widefield microscope (Zeiss Axioskop) with a 40x water immersion lens (0.8 numerical aperture). The field diaphragm was restricted to reduce light scattering and

background fluorescence. GCaMP3 was excited using an LED light source (CoolLED pE300white; QImaging) at 460±25 nm for 250 ms every 5 s. Excitation was filtered at 470±20 nm and emission was filtered at 515±17 nm (Chroma 59004). Images (12-bit) were captured on a charge-coupled device camera (Q-Click; QImaging). The LED light source and camera were controlled in Micro-Manager (Edelstein et al. 2014).

2. Using a laser scanning microscope (Olympus FV-1000, pinhole fully open) with a 25x water immersion objective (1.05 numerical aperture). Here, GCaMP3 was excited using a laser (Showa Optronics) at 488 nM. Emitted light was detected using a photomultiplier tube. Images were captured using FV10-ASW (Olympus).

I observed no difference in the response to compounds between the two systems, although bleaching only had to be corrected for when using the widefield microscope. Sections were continuously superfused with 32°C standard ACSF at a flow rate of 3-4 ml/min. All imaging was performed on PPG neurons in the NTS or GLP-1R-expressing neurons in the dLS.

2.7.3 Patch-clamp electrophysiology

As above, sections were continuously superfused with 32°C standard ACSF at a flow rate of 3-4 ml/min. NTS PPG cells expressing GCaMP3 were located using the widefield setup described in section 2.7.2. Patch pipettes were pulled on a horizontal puller (Zeitz Instrumente) from thin-walled borosilicate glass capillaries (3–7 MΩ, Harvard Apparatus). Pipettes were filled with low-Cl^- intracellular solution and fitted over the recording electrode. Cells were visualised for cell-attached recordings with a differential interference contrast filter and approached using a micromanipulator (Scientifica). Positive pressure in the patch electrode minimised blockade of the pipette tip and facilitated penetration through the brain tissue. To avoid dilution of GCaMP3 into the patch pipette, recordings were performed in the cell-attached configuration. Contact was made with the cell and positive pressure released. Light negative pressure was applied until resistance increased (usually 100 MΩ) and clear inward currents resulting from action potential firing were distinguishable from noise. Recordings were performed in voltage-clamp mode with a holding potential of -50 mV using an EPC-10 amplifier and PatchMaster software (both HEKA Elektronik). Currents were filtered at 1.5 kHz and digitized at 3 kHz.

2.8 Stereotaxic injection

2.8.1 Anaesthesia

For stereotaxic injections, adult PPG-Cre/GCaMP3, PPG-Cre/tdRFP, and GLP-1R-Cre/tdRFP mice were anaesthetised using injectable anaesthesia (ketamine hydrochloride and medetomidine in

45µl H_2O into the quadriceps) or isofluorane (1.5-2.5% at 1.5 L/min with 1.5 L/min O_2). The absence of a pedal withdrawal reflex confirmed deep anaesthesia. The skull was fixed in a stereotaxic frame and a core temperature of 37°C maintained using a heating mat.

2.8.2 Brainstem injections

Injection needles were pulled on a horizontal puller and filled with virus using negative pressure. The nose of the mouse was pushed downwards, creating a right angle between the nose and the neck to expose part of the brainstem normally covered by the cerebellum. A longitudinal incision was made from the occipital bone to the first vertebra. Obex was exposed by parting overlying muscle layers and the dura mater was pierced using a 30g needle. Virus was injected bilaterally at the following coordinates from the obex:

- 500 µm lateral
- 100 µm rostral
- 350 µm ventral

For immunohistochemical verification, 50-100 nl was injected unilaterally. For all other studies, 250 nl was injected bilaterally.

Muscle and skin were sutured using 6-0 absorbable suture. If using injectable anaesthesia, the animal was reversed with Antisedan (2.5 mg/kg). Buprenorphine (0.5 mg/kg) and 100 µl saline were administered subcutaneously and the animal was left to recover in a 34°C chamber.

2.8.3 dLS injections

Mice were anaesthetised as described in section 2.8.1 and the skull placed in a stereotaxic frame with the teeth fixed in the tooth bar pointing forwards. A longitudinal incision was made from the front of the skull to the occipital bone. Bregma and Lambda were located and the skull was levelled horizontally by measuring the vertical offset between the two landmarks and limiting it to less than 100 µm by adjusting the stereotaxic frame. The periosteum and skull were pierced using a 25-gauge needle at the following coordinates from Bregma:

- 260 µm rostral
- 450 µm lateral
- 2600 µm ventral

Next, 100-200 nl virus was injected unilaterally. The skin was sutured using 6-0 absorbable suture and the mouse left to recover in a 34°C chamber. Post-surgery bodyweights were monitored daily.

2.9 Guide cannula implantation and infusions into dLS

2.9.1 Cannulation Surgery

Mice were anaesthetised using isoflurane (Section 2.8.1) and 5 mg/kg carprofen administered subcutaneously. The absence of a pedal withdrawal reflex confirmed deep anaesthesia and the skull was fixed in a stereotaxic frame. Core temperature of 37°C was maintained using a heating blanket. An incision was made from between the eyes to the occipital bone. The pericranium, the connective tissue covering the skull, was removed by scraping with the blunt side of the scalpel. This later ensured sufficient adhesion of the cement to the skull surface. A hole was pierced in the skull using a 25g needle at the following coordinates from Bregma:

- 350 µm rostral
- 260 µm lateral
- 1600 µm ventral (injector protrudes further 1500 µm ventral).

A 2 mm, 26-gauge guide cannula was inserted halfway and a drop of superglue applied under the base of the cannula before inserting it fully. Dental cement was prepared freshly and applied to the skull surrounding the cannula. Body weights were monitored daily following surgery. Correct placement of the cannula was verified histologically.

2.9.2 Infusion via guide cannula

Mice were habituated to handling prior to infusions. A 5 µl Hamilton syringe was filled with sterile water and connected to the injector. An air bubble was introduced and the drug (saline or Ex9) aspirated. The mouse was restrained and the dummy cap removed. The injector (1500 µm protrusion after cannula) was inserted into the brain tissue via the guide cannula and fixed using an adapted dummy cap. The mouse was released and 500 nl Ex9 or saline only was infused over one min. After another min, the injector was retracted and the dummy cap replaced.

2.10 Food intake measurements

All food intake was measured using standard chow (Teklad) or vanilla Ensure liquid diet (Abbott, USA). Mice were weighed daily and habituated to 5 ml/kg i.p. saline injection and food intake measurements before experiments commenced. The role of central GLP-1 in food intake was investigated using four models (Table 2.7). The abbreviated names will be used and refer to all mice in that study, including mice expressing control constructs or receiving control infusions. At least 48 hours passed between food intake experiments on the same mouse.

Approach	Abbr. name	Experimental virus/drug	Control virus/drug	N (Exp./ Control)	Sex
PPG activation	HM3Dq	FLEX-HM3Dq	FLEX-Perceval	N=4/4	6 M, 2 F
PPG activation repeat	HM3Dq-rep	FLEX-HM3Dq	-	N=9	5 M, 4 F
PPG ablation	DTA	FLEX-DTA	FLEX-Perceval	N=7/7	8 M, 6 F
PPG acute inhibition	HM4Di	FLEX-HM4Di	FLEX-EGFP	N=12/11	9 M, 15 F
dLS GLP-1R inhibition	dLS-Ex9	Ex9	Saline	N=7/5	12 M

Table 2.7. Approaches to manipulate central GLP-1. The abbreviated names, the between-subject factors and the number and sex of subjects are listed. The within-subject factors depend on individual paradigms.

2.10.1 Normal dark phase feeding

The DTA study was a between-subjects design. The HM3Dq and HM4Di studies were mixed-model designs, and the HM3Dq-rep study was designed to be counterbalanced within-subject.

Three hours before dark onset, DTA, HM3Dq, HM3Dq-rep, and HMD4i mice were transferred to individual cages and their food was withdrawn. HM3Dq, HM3Dq-rep, and HM4Di mice were injected i.p. with saline or 2 mg/kg CNO at a dose volume of 5 ml/kg saline 30 mins prior to dark onset. Food was returned at dark onset and intakes measured manually at one, two, four, and 21 hours after dark onset. Mice were then returned to their group-housed home cages.

2.10.2 Fast-refeeding

This study was designed to be between-subjects when using DTA mice and mixed-model when using HM4Di mice. DTA and HM4Di mice were fasted six hours into dark phase and left without food until the beginning of dark phase 18 hours later. HM4Di mice were injected i.p. with saline or 2 mg/kg CNO in saline at 5 ml/kg 30 mins before dark onset. Food was returned at dark onset and intakes were manually measured at one, two, four, and 21 hours after dark onset.

2.10.3 Ensure feeding

This study was conducted as a between-subjects design. DTA mice were housed in individual cages throughout the experiment. Their food was withdrawn three hours prior to dark onset. At dark onset, they were given vanilla Ensure liquid diet (Abbott, USA) for 15 mins after which chow was returned. The mice were trained to consume Ensure over seven days. Following stabilisation of intake, both Ensure intake and one hour chow intake were measured.

2.10.4 Stress-induced hypophagia

These studies were designed as mixed-model with every animal being exposed to stress only once. All animals in the HM4Di study received 2 mg/kg CNO in 5 ml/kg saline. All cannulated mice received one infusion of saline before starting the experiment to ensure infusions did not affect food intake adversely. Data from individual animals were collected over several days.

HM4Di and dLS-Ex9 mice were transferred to individual cages and their food was withdrawn. HM4Di mice received i.p. injections of 2 mg/kg CNO in 5 ml/kg saline 60-45 mins before dark onset. dLS cannulated mice received intra-dLS infusions of either 10 µg Ex9 or saline only (500 nl) 45 mins before dark onset as described in section 2.9.2. 30 mins before dark onset, mice were restrained in transparent plastic bags with a breathing hole at the front. They were fixed in the bags using twist ties around their tails and the plastic bag. At dark onset, mice were released into their home cages and chow returned. Intake was measured at one hour, two hours, four hours, and 21 hours following dark onset.

2.11 Glucose tolerance test

Mice were fasted overnight for 16 hours from two hours prior to dark phase to two hours into light phase the next day. A small sample of blood was taken from the tail vein and the blood glucose concentration was measured using a glucose meter (Accu-Chek, Roche, UK). Glucose (1 mg/kg) was injected i.p. and blood glucose concentration was measured 15, 30, 90, and 120 mins after glucose injection.

2.12 Tail-cuff measurements

Blood pressure and heart rate of ten 7-10-week-old male naïve mice were measured using the CODA high throughput volume-pressure recording (VPR) tail-cuff system (Kent Scientific). Mice were placed in a perforated plexiglass tube, fixed tightly in place, and placed on a 32°C heat pad. An occlusion cuff and a VPR cuff were placed over the tail and 25 cycles were run. Heart rate and blood pressure were determined from accepted runs. Five animals were transferred to HFD, five were kept on normal chow. Eight weeks later tail-cuff recordings were repeated as above.

2.13 Biotelemetry probe implantation

Male, 7-10-week-old, naïve or transgenic mice (PPG-Cre/tdRFP or PPG-Cre/GCaMP3) were anaesthetised using isofluorane (1.5-2.5% at 1.5 L/min) with 1.5 L/min O_2. Body temperature was maintained at 37°C using a heat mat (World Precision Instruments). Prior to implantation, biotelemetry blood pressure probes (TA11-PA-C10, Data Science International) were rinsed in sterile saline and the tip of the catheter was filled with gel taking care to avoid any bubble formation, which would dampen the pressure transducer signal. An incision was made in the skin parallel to the trachea and the left carotid artery dissected out at the level of the carotid bifurcation. The artery was permanently occluded using non-absorbable 6-0 suture at the carotid bifurcation. The artery was then temporarily occluded proximally using non-absorbable 6-0 suture and a small hole was cut in the artery with fine scissors. The tip of the catheter was

inserted into the carotid artery, the artery occlusion released and the catheter inserted completely into the aortic arch. The catheter was fixed using non-absorbable 6-0 suture and a subdermal pocket was created on the right flank of the mouse where the transmitter was inserted. The mouse was given analgesia (5 mg/kg carprofen, subcutaneously) and left to recover for at least seven days before baseline heart rate and blood pressure were recorded. All mice were kept in individual cages after implantation.

2.14 Biotelemetry data acquisition

All recordings were done over at least 25 hours at a sample rate of 500-1000 Hz using the Dataquest ART software (Data Science International). Locomotor activity is provided by the software and is based on the mouse's distance from the centre of the platform and the location of the mouse in one of four quadrants. A larger number indicates a greater distance travelled in the 10 s bins.

2.14.1 Pharmacology

Pharmacological studies in biotelemetry probe-implanted animals were within-subject, counterbalanced designs.

To investigate the effect of systemic GLP-1R activation, mice were injected i.p. with 100 µg/kg GLP-1, 10 µg/kg Ex4, or saline only. Mice were transferred to recording platforms the day before to habituate and were injected four hours into the light phase. All injections were 100 µl and experiments were performed using a within-subject design.

For studies using atenolol, mice were injected i.p. with 2 mg/kg atenolol three hours and 45 mins into the light phase. 15 mins later, four hours into light phase, mice received a second injection of 10 µg/kg Ex4 or saline only. All injections were 100 µl.

2.14.2 Ablation of PPG neurons

This study was designed to be mixed-model with repeated measures over time and the between-subject factor being the viral transgene (i.e. Perceval vs DTA). Baseline heart rate and blood pressure were recorded one week after biotelemetry probe implantation. Following baseline recordings, mice were stereotaxically injected (section 2.8.2) with AAV8-mCherry-FLEX-DTA or AAV1/2-FLEX-Perceval as control. Heart rate and blood pressure were recorded four and six weeks post-stereotaxic surgery. Nine weeks post-surgery mice were injected i.p. in a within-subject counterbalanced design with 10 µg/kg Ex4 or saline as described in section 2.14.1. One week later, ten weeks post-surgery, mice were transferred to HFD (LabDiets). After one month

of HFD (14 weeks post-surgery), heart rate and blood pressure were recorded again. One week later (15 weeks post-surgery), mice were again injected i.p. with 10 µg/kg Ex4 or saline as before. Following the last recording, mice were anaesthetised using urethane and transcardially perfused (section 2.6.1).

2.14.3 Chemogenetic activation of PPG neurons

This study was a mixed-model design with drug treatment (saline or CNO) as a repeated measure and the between-subject factor being the expressed transgene (i.e. EGFP or HM3Dq). Mice implanted with biotelemetry probes (section 2.13) were stereotaxically injected with AAV2-FLEX-HMD3q:mCherry or AAV2-FLEX-EGFP into the NTS (Section 2.8.2). They were handled daily and habituated to i.p. injections of 5 ml/kg saline. The day before injections, mice were transferred to biotelemetry platforms. The next day mice were injected i.p. with 2 mg/kg CNO in 5 ml/kg saline 4.5 hours prior to onset of the dark phase.

2.15 Data processing and statistics

2.15.1 Ca^{2+} imaging analysis

Image stacks from *in vitro* Ca^{2+} recordings were imported into Fiji image analysis software (Schindelin et al. 2012). XY-drift was adjusted for using the StackReg plugin (Thevenaz et al. 1998). The mean pixel intensity was measured from outlined regions of interest (ROIs) and an area representing background fluorescence. For time-lapse data recorded on the widefield microscope (see section 2.7.2), background intensity was subtracted from each ROI and recordings were adjusted for bleaching using a cubic polynomial function (Balkenius et al. 2015). Fluorescence intensity is reported as the relative change in intensity from baseline, $\Delta F/F_0$, with F_0 defined as the mean fluorescence intensity five mins prior to the first stimulus and ΔF being the fluorescence intensity, F, at a given time n, F_n, minus F_0. Data were plotted in Origin 9.0 (OriginLab, US) and are presented as individual and mean traces.

Responses were quantified by calculating the area under the curve (AUC) over ten mins during the stimulus, starting at the beginning of the stimulus. Data were not normally distributed and summary data are therefore presented as box plots with whiskers. The median is shown and whiskers indicate 10^{th} and 90^{th} percentiles. Statistical significance was determined using nonparametric tests, Wilcoxon (paired two-sample), Mann-Whitney U (unpaired two-sample), Friedman (repeated measures one-way ANOVA) or Kruskal-Wallis (one-way ANOVA).

2.15.2 Patch-clamp electrophysiology analysis

Electrophysiological data was exported from PatchMaster into PulseFit (Both Heka Elektronik), from where traces were exported as ASCI files. Electrical events (i.e. currents corresponding to action potential firing) were detected using WinEDR (Strathclyde, UK) and a list of events and the interevent interval list were generated. A cell was determined to respond to drug treatment if the mean instantaneous firing frequency over one minute during the stimulus differed significantly compared to one minute prior to the stimulus, as determined by the unpaired Student's T-test. The event list was imported into The R Project for Statistical Computing, R 3.3.1 (R Core Team 2016) using RStudio (RStudio Team 2015). Firing rate was determined by creating 10 s bins of events. Plots of firing frequency over time were created in R. For correlation between firing frequency and change in GCaMP3 fluorescence, $\Delta F/F_0$ was plotted against the change in firing frequency in 10s bins. A linear function was fitted using Origin (OriginLab, Northampton, MA, USA) and plotted in GraphPad Prism 7.00 (GraphPad Software, La Jolla, California, USA).

2.15.3 Analysis of food intake experiments

Food intake experiments were designed as exploratory. When possible, studies were designed to be within-subject and randomized. Raw data were processed in Microsoft Excel and plots were generated in GraphPad Prism 7.0. Outliers were identified using Iglewicz and Hoaglin's robust test for multiple outliers with a modified Z score of 3.5 (Iglewicz and Hoaglin 1993). Statistical analysis was performed in GraphPad Prism 7.0. Three-way mixed model ANOVAs were conducted in SPSS version 22.0 (IBM Corp, NY, USA). Three-way interactions are difficult to interpret and were followed up with relevant two-way ANOVAs. For transparency, non-cumulative food intake data are presented as individual data points. Summary data are presented as mean±SEM. Statistical significance was tested using three-way mixed-model ANOVA, two-way mixed-model ANOVA, and simple main effects as indicated in figure legends and text. Results from three-way ANOVAs are presented in tables in the relevant sections.

2.15.4 Analysis of biotelemetry data

Raw biotelemetry data were extracted in 10 s bins using the DSI Analysis software and processed in Microsoft Excel and The R Project for Statistical Computing, R 3.3.1 (R Core Team 2016). Statistical significance was tested using two-way mixed-model ANOVA and simple main effects as indicated in figure legends and text.

3. Characterisation of PPG neurons *in vitro* using a genetically encoded Ca^{2+} indicator

3.1 Background

Despite the established importance of the central GLP-1 system in food intake regulation, little is known about the cellular properties of the source of central GLP-1, the PPG neurons. Until now studies have mainly employed two approaches to investigate the activity of PPG neurons:

1. Patch-clamp electrophysiology for high temporal resolution recordings of neuronal activity at the single-cell level.
2. Immunostaining for the product of the immediately early gene, *cFOS*, as a surrogate marker for recent increase in neuronal activity.

Studies using these methods have elucidated important aspects of regulation of PPG neuron activity. In 1999, Linda Rinaman discovered that GLP-1-producing neurons in the rat NTS were activated by i.p. injections of interoceptive stressors LiCl, endotoxin (LPS) and CCK. Vrang et al. (2003) later demonstrated that GLP-1-producing neurons in the NTS are activated by gastric distention in rats. These studies were reliant on immunostaining to co-localise GLP-1 and cFOS to the same cells. More recently, the development of transgenic mouse models has circumvented the problem of reliably immunostaining for GLP-1. In our laboratory, Hisadome et al. (2010) used a transgenic mouse model, the PPG-YFP mouse (Reimann et al. 2008), to selectively record the electrical activity GLP-1-producing neurons in the NTS. Using patch-clamp electrophysiology they discovered that satiety hormones, leptin and CCK, activate PPG neurons *in vitro* (Hisadome et al. 2010, 2011).

In this chapter, I aim to expand on this knowledge by investigating the modulation of PPG neuron activity by several compounds, including known satiety hormones and metabolic signals. To this end, I use a transgenic mouse expressing the genetically encoded Ca^{2+} indicator, GCaMP3, in PPG neurons only (Anesten et al. 2016; Holt et al. 2017). This mouse will be referred to as the PPG-Cre/GCaMP3 mouse. GCaMP3 is a modified enhanced green fluorescent protein (EGFP), which senses changes in intracellular [Ca^{2+}] (Tian et al. 2009). It consists of a circularly permuted EGFP, which is fused at each terminal to calmodulin and the M13 peptide of myosin light chain, respectively (Nakai et al. 2001; Tian et al. 2009). Ca^{2+} enhances the binding of calmodulin to M13 leading to a conformational change in the EGFP moiety, resulting in increased fluorescence

intensity. Neuronal activity can therefore be monitored by recording changes in GCaMP3 fluorescence intensity.

Ca^{2+} imaging was chosen as an experimental approach for two reasons:

1. It is superior to cFOS immunostaining in terms of temporal resolution and reliability. cFOS immunostaining provides a binary yes/no answer to the question "does the compound activate these neurons?" (Sagar et al. 1988). However, not all cell populations reliably increase cFOS expression upon increased activity (Labiner et al. 1993) and the detection of cFOS is dependent on the labelling protocol. GCaMP3 imaging, in contrast, provides higher temporal resolution and reliable detection of small changes in neuronal activity from a wide range of tissues (Zariwala et al. 2012) and has shed light on processes such as object localisation (O'Connor et al. 2010), place cells (Dombeck et al. 2010) and motor memory (Huber et al. 2012).
2. GCaMP3-based Ca^{2+} imaging leaves cells undisturbed and provides results from several cells simultaneously in contrast to patch-clamp electrophysiology.

I sectioned live, coronal 200 µm-thick brainstem slices from PPG-Cre/GCaMP3 mice and imaged them using either a scanning or a widefield microscope, as described in Materials and Methods. The *in vitro* slice model allows preservation of local neuronal connections and leaves the cells in their microenvironment.

Some technical considerations must be mentioned at this stage. Background fluorescence intensity was subtracted from widefield images to reduce the impact of light scattering on quantifications. All recordings are expressed as relative change in fluorescence (ΔF) from the mean over the first five minutes of the recording (F_0), as described in Materials and Methods. This is to ensure no effect of differences in expression levels of GCaMP3 on interpretation of changes in intracellular [Ca^{2+}].

Importantly, changes in intracellular [Ca^{2+}] are used as a surrogate marker for changes in neuronal activity. The method used here is not strictly quantitative, it does not provide accurate information on the absolute levels of Ca^{2+} in the cell and comparisons between recordings are therefore difficult. It is as such important that recordings serve as their own controls.

In vitro brainstem slices from PPG-Cre/GCaMP3 mice were exposed to a range of peptides, neurotransmitters, and metabolic cues. The compounds of interest were chosen based on their involvement in food intake or homeostatic regulation and potential links with the central GLP-1

system. Elucidating these interactions *in vitro* could reveal new directions for research into the neural circuits underlying GLP-1-mediated regulation of food intake behaviour.

In the next section, I will address the following questions:

1. Is the PPG-Cre/GCaMP3 model suitable for monitoring changes in PPG activity?
2. Do metabolic and homeostatic signals, such as leptin, CCK, IL-6, and hypoglycaemia, modulate PPG activity?
3. Is PPG activity modulated by stimulation of acetylcholine and ATP receptors?
4. What is the nature of 5-HT-mediated modulation of PPG activity and which receptors are involved?

3.2 Results

3.2.1 Using GCaMP3 to monitor activity of NTS PPG neurons in vitro

To begin with, I wanted to confirm that the PPG-Cre/GCaMP3 mouse strain is suitable for monitoring neuronal activity in brainstem slices *in vitro*. In this strain, Cre expression is driven by the glucagon promoter, resulting in expression of Cre in L-cells in the gut (Chimerel et al. 2014) and PPG neurons in the caudal brainstem (Anesten et al. 2016; Holt et al. 2017). Cre mediates recombination of two LoxP sites flanking a translational STOP site (Fig 3.1A). As explained in the Introduction, this leads to excision of the STOP site and enables expression of the GCaMP3 protein as detected with an anti-GFP antibody in Fig 3.1B.

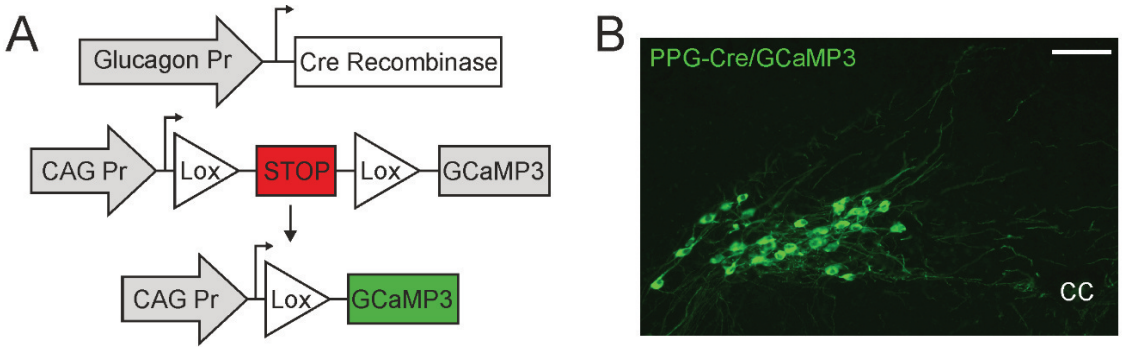

Fig 3.1 The PPG-Cre/GCaMP3 mouse model for *in vitro* recording of PPG activity. A) Glucagon promoter (PPG-Cre) mice were crossed with mice encoding CAG-promoter-STOP-GCaMP3 in the Rosa26 locus. The Rosa26 locus is active in most cell types (Zambrowicz et al. 1997; Giel-Moloney et al. 2007). In cells with active glucagon promoter, including PPG neurons, Cre is produced and excises the STOP sequence flanked by loxP sites upstream of the GCaMP3 gene. This results in cytosolic expression of GCaMP3 in these cells. **B)** GCaMP3 was detected in the NTS with an anti-GFP antibody and is shown here in green. One side of the NTS is shown here. CC: Central canal. Scale bar: 100 µm.

To ensure GCaMP3-expressing cells were in fact producing GLP-1, I double-stained fixed coronal brainstem slices for GLP-1 and GCaMP3 (Fig 3.2). GCaMP3 expression was detected in the caudal NTS, as in Fig 3.1, and filled the cytosol but was excluded from the nucleus (Fig 3.2 left panel). Immunodetection of GLP-1 revealed a punctuate stain in cells located in the NTS (Fig 3.2 middle panel). This was obvious at higher magnifications (Fig 3.2 bottom middle panel) and is most likely due to packaging of GLP-1 into vesicles. As seen in Fig 3.2 some cells were positive for GLP-1, but did not express GCaMP3, whereas all GCaMP3-positive cells were positive for GLP-1.

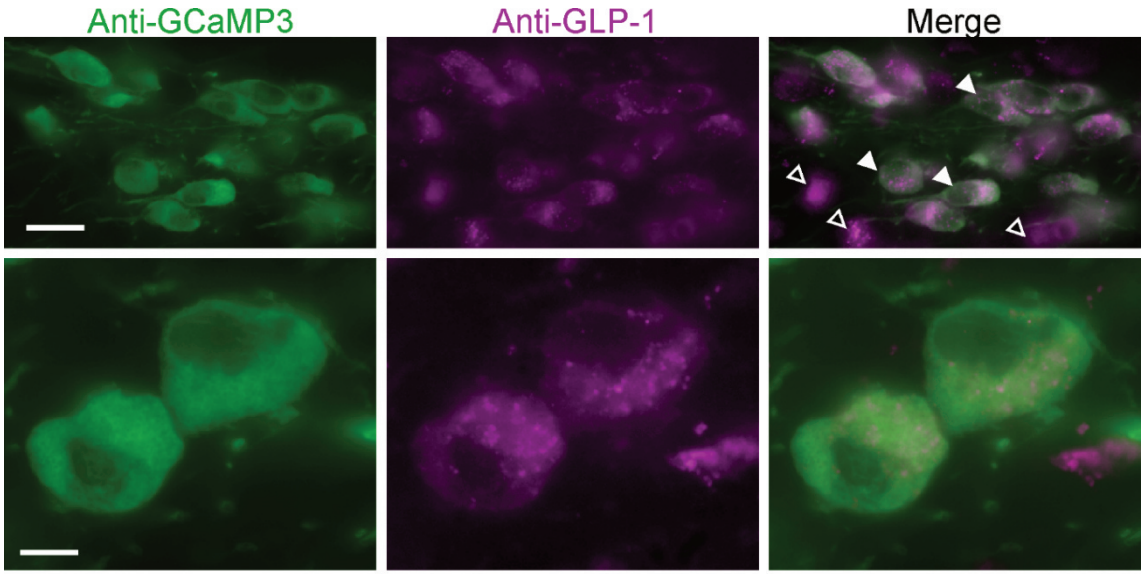

Fig 3.2 GCaMP3-positive neurons express GLP-1. PPG-Cre/GCaMP3 mice were perfuse-fixed and double-stained with anti-GFP (to detect GCaMP3, in green) and anti-GLP-1 (in magenta) antibodies. Shown here are two magnifications of cells from two different sections. White arrowheads indicate some of the double-positive neurons. Black arrowheads indicate neurons positive only for GLP-1. Scale bars: 30 µm (top panel) and 10 µm (bottom panel).

To further support this, a post-doctoral researcher in our laboratory cross-bred two transgenic strains (James E. Richards, unpublished). As explained in Materials and Methods, the PPG-Cre/tdRFP strain (Parker et al. 2012) is identical to the PPG-Cre/GCaMP3 strain with the exception of the fluorescent reporter, which is tandem-dimer red fluorescent protein (tdRFP) (Luche et al. 2007), instead of GCaMP3. The PPG-Cre/tdRFP strain was created from the same BAC construct as the PPG-YFP mouse, with expression driven by the same promoter (Reimann et al. 2008; Parker et al. 2012). However, differences in expression are still possible. We therefore crossbred PPG-Cre/tdRFP mice with PPG-YFP mice. The PPG-YFP strain is well-characterised (Hisadome et al. 2010, 2011, Llewellyn-Smith et al. 2011, 2013; Thiebaud et al. 2016). As described in the Introduction, YFP expression is under control of the glucagon promoter and single-cell RT-PCR has verified that YFP-expressing cells express the *PPG* mRNA (Hisadome et al. 2010). In the offspring, there was an almost complete overlap between cells expressing YFP and tdRFP, suggesting we can use the PPG-Cre mouse to investigate and manipulate the PPG neurons (Unpublished).

Having confirmed the validity of the PPG-Cre/GCaMP3 model, I wanted to test the ability of the GCaMP3 imaging system to detect changes in neuronal activity. I sectioned 200 µm-thick brainstem slices from PPG-Cre/GCaMP3 mice and performed simultaneous Ca^{2+} imaging and patch-clamp electrophysiology. Firing rate was monitored using cell-attached recordings to

avoid breaking the cell membrane and diluting GCaMP3 in the patch-pipette. As seen in Fig 3.3A a reduction in intracellular [Ca^{2+}] measured via change in fluorescence intensity was concurrent with a decrease in firing rate of the same neuron. This was observed repeatedly and analysis of four individual neurons revealed a positive correlation between change in firing rate and intracellular [Ca^{2+}] (Fig 3.3B), demonstrating that ongoing electrical activity is linked with intracellular Ca^{2+} levels in PPG neurons.

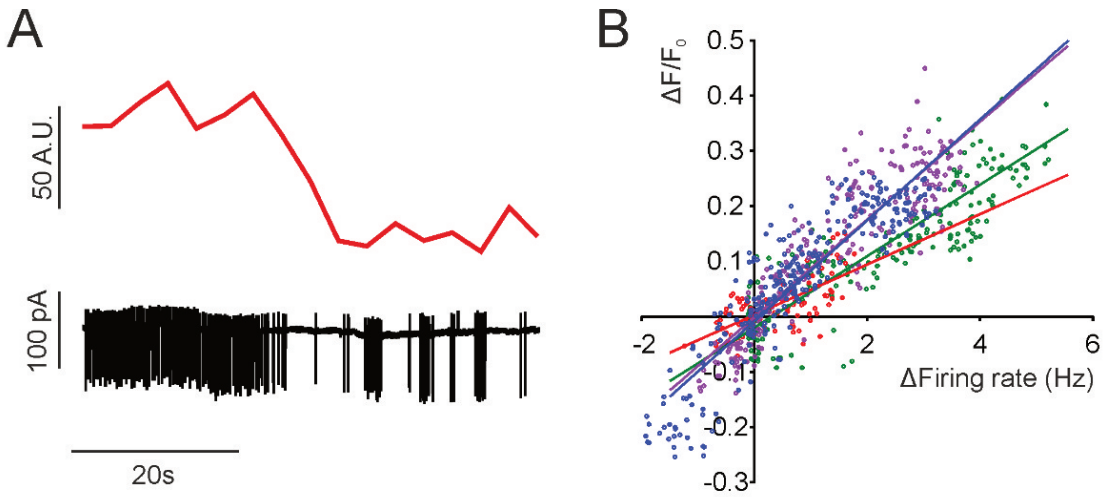

Fig 3.3 Changes in GCaMP3 fluorescence intensity correlate with changes in firing rate. A) Representative Ca^{2+} imaging (top, red) and cell-attached voltage clamp (bottom, black) traces from a single PPG neuron. **B)** Correlation between changes in firing rate and percentage change in intracellular Ca^{2+} levels from baseline for four individual cells. Each cell is represented by a unique colour, individual data points are represented by dots and a linear fit to the data is plotted in the same colour (data from 3 mice).

Having established that GCaMP3 fluorescence can be used as a surrogate marker for neuronal activity, I set out to investigate modulation of NTS PPG neuron activity. To start, I exposed the cells to 100 µM glutamate while monitoring fluorescence intensity changes (Fig 3.4). As seen from two representative cells in Fig 3.4A, GCaMP3 fluorescence intensity increased during application of 100 µM glutamate. Nine NTS PPG neurons shown in Fig 3.4B responded to 1 min of 100 µM glutamate exposure with a rapid increase in intracellular [Ca^{2+}], which decreased after washout of glutamate to baseline levels. Glutamate (100 µM) increased GCaMP3 fluorescence intensity in 89% of 143 PPG neurons imaged, demonstrating that changes in intracellular [Ca^{2+}] can be detected using *in vitro* imaging of GCaMP3 fluorescence intensity.

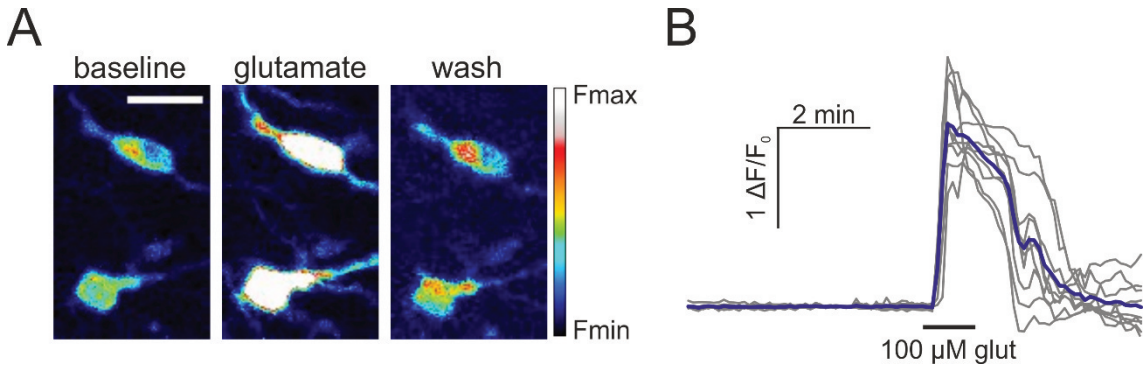

Fig 3.4 Glutamate (100 µM) increases intracellular [Ca^{2+}] in PPG neurons. Live coronal brainstem slices from PPG-Cre/GCaMP3 mice were exposed to 100 µM glutamate for 1 min. **A)** Two representative PPG neurons in the NTS, here pseudocoloured as shown on the right, before (baseline), during (glutamate) and after (wash) stimulation with 100 µM glutamate. Scale bar: 20 µm. **B)** Fluorescence intensity expressed as a fraction of the intensity at the beginning of the experiment ($\Delta F/F_0$). Glutamate application is indicated with a black bar (glut). Traces from individual cells are plotted in grey and the average response is shown in dark blue. (N=9 somata).

3.2.2 NTS PPG neurons are activated by leptin, IL-6, and CCK

As mentioned in section 3.1, Hisadome et al. (2010, 2011) studied PPG neuron activity using patch-clamp electrophysiology. These experiments were fundamental in understanding the cellular properties of PPG neurons, which were found to be directly depolarised by leptin (Hisadome et al. 2010).

Using Ca^{2+} imaging, I confirmed these findings by stimulating PPG-Cre/GCaMP3 coronal brainstem slices with 1 nM leptin (Fig 3.5A). Coronal brainstem slices from PPG-Cre/GCaMP3 mice were superfused with 1 nM leptin for 3 mins, which elicited an increase in intracellular [Ca^{2+}] as seen in images of representative cells (Fig 3.5A left) and traces from eight individual neurons (Fig 3.5A middle). Intracellular [Ca^{2+}] was monitored in 15 PPG neurons from two different mice. All imaged neurons responded to leptin with an increase in GCaMP3 fluorescence intensity, suggesting the entire PPG neuron population is activated by leptin. Responses to leptin were quantified by calculating the area under the curve (AUC) for each individual cell (Fig 3.5A right panel). These data confirm the previous study from our laboratory and demonstrate that PPG neurons respond as a population to leptin with an increase in activity.

Leptin bears structural similarities to members of the cytokine family and the lepR is closely related to class I cytokine receptors (Tartaglia et al. 1995; Frühbeck 2006). Interleukin-6 (IL-6) is a member of the cytokine family, which has been implicated in the regulation of food intake and energy expenditure (Molotkov et al. 1998; Wallenius et al. 2002; Jansson and Palsdottir 2015). Furthermore, IL-6 has been proposed to mediate the food-intake suppressive effects of GLP-1R

activation (Shirazi et al. 2013). The following data were published in collaboration with John-Olov Jansson (Anesten et al. 2016).

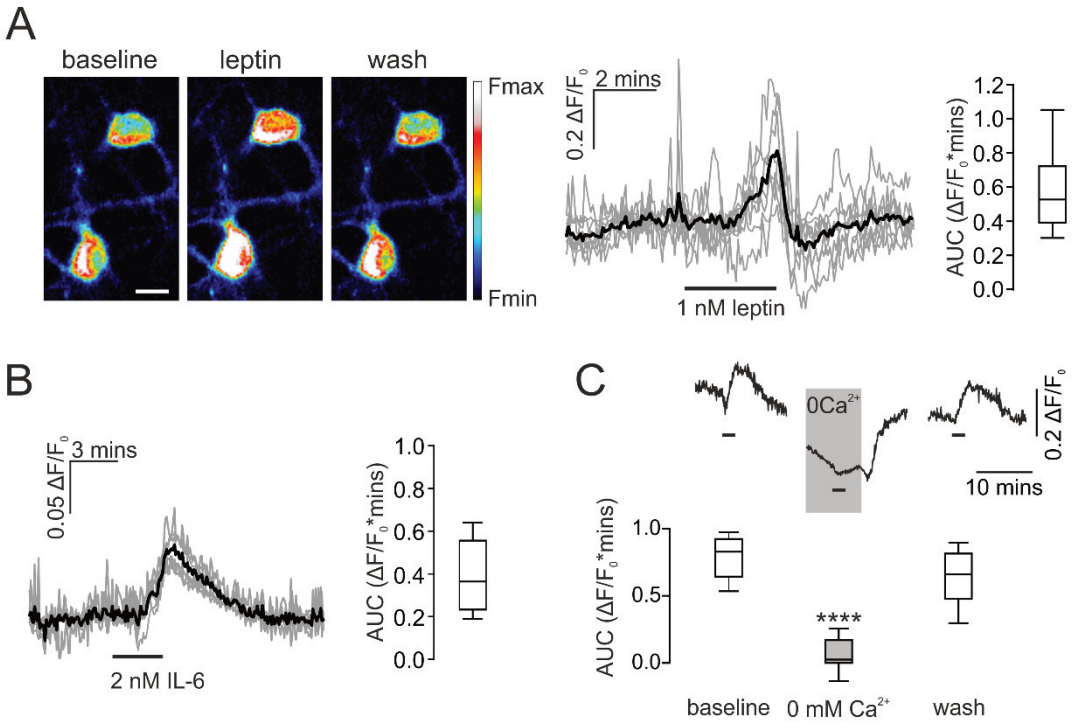

Fig 3.5 PPG neurons respond to 1 nM leptin and 2 nM IL-6 with an increase in intracellular [Ca^{2+}]. *In vitro* brainstem slices from PPG-Cre/GCaMP3 mice were exposed to 1 nM leptin or 2 nM IL-6 for 3 mins. **A)** *Left panel:* Two representative NTS PPG neurons, here pseudocoloured as shown on the right, before (baseline), during (leptin) and after (wash) stimulation with 1 nM leptin. Scale bar: 10 µm. *Middle panel:* Fluorescence intensity changes in response to 1 nM leptin expressed as a fraction of the intensity at baseline ($\Delta F/F_0$). Traces from individual cells are plotted in grey and the average response is shown in black (N=8). *Right panel:* Median AUC in response to 1 nM leptin. (N=15 somas, 2 slices). **B)** *Left panel:* Fluorescence intensity changes in response to 2 nM IL-6 expressed as $\Delta F/F_0$. Traces from individual cells are plotted in grey and the average response is shown in black (N=6). *Right panel:* Median AUC in response to 2 nM IL-6 (N=25 somas, 4 slices). **C)** *Top panel:* Representative cell responding to 2 nM IL-6 before (baseline), during (0 mM Ca^{2+}) and after (wash) removal of extracellular Ca^{2+}. The period of 0 mM Ca^{2+} is indicated with a grey bar. *Bottom panel:* Median AUC in response to 2 nM IL-6 before (baseline), during (0 mM Ca^{2+}) and after (wash) removal of extracellular Ca^{2+} (N=19-31 somas, 3 slices). Kruskal-Wallis ANOVA yielded a significant test statistic (51.42). ****p<0.0001 according to Dunn's test compared to both baseline and wash.

To investigate the link between IL-6 and PPG neuron activity, I stimulated NTS PPG neurons with 2 nM IL-6 for three minutes. This led to a clear increase in intracellular [Ca^{2+}] in six individual neurons shown in Fig 3.5B left panel. A similar pattern was seen in all 25 cells imaged, suggesting IL-6 activates PPG neurons in the NTS (Fig 3.5B right panel). This was further substantiated by

data from John-Olov Jansson's group demonstrating that PPG neurons in the NTS express IL-6 receptor-α (Anesten et al. 2016).

To investigate whether this increase in intracellular [Ca^{2+}] is dependent on influx of Ca^{2+} from the extracellular space, I repeated the stimulation with IL-6 in normal ACSF containing 2 mM Ca^{2+} followed by stimulation in ACSF in which Ca^{2+} was replaced with Mg^{2+} (Fig 3.5C). In normal ACSF, intracellular [Ca^{2+}] increased in 19 imaged NTS PPG neurons as before with a median AUC of 0.83 $\Delta F/F_0$*mins. Removal of extracellular Ca^{2+} from the ACSF slowly decreased fluorescence in the PPG neurons. Notably, the Ca^{2+} response to 2 nM IL-6 was 96% smaller in the absence of extracellular Ca^{2+} with a median AUC of 0.026 $\Delta F/F_0$*mins (Fig 3.5C, $p<0.0001$). After replenishment of extracellular Ca^{2+} the response to IL-6 returned to a similar level as baseline with a median AUC of 0.66 $\Delta F/F_0$*mins ($p=0.71$). These data demonstrate that the cytokine IL-6 activates NTS PPG neurons *in vitro* and that the resulting rise in intracellular [Ca^{2+}] is dependent on influx from the extracellular space.

In 2011, Hisadome et al. demonstrated a link between CCK and PPG neuron activity using patch-clamp electrophysiology. Of 15 recorded PPG neurons, seven were indirectly activated by CCK-8 via a noradrenergic-glutamatergic circuit. Here, I confirmed that a subset of PPG neurons is activated by CCK-8 (Fig 3.6). By monitoring the activity of several cells simultaneously, I gain more information on how PPG neurons respond to CCK as a population rather than single cells. Three imaged PPG cells are displayed in pseudocolouring in Fig 3.6A. Two somata increased intracellular [Ca^{2+}] in response to 200 nM CCK-8, whereas one soma was unresponsive. Out of 14 imaged cells, five responded to CCK-8 with an increase in intracellular [Ca^{2+}] (Fig 3.6B). After washout of CCK-8, intracellular [Ca^{2+}] returned to baseline. Nine cells exhibited no increase in [Ca^{2+}] in response to CCK-8, demonstrating that only a subset of PPG neurons respond to CCK-8 *in vitro.* In future experiments, sodium channel blocker tetrodotoxin (TTX) should be included in the ACSF to confirm that CCK-8 indirectly activates PPG neurons (Hisadome et al. 2011).

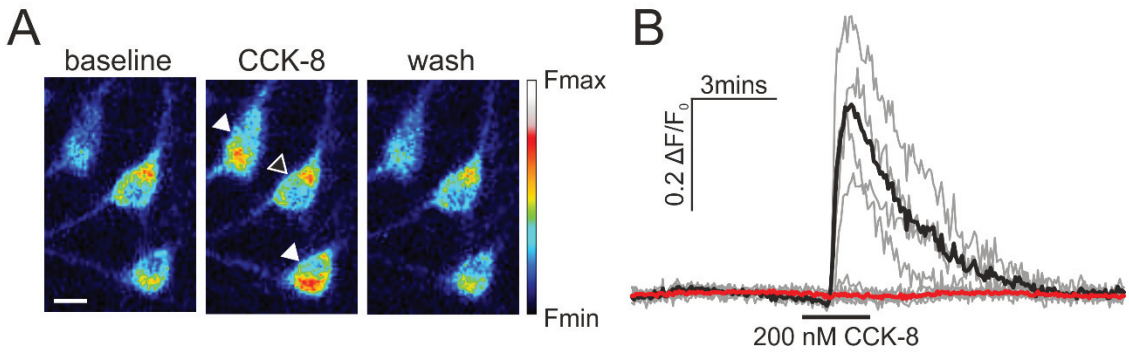

Fig 3.6 PPG neurons respond to 200 nM CCK-8 with an increase in intracellular [Ca^{2+}]. Live coronal brainstem slices from PPG-Cre/GCaMP3 mice were exposed to 200 nM CCK-8 for 3 mins. **A)** Three representative NTS PPG neurons, here pseudocoloured as shown on the right, before (baseline), during (CCK-8) and after (wash) stimulation with 200 nM CCK-8. The black arrowhead indicates one cell that did not increase [Ca^{2+}] in the presence of CCK-8. The white arrowheads indicate two responding somata. Scale bar: 10 µm. **B)** Fluorescence intensity expressed as $\Delta F/F_0$. Traces from individual cells are plotted in grey and the average response of responding cells (N=5) is shown in dark blue. The average trace of non-responding cells (N=7) is shown in black (N=12 somata in total).

3.2.3 PPG neurons are activated by hypoglycaemia

The data presented above demonstrate that leptin, IL-6, and CCK-8 activate NTS PPG neurons *in vitro,* resulting in increased intracellular [Ca^{2+}]. These compounds relay information on energy balance, visceral illness, and general homeostasis, signals which could be integrated by NTS PPG neurons. Next, I investigated the ability of a metabolic signal to regulate PPG neuron activity. The brainstem and in particular the dorsal vagal complex is a well-known site of glucosensing (Balfour et al. 2006; Thorens 2012; Lamy et al. 2014). Neurons and glia in this area have been shown to sense and respond to changing levels of extracellular glucose (Balfour and Trapp 2007; McDougal et al. 2013).

To investigate whether PPG neurons within the NTS are part of the glucosensing population in the dorsal vagal complex, I exposed *in vitro* brainstem slices from PPG-Cre/GCaMP3 mice to varying concentrations of extracellular glucose. Sections were maintained in 10 mM glucose as in previous experiments. Following baseline in 10 mM glucose, the perfusate was changed to ACSF containing only 1 mM glucose. Hypoglycaemia elicited an increase in intracellular [Ca^{2+}] (Fig 3.7), suggesting these cells are glucose-inhibited. Intracellular [Ca^{2+}] slowly increased after reduction of extracellular glucose and plateaued after 7 mins of hypoglycaemia. This same pattern was observed in 45 of 47 PPG cells imaged with a median peak change in fluorescence intensity (peak $\Delta F/F_0$) of 0.17 (Fig 3.7C). As with CCK-8, future experiments should investigate whether these responses are direct or indirect using TTX.

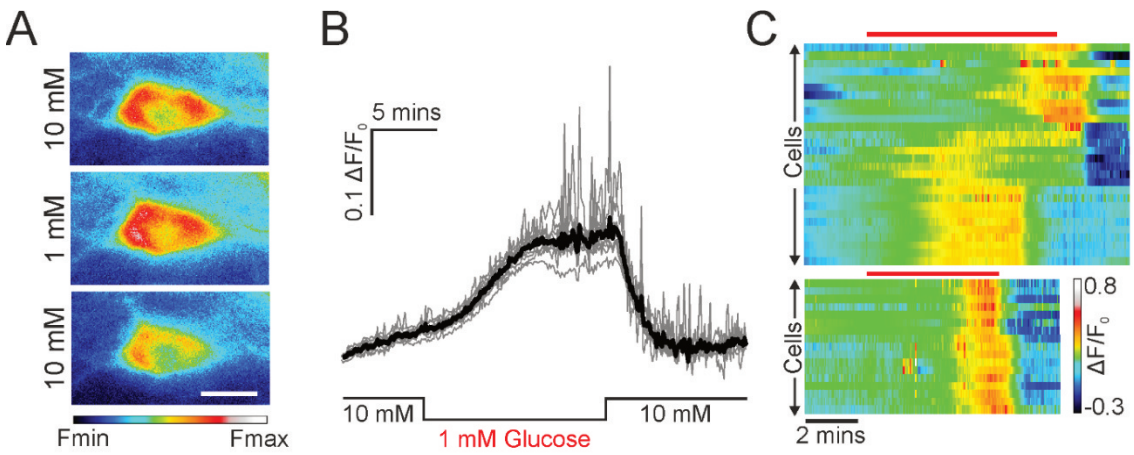

Fig 3.7 PPG neurons respond to hypoglycaemia with a rise in intracellular [Ca^{2+}]. Live coronal brainstem slices from PPG-Cre/GCaMP3 mice were exposed to 1 mM extracellular glucose for ten minutes. **A)** Representative NTS PPG neuron, here pseudocoloured as shown on the right, before (10 mM, top), during (1 mM) and after (10 mM, bottom) stimulation with low glucose (1 mM). Scale bar: 10 µm. **B)** Fluorescence intensity changes in response to low glucose expressed as $\Delta F/F_0$. Traces from individual cells are plotted in grey and the average response is shown in black. (N=10 somata). **C)** Heat map of 47 PPG cells responding to a decrease in glucose with a rise in intracellular calcium. At the top is shown a subset of experiments with slices exposed to 1 mM glucose for 15 mins. The bottom map displays a subset of experiments in which slices were exposed for only 10 mins. Red bars indicate the period of the recording in which glucose was changed from 10 mM to 1 mM

The data presented here suggest that PPG neurons not only detect the presence of homeostatic and satiety signals CCK-8, leptin and IL-6, but also monitor the levels of extracellular glucose. Surprisingly, considering the putative role of central GLP-1 in satiety, low glucose levels increased the activity of PPG neurons. I will elaborate on this point in section 3.3.2 of the Discussion. These results provide important information on the modulation of PPG neurons activity by metabolic and homeostatic cues and present interesting avenues for future research into the link between these systems and central GLP-1.

3.2.4 PPG neurons are activated by carbachol and ATP

In the previous section, I addressed the regulation of PPG neuron activity by homeostatic and satiety signals. In this section, I turn to the modulation of PPG neurons by small-molecule transmitters released from glia and neurons.

ATP is released from astrocytes in response to homeostatic stimuli such as low glucose, acidification of the microenvironment, hypoxia, and vagal stimulation (Gourine et al. 2010; McDougal et al. 2011, 2013; Accorsi-Mendonça et al. 2013; Marina et al. 2016). To investigate a potential link between gliotransmission and PPG neuron activity, I stimulated PPG neurons with 1 mM ATP (Fig 3.8).

GCaMP3 fluorescence intensity increased in all imaged neurons (N=19) in response to 1 mM ATP (Fig 3.8). Additionally, dendritic processes near PPG neurons were activated in response to 1 mM ATP (Fig 3.8A). Interestingly, the ATP-induced increase in PPG activity was abolished in the presence of TTX (0.5 µM) and glutamate receptor inhibitors DNQX (20 µM) and APV (25 µM) (Fig 3.8C). This suggests the increase in intracellular [Ca^{2+}] in response to ATP is either secondary to an increase in action potential firing and therefore suppressed by TTX, or dependent on input from other cells. These data demonstrate that 1 mM ATP is able to activate PPG neurons and provide an intriguing potential link between gliotransmission and central GLP-1, as suggested recently by Reiner et al. (2016).

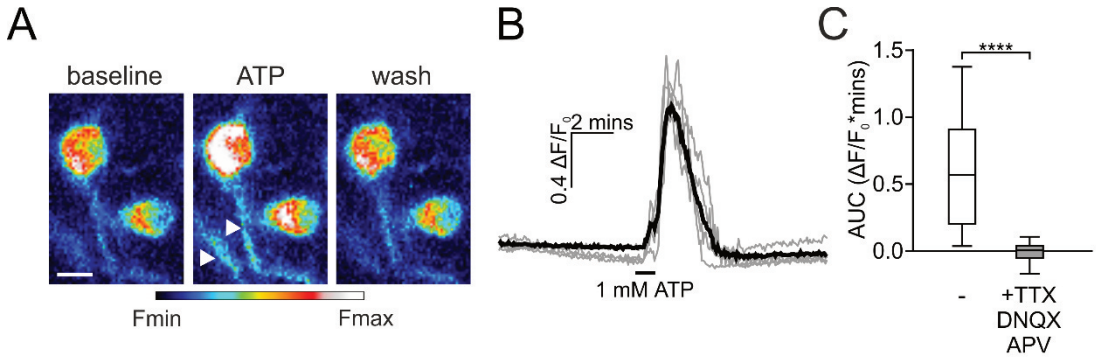

Fig 3.8 PPG neurons are activated by 1 mM ATP. Live coronal brainstem slices from PPG-Cre/GCaMP3 mice were exposed to 1 mM ATP for one minute. **A)** Two representative NTS PPG neurons, here pseudocoloured as shown below, before (Baseline), during (ATP) and after (Wash) stimulation with 1 mM ATP. White arrowheads indicate adjacent dendritic fibres responding to ATP. Scale bar: 10 µm. **B)** Fluorescence intensity changes in response to 1 mM ATP expressed as $\Delta F/F_0$. Traces from individual cells are plotted in grey and the average response is shown in black. (N=4 somata). **C)** Median AUC of PPG neuron responses after stimulation with ATP in the absence (-) and presence (+TTX, DNQX, APV) of synaptic inhibitors TTX (0.5 µM), DNQX (20 µM) and APV (25 µM). Responses were compared using Wilcoxon's signed rank test for paired data. ****$p<0.0001$. N=15 somata, 2 slices.

Next, I investigated the effect of cholinergic stimulation on PPG neuron activity. Acetylcholine excites neurons in the NTS via both muscarinic and nicotinic receptors (Shihara et al. 1999) and choline acyltransferase is expressed in dendrites in the NTS (Armstrong et al. 1988). Recently, a link has been suggested between central GLP-1 and nicotine, an AChR agonist (Tuesta et al. 2017). In addition, smoking is known to suppress appetite and activate reward pathways, an effect which may depend on central GLP-1. I stimulated PPG neurons with 100 µM carbachol for 3 mins. Carbachol is an AChR agonist, which activates both muscarinic and nicotinic receptors. Following a short baseline, sections were superfused with 100 µM carbachol, which led to a clear increase in intracellular [Ca^{2+}] in a subset of NTS PPG neurons (Fig 3.9A,B). Out of 19 PPG neurons imaged, 13 increased intracellular [Ca^{2+}] in response to cholinergic stimulation with a median

AUC of 0.76 $\Delta F/F_0$*mins (Fig 3.9C). Six PPG cells did not respond to 100 µM carbachol (Fig 3.9C). These data demonstrate that PPG neurons are activated by cholinergic stimulation. Future experiments should investigate whether this link is direct with muscarinic or nicotinic receptors expressed on the surface of PPG neurons, or whether it requires the activity of afferent inputs.

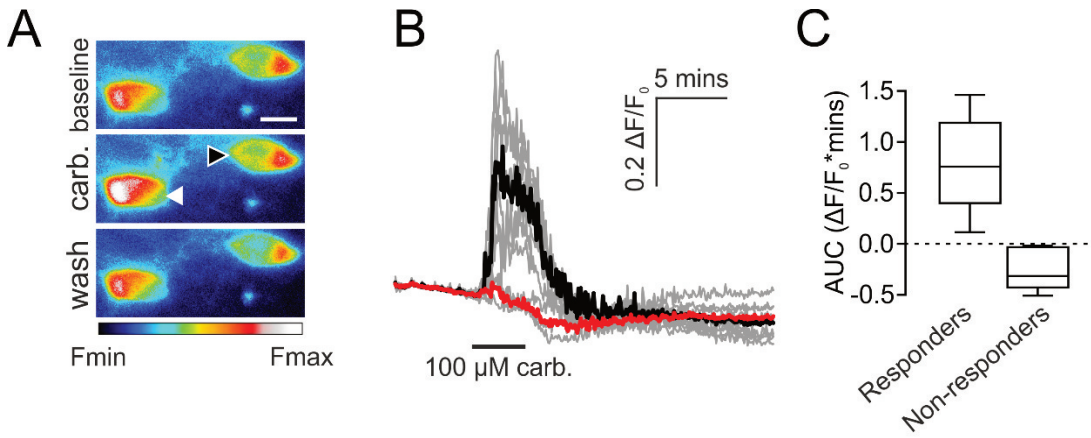

Fig 3.9 PPG neurons are activated by cholinergic stimulation. Live coronal brainstem slices from PPG-Cre/GCaMP3 mice were exposed to 100 µM AChR agonist, carbachol, for three minutes. **A)** Two representative NTS PPG neurons, here pseudocoloured as shown below, before (baseline), during (carb.) and after (wash) stimulation with 100 µM carbachol. A responding cell is indicated with a white arrow head, a non-responding cell is indicated with a black arrow head. Scale bar: 10 µm. **B)** Fluorescence intensity changes in response to 100 µM carbachol expressed as $\Delta F/F_0$. Traces from individual cells are plotted in grey and the average response of responding cells is shown in black, whereas the average trace of non-responding cells is shown in red. (N=10 somata). **C)** Median AUC of PPG neuron responses after stimulation with 100 µM carbachol split into responding and non-responding cells. N=19 somata, 2 slices.

3.2.5 Serotonergic modulation of the activity of NTS PPG neurons

In the previous section, I presented data on the regulation of PPG neuron activity by the gliotransmitter, ATP, and the AChR agonist, carbachol. These small molecules are important transmitters in the NTS and both glio- and cholinergic transmission have been implicated in hypophagia (Jo et al. 2002; Reiner et al. 2016). I will now present data on serotonergic modulation of PPG neurons *in vitro*. These data were published in (Holt et al. 2017).

5-HT (5-hydroxytryptamine, serotonin) is a key neurotransmitter in the regulation of both food intake and stress (Heisler et al. 1998, 2003, 2007; Marcinkiewcz et al. 2016). 5-HT serves diverse roles centrally and 5-HT receptor-expressing neurons are distributed throughout the brain. A range of 5-HT receptors have been implicated in the regulation of food intake including 5-HT_{1A} (Dill et al. 2013), 5-HT_3 (Hayes and Covasa 2006; Li et al. 2015), and 5-HT_{2C} receptors (Tecott et al. 1995; Vickers et al. 1999, 2001). Interestingly, mice lacking 5-HT_{2C} receptors failed to supress

food intake in response to i.p. GLP-1, suggesting there is a link between GLP-1 and serotonergic regulation of food intake (Asarian 2009; Nonogaki et al. 2011).

In collaboration with Professor Ida Llewellyn-Smith, our group discovered dense serotonergic innervation of PPG neurons in the NTS (Holt et al. 2017). Out of 358 PPG neurons, 208 received close appositions from 5-HT-immunoreactive axons, with the percentage of PPG neurons contacted in each mouse varying between 50 % and 80 % (Holt et al. 2017).

Based on this, I investigated if 5-HT would modulate the activity of NTS PPG neurons in brainstem slices *in vitro*. NTS PPG neurons were exposed to 20 µM 5-HT for one min (Fig 3.10). Only one PPG soma increased intracellular [Ca^{2+}] in response to 5-HT, although all cell bodies (N=8) were activated by 100 µM glutamate (Fig 3.10B). In total, only four out of 39 imaged PPG somata responded to 20 µM 5-HT with an increase in intracellular [Ca^{2+}]. However, dendrites adjacent to PPG somata were activated by 5-HT and had transient spikes in intracellular [Ca^{2+}] (Fig 3.10C). Although cells were only exposed to 5-HT for one minute dendritic spikes persisted for 3.5±0.2 mins. This contrasted with glutamate-induced, dendritic [Ca^{2+}] spikes, which quickly disappeared following washout of glutamate (Fig 3.10C).

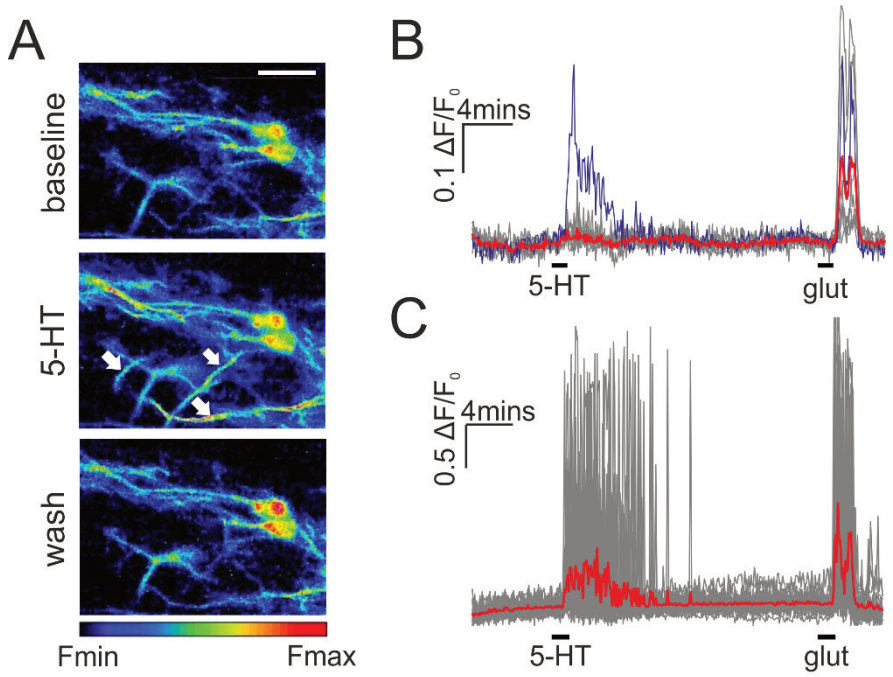

Fig 3.10 5-HT evokes intracellular [Ca^{2+}] changes mainly in distal PPG dendrites. Live coronal brainstem slices from PPG-Cre/GCaMP3 mice were exposed to 20 µM 5-HT for one min followed by stimulation with 100 µM glutamate for one min. **A)** Two representative NTS PPG neurons, pseudocoloured as indicated below the images, before (Baseline), during (5-HT) and after (Wash) stimulation with 20 µM 5-HT. White arrows indicate dendrites with transient rises in intracellular [Ca^{2+}]. Scale bar: 25 µm. **B)** Somatic fluorescence intensity changes in response to 20 µM 5-HT expressed as $\Delta F/F_0$. Traces from individual cells are plotted in grey and the average response of responding cells is shown in blue, whereas the average trace of non-responding cells is shown in red. (N=8 somata). **C)** Dendritic fluorescence intensity changes in response to 20 µM 5-HT expressed as $\Delta F/F_0$. Traces from individual dendrites are plotted in grey and the average response is shown in red (N=19 dendrites).

Dendritic [Ca^{2+}] spikes induced by 5-HT were found to be concentration-dependent with only limited activity following stimulation with 2 µM 5-HT compared to 20 µM or 200 µM (Fig 3.11). One way non-parametric ANOVA yielded a Friedman statistic of 92.57 ($p<0.0001$) and Dunn's multiple comparison's test revealed that both 20 µM and 200 µM 5-HT elicited statistically significant larger responses than 2 µM ($p<0.0001$ for both), but no difference between the response to 20 µM and 200 µM 5-HT, suggesting the response is at its maximum at 20 µM. No further PPG somata were recruited at higher concentrations of 5-HT, suggesting the reason for the limited somatic response is not insufficient stimulation of 5-HT receptors (not shown).

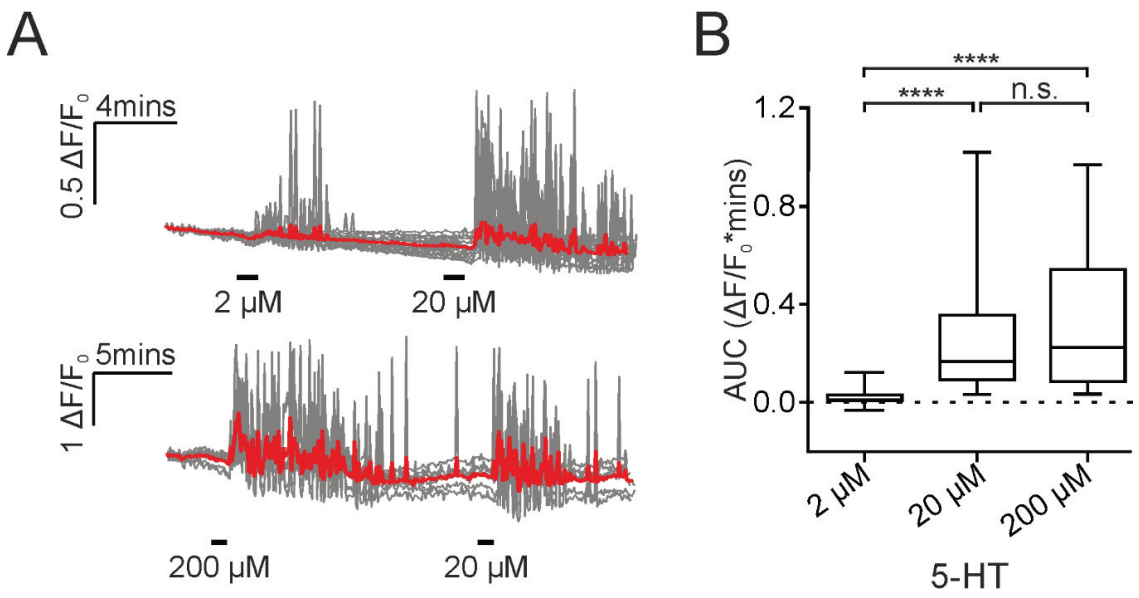

Fig 3.11 5-HT-evoked dendritic [Ca^{2+}] spikes are concentration-dependent. *In vitro* coronal brainstem slices from PPG-Cre/GCaMP3 mice were exposed to 2, 20, and 200 µM 5-HT for one min. **A)** Two independent recordings showing NTS PPG neurons responding to 2, 20, and 200 µM 5-HT. Traces from individual dendrites are plotted in grey and the mean response is shown in red. N=17 (top panel), N=7 (bottom panel). **B)** Median AUCs of dendritic Ca^{2+} spikes in response to 2, 20, and 200 µM 5-HT. (N=88 dendrites in each condition). *p<0.0001, n.s.: not significant (p>0.99) according to Dunn's adjusted multiple comparison's test.

To investigate the source of Ca^{2+} for these 5-HT-induced dendritic spikes, I repeated the stimulation with 20 µM 5-HT in the presence and absence of 2 mM extracellular Ca^{2+} (Fig 3.12). Removal of Ca^{2+} reduced dendritic [Ca^{2+}] spikes in response to 20 µM 5-HT by 69±12% (p<0.0001). While this suggests the source of Ca^{2+} for 5-HT-induced dendritic spikes is the extracellular space, I cannot exclude that prolonged exposure to Ca^{2+}-free extracellular solution provokes release from and depletion of intracellular Ca^{2+} stores (Williams et al. 1977; Weber et al. 2001).

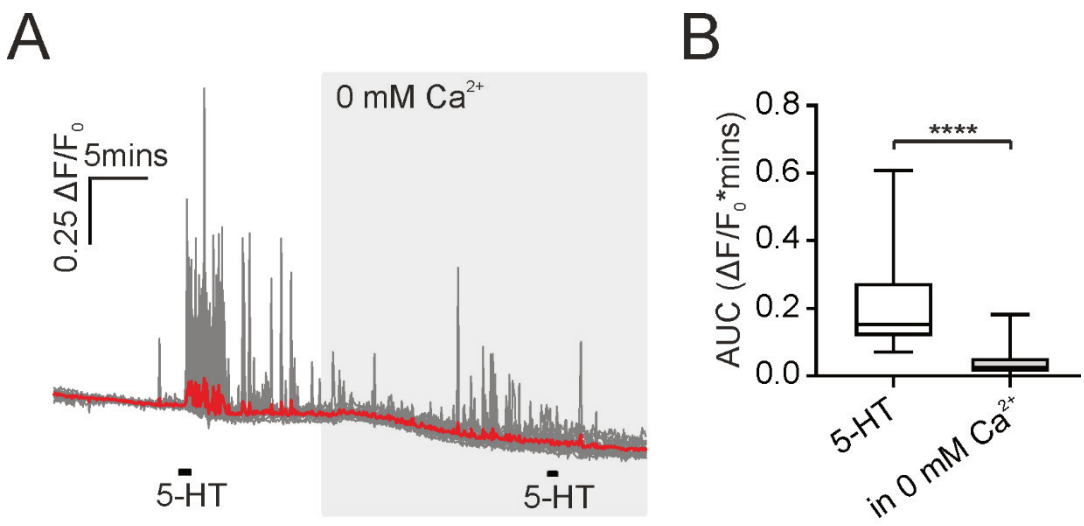

Fig 3.12 5-HT-evoked dendritic [Ca^{2+}] spikes are dependent on extracellular [Ca^{2+}]. Live coronal brainstem slices from PPG-Cre/GCaMP3 mice were exposed to 20 µM 5-HT in the presence of 2 mM or 0 mM extracellular Ca^{2+}. **A)** Dendritic fluorescence intensity changes in response to 20 µM 5-HT expressed as $\Delta F/F_0$. Sections were first exposed to 20 µM 5-HT in the presence of 2 mM extracellular Ca^{2+} after which extracellular Ca^{2+} was removed and the sections restimulated with 20 µM 5-HT. The period with 0 mM Ca^{2+} is indicated by a grey bar. **B)** Median AUC of dendrites responding to 20 µM 5-HT in the presence (5-HT) and absence (in 0 mM Ca^{2+}) of extracellular Ca^{2+}. ****p<0.0001 according to Wilcoxon matched pair signed rank test.

I next asked whether the dendritic [Ca^{2+}] spikes are dependent on the activity of neighbouring cells and voltage-gated sodium channels. To this end, I stimulated PPG neurons with 20 µM 5-HT in the absence and presence of synaptic inhibitors TTX (0.5 µM) and DNQX (20 µM). DNQX was chosen based on previous observations by our laboratory showing that more than 90% of spontaneous excitatory post-synaptic potentials were supressed in the presence of DNQX (Hisadome et al. 2010, 2011).

5-HT-evoked dendritic [Ca^{2+}] spikes were unchanged in the presence of TTX and DNQX (Fig 3.13), suggesting PPG neurons express functional 5-HT receptors and that the dendritic spikes are independent of action potential firing.

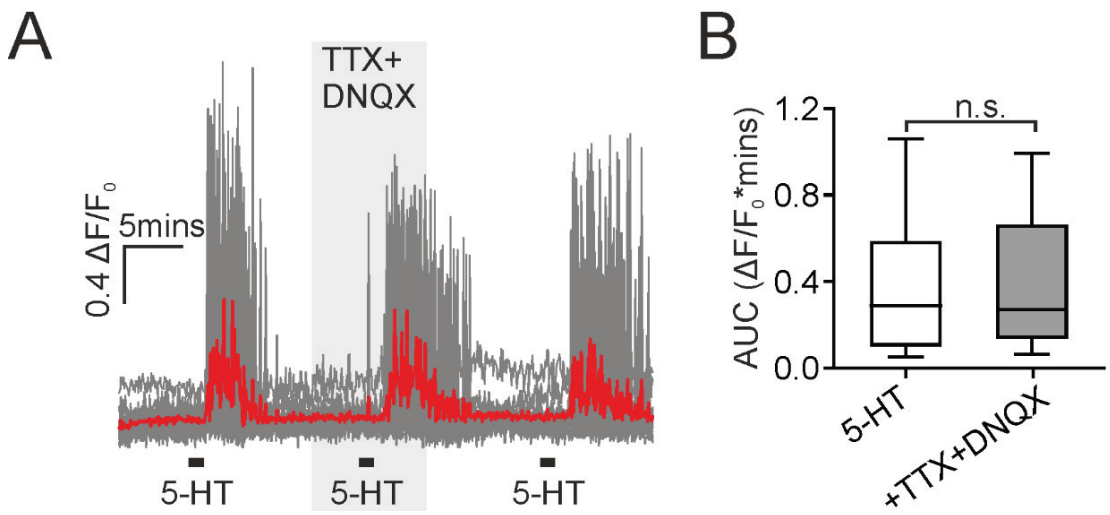

Fig 3.13 5-HT-evoked dendritic [Ca^{2+}] spikes are independent of action potentials and glutamatergic input. *In vitro* coronal brainstem slices from PPG-Cre/GCaMP3 mice were exposed to 20 µM 5-HT in the absence and presence of 0.5 µM TTX and 20 µM DNQX. **A)** Dendritic fluorescence intensity changes in response to one minute 20 µM 5-HT in the presence and absence of TTX and DNQX. Traces from individual dendrites are plotted in grey and the average response is shown in red. TTX and DNQX application in indicated with a grey bar. N=12 dendrites. **B)** Median AUCs of dendritic Ca^{2+} spikes in response to 20 µM 5-HT in the absence (5-HT) and presence (+TTX+DNQX) of synaptic inhibitors. (N=55 dendrites in each condition). n.s.: not significant according to Wilcoxon matched-pairs signed rank test (p=0.56).

The data presented until now have demonstrated that PPG neurons respond directly to 5-HT with dendritic spikes in intracellular [Ca^{2+}]. These spikes were dependent on extracellular Ca^{2+} but did not require action potential firing or glutamatergic input, suggesting NTS PPG neurons express functional 5-HT receptors. I wanted to further dissect the mechanism underlying these [Ca^{2+}] spikes and set out to determine which 5-HT receptors were involved in the response. To this end, I used selective agonists and antagonists for several 5-HT receptor subtypes.

Most 5-HT receptor subtypes can be detected in the NTS (Sévoz-Couche et al. 2000; Jordan 2005). In particular both 5-HT_2 and 5-HT_3 receptors are involved in the regulation of food intake (Vickers et al. 2001; Hayes and Covasa 2005, 2006; Schuhler et al. 2005; Li et al. 2015). I therefore assessed the contribution of each receptor subtype to the dendritic Ca^{2+} response to 5-HT.

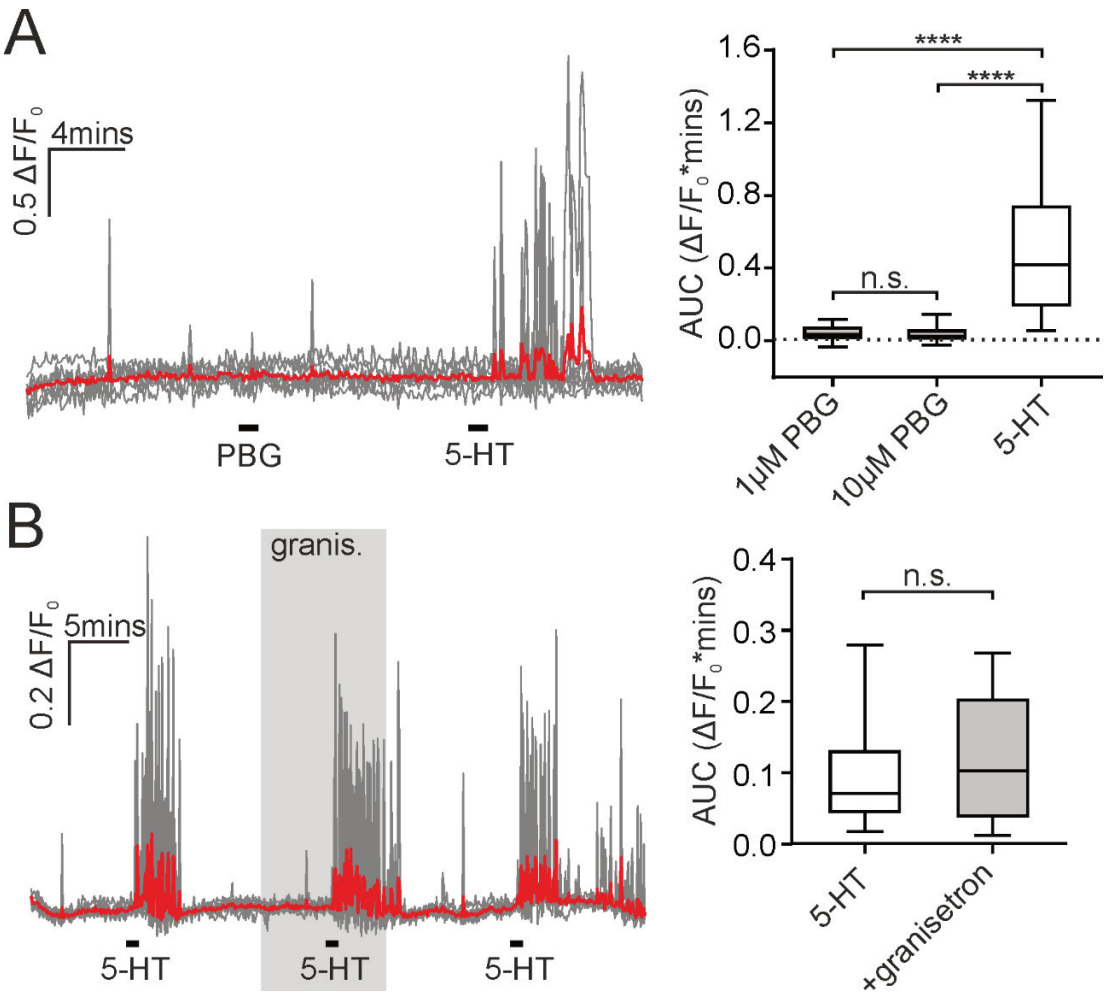

Fig 3.14 5-HT_3 receptors are not involved in the dendritic Ca^{2+} response to 5-HT. A) Stimulation with 5-HT_3 receptor agonist PBG does not elicit Ca^{2+} spikes in PPG dendrites**.** *Left panel:* Dendritic fluorescence intensity changes in response to one min 10 µM 5-HT_3 receptor agonist or 20 µM 5-HT. Traces from individual dendrites are plotted in grey and the mean response is shown in red. N=7 dendrites. *Right panel:* Median AUCs of dendritic Ca^{2+} spikes in response to 1 µM PBG (N=32 dendrites), 10 µM PBG (N=25 dendrites), and 20 µM 5-HT (N=37 dendrites) (3 mice). Kruskal-Wallis rendered a Chi-Square value of 45.9 ($p<0.0001$). Post-hoc comparisons revealed no statistically significant difference between 1µM and 10µM PBG ($p>0.999$) but showed that the responses to 20µM 5-HT were significantly different to both 1µM and 10µM PBG ($p<0.0001$). **B)** 5-HT evoked dendritic Ca^{2+} spikes are unaltered by 5-HT_3 receptor inhibition. *Left panel:* Dendritic fluorescence intensity changes in response to one min 20 µM 5-HT in the absence and presence of 5-HT_3 receptor antagonist granisetron (5 µM). Traces from individual dendrites are plotted in grey and the mean response is shown in red. Application of 5 µM granisetron is indicated with a grey bar. N=9 dendrites. *Right panel:* Median AUCs of dendritic Ca^{2+} spikes in response to 20 µM 5-HT before (white box) and during (grey box) granisetron. (N=32 dendrites, 3 mice), n.s.: not significant according to Wilcoxon matched-pairs signed rank test ($p=0.32$).

Phenylbiguanide (PBG) is a selective 5-HT_3 receptor agonist (Ireland and Tyers 1987; Chen et al. 1991). I used it here at two concentrations (1 and 10 µM) to stimulate PPG neurons *in vitro*. Two concentrations of PBG failed to elicit [Ca^{2+}] spikes, whereas dendritic [Ca^{2+}] rises were clearly seen following 20 µM 5-HT (Fig 3.14A). Kruskal-Wallis one-way ANOVA yielded a significant test statistic of 45.9 ($p<0.0001$) and Dunn's multiple comparisons test revealed a significantly larger Ca^{2+} response in 5-HT-stimulated dendrites compared to both 1 and 10 µM PBG (Fig 3.14A right panel, $p<0.0001$ for both). These findings were further supported by experiments using the 5-HT_3 receptor antagonist granisetron (5 µM). Granisetron failed to inhibit the dendritic response to 20 µM 5-HT with no difference in the response to 20 µM 5-HT before and during granisetron (Fig 3.14B, $p=0.32$). These data suggest that 5-HT_3 receptors are not involved in serotonergic modulation of NTS PPG neurons.

Next, I investigated the potential involvement of 5-HT_2 receptors in the response to 5-HT. I stimulated NTS PPG neurons with 20 µM 5-HT in the absence and presence of a 5-HT_2 receptor antagonist, ketanserin (1 µM). Inhibition of 5-HT_2 receptors attenuated the dendritic [Ca^{2+}] response to 20 µM 5-HT by 77±6 % (Fig 3.15A, $p<0.0001$). Because of the proposed link between central GLP-1 and 5-HT_{2C} receptors and because of 5-HT_{2C} receptors' known role in the regulation of food intake, I next tested whether PPG dendrites can be activated by the selective 5-HT_{2C} receptor agonist WAY161,503. In support of a role for 5-HT_{2C} receptors in the generation of PPG dendritic [Ca^{2+}] spikes, 5 µM WAY161,503 elicited transient [Ca^{2+}] rises in a total of five individual sections from five mice (Fig 3.15B).

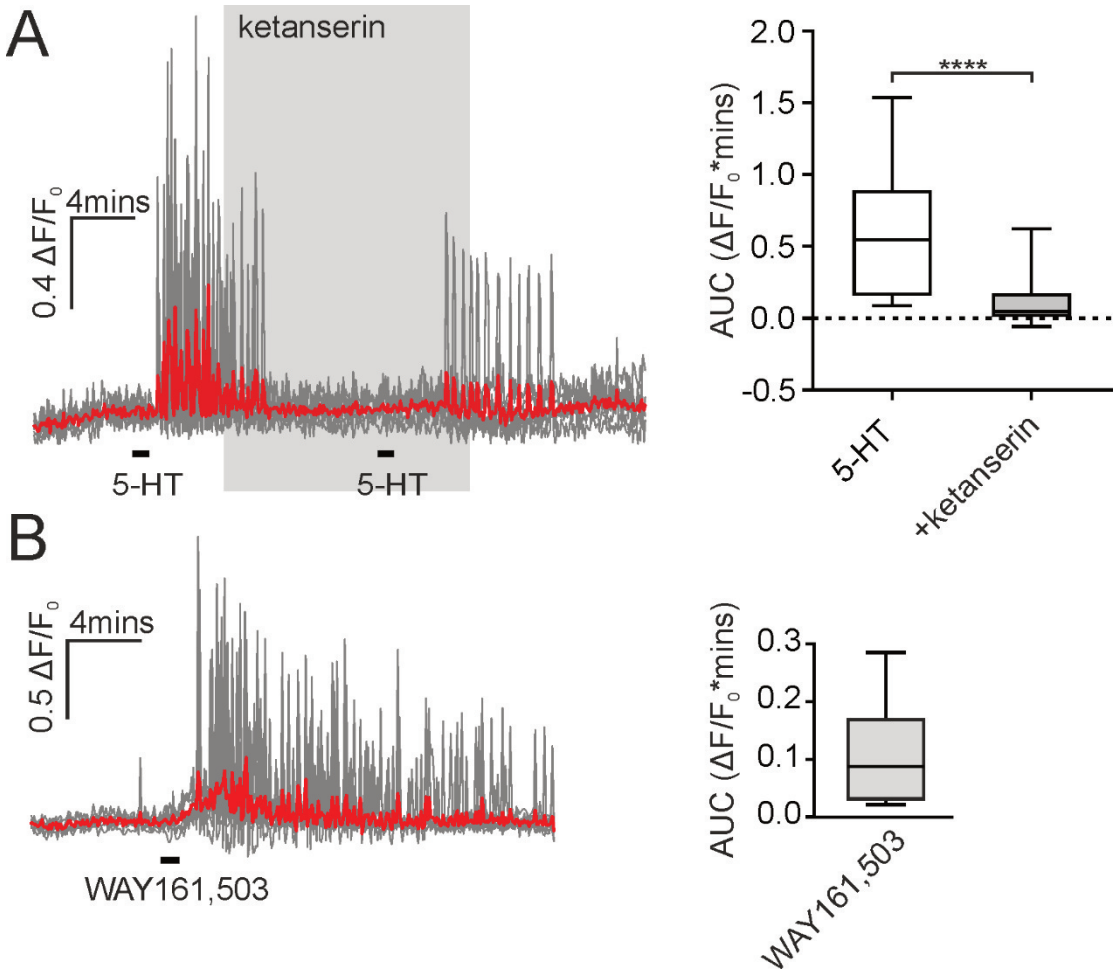

Fig 3.15 NTS PPG neurons are activated by 5-HT via 5-HT_2 receptors and 5-HT_{2C} receptor activation elicits dendritic Ca^{2+} spikes. A) 5-HT_2 receptor inhibition attenuates the dendritic response to 5-HT. *Left panel:* Dendritic fluorescence intensity changes in response to one min 20 µM 5-HT in the presence and absence of 5-HT_2 receptor antagonist ketanserin (1 µM) expressed as relative change in fluorescence from baseline, $\Delta F/F_0$. Traces from individual dendrites are plotted in grey and the mean response is shown in red. Ketanserin application is indicated with a grey bar. N=6 dendrites. *Right panel:* Median AUCs of dendritic Ca^{2+} spikes in response to 20 µM 5HT before (white box) and during (grey box) 1 µM ketanserin (N=17 dendrites, 3 mice). ****p<0.0001, Wilcoxon matched-pairs signed rank test. **B)** 5-HT_{2C} receptor activation elicits Ca^{2+} spikes in PPG dendrites. *Left panel:* Traces showing individual dendritic fibres responding to the 5-HT2C receptor agonist WAY161,503 (5 µM) with an increase in intracellular Ca^{2+} (N=9 dendrites). Traces from individual dendrites are plotted in grey and the average response is shown in red. *Right panel:* Median AUC of dendrites responding to WAY161,503 (N=32 dendrites, 5 mice).

Having discovered a potential role for 5-HT_{2C} receptors in the activation of PPG dendrites, I was curious how this was related to electrical activity at the level of the soma. I monitored the spontaneous firing patterns of NTS PPG neurons using loose-patch recordings in the cell-attached configuration.

Spontaneous firing was recorded in 16 cells, which were stimulated with 20 µM 5-HT for 3 mins (Fig 3.16). Spontaneous firing rates were similar to those seen for PPG neurons previously

(Hisadome et al. 2010, 2011). Student's t-test revealed 12 of 16 cells recorded were electrically responsive to 20 µM 5-HT. Five cells were found to increase their firing rate by 1.3±0.2 Hz (Fig 3.16A), seven reduced their firing rate by -1.0±0.2 Hz (Fig 3.16B) and four cells showed no response to 20 µM 5-HT (Fig 3.16C). Friedman one-way ANOVA yielded a significant test statistic in the activated cells (Friedman statistic: 8.4, p=0.0085) and in the inhibited cells (Friedman statistic: 10.57, p=0.0027), but not in the non-responding cells (Friedman statistic: 0.133, p>0.99). There was a significant increase in firing rate in the activated cells (p=0.013) and a significant decrease in the inhibited cells (p=0.023), but no effect of 5-HT in the non-responding cells (p>0.99), demonstrating that 20 µM 5-HT can have different effects on firing rate in different neurons.

Having found that a subset of PPG neurons was inhibited by 20 µM 5-HT, I next addressed the question, which 5-HT receptor is involved in this response. 5-HT_5 and 5-HT_1 are inhibitory receptors and couple to the $G_{i/o}$ pathway (McCorvy and Roth 2015). The 5-HT_{1A} receptor was of particular interest because of its known involvement in appetite regulation (Dill et al. 2013). I therefore tested whether the selective 5-HT_{1A} receptor antagonist, WAY-100,635 (Forster et al. 1995), was able to abolish the reduction in firing rate seen in a subset of PPG neurons.

Fig 3.17A shows a representative simultaneous recording of intracellular $[Ca^{2+}]$ (top, red) and spontaneous firing rate (bottom, black). 5-HT (20 µM) completely abolished action potential firing. This decrease in electrical activity was accompanied by a decrease in intracellular $[Ca^{2+}]$ confirming the correlation between changes in firing rate and intracellular $[Ca^{2+}]$ (Fig 3.17A top left and Fig 3.3). Inhibition of 5-HT_{1A} receptors prevented the 5-HT-induced reduction in both intracellular $[Ca^{2+}]$ and spontaneous firing frequency. Interestingly, 5-HT_{1A} suppression increased both intracellular $[Ca^{2+}]$ and firing rate independent of 5-HT application, suggesting these cells receive ongoing serotonergic inhibitory input mediated by 5-HT_{1A} receptors (Fig 3.17A).

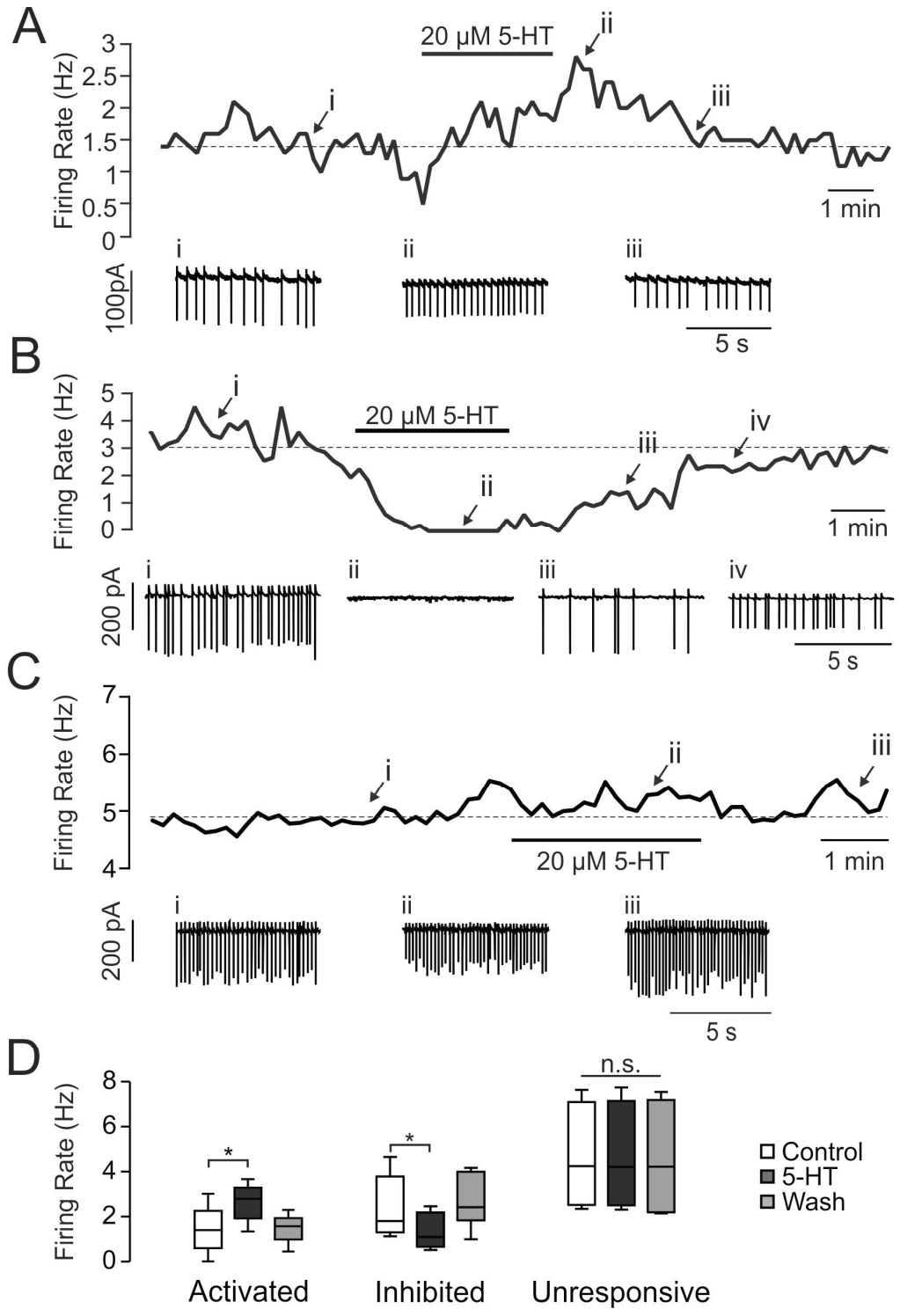

Fig 3.16 NTS PPG neuron electrical activity is modulated by 5-HT. Representative traces of spontaneous firing rates of PPG neurons either activated **(A)**, inhibited **(B)** or unaffected **(C)** by three minutes stimulation with 20 µM 5-HT. Below each representative trace are shown periods of the original voltage-clamp recordings from timepoints i, ii, iii and iv. **D)** Median firing rate of activated (N=5), inhibited (N=7) and unresponsive cells (N=4) before (white box), during (dark grey box) and after washout of (light grey box) 20 µM 5-HT. *p<0.05 according to Dunn's multiple comparisons test.

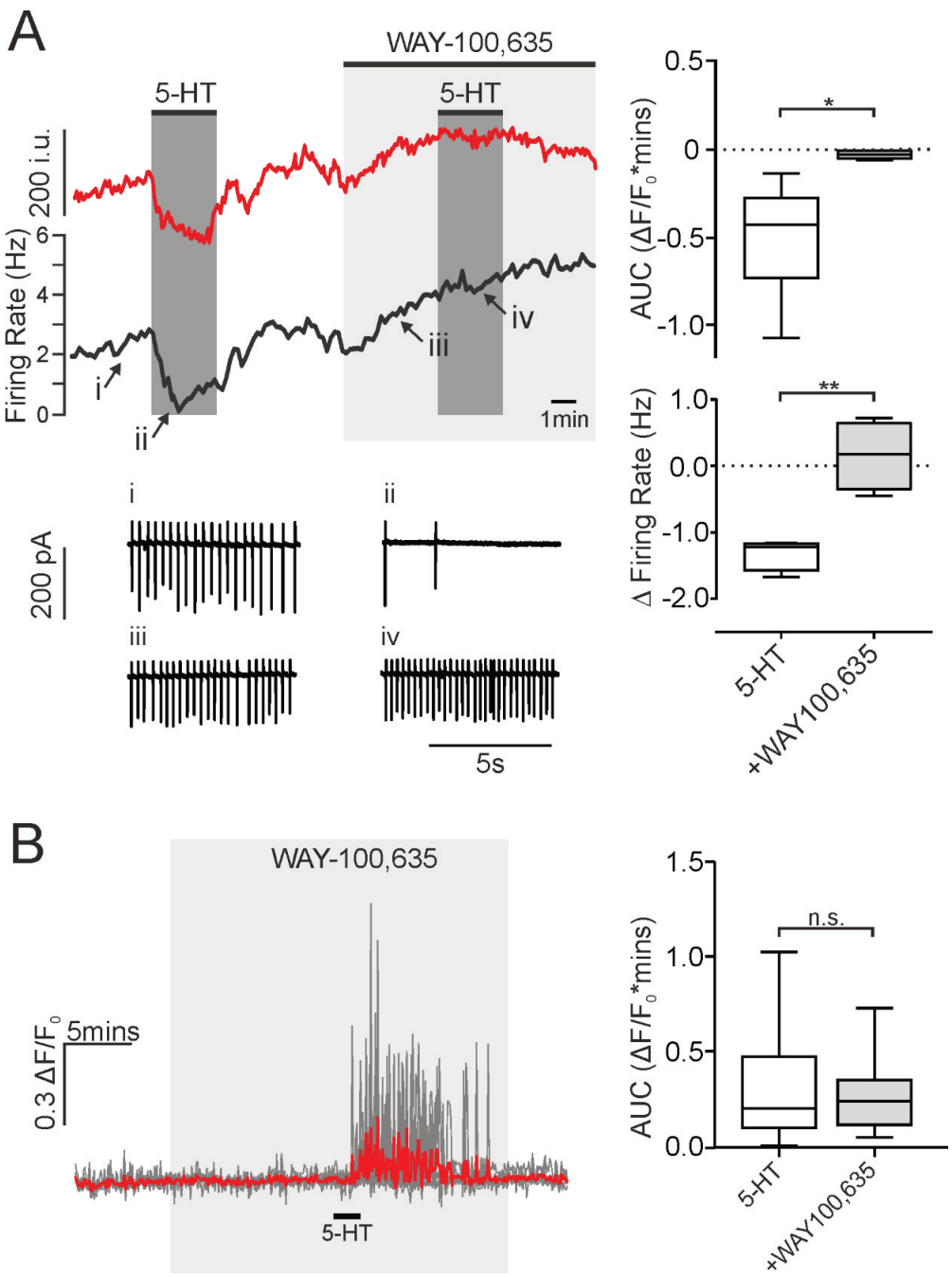

Fig 3.17 Inhibition of PPG neuron electrical activity by 5-HT is dependent on 5-HT_{1A} receptors. A) *Left panels:* Representative traces of spontaneous firing rate (middle left) and GCaMP3 fluorescence intensity (top left, i.u.: intensity units) of the same PPG neuron recorded in loose-patch configuration. Applications of 20 µM 5-HT are marked with black bars and dark grey boxes and application of 5-HT_{1A} receptor antagonist WAY-100,635 is marked by a light grey box. Original cell-attached recordings from timepoints i, ii, iii and iv are shown in the bottom left panel. *Right panels:* Median AUC (top, N=7) and firing rate (bottom, N=4) of PPG somata stimulated with 5-HT in the absence (white boxes) and presence (grey boxes) of WAY-100,635. **p<0.01 (paired Student's t-test); *p<0.05 (Wilcoxon's signed rank test) (N=4 cells, 4 mice). **B)** *Left panel:* The dendritic Ca^{2+} response to 5-HT in the presence of 20 µM WAY-100,635 (n=6 dendrites). WAY-100,635 application is indicated with a light grey box. *Right panel*: Median AUC of dendritic responses to 5-HT alone from previous experiments (n=248 dendrites) and to 5-HT in the presence of WAY-100,635 (n=20 dendrites (3 mice)). n.s.: not significant (p=0.91) according to Mann-Whitney test.

Cell-attached recordings from four independent PPG somata displayed a similar pattern to the cell shown in Fig 3.17 with firing rate decreasing by -1.3±0.1 Hz in response to 5-HT (Fig 3.17A bottom right). The 5-HT-induced decrease in action potential firing was completely abolished by 5 µM WAY-100,635 ($p=0.0047$, Student's paired t-test). Similarly, somatic Ca^{2+} recordings of seven cells showed a clear attenuation of the inhibitory response to 5-HT in the absence of 5-HT_{1A} signalling (Fig 3.17A top right). The 5-HT response was reduced by 91±6 % in the presence of WAY-100,635.

Interestingly, inhibition of 5-HT_{1A} receptors did not result in 5-HT-induced somatic excitation of PPG neurons. Furthermore, the dendritic [Ca^{2+}] response to 5-HT was not altered in the presence of WAY-100,635 (Fig 3.17B, $p=0.91$). These data suggest activation of 5-HT_{1A} receptors does not explain the lack of propagation of the dendritic [Ca^{2+}] spikes to somata in response to 5-HT.

In summary, I have demonstrated a link between serotonergic signalling and PPG activity. This link is multifaceted and consists of both inhibitory and excitatory effects. 5-HT-induced dendritic spikes were dependent on 5-HT_2 receptors and activation of 5-HT_{2C} receptors led to clear transient [Ca^{2+}] rises in PPG dendrites. However, I also demonstrated that a subset of PPG neurons was inhibited at the somatic level and that the reduction in firing rate was dependent on 5-HT_{1A} receptor signalling.

3.3 Discussion

In this chapter, I investigated the cellular regulation of PPG neuron activity by metabolic signals, hormones, and neurotransmitters. Figure 3.18 summarises the results presented here along with known inputs from the literature. Using *in vitro* Ca^{2+} imaging, I demonstrated that satiety hormones CCK and leptin increase intracellular [Ca^{2+}] in PPG neurons (Figs 3.5 and 3.6). Similarly, the cytokine IL-6 led to a rise in cytosolic [Ca^{2+}] and NTS PPG neurons were inhibited by high extracellular glucose levels (Figs 3.5 and 3.7). PPG neurons were activated by ATP in an indirect manner and carbachol, an AChR agonist, increased intracellular [Ca^{2+}] in a subset of PPG neurons (Figs 3.8 and 3.9). 5-HT modulated the activity of PPG neurons in a heterogenous way: Some cells increased firing in response to 5-HT, while others had decreased firing (Fig 3.16). Furthermore, distal dendrites showed 5-HT_{2C} receptor-mediated dendritic [Ca^{2+}] spikes that failed to propagate to the soma (Fig 3.10).

3.3.1 The activity of NTS PPG neurons is modulated by signals of satiety

In vitro Ca^{2+} imaging revealed that the satiety hormone leptin activated PPG neurons as observed previously using patch-clamp electrophysiology (Fig 3.5) (Hisadome et al. 2010). Leptin has long been known to reduce food intake in both humans and rodents (Zhang et al. 1994; Pelleymounter et al. 1995; Schwartz et al. 1996; Larsson et al. 1998; Klok et al. 2007; Patel and Ebenezer 2008). It is released from adipose tissue into the bloodstream and acts on brain lepRs to supress feeding (Campfield et al. 1995). The hypothalamus has been thought to be its main site of action (Cowley et al. 2001; Pinto et al. 2004; Takahashi and Cone 2005). However, the caudal brainstem is another key site for the food intake-suppressive effects of leptin (Grill et al. 2002; Hosoi et al. 2002; Huo et al. 2007).

Although several studies have found a link between central GLP-1 and leptin (Goldstone et al. 1997, 2000; Williams et al. 2006), the expression of lepRs by NTS PPG neurons is controversial with evidence suggesting lepRs are expressed by PPG neurons in mice (Goldstone et al. 1997; Hisadome et al. 2010; Garfield et al. 2012), but not in rats (Huo et al. 2008). I presented evidence for a link between central GLP-1 and leptin in mice. However, I did not confirm that the effect of leptin on PPG neuron activity is via direct activation of lepRs expressed on PPG neurons. Importantly, this has been demonstrated previously using patch-clamp electrophysiology (Hisadome et al. 2010). Although leptin, in contrast to GLP-1, is considered a long-term suppressor of food intake (Attele et al. 2002; Klok et al. 2007), these data suggest that it partly regulates feeding via activation of the central GLP-1 system.

PPG neurons were also activated by the inflammatory cytokine IL-6, which is known to play a role in food intake and obesity (Wallenius et al. 2002). We have found that PPG neurons express functional IL-6 receptors and respond to IL-6 with an influx of Ca^{2+} (Fig 3.5) (Anesten et al. 2016). Interestingly, GLP-1-induced suppression in feeding has been shown to be partially dependent on IL-6 receptor signalling (Shirazi et al. 2013). Whether this reflects a disease-state rather than regulation of homeostatic feeding is unclear, and it is possible that the link between IL-6 and GLP-1 in the regulation of food intake is mainly relevant during times of inflammation (Cahlin et al. 2000; Kahles et al. 2014).

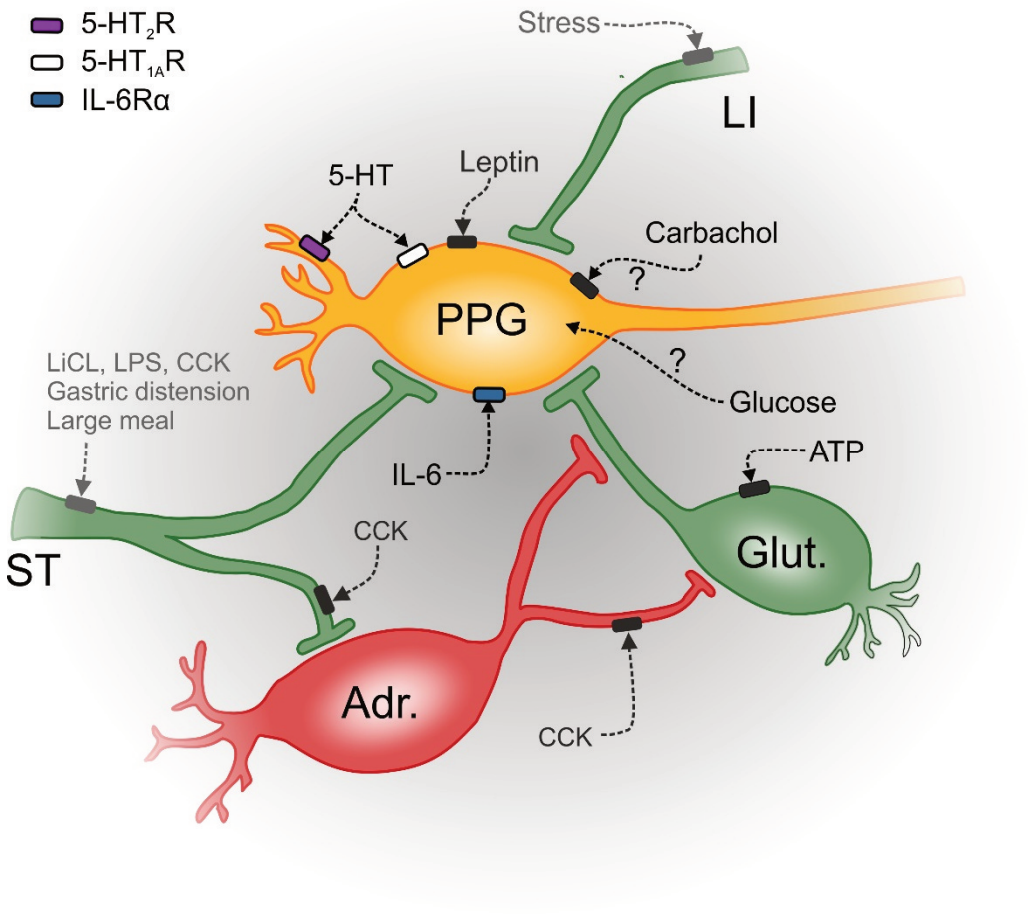

Fig 3.18 Proposed regulation of PPG neuron activity based on experimental evidence and literature. Compounds newly discovered to regulate PPG neuron activity were added to Fig 1.3. In black are shown compounds, which were investigated in this chapter. In grey are compounds previously shown to affect PPG neuron activity as described in Introduction. Using Ca^{2+} imaging, PPG neurons were found to be activated by AChR agonist, carbachol, and hypoglycaemia. The underlying mechanisms are unknown. ATP indirectly activated PPG neurons. Interleukin-6 (IL-6) increased intracellular [Ca^{2+}] in PPG neurons, which were found to express IL-6 receptor-α (IL-6Rα). 5-HT modulated PPG activity by inducing dendritic Ca^{2+} spikes via 5-HT_2 receptors (5-HT_2R) and by decreasing firing rate via 5-HT_{1A} receptors. Leptin and cholecystokinin (CCK) were confirmed to activate PPG neurons. ST: Solitary tract, LI: Limbic input, LPS: Lipopolysaccharide. Adr.: adrenergic neuron, Glut.: glutamatergic neuron.

I also demonstrated that CCK, another satiety hormone, increases intracellular [Ca^{2+}] in a subset of NTS PPG neurons. Hisadome et al. (2011) similarly found that CCK increases firing frequency indirectly in approximately 50% of PPG neurons. It is unclear whether the lack of response in the remaining neurons is due to severing of inputs in the *in vitro* slice preparation or whether it reflects the existence of different subpopulations of PPG neurons.

The origin of CCK acting on PPG neurons is uncertain. CCK-immunoreactive fibres and cell bodies are present in the NTS of rats (Takagi et al. 1984). NTS^{CCK} neurons are activated by feeding and reduce food intake through NTS → PBN and NTS → PVN circuits in mice (D'Agostino et al. 2016; Roman et al. 2016, 2017). A NTS^{CCK} → NTS^{PPG} indirect connection could provide an additional pathway for postprandial suppression of appetite. Alternatively, CCK released from the gut crosses the blood-brain barrier to activate CCK receptors in the CNS. Peripheral injection of CCK activates GLP-1-producing neurons in rats (Rinaman 1999b) and reduces food intake (McCann et al. 1989; Asin et al. 1992; Zhang and Ritter 2012). Importantly, peripheral injection of CCK also causes interoceptive stress and malaise (Ervin et al. 1995; Rinaman 1999b) and it is possible that food intake-suppressive effects of high levels of peripheral CCK are mainly mediated by induction of nausea (Verbalis et al. 1986; Shillabeer and Davison 1987; McCann et al. 1989). Both CCK and IL-6 could therefore signal states of illness rather than postprandial satiety via activation of NTS PPG neurons. The relative contributions of central and peripheral CCK in the activation of PPG neurons remains unknown.

3.3.2 PPG neurons as glucosensors

PPG neurons were found to increase their activity in response to a decrease in extracellular glucose (Fig 3.7). Other appetite-regulating neuronal populations have been found to be inhibited by high levels of extracellular glucose including hypothalamic AgRP-expressing cells (Muroya et al. 1999; Fioramonti et al. 2007; Marston et al. 2011), which are essential for the onset of feeding (Luquet et al. 2005). In contrast, satiety-inducing cells such as hypothalamic POMC-expressing neurons are excited by high levels of extracellular glucose (Ibrahim et al. 2003; Parton et al. 2007). Considering the putative role of NTS PPG neurons in satiety, it was surprising to find that they are inhibited by high levels of glucose rather than excited. Our laboratory has evidence from patch-clamp experiments, which suggests that PPG neurons are in fact glucose-excited during the dark phase and glucose-inhibited during the light phase (Hisadome et al., unpublished). A similar circadian regulation of GLP-1 secretion from the gut has been suggested (Gil-Lozano et al. 2014), suggesting both peripheral and central GLP-1-producing cells are "tuned" to respond to changes in metabolic cues during times of the day with usually high intake

of food, i.e. the dark phase in rodents. Future experiments should address the circadian rhythm of increases in PPG somatic [Ca^{2+}] in response to low glucose and whether this response is reversed during the dark phase.

It remains unclear how glucose-inhibited cells sense glucose, but there is some evidence that it is dependent on glucokinase and an intracellular drop in ATP during hypoglycaemia (Dunn-Meynell et al. 2002; Kang et al. 2006). However, there is also compelling evidence that the inhibitory effect of glucose on orexin neuron firing is independent of changes in intracellular glucose or ATP and is mediated by a potassium current (Burdakov et al. 2006). I observed a delayed increase in intracellular [Ca^{2+}] in response to hypoglycaemia, with several minutes passing between application and response. This was different to all other stimuli and suggests that the main mechanism of glucosensing in PPG neurons is dependent on metabolism of glucose, not direct activation of a glucose-sensitive current. Future experiments should address the importance of glucokinase in PPG glucosensing. If glucose-inhibition is dependent on the activity of glucokinase, inhibition of glucokinase should rapidly increase the activity of PPG neurons, as was seen for NPY neurons (Zhou et al. 2011).

Notably, I only investigated the response to relatively large changes in extracellular glucose (10 → 1 mM glucose), and could therefore not distinguish between high and low glucose sensitivity. Future experiments should address this by introducing gradual steps in glucose concentrations (e.g. 10 mM → 5 mM → 2.5 mM → 0.5 mM).

3.3.3 ATP activates PPG neurons suggesting a link between astrocytes and GLP-1

I demonstrated here that ATP is a potent stimulator of PPG neuron activity in an indirect manner. Intracellular [Ca^{2+}] of both dendrites and somata was elevated in response to 1 mM ATP (Fig 3.8). The primary source of extracellular ATP in the brain is astrocytes, which sense the brain microenvironment, including pH and glucose levels (Teschemacher et al. 2015). Interestingly, astrocytes have been shown to partly mediate the anorexic effects of hindbrain GLP-1R activation (Reiner et al. 2016), indicating some crosstalk between central GLP-1 and astrocytic signalling. The data presented here suggest that this communication occurs in the opposite direction as well, with ATP increasing the activity of PPG neurons.

Astrocytes have recently been implicated in the regulation of food intake via inhibition of AgRP neurons (Yang et al. 2015). Similar to what I observed in these experiments, ATP was found to indirectly regulate AgRP neuron activity. Since astrocytes in the NTS are known to be glucose-inhibited (McDougal et al. 2013), this could provide a parallel mechanisms by which changes in

extracellular glucose modulate PPG neuron activity. I did not investigate whether glucose directly affects the activity of PPG neurons by including TTX in the experimental solutions. It therefore remains a possibility that glucose-induced inhibition of astrocytic ATP release leads to decreased glutamatergic input to PPG neurons and decreased firing.

3.3.4 Activation of PPG neurons through acetylcholine receptor stimulation

The AChR agonist carbachol increased intracellular [Ca^{2+}] in a subset of PPG neurons, revealing a potential link between central GLP-1 and cholinergic signalling (Fig 3.9). Both nicotine, an agonist of the nicotinergic AChR, and acetylcholine activate most neurons in the NTS (Yettefti et al. 1997; Shihara et al. 1999). In particular, NTS to PVN projecting neurons are activated in response to nicotine (Feng and Uteshev 2014) and NTS second order neurons are activated by acetylcholine to regulate the sympathetic response to peripheral chemoreflexes (Furuya et al. 2014; Zoccal et al. 2014). GLP-1 released from NTS PPG neurons may act downstream of cholinergic neurons to increase sympathetic output and decrease food intake (Jo et al. 2002).

I did not address whether carbachol leads to direct activation of AChRs on PPG neurons and did not investigate whether the receptors involved were nicotinic or muscarinic. However, Kalappa et al. (2011) demonstrated that AChR-mediated activation of neurons in the caudal NTS is dependent on stimulation of presynaptic nicotinic receptors leading to enhanced release of glutamate onto NTS neurons. Similarly, Yettefti et al. (1997) demonstrated that peripheral nicotine indirectly activates NTS neurons. It is likely that PPG neurons are activated by carbachol in a similar way. This is supported by the lack of response in all neurons, suggesting some cells were lacking the necessary input. Future experiments should address this possibility by including TTX and DNQX in the experimental solutions.

The link between AChR signalling and PPG neuron activity described also provides an interesting potential mechanism for GLP-1-mediated suppression of reward and addiction. In addition to its well-known role in the regulation of food intake, GLP-1 has anti-addictive actions (Erreger et al. 2012; Egecioglu et al. 2013b; Graham et al. 2013) and reduces intake and reward of nicotine (Egecioglu et al. 2013a; Tuesta et al. 2017). The data presented encourage further investigations into the link between AChR activation, and in particular detection of nicotine, and PPG neuron activity. Future experiments should investigate the role of PPG neurons in nicotine-mediated autonomic control and appetite regulation and the potential for GLP-1-based therapies in the treatment of addiction.

3.3.5 Serotonergic modulation of NTS PPG neurons

In collaboration with Ida Llewellyn-Smith, I explored anatomical and functional links between 5-HT and NTS PPG neurons. Although, two thirds of NTS PPG neurons received somatic or proximal dendritic close appositions from serotonergic neurons, only 10% of PPG neurons increased somatic [Ca^{2+}] in response to 5-HT. In fact, [Ca^{2+}] increases in response to 5-HT were mainly observed in dendrites with no propagation of the Ca^{2+} signal to somata (Fig 3.10). TTX and DNQX did not affect the dendritic [Ca^{2+}] spikes, suggesting postsynaptic 5-HT receptors rather than presynaptic receptors are responsible for the responses, in contrast with what was observed for 5-HT effects on A2 NTS neurons (Cui et al. 2012)

Activation of 5-HT_3 receptors or inhibition of these receptors during 5-HT application did not affect dendritic [Ca^{2+}] spikes in PPG neurons (Fig 3.14). This indicates that PPG neurons do not express 5-HT_3 receptors. In contrast, I demonstrated that 5-HT induces dendritic [Ca^{2+}] spikes in PPG neurons via 5-HT_2 receptors and that 5-HT_{2C}-receptor activation increases dendritic [Ca^{2+}] in NTS PPG neurons (Fig 3.15). 5-HT_{2C} receptors reduce food intake via the melanocortin system in the hypothalamus (Lam et al. 2008). Whether PPG neurons are involved in the anorexic response to the 5-HT_{2C} receptor agonist lorcaserin is a key next question. Interestingly, the hypophagic effect of GLP-1R activation was lost in 5-HT_{2C} receptor knockout mice (Asarian 2009). However, these results appear to support a role of GLP-1 upstream from 5-HT_{2C} receptors, rather than downstream as explored in this study.

Activation of 5-HT_{2C} receptors on PPG neurons evoked [Ca^{2+}] spikes in dendrites, but failed to affect somatic [Ca^{2+}]. 5-HT_{2C} receptors are G-protein coupled receptors and lead to intracellular signalling via $G_{\alpha q}$. Although their activation on PPG dendrites presumably leads to depolarisation, opening of voltage-gated Ca^{2+} channels, and influx of Ca^{2+}, this Ca^{2+} signal does not propagate to the cell body. Importantly, the intracellular [Ca^{2+}] is tightly controlled in dendritic spines (Higley and Sabatini 2012) and dendritic [Ca^{2+}] transients are in some neurons prevented from propagating to the soma (Jarsky et al. 2005; Sjostrom et al. 2008; Higley and Sabatini 2012).

The lack of propagation of the response to 5-HT to somata could have several causes. Since 200 µM 5-HT failed to enhance the response to 5-HT, I reject that 20 µM is subthreshold for somatic activation. Alternatively, local depolarisation occurs on dendrites via 5-HT_{2C} receptors, but simultaneous activation of inhibitory 5-HT receptors prevents the signal from reaching the soma. I reject this as well, since selective activation of 5-HT_{2C} receptors did not affect somatic [Ca^{2+}] and suppression of 5-HT_{1A} receptor-mediated inhibition of PPG neurons did not allow

propagation of $[Ca^{2+}]$ spikes to cell bodies. I propose instead that 5-HT activates 5-HT_{2C} receptors on distal dendrites leading to compartmentalised increases in $[Ca^{2+}]$. Local $[Ca^{2+}]$ transient have been implicated in synaptic plasticity, enhancing somatic spike precision, and dendritic release of neuropeptides (Sjostrom et al. 2008).

In accordance with 5-HT only increasing $[Ca^{2+}]$ in few somata, firing rate increased in only 25% of recorded neurons under 5-HT. Almost half of the tested PPG cells decreased action potential frequency in response to 5-HT and this inhibitory response was dependent on 5-HT_{1A} receptors (Figs 3.16 and 3.17). These data raise the question why PPG neurons are excited by 5-HT at the dendritic level, but inhibited at the somatic level. I propose two, not mutually exclusive, explanations: 1) There exist separate populations of PPG neurons which respond oppositely to 5-HT, and 2) the dendritic compartment is functionally isolated from the soma, meaning that robust dendritic $[Ca^{2+}]$ spikes do not result in excitation of PPG cell bodies.

The heterogenous responses to 5-HT on PPG neurons align with the physiological roles of the 5-HT_{2C} and 5-HT_{1A} receptors. Indeed, 5-HT_{1A} receptor inhibition suppresses feeding (Dill et al. 2013), as disinhibition of PPG neurons is expected to. Loss of 5-HT_{2C} receptors increases food intake (Nonogaki et al. 1998), suggesting that 5-HT_{2C} receptor activation reduces appetite. Similarly, chemogenetic activation of PPG neurons dramatically suppresses feeding, as I will show in Chapter 4 and as has recently been demonstrated by others (Gaykema et al. 2017). Future experiments should build on the discoveries made here by investigating the need for PPG neurons in the hypophagic response to 5-HT_{1A} receptor antagonists and 5-HT_{2C} receptor agonists, respectively.

In summary, PPG neurons respond to a range of neurotransmitter and metabolic signals with an increase in intracellular $[Ca^{2+}]$. All the tested compounds have been implicated in the control of food intake and many of them signal changes in homeostasis, be it energy balance or inflammation. There was a clear correlation between electrical activity and intracellular $[Ca^{2+}]$, encouraging the investigation of potential inhibitory responses. Future studies should investigate known hunger-stimulating compounds such as orexin and endocannabinoid receptor agonists. With their anatomical properties, PPG neurons are ideally situated to receive and relay these signals. Future studies should work on elucidating the physiological importance of the functional links demonstrated here.

4. The physiological role of PPG neurons in food intake

4.1 Background

The role of central GLP-1 in food intake has been the topic of intense research for decades. Most studies have delivered GLP-1 or its analogues exogenously. As discussed in the Introduction (see Table 1.1), intraparenchymal injection of GLP-1 or analogues in a number of brain areas results in decreased food intake (Turton et al. 1996; Zhao et al. 2012; Mietlicki-Baase et al. 2013; Alhadeff et al. 2014; Secher et al. 2014). This hypophagia most likely mimics several different aspects of feeding, including stress-related hypophagia, hedonic feeding, and homeostatic feeding. For the purpose of this thesis, normal feeding will refer to food intake occurring throughout the day, primarily at dark onset, with no other stimuli than the normal circadian rhythm.

Studies using GLP-1R agonists are crucial in identifying brain areas involved in GLP-1-induced satiety. They do not, however, address the physiological role of central GLP-1. In particular, the approach fails to investigate the role of the source of central GLP-1, the PPG neurons, in appetite regulation. Exogenous GLP-1 is often delivered in supraphysiological doses and GLP-1R agonism does not take into account release of co-transmitters from PPG neurons, including glutamate and GLP-2.

Studies in which the GLP-1R antagonist, Ex9, is infused directly into the brain tissue, come somewhat closer to investigating the physiological role of GLP-1 in feeding (Turton et al. 1996; Alhadeff et al. 2012; Dossat et al. 2013). This approach aims to inhibit the actions of endogenously released GLP-1 onto GLP-1Rs in distinct brain nuclei, making it possible to assess the importance of different brain regions in GLP-1-mediated satiety in a physiological context.

As described in the Introduction, the most likely source of GLP-1 acting on central GLP-1Rs is PPG neurons in the lower brainstem. In Chapter 3, I investigated the modulation of PPG neuron activity by a range of compounds. In this chapter, I investigate another three aspects of the physiology of NTS PPG neurons:

1) Are NTS PPG neurons *sufficient* to reduce feeding?
2) Are NTS PPG neurons *necessary* to reduce feeding?
3) Is the homeostatic and psychological state of the animal important for recruitment of PPG neurons?

I approach these questions by chemogenetically manipulating the activity of NTS PPG neurons *in vivo* and measuring food intake in the following hours. I follow up these three initial questions with further investigations of downstream targets of PPG neurons, both anatomically and functionally.

Several different food intake paradigms were used in an effort to thoroughly investigate in which physiological context PPG neurons play a role:

- **Short fast:** Three hours fast prior to dark onset for studying normal food intake. The short fast was included to ensure simultaneous onset of feeding for all animals at dark onset. A brief fast is not expected to significantly affect hunger levels and is used routinely in food intake studies (Grill et al. 2002; Jensen et al. 2013; Terrill et al. 2016).
- **Prolonged fast:** Food-deprivation for 18 hours prior to dark onset puts the mice into negative energy balance, thus encouraging intake of a large meal at the beginning of the dark phase.
- **Ensure preload:** Following a short fast, vanilla milkshake was given to encourage consumption of a large meal in a short period of time. Ensure is a highly palatable liquid, which mice quickly learn to drink in large quantities.
- **Acute restraint stress:** Mice were subjected to 30 mins restraint before food intake measurements. As explained in the Introduction, this is a stimulus, which induces acute psychogenic stress and which may engage the central GLP-1 system.

All food intake measurements were instigated at the onset of dark phase and intake was measured during the dark phase. This is the time of day mice forage (Ellacott et al. 2010; Jensen et al. 2013) and their activity increases, as I will demonstrate in Chapter 5.

4.2 Results

4.2.1 Activation of PPG neurons in vivo dramatically reduces feeding

I set out to determine whether PPG neurons are sufficient to reduce dark onset feeding in mice, as was recently shown by Gaykema et al. (2017). To this end, I chemogenetically activated NTS PPG neurons and monitored feeding. By selectively expressing the $G_{\alpha q}$-coupled DREADD HM3Dq in NTS PPG neurons, I was able to activate them *in vitro* and *in vivo* with CNO, as illustrated in Fig 4.1. I hypothesised that this activation leads to release of GLP-1 and co-transmitters, such as glutamate, from terminals (Zheng et al. 2015b), resulting ultimately in reduced food intake. This would confirm the sufficiency of PPG neurons to reduce food intake.

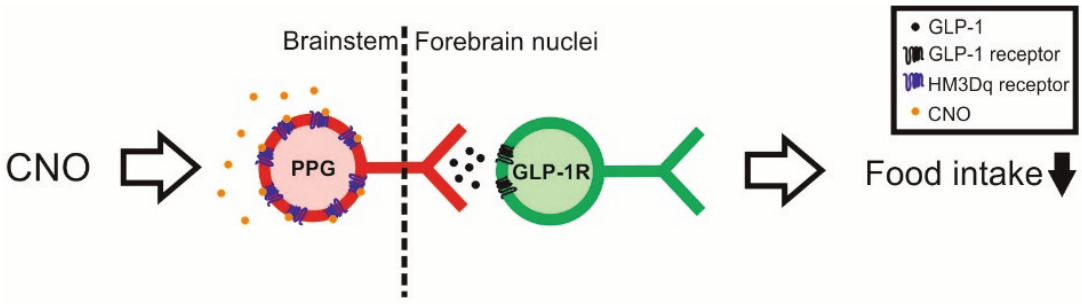

Fig 4.1 Diagram illustrating the hypothesis for hypophagia following activation of NTS PPG neurons. Expression of HM3Dq receptor (In blue) on cell surface of PPG neurons allows activation using the selective drug CNO. This leads to release of GLP-1 (and co-transmitters) in forebrain nuclei. Here GLP-1Rs are activated on downstream neurons resulting in decreased food intake.

NTS PPG neurons were infected with AAV2-FLEX-HM3Dq:mCherry or AAV1/2-FLEX-Perceval as control through bilateral, stereotaxic injection of 200 nl AAV into the NTS (Fig 4.2A). This led to clear expression of HM3Dq:mCherry or Perceval in PPG neurons only, visualized here by immunohistochemistry for either mCherry or Perceval (Fig 4.2B).

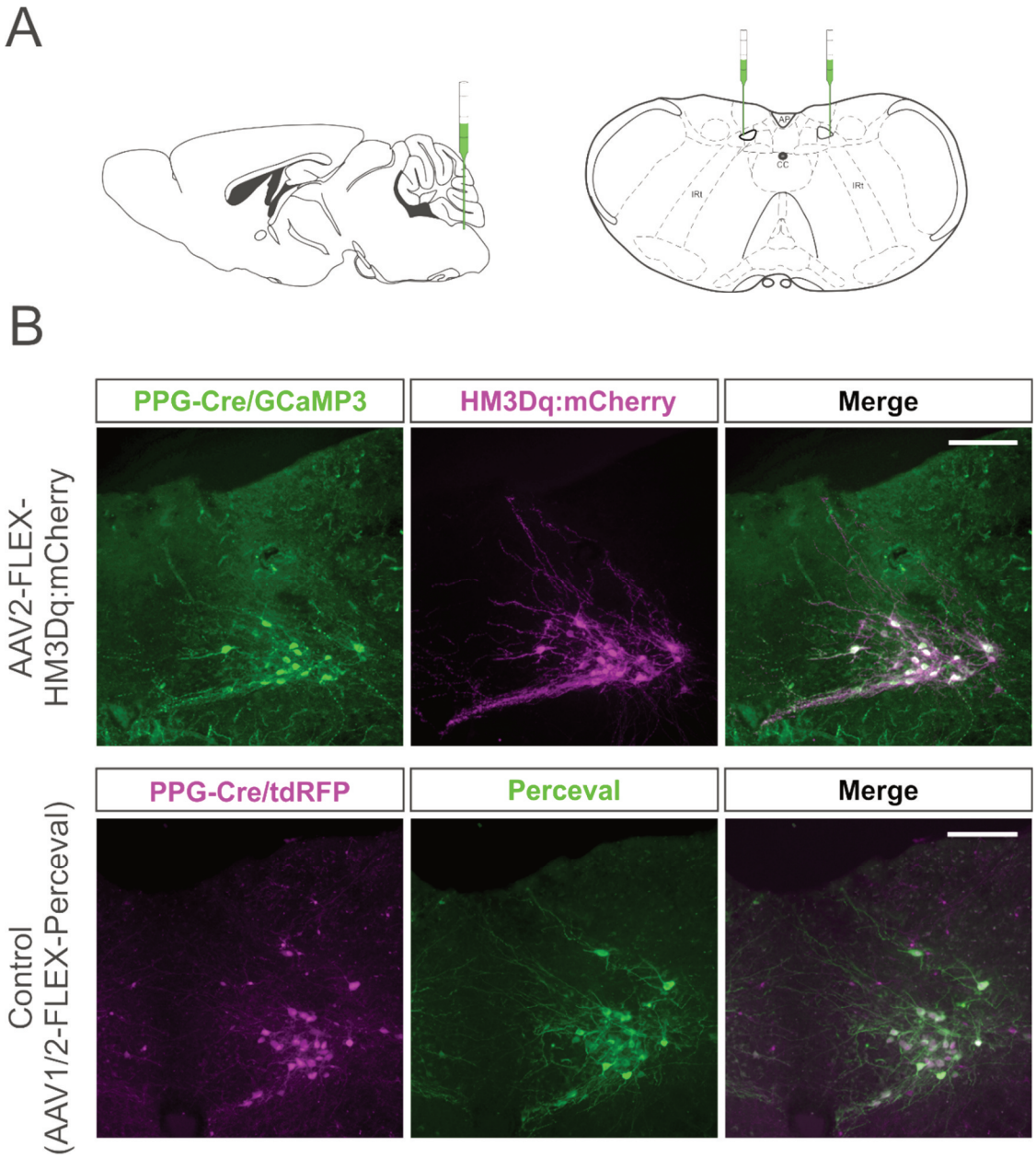

Fig 4.2 Selective expression of HM3Dq in NTS PPG neurons using viral gene delivery. A) The hypothesis described in Fig 4.1 was tested by injecting an AAV encoding HM3Dq receptor fused with mCherry (HM3Dq:mCherry) into the NTS. *Left panel:* Sagittal view of the stereotaxic injection. *Right panel*: Coronal section showing site of stereotaxic injection. Both adapted from Paxinos and Franklin's 'The mouse brain in stereotaxic coordinates' (Franklin and Paxinos 2008). **B)** Immunofluorescent images showing expression of HM3Dq:mCherry or Perceval in PPG neurons in the NTS. *Top panels:* HM3Dq:mCherry expression was detected using an anti-dsRed antibody, displayed in magenta. PPG neurons expressing GCaMP3 were detected using an anti-GFP antibody, shown in green. *Bottom panels:* Perceval was detected using an anti-GFP antibody, shown in green. PPG neurons expressing tdRFP were detected using an anti-dsRed antibody, shown in magenta. Scale bars: 100 µm.

Having successfully targeted the expression of HM3Dq to NTS PPG neurons, I verified *in vitro* that this approach allows activation of PPG neurons. PPG-Cre/GCaMP3 mice were injected with AAV2-FLEX-HM3Dq:mCherry into the NTS as shown in Fig 4.2A. As explained in Chapter 3, GCaMP3 is stably expressed from the Rosa26 locus in PPG neurons in these mice. Co-expression with HM3Dq made it possible to monitor intracellular [Ca^{2+}] while activating HM3Dq with CNO. As demonstrated in Chapter 3, GCaMP3 fluorescence intensity positively correlates with firing rate of PPG neurons and can therefore be used as a surrogate marker for neuronal activity.

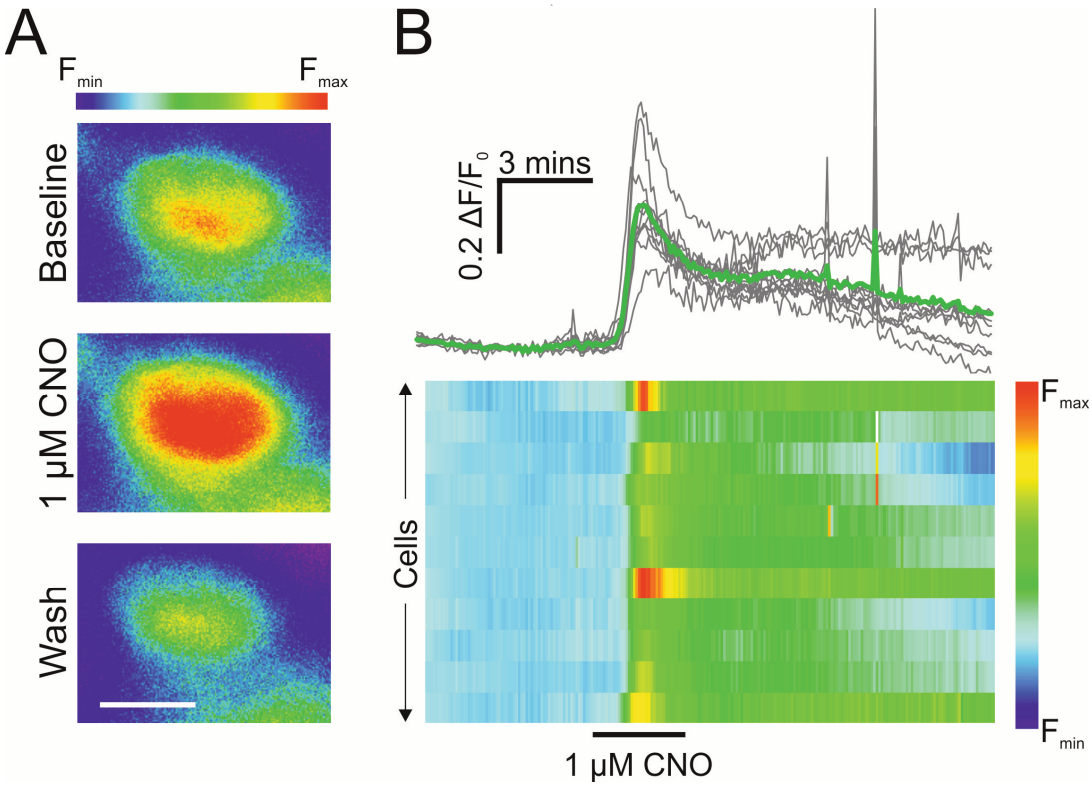

Fig 4.3 PPG neurons expressing HM3Dq increase intracellular [Ca^{2+}] in response to CNO. A) Fluorescence intensity levels of one pseudocoloured, representative GCaMP3+/HM3Dq+ cell during baseline (top), superfusion with 1 µM CNO (middle), and after washout of CNO (Bottom). Blue corresponds to F_{min} and red to F_{max} as shown in the bar above the images. Scale bar: 10 µm. **B)** Traces (*top panel*) and heat map (*bottom panel*) showing 11 individual cells responding to 1 µM CNO with an increase in intracellular [Ca^{2+}]. *Top panel:* Individual cells shown in grey and the average trace shown in green. *Bottom panel:* Heat map with blue denoting F_{min} and red denoting F_{max} showing the same 11 cells as in the top panel responding to 1 µM CNO. Each cell is represented by a row in the map. Application of 1 µM CNO is indicated with a black bar and applies to both the top and bottom panel. The heat map pseudocolouring levels are indicated by the bar on the right.

Three weeks after injection, mice were anaesthetised and decapitated and brainstem slices were sectioned for *in vitro* Ca^{2+} imaging. HM3Dq-expressing cells were identified as mCherry-positive throughout the NTS and overlapped with GCaMP3 expression. GCaMP3 expression was noticeably reduced in these sections as compared to non-transduced mice used for the

recordings in Chapter 3. This was most likely due to overexpression of HM3Dq:mCherry and resulting downregulation of the expression of GCaMP3. However, with short incubation times after stereotaxic injection to limit overexpression (no more than 21 days), GCaMP3 was clearly detectable in brainstem slices.

Fig 4.3A shows a representative, pseudocoloured GCaMP3-expressing cell responding to 1 µM CNO with an increase in intracellular [Ca^{2+}]. Intracellular [Ca^{2+}] increased in all 11 cells recorded here, as displayed in two different ways in Fig 4.3B. [Ca^{2+}] peaked in the minutes following CNO application and subsequently declined, most likely due to Ca^{2+} buffering. Importantly, after CNO stimulation, intracellular [Ca^{2+}] remained higher than baseline for most cells during the recording, suggesting the effect does not readily wash out.

Having established that HM3Dq-expressing PPG neurons increase intracellular [Ca^{2+}] in response to CNO *in vitro,* I next determined the effect of PPG neuron activation on feeding. Eight PPG-Cre/tdRFP mice were injected into the caudal NTS (200 nl bilaterally) with either AAV2-FLEX-HM3Dq:mCherry or AAV1/2-FLEX-Perceval as control. Perceval is a modified EGFP designed to detect changes in the ATP/ADP ratio. Since Perceval does not affect the activity of neurons it was used in this study as a control for viral expression (Berg et al. 2009; Tantama et al. 2013). Expression of the two transgenes was confirmed immunohistologically at the end of the experiment (Fig 4.2B). All animals expressed the expected transgene, no animals were excluded due to lack of expression.

All animals received both 2 mg/kg CNO and vehicle. Prior to the food intake experiments, mice were habituated to i.p. injections of 5 ml/kg saline. On the day of the experiment, food was removed for three hours until dark onset. This mild fast was to ensure all mice had their first meal at dark onset. Mice were injected i.p. 30 mins before dark onset with either saline or 2 mg/kg CNO. Food was returned at dark onset and intake measured at one and two hours after dark onset (Fig 4.4).

Three-way mixed model ANOVA revealed no significant interaction, time x drug x virus ($F(1, 6) = 0.439$, $p=0.532$), whereas there was a significant two-way interaction between drug and virus ($F(1,2) = 22.92$, $p<0.0001$). Two-way mixed-model ANOVA at both hour 1 and hour 2 revealed significant interactions between drug and virus (Hour 1: $F(1, 6) = 17.19$, $p=0.006$; Hour 2: $F(1, 6) = 8.647$, $p=0.0259$), suggesting i.p. injection of CNO affects food intake differently in control and HM3Dq-expressing mice.

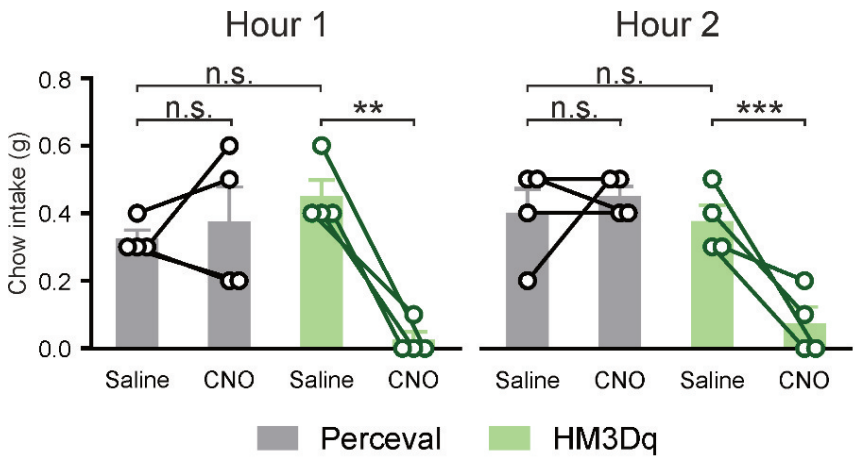

Fig 4.4 Chemogenetic activation of PPG neurons reduces dark onset feeding. Chow intake during the first hour (*left panel)* and second hour (*right panel*) after dark onset in mice expressing either HMD3q (green, N=4) or Perceval (grey, N=4) and injected i.p. with 2 mg/kg CNO or saline only. Data from mice are shown as individual data points and lines connect data from the same mouse. **p<0.01, ***p>0.001, n.s.: not significant. **p<0.01, ***p<0.001, n.s.: not significant according to Sidak's multiple comparions test.

Importantly, Perceval and HM3Dq mice injected with saline ate similar amounts of chow in both hour 1 and hour 2 (p=0.30 and p=0.93, respectively), suggesting expression of HM3Dq does not affect food intake in the absence of stimulation with CNO. Similarly, i.p. injection of 2 mg/kg CNO had no effect on food intake in mice expressing the control virus, Perceval, at both hour 1 (p=0.81) and hour 2 (p=0.82). In contrast, i.p. injection of 2 mg/kg CNO significantly reduced food intake in HM3Dq-expressing mice. In hour 1, activation of NTS PPG neurons reduced food intake by 94±6 % (p=0.0038). Similarly, food intake was reduced by 77±16 % in hour 2 (p=0.024).

I draw three crucial conclusions from these data:

1) The expression of HM3Dq in itself does not affect food intake, since there was no difference between chow consumption of HM3Dq and Perceval mice.
2) CNO in itself does not affect chow intake, as there was no difference in chow intake between saline and CNO in the control group. This is an important observation considering a recent report that the CNO metabolite, clozapine, is the active ligand for HM3Dq (Gomez et al. 2017) and that clozapine may have off-target effects (MacLaren et al. 2016).
3) Chemogenetic activation of PPG neurons dramatically reduces feeding in mice.

To expand on these data, I injected another cohort of nine animals with AAV2-FLEX-HM3Dq:mCherry only. Since expression of HM3Dq and i.p. injection of CNO do not affect food

intake, the control group was omitted in this experiment. The study was performed following a counterbalanced, crossover design with each animal receiving both 2 mg/kg CNO and saline alone.

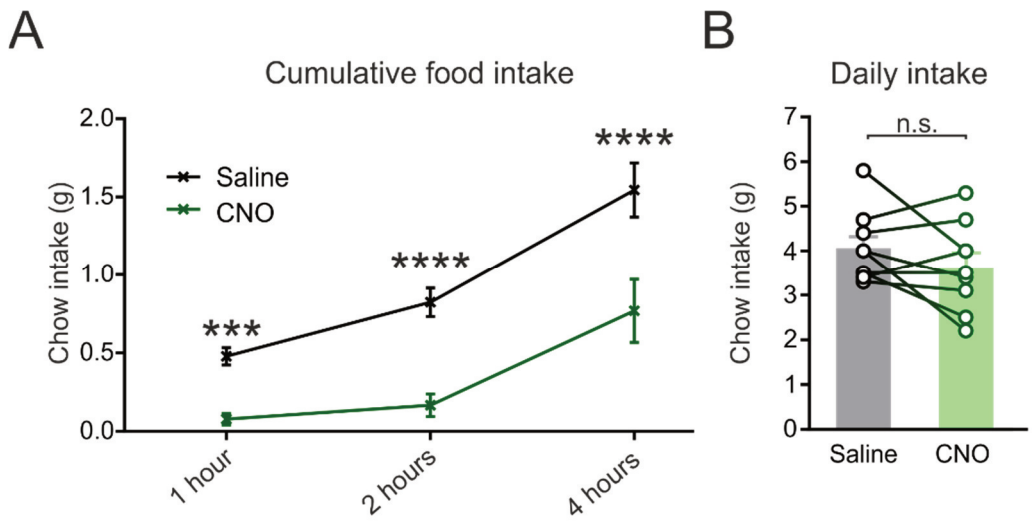

Fig 4.5 PPG neurons are sufficient to reduce food intake four hours into the dark phase. A) Mean cumulative chow intake 1, 2, and 4 hours into the dark phase following saline (black) or 2 mg/kg CNO (green). Data are displayed as mean±SEM. **B)** Mean daily cumulative chow intake following saline (grey) or 2 mg/kg CNO (green) measured 21 hours after dark onset. Data from individual mice are shown as circles and paired data connected with lines. ***p<0.001, ****p<0.0001, n.s.: not significant according to Sidak's multiple comparisons test.

Chow intake was significantly reduced up to four hours after dark onset (Fig 4.5). Repeated measures two-way ANOVA of data from the first four hours revealed a significant interaction between time and drug treatment ($F(2,16)=5.626$, $p=0.0141$) and Sidak's multiple comparisons test yielded a statistically significant effect of CNO at one, two, and four hours ($p=0.0005$, $p<0.0001$, and $p<0.0001$, respectively, Fig 4.5A). NTS PPG activation reduced food intake by as much as 83±7 % in the first hour and some animals did not eat at all in the first four hours. Interestingly, the effect of CNO had disappeared the following day with cumulative daily chow intake unaffected by PPG activation ($p=0.20$, Fig 4.5B). These data suggest mice compensate following the initial decrease in chow intake.

Analysis of the non-cumulative data revealed a transient decrease in dark phase food intake over the first four hours following PPG activation (Fig 4.6). Repeated-measures two-way ANOVA of the non-cumulative data revealed a significant effect of drug treatment ($F(1,8)=17.31$, $p=0.0032$) and of time ($F(2,16)=20.62$, $p<0.0001$), but no interaction between the two ($F(2, 16) = 2.897$, $p=0.0844$). PPG activation affected chow intake in the first ($p=0.0005$) and second ($p=0.013$) hour after dark onset, but the effect had faded during hours 3-4 ($p=0.15$) (Fig 4.6A).

Interestingly, the effect appeared to reverse overnight (hours 5-21) so that mice ate 16±11 % more after being injected with CNO compared to saline, although this did not reach statistical significance (Fig 4.6B, p=0.17).

These data demonstrate that PPG activation is a strong driver of hypophagia and that even when mice are most likely to eat, during the beginning of dark phase, activation of NTS PPG neurons is sufficient to dramatically reduce chow intake.

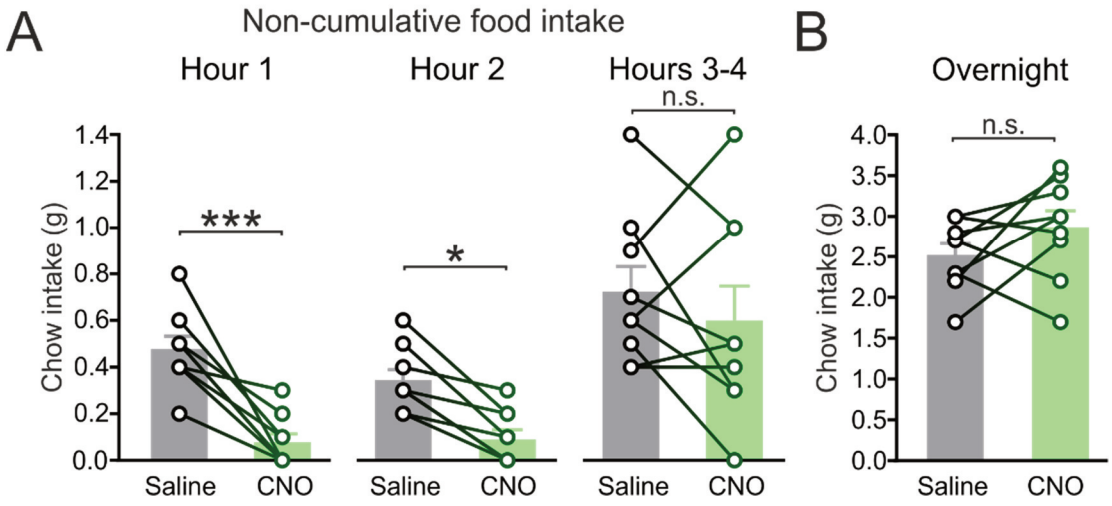

Fig 4.6 Chow intake is reduced following PPG activation, but recovers overnight. A) Mean non-cumulative chow intake at hours 1, 2, and 3-4 after onset of the dark phase following i.p. injection of 2 mg/kg CNO (green) and saline (black). **B)** Mean overnight (hours 5-21) non-cumulative chow intake. Data are displayed as mean±SEM. Data from individual mice are shown as circles connected with lines. *p<0.05, ***p<0.001, n.s.: not significant according to Sidak's multiple comparisons test.

4.2.2 Ablation of PPG neurons does not affect normal dark onset feeding

Having established that activation of NTS PPG neurons is sufficient to decrease dark onset feeding in mice, I next investigated the necessity of NTS PPG neurons in the regulation of feeding. To this end, I employed two different models of PPG neuron inactivation: ablation and acute inhibition. I hypothesised that they would both increase food intake (Fig 4.7).

As described in the Introduction, in the first approach NTS PPG neurons were ablated by inhibiting protein synthesis, ultimately leading to cell death (Fig 1.4). For this, I used a Cre-dependent virus, AAV8-mCherry-FLEX-DTA, to express DTA selectively in PPG neurons. This virus also leads to expression of the fluorescent protein mCherry. All cells infected with the virus express mCherry, with the exception of PPG neurons. In these cells, Cre mediates homologous recombination, mCherry expression is turned off, and DTA expression is turned on (Wu et al. 2014). This means only cells positive for Cre will die, allowing selective ablation of PPG neurons.

The second model uses the inhibitory DREADD, HM4Di, to acutely inactivate PPG neurons (Armbruster et al. 2007). Expression of HM4Di is Cre-dependent, allowing selective expression in NTS PPG neurons. I use a virus, AAV2-FLEX-HM4Di:mCherry in which the fluorescent reporter mCherry is fused to HM4Di to facilitate identification of HM4Di-expressing cells. Both these models allow me to investigate the importance of endogenous activity of PPG neurons during feeding.

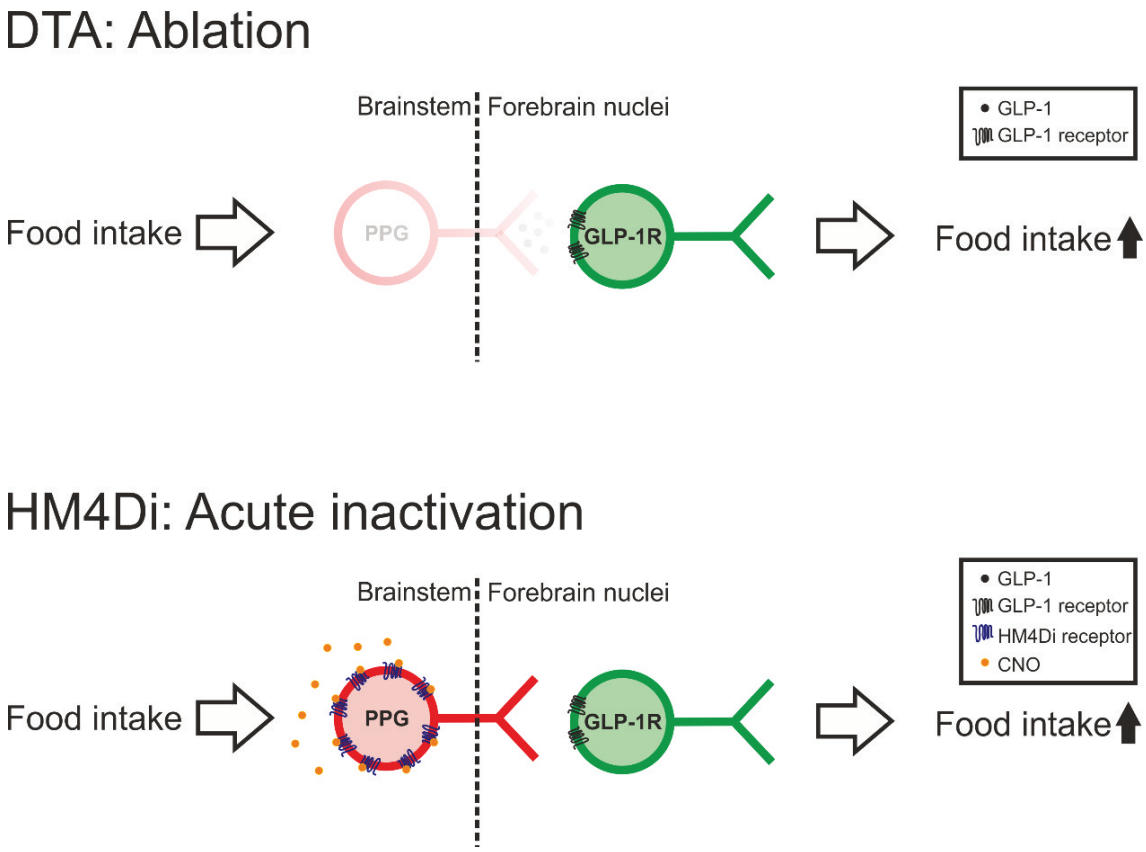

Fig 4.7 Hypotheses for the effect of PPG inactivation or ablation on feeding. *Top panel:* Ablation with AAV8-mCherry-FLEX-DTA leads to loss of NTS PPG neurons. This results in no release of GLP-1 or co-transmitters in forebrain nuclei and increased food intake as compared to control mice. *Bottom panel:* In this model the inhibitory DREADD, HM4Di:mCherry, is selectively expressed in PPG neurons. Activation of HM4Di with CNO leads to inactivation of PPG neurons and reduced synaptic release of GLP-1 and co-transmitters. Ultimately, this blocks the hypophagic effect and leads to an increase in food intake as compared to control mice.

I first confirmed that expression of DTA leads to selective ablation of NTS PPG neurons. To establish the time course of ablation following viral injections, three PPG-Cre/GCaMP3 mice were injected unilaterally with 50 nl AAV8-mCherry-FLEX-DTA. The mice were perfuse-fixed four, seven, or 14 days after injection and coronal brainstem sections were immunostained for both mCherry and the fluorescent marker for PPG neurons, GCaMP3.

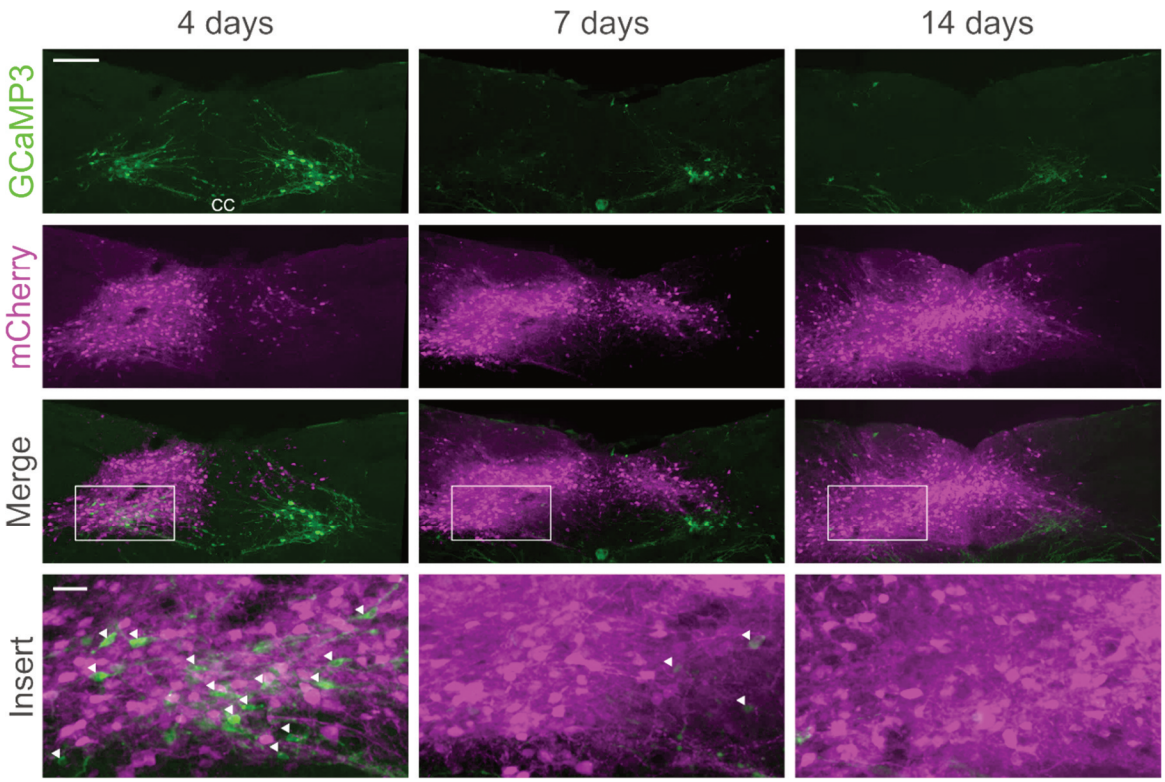

Fig 4.8 Time course of ablation of NTS PPG neurons with AAV8-mCherry-FLEX-DTA. Coronal sections from three PPG-Cre/GCaMP3 mice injected unilaterally into the NTS on the left side with 50-100 nl AAV8-mCherry-FLEX-DTA at day 0 and perfuse-fixed at day 4, 7, and 14, respectively. *Top panel:* Immunohistochemistry for GCaMP3 in green detecting PPG neurons in the NTS. Scale bar: 100 µm. CC: Central canal. *Second from top panel:* Immunohistochemistry for mCherry in magenta showing the spread of the AAV8-mCherry-FLEX-DTA virus from the injection site. *Third from top panel:* Composite of the first two panels showing an overlay of GCaMP3- and mCherry-positive cells in the NTS. *Bottom panel:* Inserts indicated in merged images. GCaMP3-positive cells are clearly seen at day 4, only a few at day 7, and none at day 14. Scale bar: 20 µm. Arrowheads point to GCaMP3-positive PPG neurons.

Cells expressing mCherry were detected in the NTS as early as four days after injection (Fig 4.8). The expression was more diffuse at days 7 and 14, suggesting mCherry was reaching axonal and dendritic fibres around cell bodies. At day 4, many GCaMP3-expressing PPG neurons were still visible at the side of injection, despite surrounding cells clearly expressing mCherry. At day 7, very few GCaMP3-positive cells were seen on the side of injection and the contralateral side seemed to be affected as well with some mCherry expression visible. A similar pattern was seen at day 14, when all PPG neurons had been ablated on the side of injection and very few were visible on the contralateral side.

No double-positive cells were observed, in agreement with the mechanism of the AAV8-mCherry-FLEX-DTA described above. In PPG neurons, where Cre is present, mCherry expression is turned off while DTA expression is turned on through homologous recombination. The reason

for no double-positive neurons is therefore that the AAV8-mCherry-FLEX-DTA has successfully infected cells throughout the NTS including PPG neurons, but that Cre expressed in PPG neurons has turned off mCherry expression. This also implies that DTA expression has been turned on in the same cells. The fact that the cells are still visible suggests that the DTA-mediated prevention of protein synthesis has yet to result in cell death at day 4. These data suggest that infection and expression from this virus happen within four days of injection and that PPG cells are successfully ablated within 14 days of incubation of the virus. Using the PPG ablation model, our laboratory has found that up to 80% of hypothalamic GLP-1 is lost following NTS PPG ablation, demonstrating that the PPG neurons are the main source of central GLP-1 (James E. Richards and Stefan Trapp, unpublished data).

The data discussed above demonstrate that injection of AAV8-mCherry-FLEX-DTA leads to selective ablation of PPG neurons in the NTS. To investigate the effect of loss of NTS PPG neurons on food intake, I injected 14 PPG-Cre/RFP mice bilaterally with 250 nl of either AAV8-mCherry-FLEX-DTA or AAV1/2-FLEX-Perceval as control.

In 2011, Barrera et al. demonstrated that siRNA-mediated knock-down of GLP-1 in rat brainstem leads to increased body weight gain. Considering these results and the bulk of evidence for a role of central GLP-1 in satiety (Tang-Christensen et al. 1996; Turton et al. 1996; Larsen et al. 1997b; Williams et al. 2009), I monitored body weight changes over 80 days following transduction with AAV8-mCherry-FLEX-DTA to determine whether loss of PPG neurons affects body weight.

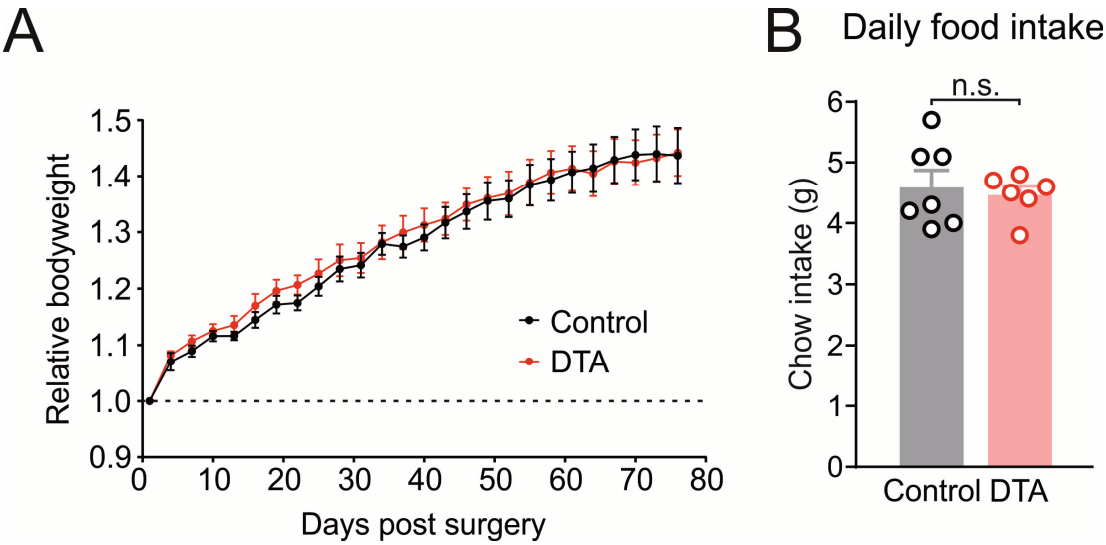

Fig 4.9 Ablation of NTS PPG neurons does not affect body weight or daily food intake. A) Mean relative bodyweight gain following injection of either AAV1/2-FLEX-Perceval (Control, grey, N=7) or AAV8-mCherry-FLEX-DTA (DTA, red, N=7). Bodyweights were normalised to the first day after surgery. One data point displaying mean±SEM every three days starting on day one. **B)** Mean daily cumulative food intake of AAV1/2-FLEX-Perceval (control, grey, N=7) or AAV8-mCherry-FLEX-DTA (DTA, red, N=6). Data from individual mice are shown as circles. n.s.: not significant. Data from one DTA mouse were excluded as an outlier as described in Materials and Methods.

Following stereotaxic injections mice lose up to 10% bodyweight. Since this decrease in bodyweight happens mainly over the first day post-surgery, body weights were normalised to the first day after surgery. Keeping in mind that PPG neurons are still present four days after surgery (Fig 4.8), virus type should not have a phenotypic effect the first day following surgery. Body weight increased over 80 days to a similar degree for control and DTA mice (Fig 4.9A). Indeed, mixed-model two-way ANOVA revealed a significant main effect of time on bodyweight ($F(25,300)=116.8$, $p<0.0001$), but there was no difference in the body weight gain of control and DTA animals ($F(1,12)=0.08578$, $p=0.7746$). Accordingly, there was no significant difference in daily cumulative chow intake with control animals eating 4.66±0.3 g and DTA mice eating 4.4±0.14 g (Fig 4.9B, unpaired t-test: $p=0.45$).

Although no overall effects on bodyweight or daily food intake were observed, it is possible that the effect is only on early dark phase meals, as was seen in the case of PPG activation with HM3Dq (Fig 4.6). To investigate this possibility, I monitored normal, dark onset feeding of the same group of PPG-ablated and control mice (Fig 4.10).

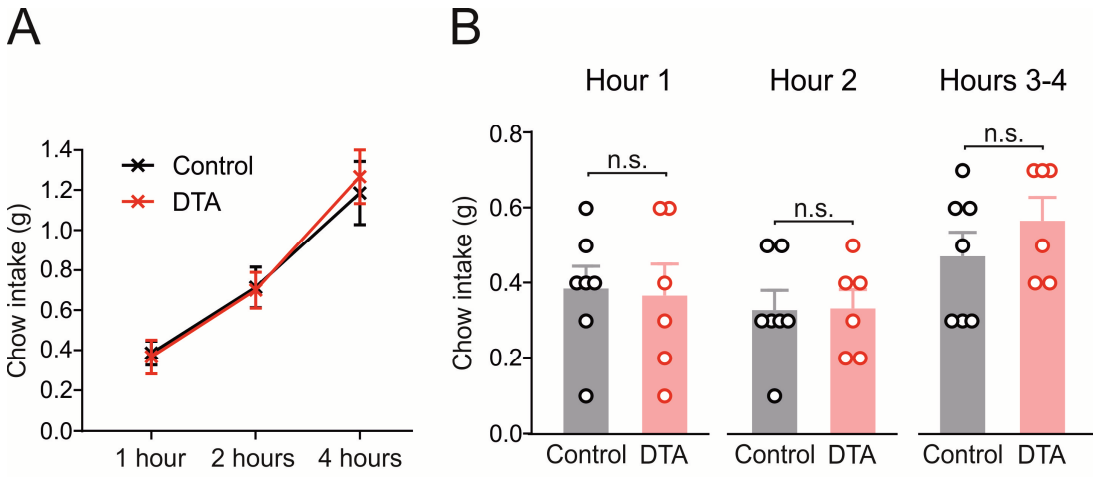

Fig 4.10 Ablation of NTS PPG neurons does not affect dark onset feeding. A) Mean cumulative food intake 1, 2, and 4 hours after dark onset. Perceval (Control) data in black and DTA data in red. **B)** Normal dark onset feeding in Perceval (Control, grey) and DTA (red) mice. Summary data represent the mean±SEM. Data from individual mice are shown as circles. n.s.: Not significant. N=7 (control), N=6 (DTA). Data from one DTA mouse were excluded as described in Materials and Methods.

Cumulative food intake was unaffected by PPG ablation (Fig 4.10A). A mixed-model two-way ANOVA yielded no significant interaction between time and virus type ($F(2,22)=0.5406$, $p=0.5900$). There was a significant main effect of time ($F(2,22)=124.7$, $p<0.0001$) as expected from cumulative food intake data, but no main effect of virus type ($F(1,11)=0.01224$, $p=0.9139$). Similarly, analysis of the non-cumulative chow intake using mixed-model two-way ANOVA revealed no interaction between time and virus ($F(2,22)=0.834$, $p=0.4476$). There was a main effect of time ($F(2,22)=8.845$, $p=0.0015$), but again no effect of virus ($F(1,11)=0.1472$, $p=0.7085$) (Fig 4.10B). These data suggest loss of NTS PPG neurons does not affect feeding in mice.

4.2.3 Acute inhibition of PPG activity has no effect on normal feeding

Importantly, PPG ablation could have led to compensation over the three weeks of incubation, allowing the animal to rely on other satiety systems to regulate feeding. To rule out any confounding factors from such compensation, I also used an acute model of inactivation, as described in Fig. 4.7. I performed stereotaxic, bilateral injections of 250 nl AAV2-FLEX-EGFP or AAV2-FLEX-HM4Di:mCherry on 23 PPG-Cre/GCaMP3 and PPG-Cre/tdRFP mice. Mice belonged to an EGFP (control) group or an HM4Di group and received saline and CNO in a counterbalanced manner.

Mice were perfuse-fixed following feeding studies and, as seen in Fig 4.11, there was clear expression of HM4Di:mCherry in PPG neurons in the NTS. This was seen in all animals, no animals

were excluded due to lack of expression of the desired transgene (HM4Di:mCherry or EGFP). Surprisingly, a few cells were found to be mCherry-positive without obvious expression of GCaMP3. As mentioned previously, overexpression of a virally-delivered transgene was found to reduce expression of the fluorescent reporter, GCaMP3 (see section 4.2.1). This could explain the lack of GCaMP3 expression in HM4Di-expressing cells. Importantly, I found no impact of this on phenotype both *in vitro* and *in vivo.* At higher magnification, the HM4Di:mCherry signal had a punctate morphology, suggesting some of the fusion protein was present in intracellular compartments (Fig 4.11). Patch-clamp electrophysiology confirmed that 1 µM CNO attenuated action potential firing in HM4Di-expressing PPG neurons (N=5 cells, experiments performed by Stefan Trapp on mice injected by me, unpublished data not shown).

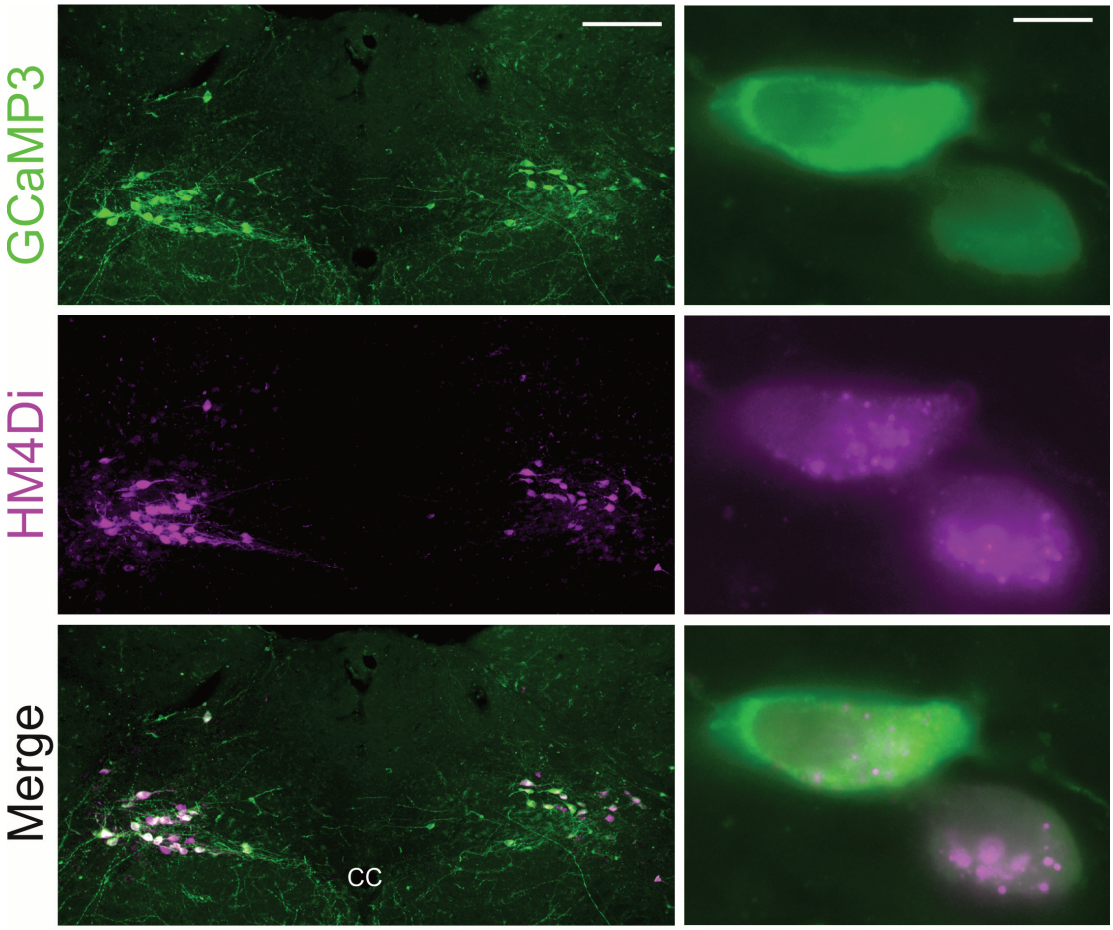

Fig 4.11 Selective expression of HM4Di:mCherry in NTS PPG neurons. Immunofluorescence images showing expression of HM4Di:mCherry in PPG neurons in the NTS. HM4Di:mCherry expression was detected using an anti-dsRed antibody, displayed in magenta. PPG neurons expressing GCaMP3 were detected using an anti-GFP antibody and are shown in green. Low magnification images (scale bar: 100 µm) are shown on the left. High magnification images (scale bar: 10 µm) are shown on the right.

Two weeks days after stereotaxic surgery, mice were habituated to i.p. injection and food intake measurements until the stress of handling no longer affected food intake and body weight (Ellacott et al. 2010). Following habituation, food intake was measured as before.

Cumulative food intake did not vary between any of the groups and PPG inhibition had no effect on food intake (Fig 4.12A). There was no three-way interaction between virus, drug and time (Table 4.1, p=0.84). In addition, there were no significant two-way interactions and only one significant main effect was found: a main effect of time (p<0.0001) as expected from cumulative food intake data. There was also no effect of PPG inhibition on daily chow intake (Fig 4.12B).

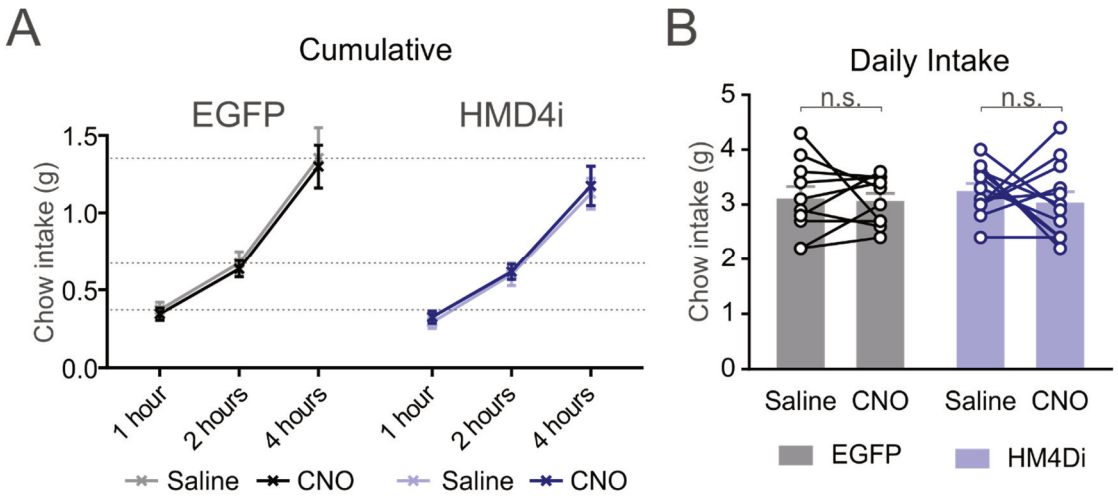

Fig 4.12 Acute inhibition of NTS PPG neurons does not affect cumulative food intake. A) EGFP (black and grey) and HM4Di-expressing (blue) mice were injected i.p. with 2 mg/kg CNO or saline 30 mins before dark onset and food intake was measured one, two, and four hours later. Cumulative data are shown here as mean±SEM. **B)** Daily food intake following 2 mg/kg CNO in EGFP (grey, N=10) and HM4Di (blue, N=12) mice. Data from individual mice are shown as circles and paired data connected with lines. One EGFP animal was excluded as an outlier as described in Materials and Methods. n.s.: not significant.

Source of variability	F statistic	p-value	Significance
Time x Virus x Drug	F(1.249, 26.229) = 0.074	p=0.841	n.s.
Time x Virus	F(1.1859, 40) = 0.058	p=0.933	n.s.
Time x Drug	F(1.249, 26.229) = 0.016	p=0.938	n.s.
Virus x Drug	F(1, 21) = 0.304	p=0.587	n.s.
Time	F(1.149, 24.123) = 132.918	p>0.001	***
Drug	F(1, 21) = 0.002	p=0.964	n.s.
Virus	F(1, 21) = 1.188	p=0.288	n.s.

Table 4.1 Three-way mixed model ANOVA result of HM4Di cumulative data. Data failed Mauchly's test of sphericity and Greenhouse-Geisser adjustment was applied. N=10 (EGFP), N=12 (HM4Di). One EGFP animal was excluded as an outlier as described in Materials and Methods. n.s.: not significant.

Fig 4.13 shows the non-cumulative food intake data from the same experiment. In accordance with the data shown above there were no obvious differences between the groups. Control and HM4Di-expressing mice ate similar amounts of chow under both saline and CNO conditions. As with the cumulative data, there was no three-way interaction time x virus x drug, no two-way interactions were found and only one main effect: time ($p<0.0001$) (Table 4.2). These data provide two important conclusions:

1) Expression of HM4Di in the absence of CNO does not affect feeding.
2) Acute PPG inhibition has no impact on feeding during the dark phase.

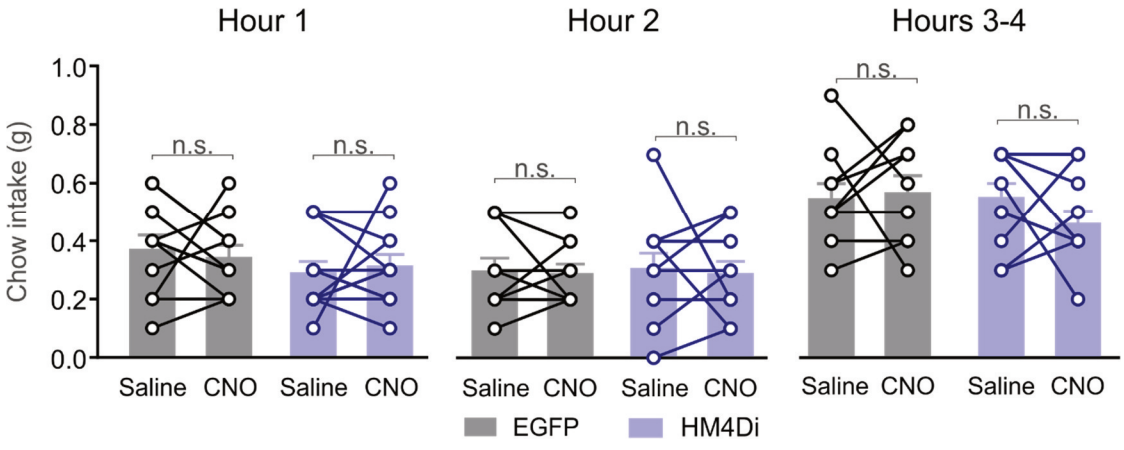

Fig 4.13 Acute inhibition of NTS PPG neurons does not affect feeding. Non-cumulative chow intake during hour one, two and hours 3-4 after dark onset. Both EGFP (grey) and HM4Di (blue) mice were injected with 2 mg/kg CNO 30 mins before dark onset. N=10 (EGFP), N=12 (HM4Di). One EGFP animal was excluded as an outlier as described in Materials and Methods. n.s.: Not significant.

Source of variability	F statistic	p-value	Significance
Time x Virus x Drug	F(1.390, 27.793) = 0.061	p=0.881	n.s.
Time x Virus	F(1.863, 37.266) = 0.389	p=0.666	n.s.
Time x Drug	F(1.390, 27.739) = 0.157	p=0.776	n.s.
Virus x Drug	F(1, 20) = 0.045	p=0.834	n.s.
Time	F(1.863, 37.266) = 31.341	p<0.001	***
Drug	F(1, 20) = 0.045	p= 0.834	n.s.
Virus	F(1, 20) = 0.108	p=0.746	n.s.

Table 4.2 Three-way mixed model ANOVA result of HM4Di non-cumulative data. Data failed Mauchly's test of sphericity and the Greenhouse-Geisser adjustment was used. N=10 (EGFP), N=12 (HM4Di). One EGFP animal was excluded as an outlier as described in Materials and Methods. n.s.: not significant.

The data presented here demonstrate that both chronic ablation and acute inactivation of NTS PPG neurons have little impact on food intake during the dark phase, suggesting PPG neurons do not play a role in the regulation of normal feeding. This was surprising, considering the robust effect of activation of PPG neurons on dark onset feeding. It is worth noting that activation with HM3Dq simply demonstrates the sufficiency of PPG neurons in suppressing food intake. It does not prove a role in physiological regulation of appetite. By inhibiting PPG activity in two different ways, I demonstrate here that PPG neuron activity is not necessary for regulation of normal food intake.

4.2.4 PPG neurons regulate hyperphagia following a large meal

I next wondered whether PPG neurons may need stimulation beyond normal feeding to be recruited. In rats, GLP-1-expressing neurons only become significantly activated following a very large meal (Kreisler et al. 2014; Kreisler and Rinaman 2016). I hypothesised that a large meal following a prolonged fast would engage the brain GLP-1 system. If correct, PPG inactivation would increase food intake under these conditions. To investigate this, DTA and control mice were food-deprived for 18 hours to induce energy deficiency and drive feeding. Chow was returned at dark onset and their intake was measured in the following hours as before.

After a prolonged food-deprivation, mice ate larger meals than observed with a short fast of three hours. Following 18 hours without access to food, control animals ate 0.6±0.05 g chow in the first hour compared to 0.4±0.06 g when food-restricted only briefly (Fig 4.14 and Fig 4.10, respectively). Intriguingly, in the first hour, DTA animals ate 0.9±0.11 g with some animals eating as much as 1.2 g of chow (Fig 4.14). Two-way mixed model ANOVA of the non-cumulative data

yielded no significant interaction between time and virus (F(2, 22) = 0.7462, p=0.49) and there was no main effect of time (F(2, 22) = 0.3227, p=0.7276), suggesting intake was similar at all timepoints measured as displayed in Fig 4.14. However, there was a main effect of virus on feeding (F(1, 11) = 6.099, p=0.0311) with DTA animals eating on average 0.18 g more than control animals at each timepoint (hour 1, hour 2, and hours 3-4). The largest effect was seen in hour 1, where DTA animals ate 0.29±0.13 g more than control animals. These data suggest PPG ablated animals eat consistently more following a prolonged fast than control animals.

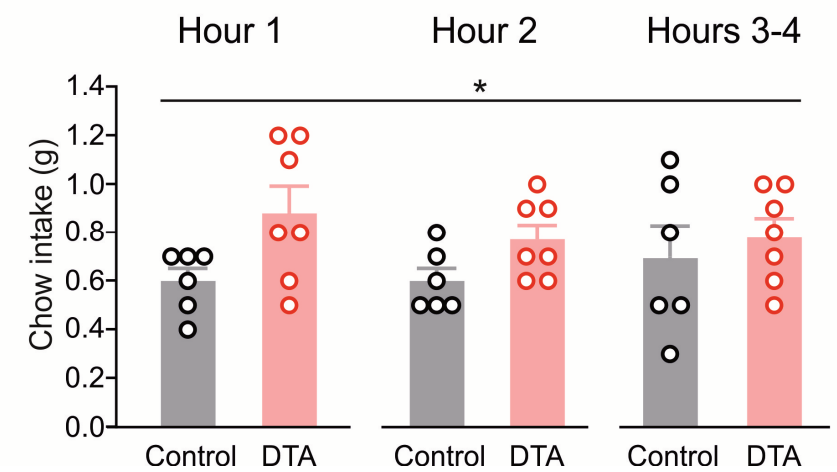

Fig 4.14 Ablation of PPG neurons increases feeding after a prolonged fast. **A)** Food intake of Perceval (control, black, N=6) and DTA (red, N=7) mice following 18 hour fast at hours 1, 2 and 3-4 after dark onset. One control animal was excluded as an outlier as described in Materials and Methods. *p<0.05, main effect of virus according to two-way mixed-model ANOVA. There was no interaction (p=0.49) and no main effect of time (p=0.73).

Turning to the cumulative data, I found that the consistently higher intake over the first hours after dark onset resulted in PPG-ablated animals eating in total 0.54±0.22 g more than control animals over four hours (Fig 4.15A). Two-way mixed model ANOVA yielded no significant interaction (F(2, 22) = 1.81, p=0.19), but a significant main effect of time (F(2, 22) = 215.5, p<0.0001). As with the non-cumulative data, this analysis also revealed a significant effect of virus on feeding (F(1, 11) = 7.994, p=0.016), suggesting that at all timepoints DTA animals had significantly higher intake. In addition, daily chow intake was 0.83 g higher in DTA mice, although this did not reach significance (Fig 4.15B, p=0.056).

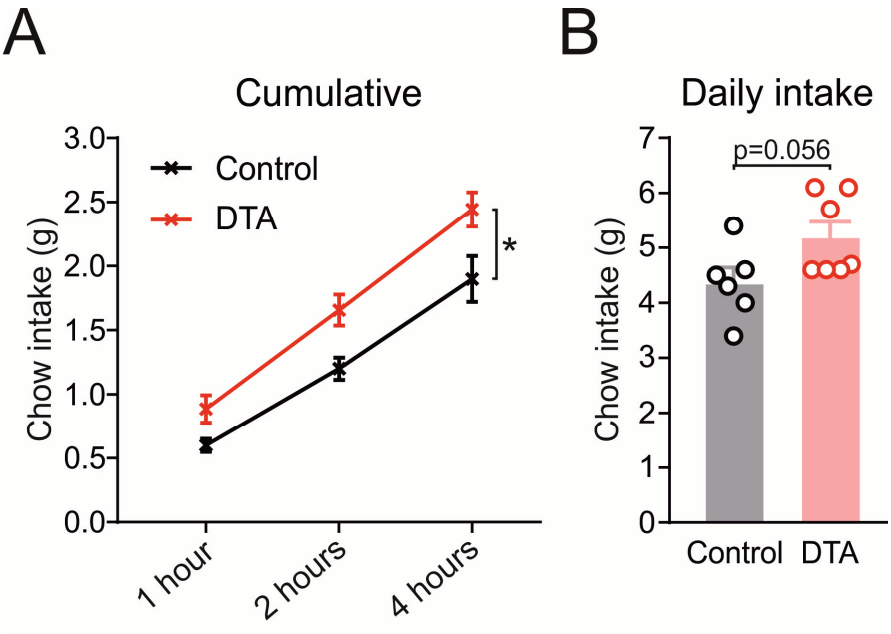

Fig 4.15 Ablation of PPG neurons increases refeeding following prolonged fasting. A) Cumulative food intake of Perceval (control, black, N=6) and DTA (red, N=7) mice following 18-hour fast at one, two and four hours after dark onset. *p<0.05, main effect of virus according to two-way mixed-model ANOVA **B)** Daily chow intake (21 hours post dark onset) following 18 hours fast. Student's t-test. One control animal was excluded as an outlier as described in Materials and Methods

In conclusion, loss of NTS PPG neurons increases normal chow intake over several hours following refeeding after a long fast. These results point to a role for PPG neurons in the prevention of overconsumption. To confirm these findings in a model of acute PPG inhibition, I repeated this experiment in mice expressing HM4Di. Again, to encourage intake of a large meal, I food-deprived mice for 18 hours and injected (i.p.) them with 2 mg/kg CNO or saline 30 mins prior to dark onset.

As in the previous experiment, control mice ate a large meal following a prolonged fast. EGFP mice injected with saline ate 0.85±0.1 g of chow (Fig 4.16), which was substantially more than the 0.37±0.05 g eaten following a brief fast of three hours (Fig 4.13). Similarly, HM4Di mice injected with saline ate 0.68±0.08 g of chow (Fig 4.16) as compared to 0.29±0.04 g after a shorter fast of three hours (Fig 4.13), demonstrating that a prolonged fast drives intake of a larger meal independent of the viral transgene expressed.

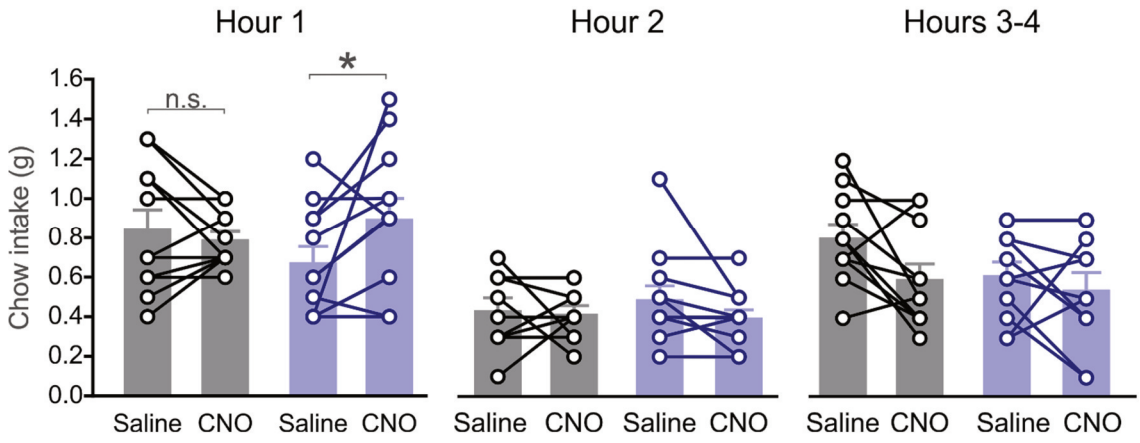

Fig 4.16 The effect of PPG inhibition on hourly food intake following a long fast. A) Non-cumulative food intake of HM4Di mice following 18 hours fast. EGFP (grey, N=11) and HM4Di (blue, N=12) mice were injected with either saline or 2 mg/kg CNO and intake was measured at hours one, two and three-four after dark onset. In the event of a significant interaction virus x drug, main effects were tested post-hoc using Sidak's multiple comparisons test. *p<0.05, n.s.: not significant according to Sidak's multiple comparisons test or two-way mixed model ANOVA.

Source of variability	F statistic	p-value	Significance
Time x Virus x Drug	F(2, 42) = 2.227	p=0.120	n.s.
Time x Virus	F(2, 42) = 1.063	p=0.355	n.s.
Time x Drug	F(2, 42) = 2.569	p=0.089	n.s.
Virus x Drug	F(1, 21) = 5.369	p=0.031	*
Time	F(2, 42) = 23.635	p<0.001	***
Drug	F(1, 21) = 0.588	p= 0.452	n.s.
Virus	F(1, 21) = 0.838	p=0.370	n.s.

Table 4.3 Three-way mixed model ANOVA result of HM4Di refeeding non-cumulative data. Data passed Mauchly's test of sphericity. N=11 (EGFP) and N=12 (HM4Di). n.s.: not significant.

The effect of acute PPG inhibition on refeeding after a long fast was less pronounced and shorter-lived than that of chronic ablation (Fig 4.16 and Fig 4.14). There was no significant three-way interaction between drug, time, and virus (Table 4.3, p=0.120). However, the analysis revealed a significant two-way interaction between virus and drug (p=0.031), suggesting the effect of CNO varies between EGFP- and HM4Di-expressing mice. This interaction is difficult to interpret independently of time, so I analysed each timepoint individually.

During hour 1, HM4Di mice ate 0.23±0.1 g more after PPG inhibition than after a saline injection (Fig 4.16 Hour 1). Two-way mixed-model ANOVA revealed a statistically significant interaction between virus and drug ($F(1, 21) = 4.733$, $p=0.0411$). At this timepoint, CNO did not affect food intake in the EGFP group ($p=0.81$). In contrast, HM4Di-expressing mice had significantly higher intakes after CNO compared to saline ($p=0.038$), demonstrating that inhibition of PPG neurons leads to increased food intake following a long fast. There were no significant interactions and no significant main effects on chow intake at hour 2 and hours 3-4 (Fig 4.16). These data suggest the effect of acute inhibition of PPG neurons on refeeding following a long fast is limited to the first hour following dark onset.

To confirm the effect of PPG inhibition is sustained over several hours, I inspected the cumulative data. Intake was increased over four hours after dark phase in the PPG inhibited animals as compared to HM4Di animals injected with saline only (Fig 4.17A). In contrast, EGFP animals injected with CNO did not increase their food intake.

There was no three-way interaction between virus, drug, and time (Table 4.4, $p=0.194$). There was, however, two significant two-way interactions: time x drug ($p=0.043$) and drug x virus ($p=0.039$). I therefore conducted further two-way ANOVAs at each timepoint, which revealed a significant interaction between virus and drug at hour 1, corresponding to what was seen in the non-cumulative data in Fig 4.16 (($F(1, 21) = 4.733$, $p=0.0411$). There was no difference two and four hours after dark onset, suggesting the effect of PPG inhibition is not sustained over several hours. Similarly, there was no effect of PPG inhibition on 21-hour chow intake (Fig 4.17B).

These results support the data from the previous experiment, in which ablation of NTS PPG neurons increased dark onset feeding following a long fast. Based on these sets of data, I conclude that, although PPG neurons may not be important in the regulation of normal feeding, a large meal following a long fast recruits NTS PPG neurons to suppress feeding. Importantly, both PPG ablation and acute inhibition resulted in increased chow intake following a long fast.

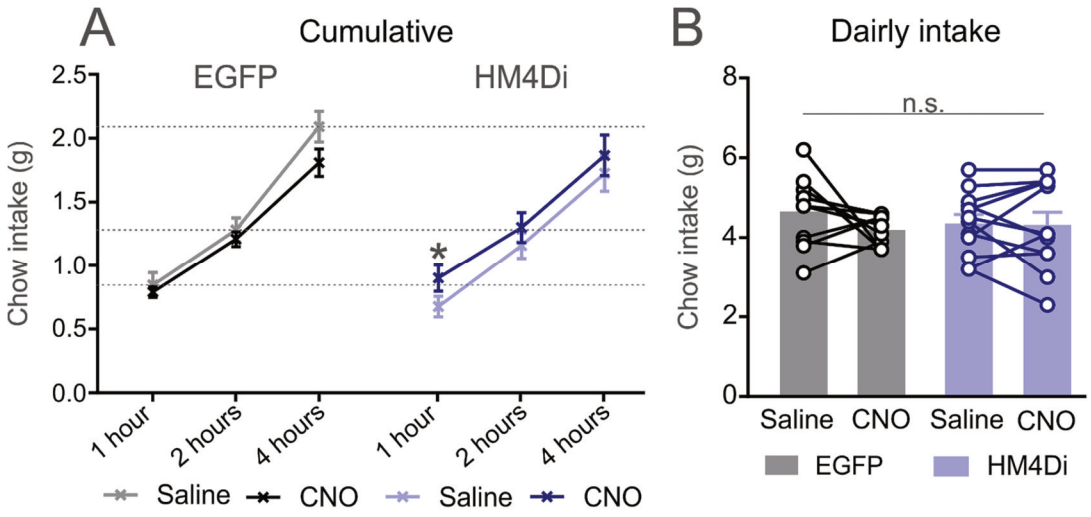

Fig 4.17 The effect of PPG inhibition on food intake following a long fast. A) Cumulative food intake of HM4Di mice following 18-hour fast. EGFP (N=11, black and grey) and HM4Di (N=12, light and dark blue) mice were injected with either saline (grey and light blue) or 2 mg/kg CNO (black and dark blue) and intake was measured at one, two and four hours after dark onset. **B)** Daily chow intake (21 hours post dark onset) following 18 hours fast in EGFP (grey, N=11) and HM4Di (blue, N=12) animals. *p<0.05 according to Sidak's multiple comparisons test. n.s.: no significant interaction or main effects according to two-way ANOVA.

Source of variability	F statistic	p-value	Significance
Time x Virus x Drug	F(1.488, 31.257) = 1.761	p=0.194	n.s.
Time x Virus	F(1.359, 28.541) = 1-486	p=0.240	n.s.
Time x Drug	F(1.488, 31.257) = 3.859	p=0.043	*
Virus x Drug	F(1, 21) = 4.859	p=0.039	*
Time	F(1.359, 28.541) = 299.694	p<0.001	***
Drug	F(1, 21) = 0.057	p= 0.814	n.s.
Virus	F(1, 21) = 0.303	p=0.588	n.s.

Table 4.4 Three-way mixed model ANOVA result of HM4Di refeeding cumulative data. Data did not pass Mauchly's test of sphericity and the Greenhouse-Geisser adjustment was used. N=11 (EGFP) and N=12 (HM4Di). n.s.: not significant. *p<0.05 ****p<0.0001.

4.2.5 PPG ablation blunts preload-induced hypophagia

From the data shown here, we know that PPG neurons are sufficient but not necessary for suppression of feeding during dark onset. It is also clear from two experiments involving inhibition of endogenous PPG activity that prolonged food-deprivation can encourage the intake of a large meal and that this may recruit PPG neurons to limit overeating. The next experiment

confirms that a large meal activates NTS PPG neurons. I encouraged intake of a large meal, in this experiment not by fasting the mice for a long time, but by providing them with highly-palatable diet before measuring chow intake. Ensure liquid diet tastes of vanilla and mice are quickly habituated to drinking a large amount over a short period of time.

To start, animals were trained to consume a large preload of Ensure. DTA and control mice were fasted for three hours and given Ensure in place of drinking water for 15 mins at dark onset. During the first training session, DTA and control mice drank 0.45±0.06 g of Ensure (Fig 4.18A). At this stage, there was no difference in the consumption of Ensure between the two groups (p=0.31). The intake increased during the following three sessions and stabilised at 1.4±0.04 g. After stabilisation of preload intake, there was still no difference in the intake between DTA and control mice (Fig 4.18B, p=0.70).

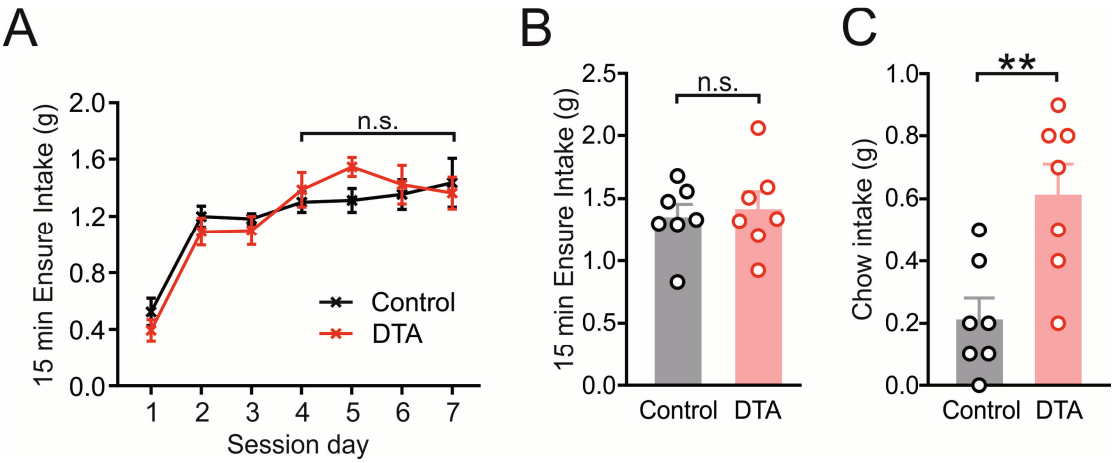

Fig 4.18 PPG ablation increases chow intake following a preload. A) Training of control (black, N=7) and DTA (red, N=7) mice to drink Ensure over 15 mins at dark onset. **B)** 15 mins Ensure intake in control (grey) and DTA (red) mice at dark onset. n.s.: no significant interaction or main effects according to two-way ANOVA. **C)** Chow intake one hour after 15 mins Ensure preload. **p<0.01 according to Student's t-test.

Following 15 mins of Ensure access, the liquid diet was removed and water and chow returned to the cages. An hour later, chow intake was measured. Intake was lower in the control group than usually seen for the first hour of dark phase with control mice eating roughly half their normal intake (Fig 4.18C, 0.21±0.06 g in comparison with 0.4±0.06 g as in Fig 4.10). In contrast, DTA animals ate significantly more than control animals with 0.61±0.1 g of chow eaten in the hour following the Ensure preload (Fig 4.18C, p=0.0052).

I conclude from these data that a large meal at dark onset decreases food intake in the following hour as would be expected if satiety systems are engaged. However, this decrease was only seen in control animals. In animals lacking NTS PPG neurons, intake was higher. Interestingly, the

intake of Ensure, a highly palatable diet, was itself unaffected by the lack of NTS PPG neurons, which could suggest that these neurons are not involved in the regulation of hedonic feeding in mice, although this would need further experimental evidence. Importantly, these results confirm the previous study in which DTA mice were less sensitive to satiety elicited by the intake of a large meal after a long fast. Taken together this suggests NTS PPG neurons could play a role in the prevention of overeating, and may be less essential in the control of normal feeding.

4.2.6 Central GLP-1 drives stress-induced hypophagia

Evidence is mounting for a role of central GLP-1 in the regulation of stress (Ghosal et al. 2013; Maniscalco et al. 2015; Holt and Trapp 2016; Kreisler and Rinaman 2016). When subjected to acute restraint stress, rats suppress their food intake significantly (Krahn et al. 1990). Interestingly, restraint stress is known to activate GLP-1-producing neurons in the rat (Maniscalco et al. 2015). On this basis, I hypothesised acute restraint stress activates NTS PPG neurons which release GLP-1 into forebrain nuclei leading to a reduction in food intake (Fig 4.19).

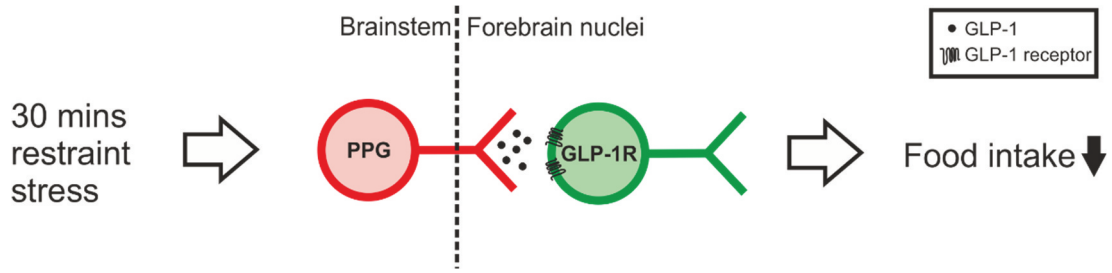

Fig 4.19 Hypothesis of PPG neuron control of stress-induced hypophagia. Restraint stress for 30 mins activates NTS PPG neurons, which then release GLP-1 (and co-transmitters) into forebrain nuclei. Activation of GLP-1 and co-transmitter receptors ultimately leads to a decrease in food intake.

To test this hypothesis, I returned to the acute inhibition model using HM4Di. The same 23 mice expressing either HM4Di or EGFP were exposed to acute stress in the following way: Food was removed three hours before dark onset. 45 mins prior to dark onset all animals were injected with 2 mg/kg CNO. The experiment was designed without a control injection of saline so as to only expose animals to stress once. Importantly, earlier experiments confirmed that injection of 2 mg/kg CNO alone does not affect chow intake in mice expressing a control virus (Fig 4.4 and 4.13). Half an hour before dark onset (15 mins after the injection of 2 mg/kg CNO), mice were either left undisturbed in their cages or exposed to restraint stress. For stress exposure, mice were placed tightly in transparent conical plastic bags with a breathing hole at the front as described in Materials and Methods. Their movement was restricted this way for 30 mins. At dark onset, all mice were returned to their cages and given chow.

Acute restraint stress was sufficient to reduce dark onset feeding over four hours in the EGFP group (Fig 4.20A). A two-way within-subjects ANOVA revealed a significant effect of both time ($F(2, 16) = 123.9$, $p<0.0001$) and stress ($F(1, 8) = 14.14$, $p=0.0055$), but no interaction between the two ($F(2, 16) = 0.4299$, $p=0.6578$). In contrast, HM4Di mice exposed to stress on average did not reduce their intake with mice eating only 4±8 % less at each of the three timepoints following restraint stress (Fig 4.20A). Indeed, a two-way within-subjects ANOVA revealed a significant effect of time ($F(2, 22) = 134.5$, $p<0.0001$), but no effect of stress ($F(1, 11) = 0.8684$, $p=0.37$) and no interaction between the two ($F(2, 22) = 0.212$, $p=0.81$). These data suggest that acute stress does not suppress feeding in the absence of PPG activity.

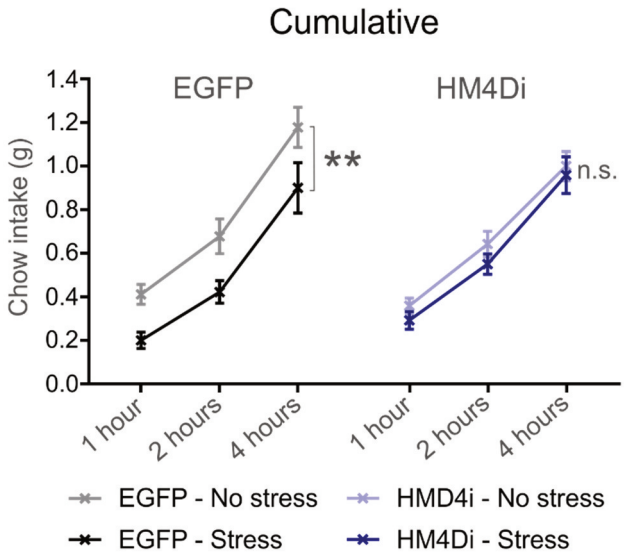

Fig 4.20 Acute stress reduces food intake in control animals, an effect which was attenuated in PPG inhibited mice. 30 mins restraint stress induced clear hypophagia sustained over four hours in EGFP mice (in grey and black, N=9), but not in HM4Di (light and dark blue, N=12) mice. Data from two EGFP mice were as outliers as described in Materials and Methods. **p<0.01, n.s.: not significant, main effect of stress (two-way ANOVA).

To further investigate at which timepoints the effect of PPG inhibition is most pronounced, I investigated the non-cumulative data (Fig 4.21). Three-way ANOVA did not reveal a significant interaction between time, virus, and stress (Table 4.5, $p=0.51$). There was however a significant two-way interaction between stress and time (Table 4.5, $p=0.041$).

At hour 1, there was a significant interaction between stress and virus ($F(1, 19) = 4.906$, $p=0.0392$). Acute stress suppressed food intake in EGFP mice by 50±8 % ($p=0.0008$). In contrast, there was no effect of stress in the HM4Di group in the first hour ($p=0.2516$). There was no interaction between stress and virus at hours 2 and 3-4 ($F(1, 19) = 0.09128$, $p=0.7658$ and $F(1, 18) = 0.08055$, $p=0.7798$, respectively) and the effect of stress had disappeared in hour 2 and hours 3-4 ($F(1, 19) = 1.164$, $p=0.2941$ and $F(1, 19) = 0.05775$, $p=0.8127$, respectively).

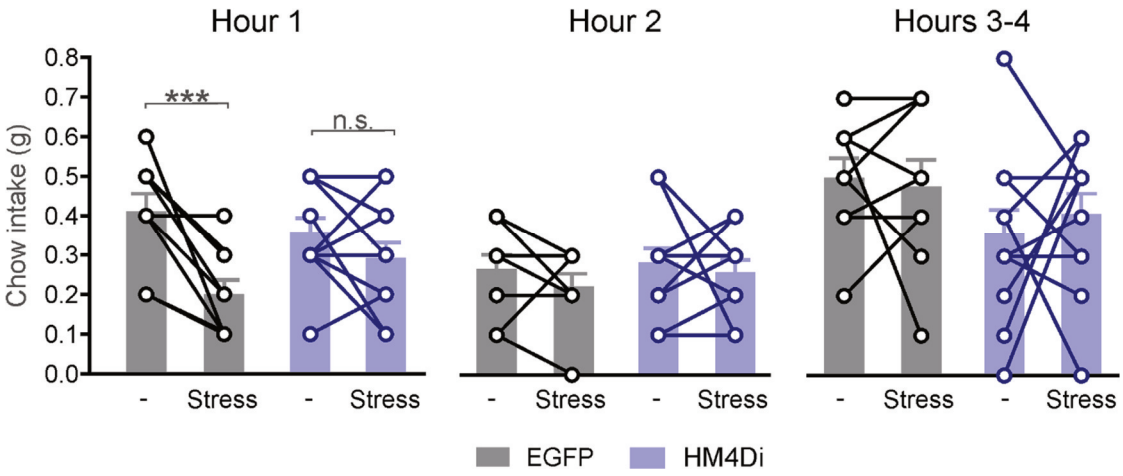

Fig 4.21 PPG inhibition suppresses stress-induced hypophagia. Non-cumulative data from hours 1, 2, and 3-4 after onset of dark. EGFP (grey, N=9) and HM4Di (blue, N=12) mice were left undisturbed (-) or exposed to acute restraint stress for 30 mins prior to dark phase. All animals were injected with 2 mg/kg CNO. Data from two EGFP mice were excluded as outliers as described in Materials and Methods. In the event of a significant interaction stress x virus, effects were tested using Sidak's multiple comparisons test. n.s.: not significant. *p<0.05, ***p<0.001.

Source of variability	F statistic	p-value	Significance
Time x Virus x Stress	F(1.583, 30.08) = 0.625	p=0.506	n.s.
Time x Virus	F(1.581, 30.031) =2.654	p=0.098	n.s.
Time x Stress	F(1.583, 30.08) = 3.869	p=0.041	*
Virus x Stress	F(1, 19) = 2.029	p=0.171	n.s.
Time	F(1.581, 30.031) = 15.970	p<0.0001	****
Stress	F(1, 19) = 3.714	p= 0.069	n.s.
Virus	F(1, 19) = 0.396	p=0.537	n.s.

Table 4.5 Three-way mixed model ANOVA result of HM4Di and EGFP non-cumulative data under acute stress. Data from hour 1, hour 2, and hours 3-4. The data failed the test of sphericity and the Greenhouse-Geisser adjustment was used. N=9 (EGFP), N=12 (HM4Di). Data from two EGFP mice were excluded as outliers as described in Materials and Methods. n.s.: not significant.

The data shown here suggest that during the first hour following acute stress, PPG activity is necessary for suppression of feeding. Since there was no effect of acute stress on food intake at hours 2 and 3-4 it is difficult to determine whether PPG inhibition would have an effect at those timepoints. These data encourage further exploration of the involvement of NTS PPG neurons in the regulation of stress-induced hypophagia.

Until this point, I have addressed the question of the physiological role of NTS PPG neurons in the regulation of food intake. I have explored different types of feeding: normal dark onset chow intake, intake following a prolonged fast, intake after a large preload of liquid diet, and intake following acute restraint stress. I found that NTS PPG neurons are not involved in regulation of normal feeding, but that after certain challenges, such as a very large meal or following acute stress, PPG neurons play a role in satiety.

4.2.7 Neurons in the dLS express GLP-1R

Having revealed a possible role for PPG neurons in stress-induced hypophagia, I was interested in the relevant downstream targets of PPG neurons. As discussed in the Introduction, PPG neurons project widely and GLP-1Rs are found throughout the brain. Of particular interest for this study was the dLS, due to its established involvement in the regulation of stress, fear, and anxiety (Reis et al. 2010; Singewald et al. 2011; Anthony et al. 2014) and its ability to suppress feeding in response to GLP-1 (Terrill et al. 2016).

To investigate the importance of dLS GLP-1Rs in stress-induced hypophagia, I used another transgenic mouse strain, GLP-1R-Cre/tdRFP, which expresses Cre under the control of the GLP-1R promoter (Richards et al. 2014; Cork et al. 2015). In these mice, GLP-1R-expressing cells also produce Cre and consequently the fluorescent reporter tdRFP (Luche et al. 2007) as explained in the Introduction. This model allows both visualisation of these cells via tdRFP and selective transgene expression using Cre-dependent viruses. We have previously shown that GLP-1R-expressing cells are located throughout the dLS (Cork et al. 2015).

To be able to further characterise these cells, anatomically and functionally, I created and produced a rAAV encoding the GCaMP3 open reading frame (ORF) in a Cre-dependent manner. The GCaMP3 ORF was cloned into the Cre-dependent plasmid, pAAV-CBA-FLEX (Murray et al. 2011) as shown in Fig 4.22.

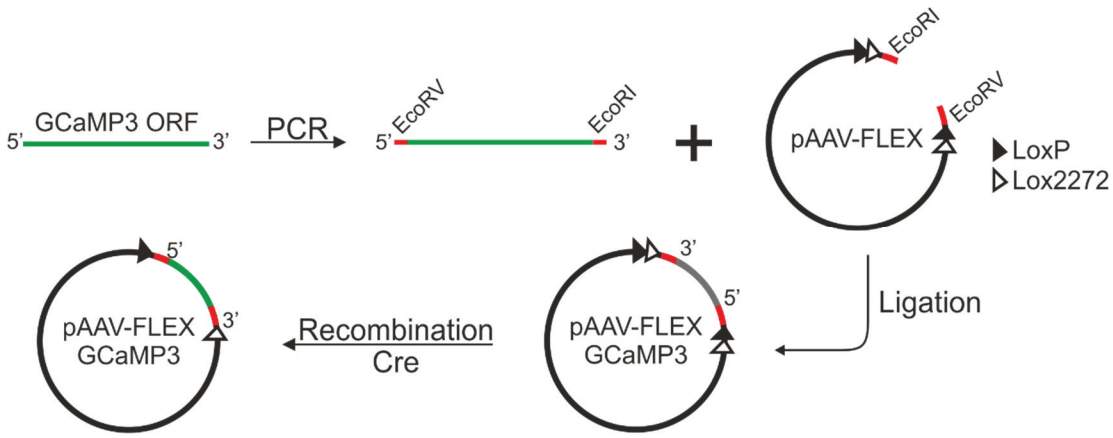

Fig 4.22 Cloning strategy for creating Cre-dependent pAAV-FLEX-GCaMP3. The GCaMP3 ORF was amplified from PPG-Cre/GCaMP3 brainstem tissue. Restriction enzyme sites were incorporated at the time of ORF amplification. EcoRV was added to the 5' end, whereas EcoRI was added to the 3' end of the amplicon. The GCaMP3 ORF was ligated into the backbone so that the ORF was in the reverse orientation with relation to the promoter ensuring that no functional GCaMP3 protein would be produced in the absence of Cre. In the presence of Cre, two recombination events between lox sites lead to inversion of the GCaMP3 ORF and successful expression of the protein. Sequencing of the flanking regions and insert confirmed correct (reverse) orientation of the insert.

rAAV particles were packaged in AD293T cells and purified on a heparin column as described in Materials and Methods. The purified virus was injected into the NTS of PPG-Cre/tdRFP mice to confirm Cre-dependent expression. Images in Fig 4.23 are representative images from live brainstem slices showing four tdRFP- and GCaMP3-expressing cells in the NTS. Expression of tdRFP filled the cell bodies of PPG neurons in the NTS. As with the transgenic PPG-Cre/GCaMP3 mouse, GCaMP3 expression was seen throughout the cytosol and was excluded from the nucleus (Fig 4.23). There was no expression of GCaMP3 in tdRFP-negative cells.

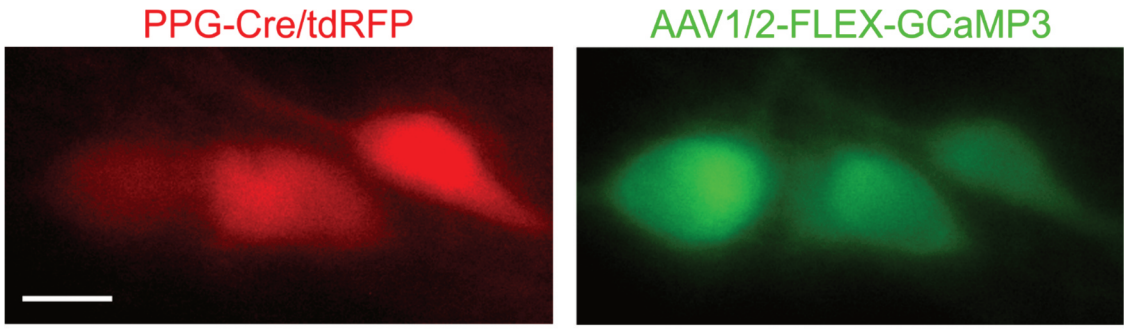

Fig 4.23 Selective expression of AAV1/2-FLEX-GCaMP3 in NTS PPG neurons. Live brainstem slice with four cells co-expressing the fluorescent reporter tdRFP (red, left) and the viral transgene GCaMP3 (green, right). GCaMP3 expression was strongest in the cytoplasm and was largely excluded from the nucleus. Scale bar: 10 µm.

To confirm functionality of the GCaMP3 construct, I exposed *in vitro* brainstem slices to 100 µM glutamate and monitored GCaMP3 fluorescence intensity as a surrogate marker for neuronal

activity. Fig 4.24A shows a representative cell responding to 100 µM glutamate with an increase in intracellular [Ca^{2+}]. As seen in Fig 4.24B, fluorescence intensity decreased after washout of glutamate. However, cytosolic [Ca^{2+}] did not immediately return to baseline. The response to glutamate was biphasic with an initial peak in fluorescence followed by a slight decrease and a second smaller peak. Increases in intracellular Ca^{2+} were observed in five independent PPG neurons with a median peak response of 0.7 $\Delta F/F_0$, confirming that expression of GCaMP3 from a viral vector can be used to monitor intracellular [Ca^{2+}] as seen with the transgenic model PPG-Cre/GCaMP3 in Chapter 3.

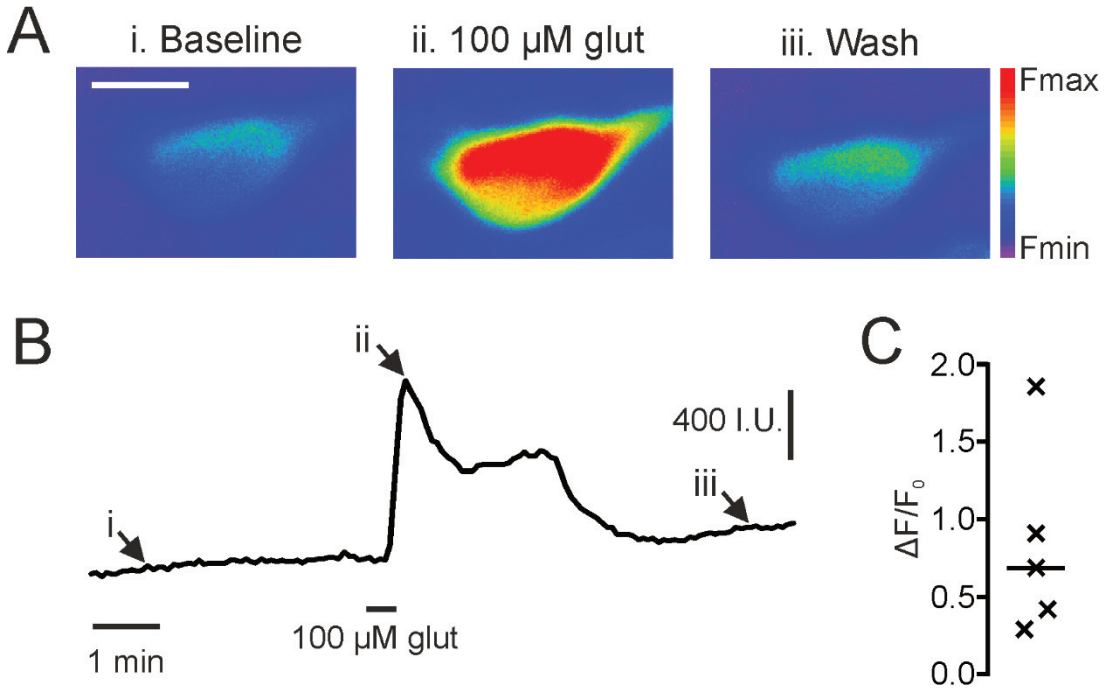

Fig 4.24 Representative PPG neuron responding to 100 µM glutamate with an increase in intracellular [Ca^{2+}]. A) Images of live brainstem slice with one pseudocoloured PPG neuron transduced with AAV1/2-FLEX-GCaMP3. During baseline (i. Baseline), glutamate (ii. 100 µM glut) and after washout of glut (iii. Wash). Scale bar: 10 µm. **B)** Trace showing fluorescence intensity changes of cell in A). i, ii and iii indicate timepoints shown in A). I.U.: Intensity units. **C)** Relative change in fluorescence intensity from baseline following stimulation with 100 µM glutamate in five cells from one mouse shown as individual data points. The line indicates the median.

Next, I set out to investigate the properties of GLP-1R-expressing neurons in the dLS. I first confirmed that GCaMP3 can be successfully expressed from the viral vector in dLS GLP-1R-expressing neurons. I unilaterally injected GLP-1R-Cre/tdRFP mice with AAV1/2-FLEX-GCaMP3 into the dLS. Three weeks days later, the mice were transcardially perfuse-fixed and coronal sections were stained for both tdRFP and GCaMP3. Fig 4.25 shows the overlapping expression of tdRFP and GCaMP3 at two sites of the dLS along the rostrocaudal axis. At both sites, dLS GLP-1R-producing neurons were expressing GCaMP3. Not all tdRFP positive neurons were also

positive for GCaMP3, in particular those in the more dorsal part of the dLS, suggesting the virus had not spread throughout the entire dLS.

A few neurons were found to be GCaMP3-positive, but tdRFP-negative. The Cre-dependence of GCaMP3-expression from the AAV1/2-FLEX-GCaMP3 construct was confirmed both in HEK293 cells *in vitro* and in sections from animals stereotaxically injected into the NTS with AAV1/2-FLEX-GCaMP3, suggesting this is not the cause of GCaMP3 expression in cells seemingly not expressing GLP-1R. Rather I propose that overexpression of a virally delivered transgene leads to a decrease in expression of the other fluorescent reporter. I have observed this phenomenon using several different constructs. As mentioned previously, when discussing the expression of HM4Di:mCherry in PPG neurons, this could imply that transgene overexpression from viral particles leads to suppression of expression of other proteins. The implications for cell function are not known, although both PPG and dLS GLP-1R cells were still responsive to activation and I have not observed any *in vivo* phenotypes of viral transduction (Fig 4.24 and 4.26).

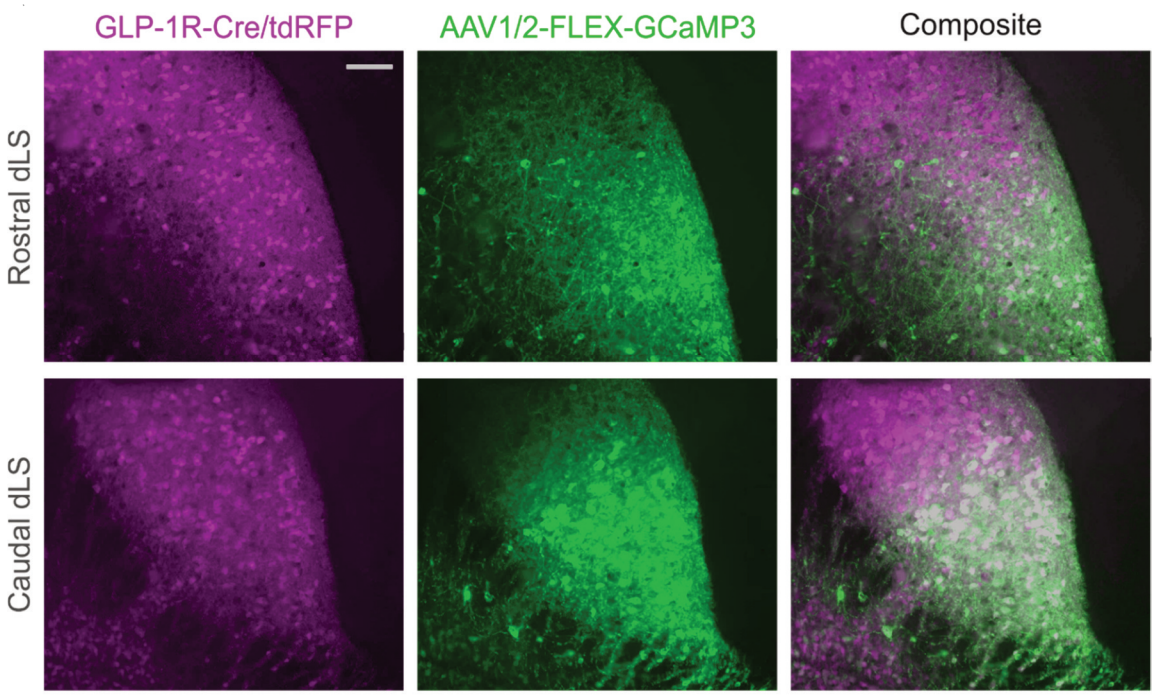

Fig 4.25 Selective expression of AAV1/2-FLEX-GCaMP3 in dLS GLP-1R neurons. Immunostaining of GLP-1R-expressing neurons transduced with AAV1/2-FLEX-GCaMP3. Images were taken of both the rostral and caudal dLS. The fluorescent reporter for GLP-1-expressing cells, tdRFP, was detected using an anti-dsRed antibody and is pseudocoloured in magenta. Cre-dependent GCaMP3 expression from AAV1/2-FLEX-GCaMP3 was detected using an anti-GFP antibody and is pseudocoloured in green. Merged images are seen on the right. White colour indicates overlap of magenta and green. Scale bar: 100 µm.

In vitro calcium imaging was performed on GLP-1R-expressing neurons in the dLS with the final aim of determining the responsiveness of these neurons to GLP-1 *in vitro*. GLP-1R-Cre/tdRFP mice were unilaterally injected into the dLS with AAV1/2-FLEX-GCaMP3. Three weeks later, live brainstem sections were obtained and *in vitro* Ca^{2+} imaging was performed. Sections were superfused with ACSF and exposed to 15 mM KCl for 15 s to induce robust depolarisation.

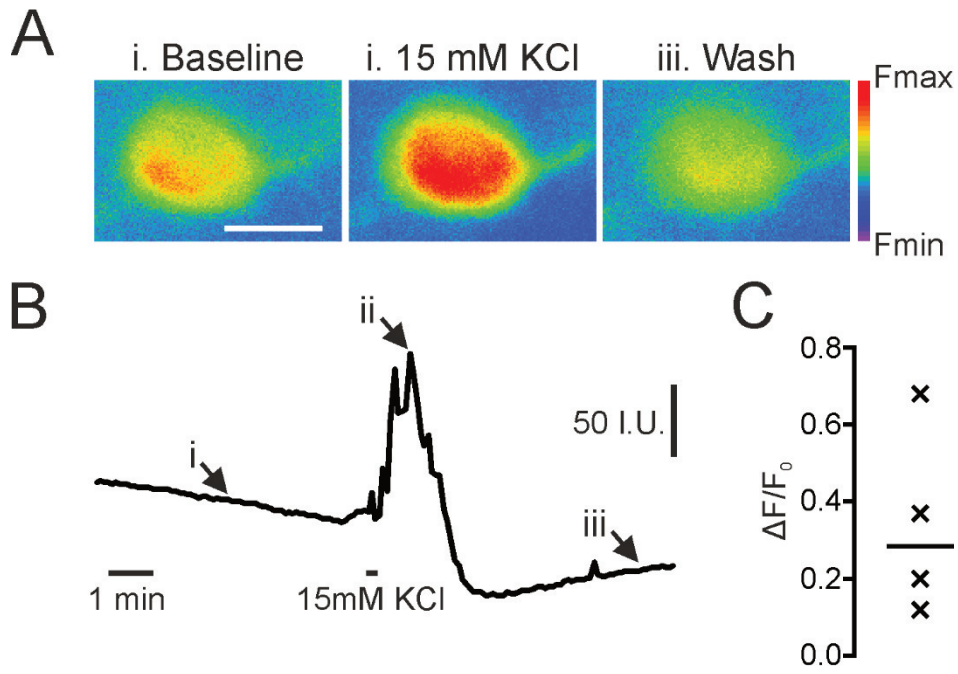

Fig 4.26 *In vitro* Ca^{2+} imaging of dLS GLP-1R-expressing neurons. A) One representative, pseudocoloured dLS GLP-1R-expressing neuron transduced with AAV1/2-FLEX-GCaMP3. Fluorescence intensity is shown before (i. Baseline), during (ii. 15 mM KCl) and after washout of KCl (iii. Wash). Scale bar: 10 µm. **B)** Trace showing fluorescence intensity changes of cell in A). i, ii and iii indicate timepoints shown in A). I.U.: Intensity units. **C)** Relative change in fluorescence intensity from baseline following stimulation with 15 mM KCl in four individual cells shown as data points. The line indicates the median.

Fig 4.26A shows a dLS GLP-1R-expressing neuron responding to 15 mM KCl with an increase in intracellular [Ca^{2+}]. Following washout of KCl intracellular [Ca^{2+}] decreased to levels lower than baseline, presumably due to Ca^{2+} buffering, although some contribution from bleaching cannot be excluded. In Fig 4.26B these changes in intracellular [Ca^{2+}] are clearly seen with 15 mM KCl stimulating a rise in intracellular [Ca^{2+}]. After washout of KCl, intracellular [Ca^{2+}] quickly decreased to a level lower than baseline and slowly recovered towards baseline. Intracellular [Ca^{2+}] was recorded from four different dLS GLP-1R neurons, which all exhibited similar responses to 15 mM KCl with a median peak response of 0.29 $\Delta F/F_0$. These data demonstrate that viral delivery of AAV1/2-FLEX-GCaMP3 is a useful tool to investigate the cellular properties of dLS GLP-1R-expressing neurons. Future experiments should assess the response to GLP-1.

4.2.8 Endogenous GLP-1 in the dLS mediates stress-induced hypophagia

We know from the previous sections that inhibition of NTS PPG neuron activity attenuates the hypophagia following acute restraint stress (Fig 4.20 and Fig 4.21). Next, I investigated whether GLP-1 released into the dLS mediates this hypophagia. The following experiments were conducted at Florida State University in collaboration with Dr Diana Williams. I implanted unilateral cannulae into the dLS as described in Materials and Methods and hypothesised that by inhibiting GLP-1Rs in the dLS, I could attenuate the suppression in food intake following acute stress (Fig 4.27).

As in previous experiments, mice were exposed to restraint stress once. Consequently, the study was a counter-balanced mixed-model design, with drug infusion as the between-subject factor and stress exposure as the within-subject factor. Control mice had infusions of saline and confirmed the ability of acute stress to suppress feeding, a well-known phenomenon (Ellacott et al. 2010; Maniscalco et al. 2015). The experimental group received infusions of 10 µg Ex9.

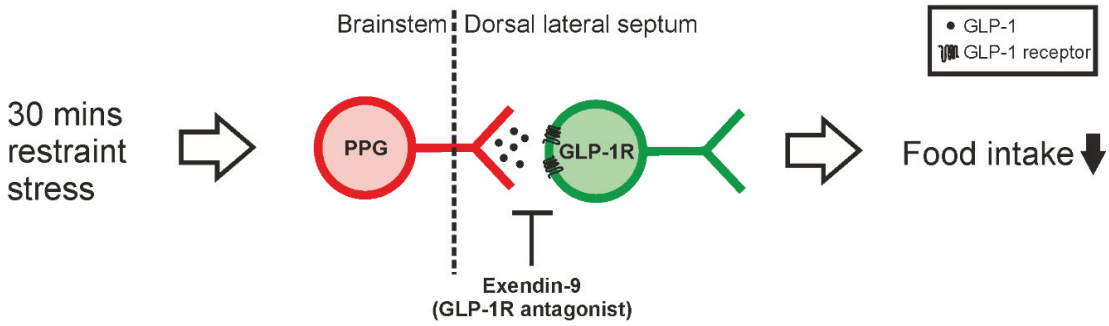

Fig 4.27 Hypothesis for the role of dLS GLP-1 in the hypophagic response to acute stress. 30 mins restraint stress leads to activation of PPG neurons in the caudal brainstem. This results in release of GLP-1 into the dLS. Activation of downstream GLP-1R-expressing neurons (GLP-1R) results in suppression of food intake. I hypothesise that this hypophagia can be blunted by infusing the GLP-1R antagonist Ex9 into the dLS.

Cannula placements were verified at the end of the experiment and only mice with correct placements into the dLS were included in the final analysis. A representative image from one cannulated mouse is shown in Fig 4.28. Damage from the injector is clearly seen on the right hand side at the most dorsal part of the dLS just ventral of the corpus callosum (arrow).

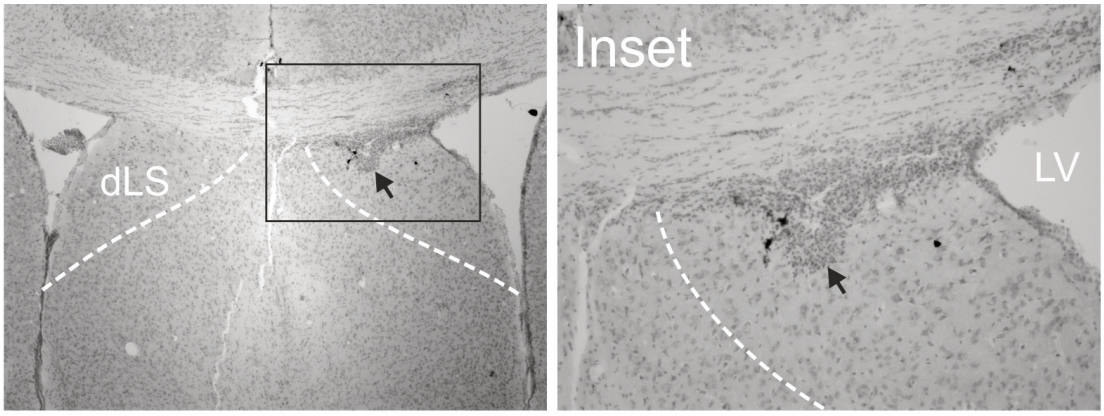

Fig 4.28 Representative cannula placement for infusions into the dLS. Representative image at 4x (left) and 10x (right, inset) magnification. Sections were stained with thionin and images captured on a brightfield microscope. Tissue damage from the injector is indicated with a black arrow just ventral of the corpus callosum. dLS: dorsal lateral septum; LV: lateral ventricle.

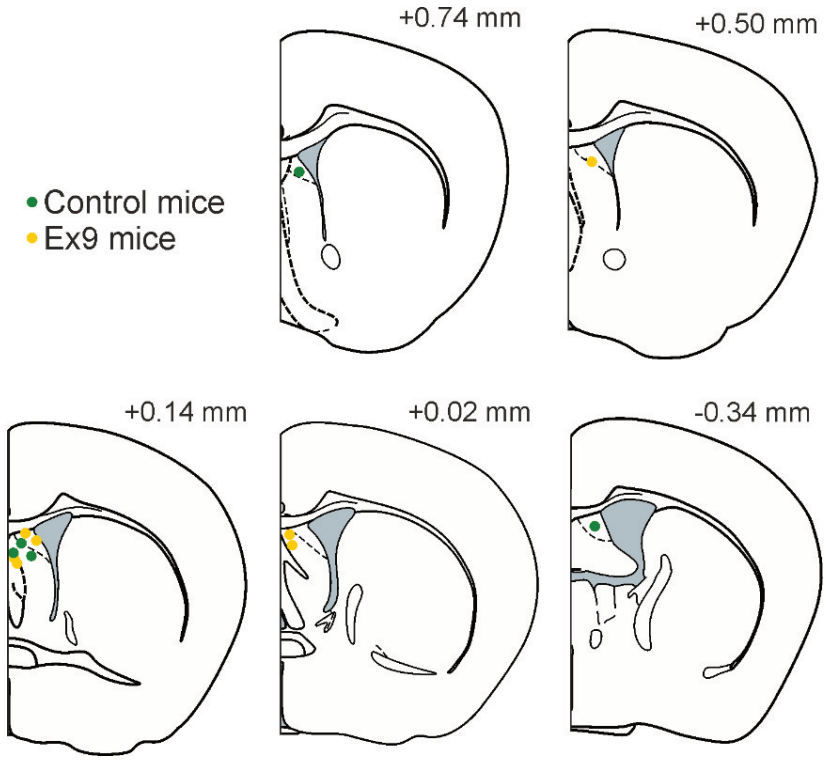

Fig 4.29 Cannula placements for infusions into the dLS. Schematics of forebrain sections containing the dLS and indicating successful targeting of dLS with infusions of either saline (control mice, n=5, green) or Ex9 (Ex9 mice, n=7, yellow). Numbers refer to rostrocaudal distance from Bregma with positive numbers being rostral and negative being caudal of Bregma.

The most ventral damage to tissue created by the injector was located in each mouse. Fig 4.29 shows a schematic of the injector sites in mice included in the final analysis. Data were included from mice with injector damage in the dLS between -0.34 mm and +0.74 mm from Bregma. Five control and three Ex9 mice were excluded on the basis of incorrectly placed cannula implantations.

On each experimental day, mice were fasted for three hours prior to dark onset. Saline or Ex9 were infused 60-45 mins prior to dark onset. Mice were exposed to restraint stress 15 mins later or left undisturbed in their cages. At dark onset, chow was returned. Restraint stress induced a clear reduction in food intake at hours 1, 2, and 3-4 after dark onset in both saline and Ex9-infused mice, confirming again the ability of acute stress to reduce food intake (Fig 4.30). I noted that acute stress had a more sustained suppressive effect on feeding in the experiments conducted at Florida State University than the ones described in section 4.2.5. This is most likely due to differences in the environment and the conical bags used to induce stress.

There was a significant three-way interaction, stress x time x drug treatment (Table 4.6, $p=0.042$) and a significant two-way interaction between drug and stress at hours 5-21 ($F(1, 10) = 6.052$, $p=0.0337$). At this timepoint, stress significantly suppressed intake in saline-treated mice ($p=0.0049$), but failed to affect intake in the Ex9-infused group (Fig 4.30, $p=0.60$). There were no significant two-way interactions at hours 1, 2, and 3-4. Ex9 infusions had no effect on chow intake in the absence of stress ($p=0.35$). These data demonstrate that suppression of endogenous GLP-1 in the dLS does not affect normal feeding, but attenuates the hypophagic response to acute stress at later timepoints.

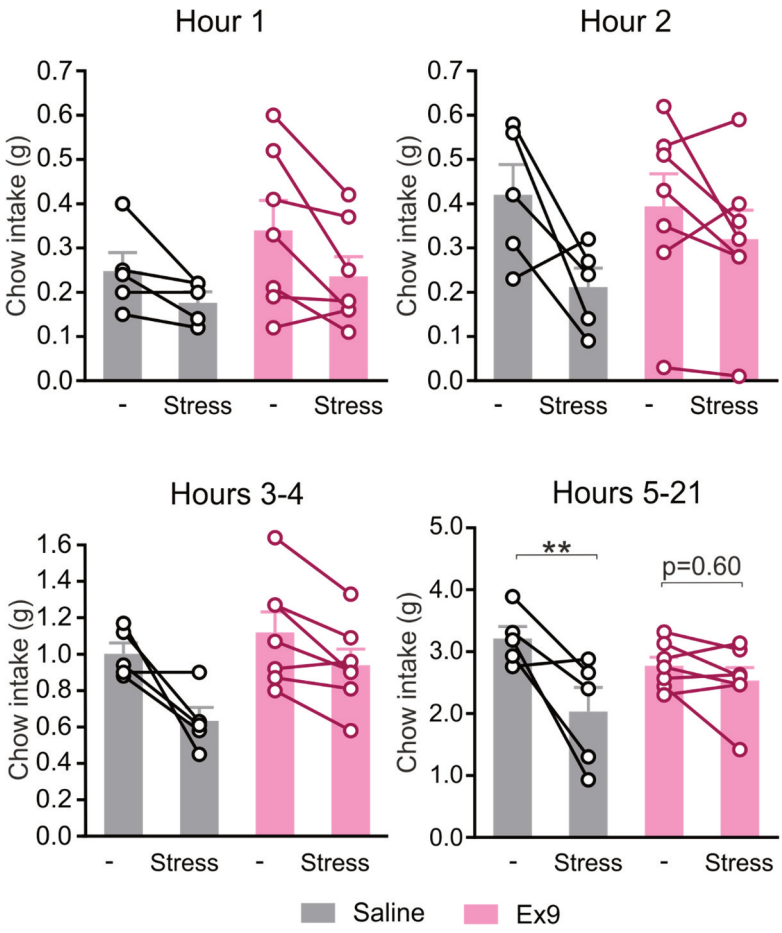

Fig 4.30 Inhibition of dLS GLP-1Rs attenuates stress-induced hypophagia. Effect of restraint stress on non-cumulative food intake at hours 1, 2, 3-4, and 5-21 after dark onset. saline- (grey) and Ex9-infused (magenta) mice were left undisturbed (-) or exposed to acute restraint stress for 30 mins prior to dark phase. N=5 (Saline), N=7 (Ex9). Two-way mixed-model ANOVA was conducted at each timepoint. In the event of a significant interaction stress x drug, main effects were tested post-hoc using Sidak's multiple comparisons test. **p<0.01.

Source of variability	F statistic	p-value	Significance
Time x Drug x Stress	F(1.250, 12.496) = 4.792	p=0.042	*
Time x Drug	F(1.5472, 14.719) =0.295	p=0.682	n.s.
Time x Stress	F(1.250, 12.496) = 7.975	p=0.041	n.s.
Drug x Stress	F(1, 10) = 6.943	p=0.025	*
Time	F(1.472, 14.719) = 205.549	p<0.0001	****
Stress	F(1, 10) = 26.715	P<0.0001	****
Drug	F(1, 10) = 1.157	p=0.307	n.s.

Table 4.6 Three-way mixed model ANOVA result of Ex9 and saline-infusions under acute stress - non-cumulative data. Data from hour 1, hour 2, hours 3-4, and hours 5-21. Data failed the test of sphericity and the Greenhouse-Geisser adjustment was used. N=5 (saline), N=7 (Ex9). n.s.: not significant.

This conclusion was supported by the cumulative data from the same experiment (Fig 4.31A). Acute restraint stress induced hypophagia in saline-infused animals. Food intake remained suppressed overnight (4.31B). The suppression was more pronounced in saline-infused than Ex9-infused mice. In support, there was a significant three-way interaction time x stress x drug treatment (Table 4.7). There were no significant interactions between stress and drug treatment at one, two, and four hours. There was however a significant main effect of stress at all these timepoints, suggesting stress reduces food intake in both saline and Ex9 mice at the beginning of dark phase. In contrast, at 21 hours after dark onset, there was a significant interaction between stress and drug (F(1, 10) = 6.943, p=0.0249). At this late timepoint, there remained an intake-suppressive effect of stress in the saline-infused mice (Fig 4.31B, p=0.0009). In contrast, mice infused with Ex9 exhibited no hypophagia at 21 hours (p=0.15).

These results demonstrate that unilateral infusion of the GLP-1R antagonist, Ex9, into the dLS attenuates stress-induced hypophagia in mice, suggesting endogenous GLP-1 within the dLS is involved in suppression of feeding in response to stress.

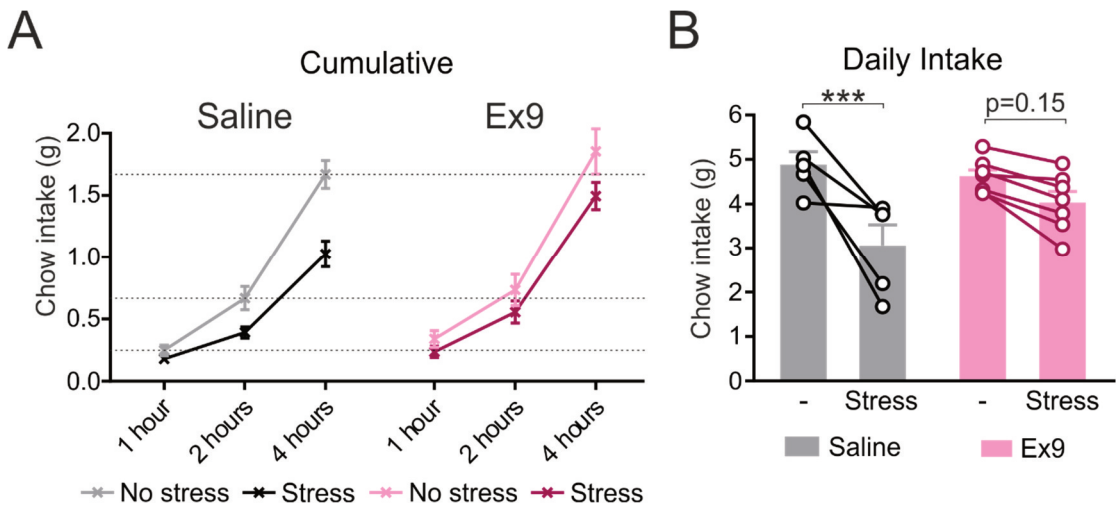

Fig 4.31 Infusion of Ex9 into the dLS attenuates the hypophagic response to acute restraint stress. Mice were infused into the dLS with either saline (N=5) or Ex9 (N=7) and subsequently exposed to 30 mins restraint stress or left in their cages. **A)** Acute stress reduced cumulative food intake over 4 hours in animals infused with saline, but not in animals infused with Ex9. **B)** Daily (21 hours) cumulative food intake was significantly reduced following acute stress in animals infused with saline into the dLS. Inhibition of dLS GLP-1Rs attenuated the stress-induced hypophagia resulting in no effect of stress on daily food intake. Main effects were tested post-hoc using Sidak's multiple comparisons test. ***p<0.001.

Source of variability	F statistic	p-value	Significance
Time x Treatment x Stress	F(1.172, 11.720) = 6.444	p=0.023	*
Time x Treatment	F(1.320, 13.202) =0.729	p=0.446	n.s.
Time x Stress	F(1.172, 11.720) = 19.515	p=0.001	**
Treatment x Stress	F(1, 10) = 5.340	p=0.043	*
Time	F(1.320, 13.203) = 437.298	p<0.001	****
Stress	F(1, 10) = 35.069	P<0.001	****
Treatment	F(1, 10) = 2.424	p=0.151	n.s.

Table 4.7 Three-way mixed model ANOVA result of Ex9 and saline-infusions under acute stress - cumulative data. Data from hour 1, hour 2, hours 3-4, and hours 5-21. Data failed the test of sphericity and the Greenhouse-Geisser adjustment was used. N=5 (saline), N=7 (Ex9). n.s.: not significant.

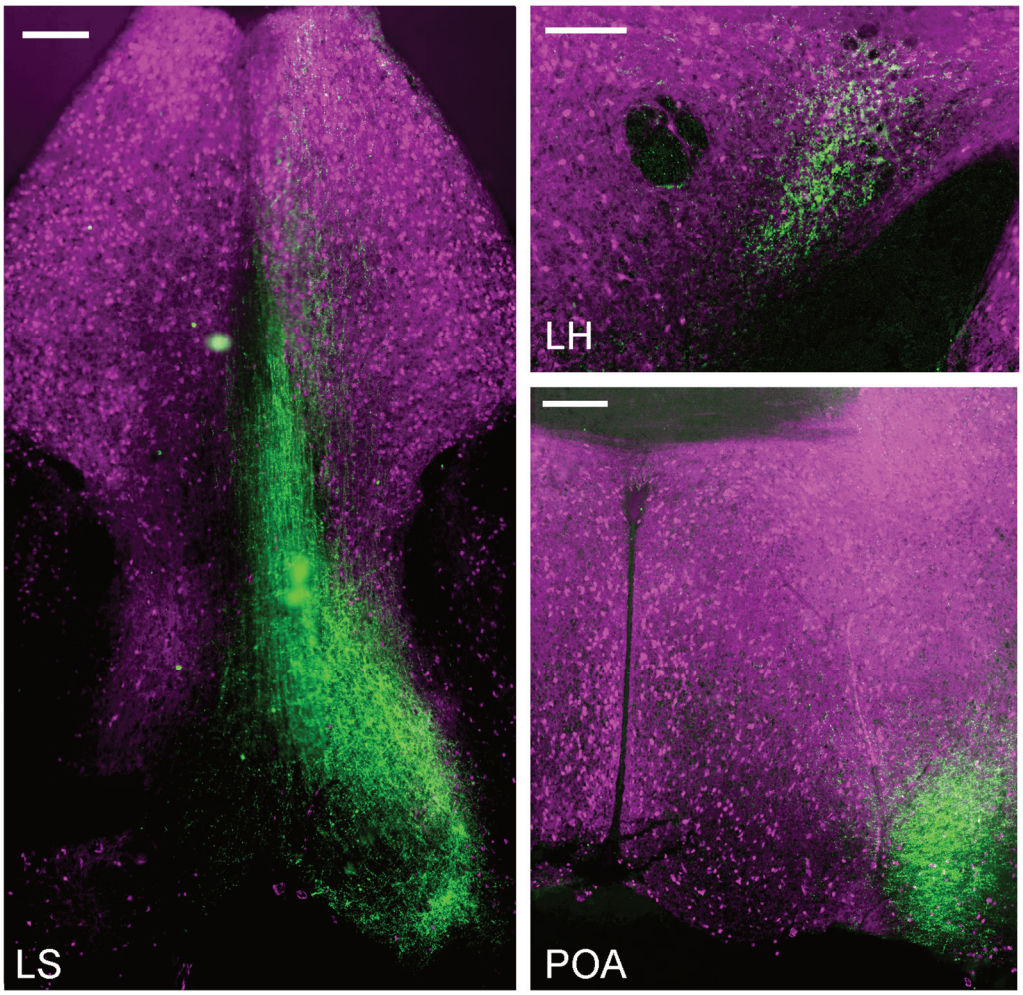

Fig 4.32 Projections of dLS GLP-1R-expressing neurons. Unilateral transduction of dLS GLP-1R-expressing neurons with AAV1/2-FLEX-GCaMP3. See Fig 4.25 for image of transduced dLS cells bodies. Axonal fibres and terminals were identified in the lateral septum (LS), lateral hypothalamus (LH), and the preoptic area of the hypothalamus (POA). GCaMP3-expressing GLP-1R neuronal fibres were detected with an anti-GFP antibody and are shown in green. Expression of tdRFP was detected with an anti-dsRed antibody and is shown in magenta. Scale bars: 200 µm (LS and POA) and 100 µm (LH).

Given the importance of both NTS PPG neurons and dLS GLP-1Rs in the hypophagic response to stress, I was interested in the downstream targets of this stress circuit. Coronal forebrain sections from GLP-1R-Cre/tdRFP mice previously transduced with AAV1/2-FLEX-GCaMP3 were immunostained for tdRFP and GCaMP3 (Fig 4.32).

As shown in Fig 4.25, GCaMP3 was clearly expressed in dLS GLP-1R-expressing neurons. GCaMP3-positive non-varicose axons extended through the intermediate LS and terminated in the preoptic area (POA). GCaMP3-positive axons were also detected in the lateral hypothalamus (LH) (Fig 4.32), whereas no GCaMP3-positive terminals were found in the PVN (not shown). The connections from GLP-1R-expressing neurons in the dLS to these two hypothalamic areas could be important in the physiological responses to stress, including suppression of appetite.

4.3 Discussion

In this chapter, I explored the role of PPG neurons in the regulation of feeding. Chemogenetic activation of PPG neurons robustly suppressed food intake. On the other hand, loss or inhibition of PPG neurons did not increase normal feeding. I discovered that PPG neurons are necessary for satiety following a large meal, suggesting these neurons are mainly involved in the regulation of overeating, not daily feeding. This was further substantiated, when I found that acute restraint stress suppresses food intake in a PPG neuron-dependent manner. Experimental evidence in this chapter suggests that stress-induced anorexia is mediated by GLP-1 released into the dLS and that GLP-1R-expressing neurons project from there to several hypothalamic areas.

4.3.1 NTS PPG neurons have the ability to suppress feeding

I show here that acute chemogenetic activation of NTS PPG neurons is sufficient to produce robust anorexia in mice (Fig 4.4-4.6). This hypophagic effect was mainly visible in the first two hours following dark onset, similar to what was recently reported in a parallel study by Gaykema et al. (2017). It is unclear whether the fading of the effect reflects activation of compensatory mechanisms preventing extended hypophagia, or if it is a result of the half-life of CNO. CNO is present for up to two hours after i.p. injection in mice (Guettier et al. 2009), but behavioural effects of CNO activation of virally expressed HM3Dq-receptors have been reported to last for up to eight hours in neurons expressing AgRP (Krashes et al. 2011). Additionally, although observing a time-limitation on the response in lean animals, Gaykema et al. reported (2017) clear hypophagic effects at four hours in diet-induced obese mice. This evidence suggests the most likely explanation for the lack of lasting effects is activation of compensatory mechanisms, which ensure sufficient food intake. Indeed, in my experiments, the effect of PPG activation appeared to reverse overnight with PPG activated mice eating more than controls, suggesting some level of compensation (Fig 4.6).

Although the *in vivo* effects of PPG activation observed by Gaykema et al. (2017) were similar to those presented here, I observed more robust *in vitro* responses. Gaykema et al. (2017) observed no effect of 1 µM CNO on electrophysiological properties of HM3Dq-expressing PPG neurons and reported only very small increases in activity following 9 µM CNO for ten minutes. This is surprising, considering the robust increase in intracellular [Ca^{2+}] in response to 1 µM CNO, demonstrated here (Fig 4.3) as well as the dramatic *in vivo* effects observed by me and Gaykema et al. (2017). Importantly, it is difficult to compare electrophysiological and Ca^{2+} imaging data and I have not categorically shown that HM3Dq-mediated activation of PPG neurons leads to an

increase in firing frequency. However, I observed a clear correlation between change in firing rate and intracellular [Ca^{2+}] in Chapter 3 and Alexander et al. (2009) convincingly demonstrated an increase in firing frequency in hippocampal neurons expressing HM3Dq. I am surprised by the lack of spontaneous firing in any of the cells recorded from by Gaykema et al. (2017). In our hands, PPG neurons *in vitro* have resting firing rates of 1.5-2 Hz with 124 of 135 recorded PPG neurons being spontaneously active (Hisadome et al. 2010; Holt et al. 2017). Notably, Gaykema et al. (2017) performed whole-cell recordings, whereas Hisadome et al. (2010, 2011) recorded in perforated-patch and my recordings were done in the cell-attached configuration. It is possible that in the whole-cell recordings presented by Gaykema et al. (2017), dilution of intracellular ATP into the electrode leads to opening of K_{ATP} channels and resulting hyperpolarisation.

4.3.2 PPG neurons are not necessary for the regulation of normal feeding

The sufficiency of PPG neurons to reduce food intake does not prove that these neurons are necessary for the regulation of feeding. It is unclear whether activation using HM3Dq recapitulates endogenous stimulation of PPG neurons by afferent neurons and circulating peptides. On the other hand, PPG inactivation or ablation prevents the endogenous release of GLP-1 in response to physiological stimuli. There is significant strength in having two different approaches to inactivation. Ablation using viral delivery of DTA is irreversible and not reliant on injection of CNO. As such, minimal handling of the animal is needed. HM4Di-mediated inhibition is a complementary technique achieving the same final goal of inactivation, while avoiding any risks of compensatory mechanisms developing due to chronic loss of GLP-1 signalling.

Loss or inactivation of NTS PPG neurons did not affect normal feeding during the dark phase (Figs 4.10, 4.12-4.13) and NTS PPG neurons were not necessary for bodyweight regulation (Fig 4.9). In support of my findings, global and central knockdown of GLP-1R was found to have little impact on food intake and body weight in mice (Scrocchi et al. 1996; Sisley et al. 2014). Somewhat surprisingly, a recent study in mice found that hypothalamic GLP-1Rs are necessary for satiety (Burmeister et al. 2017). This is difficult to reconcile with a lack of effect of global and brain knock-out of GLP-1R on food intake and bodyweight and does not align with my findings that permanent loss of PPG neurons has no effect on *ad libitum* feeding.

In rats, Barrera et al. (2011) found that shRNA-mediated knockdown of GLP-1 in the hindbrain led to hyperphagia and increased bodyweight. Furthermore, two recent studies in rats demonstrated that GLP-1Rs in the NTS (Alhadeff et al. 2017) and LH (López-Ferreras et al. 2017) are essential for satiety and food reward. GLP-1R knockdown using virally delivered shRNA in

these areas led to increased food intake and heightened motivation to work for food, in accordance with the effects seen following exogenous delivery of GLP-1 into these areas. Notably, the effects on bodyweight observed by Barrera et al. (2011) were measured soon after stereotaxic surgery and could be confounded by surgery-induced inflammation. However, these discrepancies could also reflect species differences between mice and rats and should be kept in mind when interpreting data and comparing studies conducted in different species. Importantly, GLP-1R inhibition did not affect food intake in humans (Melhorn et al. 2014; Steinert et al. 2014), supporting the results from mice presented here and by Scrocchi et al. (1996) and Sisley et al. (2014).

4.3.3 NTS PPG neurons are necessary for the prevention of overeating

I demonstrate here that, after overnight food deprivation, NTS PPG neurons play a role in the regulation of food intake. Both PPG-ablated and PPG-inhibited mice had significantly elevated intakes, compared to control mice, when food was returned after 18 hours of food deprivation (Figs 4.14-4.17). There is some evidence to suggest the energy balance of the animal is important for the effect of both GLP-1R stimulation and inhibition. In their milestone paper, Turton et al. (1996) observed hyperphagia in response to central GLP-1R blockade only in sated, not food-deprived, rats. Similarly, GLP-1 and Ex4-induced hypophagia disappeared following a 24-hour fast (Williams et al. 2006) and activation of GLP-1 neurons in response to CCK-8 or restraint stress is attenuated after overnight food deprivation (Maniscalco and Rinaman 2013; Maniscalco et al. 2015).

Fasting could silence the central GLP-1 system through several different mechanisms: 1) food-deprivation may reduce the activity of PPG neurons and the release of GLP-1, and 2) it may reduce sensitivity at the level of the GLP-1Rs by suppressing expression or availability at the cell membrane. It is possible that a large meal in turn activates NTS PPG neurons sufficiently to have an impact on food intake (Kreisler et al. 2014) and I therefore propose that the timing of interventions and measurements is essential. In support of this, 40 mins of refeeding after a prolonged fast was found to re-sensitise rats to GLP-1-induced hypophagia (Ronveaux et al. 2014). Furthermore, hindbrain GLP-1R blockade had no effect on food intake in food-deprived rats, whereas Ex9 attenuated hypophagia following a large meal (Hayes et al. 2009). I therefore hypothesised that intake of a large meal leads to recruitment of NTS PPG neurons.

In support of this, I found that although PPG ablation did not affect the intake of Ensure itself, chow intake in the next hour was significantly larger in mice lacking NTS PPG neurons (Fig 4.18). GLP-1R stimulation has previously been shown to decrease intake of highly-palatable food

(Dossat et al. 2011, 2013; Alhadeff et al. 2012; Dickson et al. 2012; Mietlicki-Baase et al. 2013, 2014), nicotine (Tuesta et al. 2017), and cocaine (Graham et al. 2013; Schmidt et al. 2016). The lack of effect of PPG ablation on Ensure intake is most likely due to 15 mins being insufficient time to detect a robust effect of recruitment of the central GLP-1 system. Importantly, I did not directly test the animals' willingness to work for food. Future studies could reveal the importance of PPG neurons in addiction by exposing PPG-ablated mice to operant conditioning and conditioned place preference experiments.

Taken together these data point to a role for PPG neurons in appetite control. Interestingly, PPG neurons are not important for the regulation of normal feeding, in contrast to POMC, AgRP and CGRP neurons. Rather, they prevent overconsumption of food. Intake of large meals is disruptive to the interior environment of the organism and can lead to nausea and malaise (Woods 1991). The importance of PPG neurons in the prevention of overeating could be indicative of a role in the response to homeostatic disruptions, including overconsumption of food. Challenges to well-being are not necessarily related to food intake and could include interoceptive stress in the form of visceral illness as well as psychogenic stress (Rinaman 1999b; Kinzig et al. 2003; Holt and Trapp 2016; Kreisler and Rinaman 2016).

4.3.4 Acute stress suppresses food intake via NTS PPG neurons and the dLS

To investigate the role of PPG neurons in the response to psychogenic stress, I exposed PPG-inhibited mice to acute restraint stress. PPG neuron activity was necessary for the hypophagic effects of restraint stress (Fig 4.20-4.21), demonstrating for the first time the importance of PPG neurons in the regulation of stress-induced hypophagia. In support of this, acute stress activates GLP-1-producing neurons (Maniscalco et al. 2015) and central GLP-1R signalling is required for the hypophagic, neuroendocrine, and cardiovascular responses to stress (Kinzig et al. 2003; Maniscalco et al. 2012; Ghosal et al. 2017).

I found that endogenous GLP-1 released into the dLS mediates the anorectic response to acute stress (Fig 4.30-4.31), revealing a novel site for modulation of stress by central GLP-1 in addition to the already established PVN and amygdala (Kinzig et al. 2003; Ghosal et al. 2017). Surprisingly, although the anorexic effect of restraint was evident after one hour, the effect of Ex9 on stress-induced hypophagia was only significant much later than that of PPG inactivation. This observation has several potential explanations. First, there could be a delay in the time it takes for Ex9 to have its effect on GLP-1Rs in the nucleus. However, other studies have shown much faster effects of Ex9, suggesting this is not the case (Williams et al. 2009; Alhadeff et al. 2012; Terrill et al. 2016). Second, it is conceivable the release of co-transmitters from PPG neurons

contributes to a much earlier hypophagic response than that of GLP-1. This would mean that inactivation of PPG neurons attenuates an early and late phase of stress-induced hypophagia whereas Ex9 blockade of dLS GLP-1Rs only inhibits the late phase of anorexia. Third, I cannot exclude that the Ex9-stress experiments were underpowered and that larger numbers of mice would reveal an earlier effect of dLS GLP-1R blockade on food intake suppression. Future experiments should aim to reproduce these findings before expanding further.

Surprisingly, acute restraint stress had a shorter-lived effect on food intake when measured in our facilities at University College London, compared to Florida State University. This discrepancy is most likely due to differences between the two environments, including temperature, ambient stressors, and slight variances in the equipment used. It is worth noting that HM4Di-mice tended to eat marginally less than control mice in both normal feeding and stress experiments (Figs. 4.12-13 and 4.20-21). This difference in intake was not statistically significant as demonstrated in Figs 4.12-4.13 and was consistent over several experiments, suggesting this group of mice simply had marginally lower intakes than the control group. In the future, stress experiments could be performed as within-subject designs in which HM4Di-expressing mice are either left undisturbed or exposed to stress following CNO or saline only. However, the experiments described here were deliberately not designed in this way due to the risk of habituating animals to stress through repeated exposures (Krahn et al. 1990).

To further investigate the cellular properties of GLP-1R-expressing neurons in the dLS, I created a Cre-dependent virus encoding GCaMP3. Selective expression of GCaMP3 in dLS GLP-1R allowed recordings of intracellular [Ca^{2+}] and revealed a robust response to a strong depolarising stimulus, 15 mM KCl (Fig 4.26). Future experiments will investigate the sensitivity of these neurons to GLP-1. Activation of the GLP-1R has been largely thought to be stimulatory via coupling to $G_{\alpha s}$ and increased levels of cAMP (Drucker et al. 1987; Thorens 1992; Zhang et al. 2017). Indeed, GLP-1 has been demonstrated to depolarise vagal neurons (Holmes et al. 2009). However, Ong et al. (2017) recently found that neurons in the paraventricular nucleus of the thalamus are in fact inhibited by GLP-1. Similarly, we have observed both excitatory and inhibitory responses to GLP-1 in the hippocampus and BNST (Cork et al. 2015; I E Edwards and S Trapp, unpublished). These findings suggest the effects of GLP-1R stimulation could be heterogenous and may depend on the tissue or site being investigated.

Neurons within the LS are primarily GABAergic (Zhao et al. 2013) and project to the PVN, LH, and POA (Meibach and Siegel 1977; Swanson and Cowan 1979; Berk and Finkelstein 1981). Surprisingly, I did not see any evidence for $dLS^{GLP\text{-}1R} \rightarrow$ PVN connections, whereas there were

clear fibres of passage through the LS terminating in the POA and LH (Fig 4.32). The importance of each of these circuits in stress-induced hypophagia is an interesting topic for further research. This could be investigated using circuit-specific expression of chemo- or optogenetic tools as described for the appetite-suppressing circuit between neurons in the PBN and the central amygdala (Carter et al. 2013).

Importantly, without knowing whether GLP-1 excites or inhibits individual neurons in the dLS, and whether this is in fact a heterogeneous response, it is difficult to decide on a strategy for chemogenetic manipulation of dLS GLP-1R-expressing neurons. In the case of a heterogenous response to GLP-1 it may not be desirable to manipulate the whole population simultaneously. The same caution may be necessary when investigating other neuronal targets of GLP-1.

In this chapter, I used state-of-the-art chemogenetic tools to manipulate the activity of NTS PPG neurons. Because viral transduction was confined to the NTS and rarely spread further ventral (Fig 4.8), I did not target PPG neurons found in the IRT and along the midline (Merchenthaler et al. 1999; Llewellyn-Smith et al. 2011). It is possible that only few neurons are needed to maintain satiety in response to normal food intake and that complete loss or inactivation of PPG neurons, including those in the IRT, would reveal a role in normal feeding. The cataplexy phenotype, a symptom of narcolepsy, was only observed in mice after loss of 90% orexin neurons, suggesting some systems only need few neurons to uphold normal function (Tabuchi et al. 2014). I also cannot exclude that more sensitive methods of monitoring food intake could reveal subtle differences in meal patterns between PPG-inactivated and control mice.

Viral delivery of HM4Di, HM3Dq, and GCaMP3 all decreased expression of other fluorescent reporters. Importantly, these changes in reporter expression did not affect spontaneous firing frequency (1.5-2 Hz) or responsiveness to 15 mM KCl and 100 µM glutamate of the cells and there was no *in vivo* phenotype suggesting the cells function as normal.

The data presented in this chapter clarify the role of PPG neurons in food intake and specifically reveal that NTS PPG neurons are important for satiety in the context of overeating. Central infusions of GLP-1 have been shown to induce conditioned taste aversion in rodents (Thiele et al. 1997; Lachey et al. 2005), although the brain nuclei responsible for this seem to be distinct from the sites mediating the food-intake suppressive effects (McMahon and Wellman 1998; Kinzig et al. 2002). Future investigations should address the potential initiation of nausea in response to a large meal and whether PPG neurons are involved in initiation of malaise and conditioned taste aversion after overeating. Additionally, I identified a role for PPG neurons and

dLS GLP-1Rs in the regulation of stress-induced hypophagia. Future experiments should investigate whether this NTS^{PPG} → dLS circuit is sufficient to induce hypophagia and whether it is necessary for stress-induced hypophagia.

5. The role of PPG neurons in cardiovascular control

5.1 Background

The role of GLP-1 within the brain is not limited to regulation of food intake. Rather, the hypophagic effects of central GLP-1 may be part of a complex physiological response to acute stress (Ghosal et al. 2013; Holt and Trapp 2016). In Chapter 4, I demonstrated that PPG neuron activity is necessary for the hypophagic response to acute stress. In this chapter, I expand on those findings by investigating the role of GLP-1 in cardiovascular control.

Peripheral (i.p. or i.v.) or central (i.c.v.) administration of GLP-1 or its analogues increases heart rate in rats (Barragán et al. 1994; Yamamoto et al. 2002), mice (Griffioen et al. 2011), cattle (Edwards et al. 1997), and humans (Mark et al. 1998; Robinson et al. 2013). In contrast, the effect of GLP-1R stimulation on blood pressure has been variable with some studies observing robust hypertensive effects of GLP-1 analogues (Barragán et al. 1994; Yamamoto et al. 2002), whereas others found little evidence for an effect on blood pressure (Edwards et al. 1997). These differences could arise from variability between species and to my knowledge no study has reported an effect of GLP-1R activation on blood pressure in mouse.

Although the tachycardic effects of GLP-1R stimulation have proven robust and reproducible, the underlying mechanisms remain unclear. GLP-1R-mediated cardiovascular effects may involve a combination of peripheral and central pathways involving GLP-1Rs both in the brain and on the heart (Barragán et al. 1999; Gros et al. 2003; Hayes et al. 2008; Baggio et al. 2017). Furthermore, both the parasympathetic (Barragán et al. 1994, 1999; Cabou et al. 2008; Griffioen et al. 2011) and sympathetic nervous system (Yamamoto et al. 2002, 2003; Baggio et al. 2017; Ghosal et al. 2017) have been implicated in the tachycardic response to GLP-1R stimulation. Contributions from the autonomic nervous system to GLP-1-mediated tachycardia are therefore still controversial.

Although important for the understanding of the effects of treatments with GLP-1 analogues, these studies do not address the question of the involvement of endogenous GLP-1. The literature is sparse when it comes to the role of endogenous GLP-1 in cardiovascular control. In 1999, Barragan et al. found no effect of i.c.v. infusion of GLP-1R antagonist, Ex9, on heart rate and blood pressure (Barragán et al. 1999). However, these studies were done in anaesthetised rats in which autonomic function could be altered dependent on the choice of anaesthetic agent.

Genetic knockdown of GLP-1Rs had complicated effects on cardiovascular parameters. Although bradycardia was observed at two months of age, this effect disappeared in older mice (Gros et al. 2003). Importantly, results from genetic knockdown studies are confounded by the possibility of compensation occurring during development. Considering the robust effects of central and peripheral GLP-1R stimulation, I was curious if endogenous GLP-1 is relevant in cardiovascular control. In this chapter, I investigate the role of GLP-1 in cardiovascular control and, in particular, the contribution of NTS PPG neurons to regulation of heart rate and blood pressure. To this end, I address the following questions:

1. Which is an appropriate experimental model for elucidating the role of NTS PPG neurons in cardiovascular control?
2. What is the effect of systemic GLP-1R activation on heart rate, blood pressure, and activity in this model?
3. Are PPG neurons necessary for maintenance of normal heart rate and blood pressure?
4. How does diet-induced obesity affect cardiovascular parameters and do NTS PPG neurons play a role?
5. Is NTS PPG neuron activity sufficient to increase heart rate?

These questions were addressed using stereotaxic brainstem injections of Cre-dependent viruses and biotelemetry blood pressure probe implantation. In summary, I confirmed the tachycardic effects of peripheral injections of Ex4, but I found no evidence for a role of NTS PPG neurons in the physiological regulation of heart rate, although activation of PPG neurons was sufficient to increase heart rate in mice.

5.2 Results

5.2.1 Methods to measure heart rate and blood pressure in awake mice

To begin, I had to determine the most appropriate method for monitoring heart rate and blood pressure in mice that would allow me to investigate the role of central GLP-1 in cardiovascular control. It was important to avoid any effects of anaesthesia on heart rate and blood pressure. Furthermore, I was interested in methods, which allow repeated measurements from the same mouse. I therefore explored two approaches:

- Blood pressure recordings using a volume-pressure recording (VPR) tail-cuff system
- Implantable biotelemetry in freely-behaving mice

In the VPR tail-cuff system, awake mice are placed in tight plexiglass tubes with breathing holes as seen in Fig 5.1. An occlusion cuff is placed around the most proximal part of the tail and a recording cuff, which senses blood flow, is placed distally. The mouse is then placed on a heating pad to ensure stable core temperature and sufficient blood flow to the tail. Importantly, mice are conscious throughout the procedure allowing me to monitor heart rate and blood pressure without any effects of anaesthesia.

Heart rate and blood pressure were recorded from five male adult mice (Fig 5.1B). Heart rate and mean arterial blood pressure (MAP) were averaged for each mouse over 18-24 consecutive recordings. Mean heart rate ranged from 523 to 637 bpm and MAP varied between 99.8 and 135.5 mmHg (Fig 5.1B).

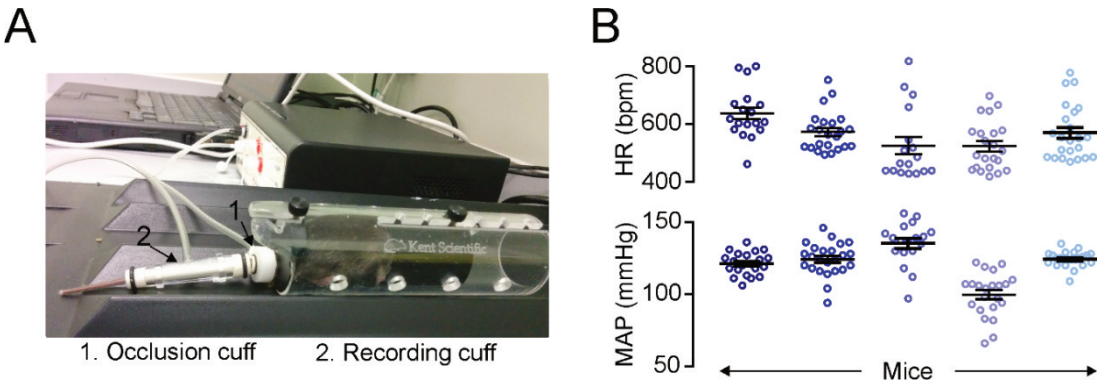

Fig 5.1 VPR tail cuff for monitoring heart rate and blood pressure in awake mice. A) A mouse restrained in a transparent plexiglass tube during blood pressure recordings. The two cuffs for blood pressure measurements are indicated. The occlusion cuff (1) inflates and restricts blood flow to the tail. As pressure is released blood returns to the tail and is detected by the recording cuff (2). **B)** Five mice were exposed to 25 cycles of measurements resulting in 18-24 accepted cycles. Data from individual mice are displayed in shades of blue and means±SEM are indicated. Heart rate (HR) in beats per minute (bpm) and mean arterial blood pressure (MAP) are shown.

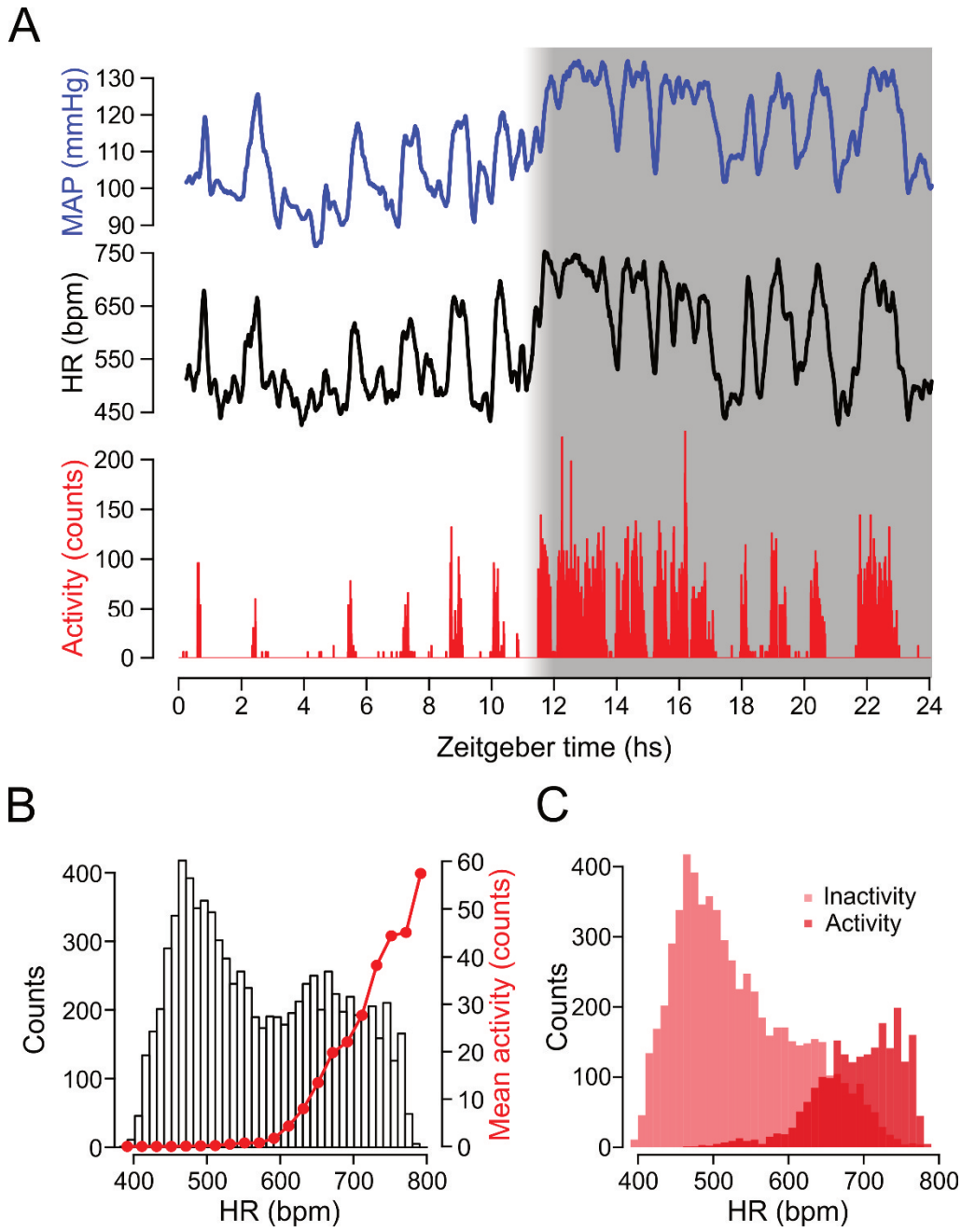

Fig 5.2 The biotelemetry system for monitoring heart rate and mean arterial blood pressure in awake, freely-behaving mice. A) Mean arterial blood pressure (MAP, blue, top), heart rate (HR, black, middle) and locomotor activity (red, bottom) measured from a single mouse over 24 hours as indicated in zeitgeber time. Dark phase is indicated with a grey box with the gradient indicating a half hour "twilight" period in which lights were dimmed. Traces are running averages over 20 mins. **B)** Histogram displaying the distribution of heart rate values in 10 bpm bins recorded from a single mouse over 24 hours is shown in white bars. Notice the bimodal distribution of heart rate values. Overlain in red is a plot of the mean activity counts at the heart rate levels indicated on the x-axis. **C)** The distribution of heart rate values from B) split into two histograms according to activity levels with the distribution of heart rate values at inactivity (when activity=0) displayed in light red, and the distribution of heart rate values during active times in dark red.

I demonstrated in Chapter 4 that restraint stress profoundly reduces food intake. I was therefore concerned that restraint during VPR tail-cuff measurements would cause stress and thus affect heart rate and blood pressure of the mice. Furthermore, VPR tail cuff measurements were variable within the same mouse with the heart rate of one mouse ranging between 428 and 818 bpm.

For these reasons, I explored an implantable biotelemetry system for monitoring heart rate and blood pressure. Male mice, 7-10 weeks old, were implanted with biotelemetry blood pressure probes as described in Materials and Methods.

Fig 5.2 shows an example of how MAP, heart rate, and activity fluctuate in a synchronised manner over 24 hours. The lowest values of MAP (~90 mmHg) and heart rate (~440 bpm) occurred at times of no activity and the highest levels of MAP (~135 mmHg) and heart rate (~750 bpm) were found at times of prolonged intense activity. For example, at the onset of dark phase, high activity levels were more frequent and coincided with a rise in both MAP and heart rate (Fig 5.2A).

Because of these fluctuations, it is not appropriate to simply report average heart rate and MAP for each mouse. As seen in Fig 5.2B, heart rate values recorded over 24 hours are not normally distributed, but rather follow a bimodal distribution. Based on the synchrony in heart rate and activity fluctuations observed in Fig 5.2A, I hypothesised that heart rate is positively correlated with activity. To confirm this, I binned heart rates in 20 bpm bins and calculated mean activity levels for each bin (Fig 5.2B). Activity levels were close to 0 at heart values between 390 and 570 bpm. At higher heart rate values, between 590 and 800 bpm, mean activity levels were positively correlated with heart rate.

To further investigate the relationship between activity and cardiovascular parameters, I filtered heart rate values according to activity levels. Inactivity was defined as any timepoint with Activity=0. Conversely, activity was defined as any timepoint with Activity>0. From this filtering, it was clear that the bimodal distribution could be split into two unimodal histograms (Fig 5.2C). Importantly, neither distribution was normal with inactive heart rate values skewed to the right and active heart rate values skewed to the left. For this reason, values reported in this chapter are all based on the median, with the exception of circadian fluctuations in heart rate and blood pressure which are displayed as averages every 30 mins over 24 hours.

To begin with, I determined resting heart rate and MAP by extracting data from timepoints when the animals are inactive and computing the median. Although it is argued that animals subjected

to the VPR tail-cuff method are at rest, HR and blood pressure were both significantly higher in mice during VPR tail-cuff measurements than in animals in which blood pressure and heart rate were monitored with biotelemetry (Fig 5.3). Mice subjected to tail-cuff measurements had an average resting heart rate of 565±21 bpm, whereas mice implanted with biotelemetry probes had significantly lower resting heart rates of 505±12 bpm (Fig 5.3A, p=0.02). Similarly, resting MAP was significantly lower in mice with biotelemetry probes (103±1 mmHg) than mice subjected to VPR tail-cuff measurements (121±6 mmHg, p=0.0005). These findings suggest that the VPR tail-cuff method does not provide true resting values, most likely due to stress induced by the restraint during tail-cuff measurements. Furthermore, VPR tail-cuff measurements do not provide circadian data or any temporal resolution of responses, since measurements are only snapshots of cardiovascular parameters. I therefore continued my investigations using biotelemetry focussing on both resting and active median heart rate and MAP.

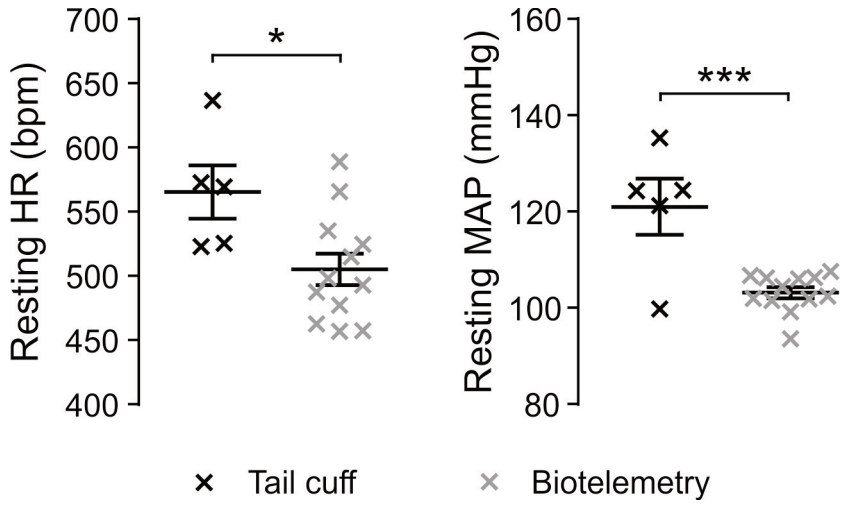

Fig 5.3 Resting HR and MAP as measured with biotelemetry and VPR tail cuff. Resting heart rate (HR, left) and MAP (right) measured using tail cuff (black symbols) or biotelemetry (grey symbols). N=5 (tail cuff) and N=12 (biotelemetry). *p<0.05, ***p<0.001, Student's unpaired t-test.

5.2.2 Systemic Ex4 increases heart rate via the sympathetic nervous system

Having identified an appropriate method for monitoring heart rate and blood pressure, I set out to investigate the role of GLP-1 in cardiovascular control. Knowing from previous studies that GLP-1R activation increases heart rate in both rats and mice (Barragán et al. 1994; Yamamoto et al. 2002; Griffioen et al. 2011), I wanted to confirm this tachycardia in the biotelemetry model. As seen in Fig 5.4, i.p. injection of 100 µl saline led to a rapid increase in heart rate as expected when inducing brief stress due to handling of the mouse. However, 30 mins later heart rate had returned to baseline and continued to fluctuate as normal with frequent returns to high values

during dark phase as typically seen (Fig 5.4 top panel). Similarly, i.p. injection of 100 µg/kg GLP-1 led to a transient increase in heart rate, which returned to baseline within 30 mins (Fig 5.4 middle panel). Importantly, the tachycardic response to handling stress may have masked any GLP-1-induced effects on heart rate. In contrast, i.p. injection of the long-acting GLP-1 analogue, 10 µg/kg Ex4, led to a sustained increase in heart rate over eight hours, which did not return to baseline until several hours into dark phase (Fig 5.4 bottom panel). Heart rate did not reach maximum values, since both handling stress and high activity during dark phase led to higher heart rate values. Ex4 appeared to increase the minimum level of heart rate, suggesting the effect was mainly on resting heart rate.

The doses of GLP-1 (100 µg/kg) and Ex4 (10 µg/kg) were chosen based on previous studies finding significant effects on food intake at these levels (Mack et al. 2006; Barrera et al. 2009; Williams et al. 2009; Kanoski et al. 2011; Dickson et al. 2012; Jessen et al. 2012; Saito et al. 2016).

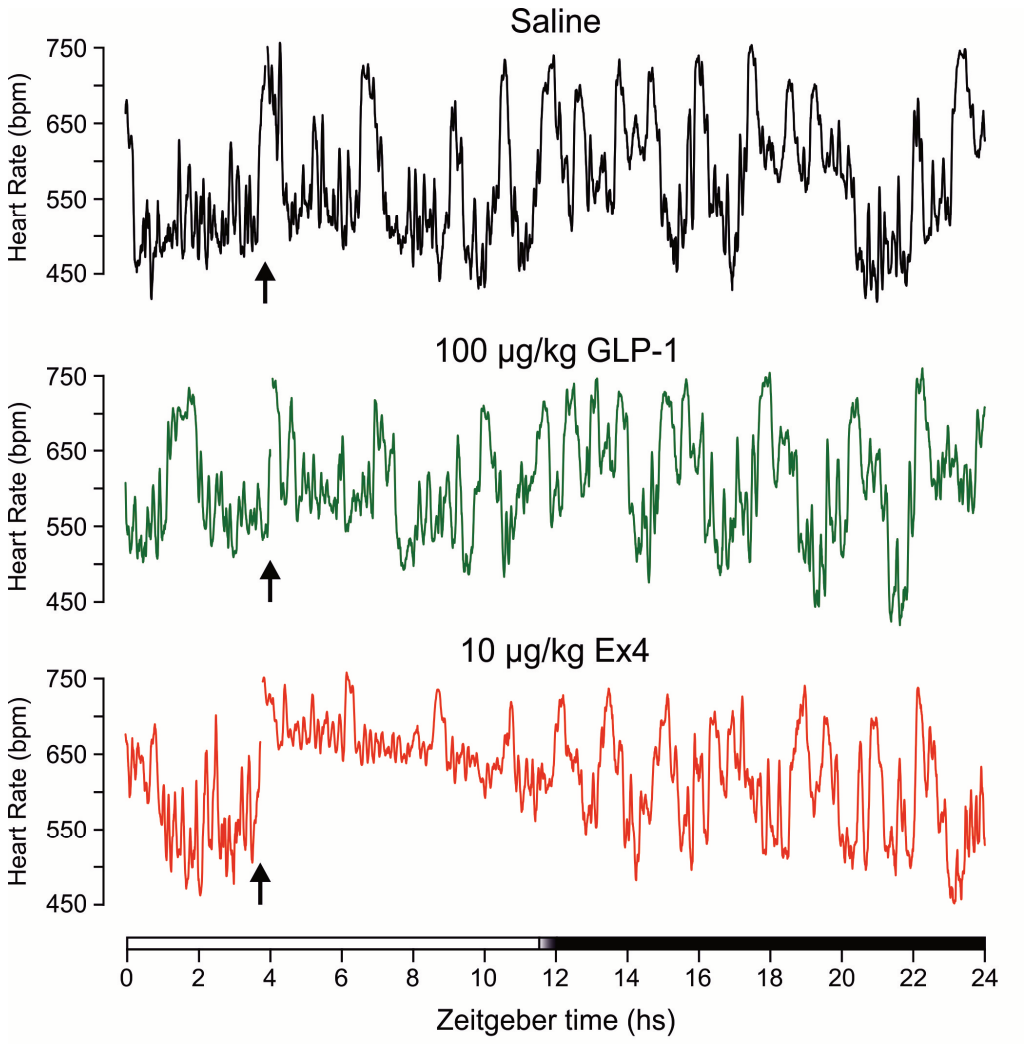

Fig 5.4 Systemic activation of GLP-1Rs induces tachycardia. Heart rate of a single mouse injected i.p. with either saline (black, top), 100 µg/kg GLP-1(7-36) (GLP-1, green, middle), and 10 µg/kg Ex4 (red, bottom) recorded over 24 hours as indicated by zeitgeber time at the bottom. Arrows indicate times of injection and the bar at the bottom indicates light (white bar) and dark (black bar) phases with a brief period of half-light indicated by a white to black gradient. Traces are running averages over 200 s.

This experiment was repeated in another three mice in a counterbalanced manner with a similar outcome. Fig 5.5 displays heart rate and blood pressure values averaged every 30 mins over a 24-hour recording. Saline injections transiently increased heart rate, whereas 10 µg/kg Ex4 i.p. led to a sustained rise in heart rate which slowly decreased over the following eight hours. Interestingly, MAP was unaffected by GLP-1R activation and only displayed a brief increase following handling (Fig 5.5B).

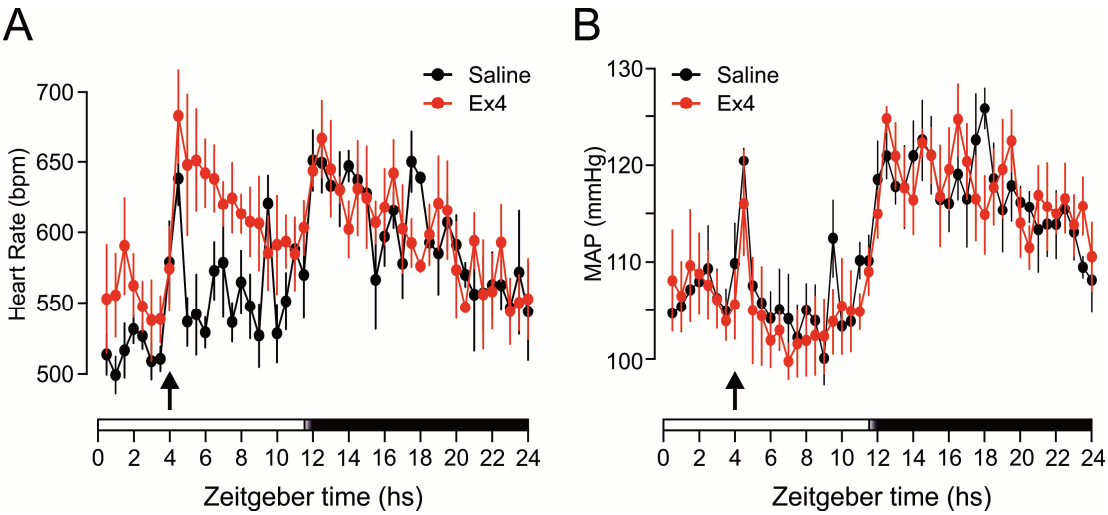

Fig 5.5 I.p. injection of Ex4 increases heart rate but not MAP in freely-behaving animals. A) Heart rate and **B)** MAP of four mice exposed to saline (black) and 10 µg/kg Ex4 (red) four hours into light phase. Heart rate and MAP were averaged every 30 mins for each mouse. Shown here are mean±SEM of four mice taken every 30 mins over 24 hours as indicated by zeitgeber time on the x-axis. Arrows indicate times of injection and the bars at the bottom indicate light (white bar) and dark (black bar) phases with a brief period of half-light indicated by a white to black gradient.

To quantify these responses, I calculated the median resting heart rates before and after drug treatments. To avoid any contribution to heart rate from the stress induced by handling of the mice, calculations were based on values 1-2 hours after injection (hours 5-6 into light phase). Furthermore, by only including heart rates during zero activity, any effects of changes in activity were avoided. I extracted heart rate values at inactivity during baseline (2-3 hours into light phase, 1-2 hours before injection) and 1-2 hours after drug injections (5-6 hours into light phase) (Fig 5.6A). Two-way repeated measures ANOVA revealed a significant interaction between time and treatment ($F(1, 3) = 22.35$, $p=0.018$). Sidak's multiple comparisons test yielded no significant effect of saline ($p=0.34$) nor GLP-1 ($p=0.29$). In contrast, there was a statistically significant effect of Ex4 on heart rate with median resting heart rate increasing from 517.4±23 to 647.6±36 bpm ($p<0.0001$).

Because mice have variable resting heart rate values, I calculated the change in resting heart rate from baseline (Fig 5.6B). Resting heart rate increased by significantly more bpm in response to 10 µg/kg Ex4, compared to saline ($p=0.0043$), whereas there was no difference in the effect of saline and GLP-1 treatment ($p=0.997$).

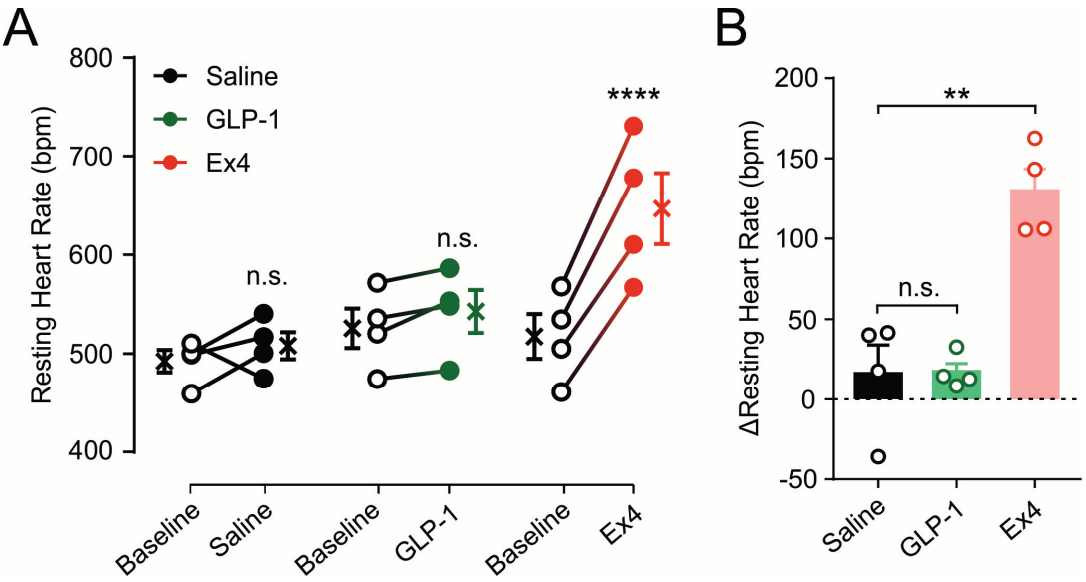

Fig 5.6 I.p. injection of Ex4 increases resting heart rate in freely-behaving mice. A) Four mice implanted with biotelemetry probes were injected i.p. with saline (black), 100 µg/kg GLP-1 (green), and 10 µg/kg Ex4 (red) four hours into light phase. Median resting heart rates of individual mice were determined before (hours 2-3) and after (hours 5-6) i.p. injections. Matched data from individual mice are plotted as well as mean±SEM values (N=4). ****p<0.0001, n.s.: not significant, Sidak's matched pairs multiple comparisons test. **B)** Change in heart rate from baseline determined from A) following injections of saline (black), GLP-1 (green), and Ex4 (red). Data from individual mice are shown as well as mean±SEM for each treatment (N=4). **p<0.01, n.s.: not significant, Dunnett's multiple comparisons test.

Although GLP-1R activation has been shown to decrease locomotor activity (Mack et al. 2006; Erreger et al. 2012; Egecioglu et al. 2013a), I found no effect of i.p. Ex4 treatment on activity as compared to treatment with saline (Fig 5.7). To quantify this, I determined the time each animal spent active as a percentage of total time during baseline (hours 1-4) and after injection of saline or 10 µg/kg Ex4 (hours 5-8) (Fig 5.8). Mice spent 14±2% of their time active during baseline. This did not change in response to saline (14±3%) and was only marginally lower following Ex4 treatment (11±2%) (Fig 5.8A). Indeed, two-way repeated measures ANOVA yielded no significant interaction between time and treatment ($F(1,3) = 0.034$, $p=0.87$) and there were no significant main effects (time: $p=0.29$, treatment: $p=0.39$). Importantly, the lack of effect on activity demonstrates that any cardiovascular consequences of GLP-1R stimulation are not secondary to changes in locomotor activity.

As expected locomotor activity increased at the onset of dark phase. This increase was similar following saline (15±3% to 35±2%) and Ex4 treatment (14±2% to 35±6%) (Fig 5.8B). Two-way repeated measures ANOVA revealed no significant interaction between time and treatment ($F(1, 3) = 0.09634$, $p=0.7766$) and there was no main effect of treatment ($p=0.83$). However, the analysis did reveal a significant main effect of time ($p=0.0058$), suggesting both saline and Ex4-

treated mice spent significantly more time active during early dark phase than during late light phase, but that systemic GLP-1R activation does not affect locomotor activity at dark onset. It is possible that Ex4 was no longer present at high enough concentrations at these later timepoints. To specifically investigate the effect of Ex4 on dark onset activity, future studies should inject the agonist immediately prior to the dark phase.

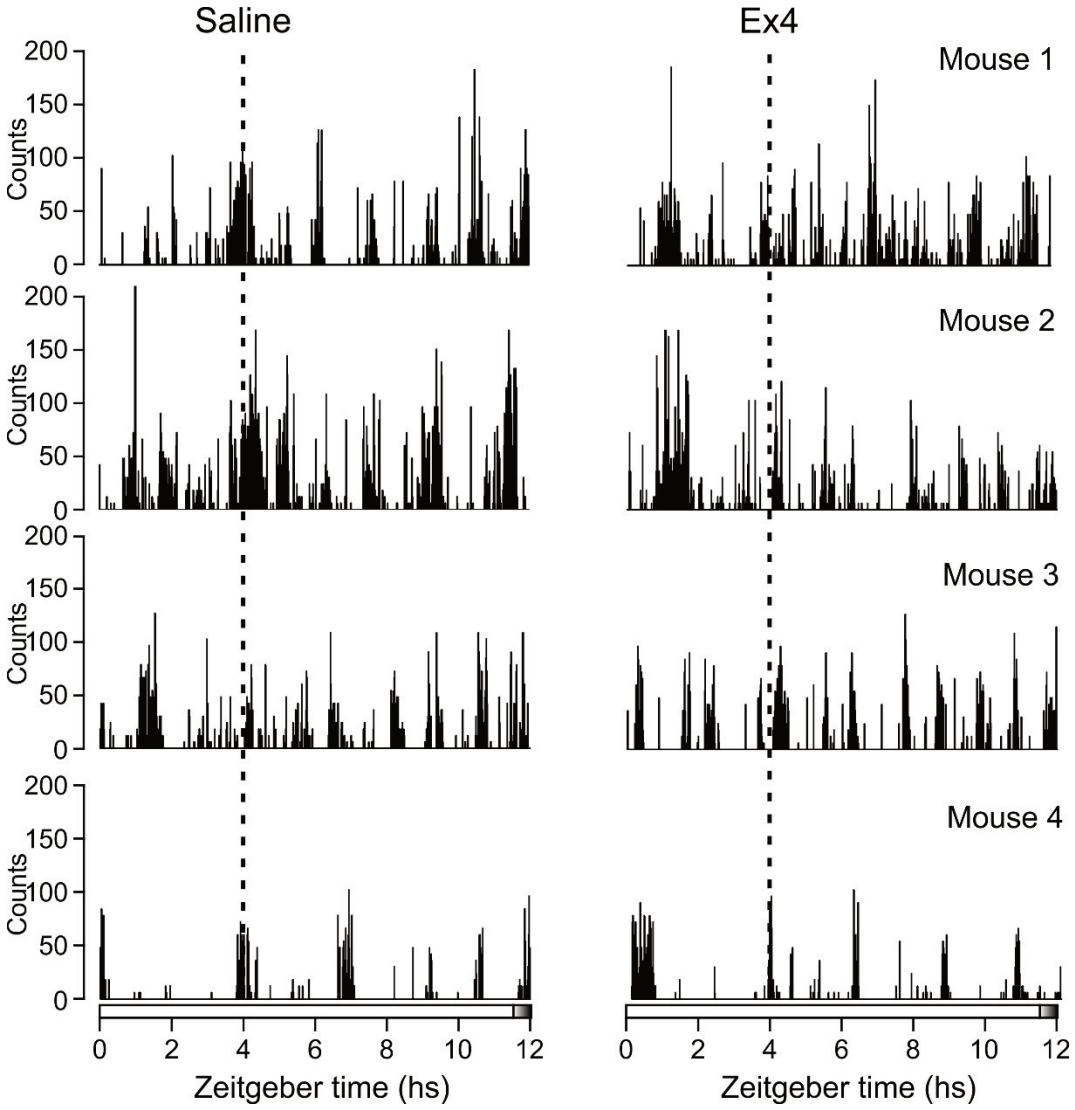

Fig 5.7 I.p. injection of Ex4 does not affect locomotor activity. A) Four mice implanted with biotelemetry probes were injected i.p. with saline (left) or 10 µg/kg Ex4 (right) four hours into light phase. Activity levels were monitored over 12 hours during light (white bar) and twilight phase (gradient bar). Zeitgeber time is indicated at the bottom. Times of i.p. injections with either saline or Ex4 are indicated with dotted lines.

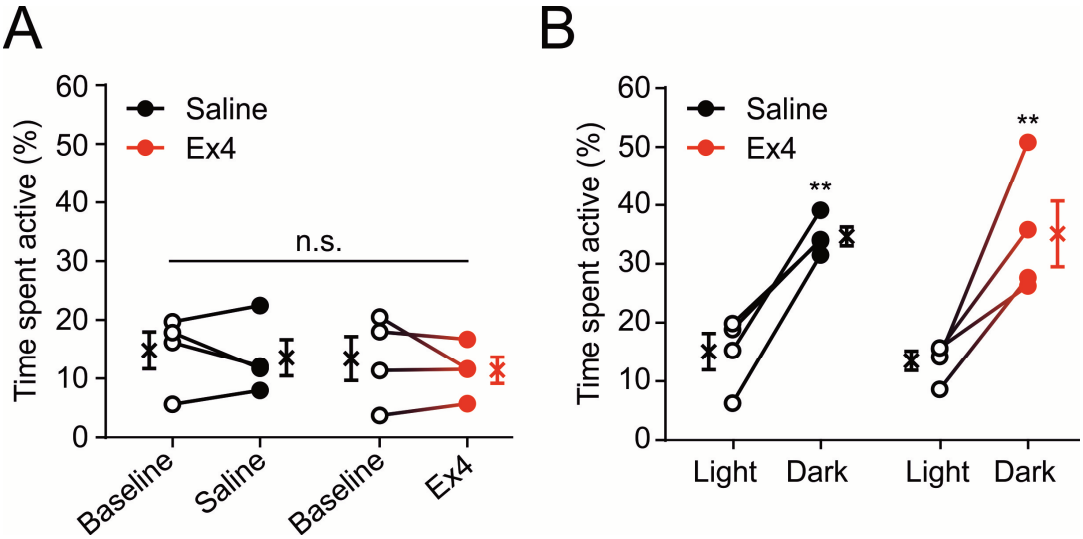

Fig 5.8 I.p. injection of Ex4 does not affect the time mice spend active. Four mice implanted with biotelemetry probes were injected i.p. with saline (black) or 10 µg/kg Ex4 (red) four hours into light phase. **A)** Percentage time spent active before (Baseline, hours 1-4, open circles) and after (Saline/Ex4, hours 5-8, filled circles) drug treatment (N=4). n.s.: no significant interaction according to two-way repeated measures ANOVA. **B)** Percentage time spent active during light (open circles, hours 8-11) and dark phase (filled circles, hours 12-15) following injection of Ex4. **p<0.01 indicating a main effect of time on activity levels in both treatment groups according to two-way ANOVA.

The data presented here clearly demonstrate that systemic GLP-1R activation with 10 µg/kg Ex4 leads to an increase in heart rate, but not MAP. GLP-1 increased heart rate only transiently, an effect which was indistinguishable from the stress-induced tachycardia seen after injection of saline. This is most likely due to rapid degradation of GLP-1 by DPP-IV in the bloodstream as explained in the Introduction.

Tachycardic effects of GLP-1R activation have been attributed to changes in activity of either the parasympathetic or sympathetic nervous system (Yamamoto et al. 2002, 2003; Griffioen et al. 2011). Furthermore, NTS PPG neurons project to sympathetic preganglionic neurons in the spinal cord (Llewellyn-Smith et al. 2015). To test whether the tachycardic effect observed in response to Ex4 was dependent on sympathetic outflow, Ex4 injections were repeated in the absence and presence of the β1-recepter antagonist, atenolol.

Six mice implanted with biotelemetry probes were injected with 2 mg/kg atenolol or saline four hours into the light phase. This dose was chosen based on previous studies in which sympathetic input to the heart was significantly attenuated (Just et al. 2000; Khor et al. 2016). 15 mins after atenolol/saline treatment mice were injected i.p. with 10 µg/kg Ex4.

As described above, i.p. injections led to a brief rise in heart rate due to handling stress. Injection of 10 µg/kg Ex4, alone induced a sustained increase in heart rate over several hours (Fig 5.9 left panel). Pre-treatment with 2 mg/kg atenolol reduced the effect of handling stress on heart rate, consistent with a decrease in sympathetic outflow to the heart. Intriguingly, Ex4 failed to increase heart rate in the absence of β1-receptor activity, suggesting Ex4 induces tachycardia via an increase in sympathetic activity (Fig 5.9 right panel).

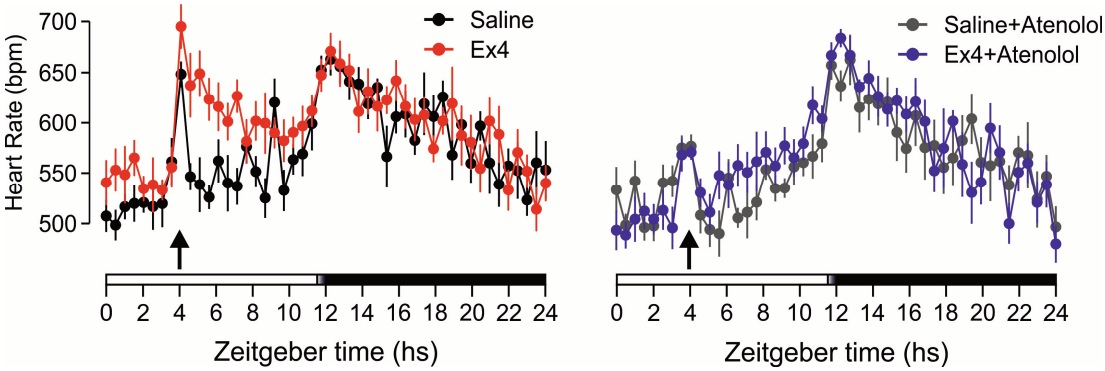

Fig 5.9 β1-receptor antagonism prevents tachycardic effects of systemic GLP-1R activation. Mice implanted with biotelemetry probes were injected i.p. with saline (black and grey) or 10 µg/kg Ex4 (red and blue) four hours into light phase in the absence (left panel) or presence (right panel) of 2 mg/kg β1-receptor antagonist, atenolol. Shown here are mean±SEM taken every 30 mins over 24 hours as indicated by zeitgeber time on the x-axis. Arrows indicate times of injection and the bars at the bottom indicate light (white bar) and dark (black bar) phases with a period of half-light indicated by a white to black gradient. N=7.

These results were quantified by calculating median resting heart rates before (hours 2-3) and after (hours 5-6) i.p. injections. Fig 5.10A depicts the median resting heart rates in response to saline, 10 µg/kg Ex4, saline + 2 mg/kg atenolol, and 10 µg/kg Ex4 + 2 mg/kg atenolol. Two-way repeated measures ANOVA found a significant interaction between drug treatments ($F(1, 6) = 10.67$, $p=0.0171$). Injection of 2 mg/kg atenolol alone did not significantly decrease heart rate as compared to saline ($p=0.88$). In the absence of 2 mg/kg atenolol, median resting heart rates were significantly increased in response to 10 µg/kg Ex4 as compared to saline ($p=0.0041$). In contrast, there was no effect of 10 µg/kg Ex4 in the presence of atenolol ($p=0.55$) and resting heart rates were comparable to following saline treatment ($p=0.99$). Furthermore, resting heart rates were significantly lower in response to Ex4 in mice pre-treated with atenolol as compared to mice with active β1-receptor signalling ($p=0.0072$).

To avoid any potential effects of different baseline resting heart rate levels between treatments, I inspected the changes in resting heart rate from baseline (Fig 5.10B). The results echoed the observations from absolute resting heart rate levels. Two-way repeated measures ANOVA revealed a significant interaction between pre-treatment with atenolol and Ex4 ($F(1, 6) = 13.84$,

p=0.0099). In the absence of 2 mg/kg atenolol, resting heart rate increased by 117.2±12 bpm as compared to 7.3±11 bpm in response to saline. In contrast, the rise in resting heart rate was significantly attenuated in the presence of atenolol with a mean increase of only 37.5±25 bpm (p=0.0038; Ex4 vs Ex4+atenolol). This was not significantly different from the change in heart rate observed in response to saline only (p=0.26).

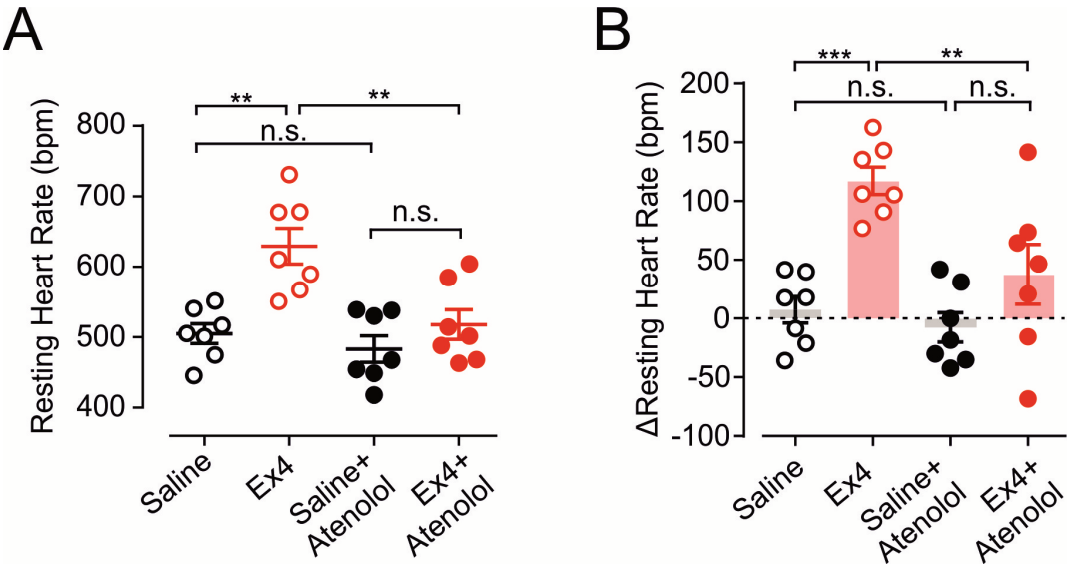

Fig 5.10 GLP-1-mediated increases in resting heart rate are dependent on the sympathetic nervous system. A) Absolute resting heart rates (5-6 hours) and **B)** change in resting heart rates from baseline (2-3 hours) in response to saline (black) or Ex4 (red) in the absence (empty circles) or presence (filled circles) of 2 mg/kg β1-receptor antagonist atenolol (N=7). **p>0.01, ***p<0.001 and n.s.: not significant, Sidak's multiple comparisons test.

The data presented in this section provide evidence for a tachycardic effect of systemic GLP-1R activation in freely-behaving mice, while GLP-1R agonism did not affect blood pressure or locomotor activity. Furthermore, these data demonstrate an involvement of the sympathetic nervous system in this response, as suggested previously by Yamamoto et al. (2002, 2003) and recently by Baggio et al. (2017).

5.2.3 NTS PPG neurons are not necessary for cardiovascular control or regulation of locomotor activity

In the previous section, I confirmed the tachycardic effect of GLP-1R activation and demonstrated an involvement of the sympathetic nervous system. Next, I was specifically interested in the involvement of central GLP-1 and the physiological role of NTS PPG neurons in cardiovascular control. In this section, I chronically ablate NTS PPG neurons and investigate the effect on cardiovascular parameters using biotelemetry in a longitudinal study.

Biotelemetry probes were implanted into 12 male PPG-Cre/GCaMP3 or PPG-Cre/tdRFP mice. Baseline heart rate, blood pressure and activity were recorded and two weeks later mice were stereotaxically injected into the NTS with either AAV8-mCherry-FLEX-DTA or AAV1/2-FLEX-Perceval as control (Fig 5.11A and B). It is clear from data shown in Chapter 4 (Fig 4.7) that DTA causes loss of PPG neurons by 14 days post-surgery. Heart rate and blood pressure were recorded again four and six weeks after viral gene delivery. At nine weeks, DTA and control animals received i.p. injections of saline and 10 µg/kg Ex4. One week later, mice were transferred to a high-fat diet (HFD, 60% caloric content from fat) for one month and blood pressure and heart rate were again recorded. A week later, at 15 weeks after surgery, saline and Ex4 injections were repeated (Fig 5.11A). At the end of the experiment, mice were transcardially perfuse-fixed and coronal brainstem sections were immunostained for the fluorescent reporters mCherry or Perceval as markers for successful transduction of NTS neurons (Fig 5.11C). All mice were expressing the expected transgene at the end of the experiment.

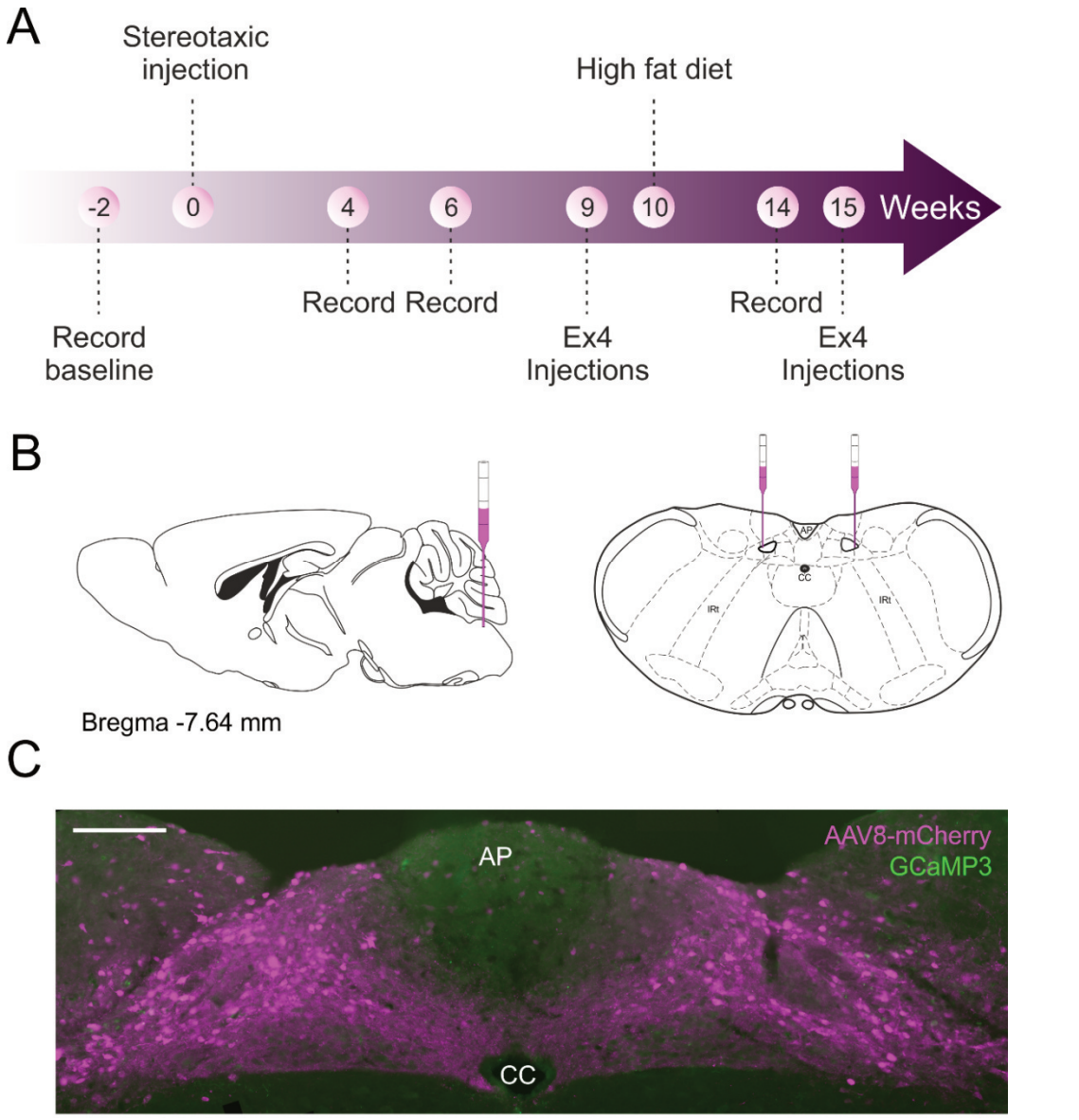

Fig 5.11 Ablation of PPG neurons using AAV8-mCherry-FLEX-DTA for investigations of the physiological role of central GLP-1 in cardiovascular control. A) Work flow for DTA ablation of PPG neurons and biotelemetry monitoring of cardiovascular consequences. Heart rate and blood pressure were measured at times indicated with "Record". **B)** Stereotaxic injections of the Cre-dependent viruses AAV8-mCherry-FLEX-DTA or AAV1/2-FLEX-Perceval into the NTS to selectively target PPG neurons. **C)** Immunofluorescent images showing caudal brainstem tissue from a PPG-Cre/GCaMP3 transgenic mouse injected with AAV8-mCherry-FLEX-DTA. Expression of mCherry was detected using an anti-dsRed antibody, displayed here in magenta. PPG neurons expressing GCaMP3 were completely lacking and could not be detected using an anti-GFP antibody (green). Scale bar: 100 µm. CC: Central canal, AP: Area postrema.

There were no obvious biological effects of ablating PPG neurons on cardiovascular parameters or locomotor activity. Consequently, in this section, I systematically explore numerous parameters, which could be affected by PPG ablation.

There was no difference in heart rate and blood pressure recorded over 24 hours between the two cohorts before ablation, confirming that these mice did not have different heart rate and MAP prior to any intervention (Fig 5.12). Furthermore, heart rate and MAP increased at the onset of dark to a similar level in both cohorts. At four and six weeks, no significant difference was seen between control and DTA animals, suggesting ablation of PPG neurons does not affect the normal regulation of blood pressure and heart rate (Fig 5.12).

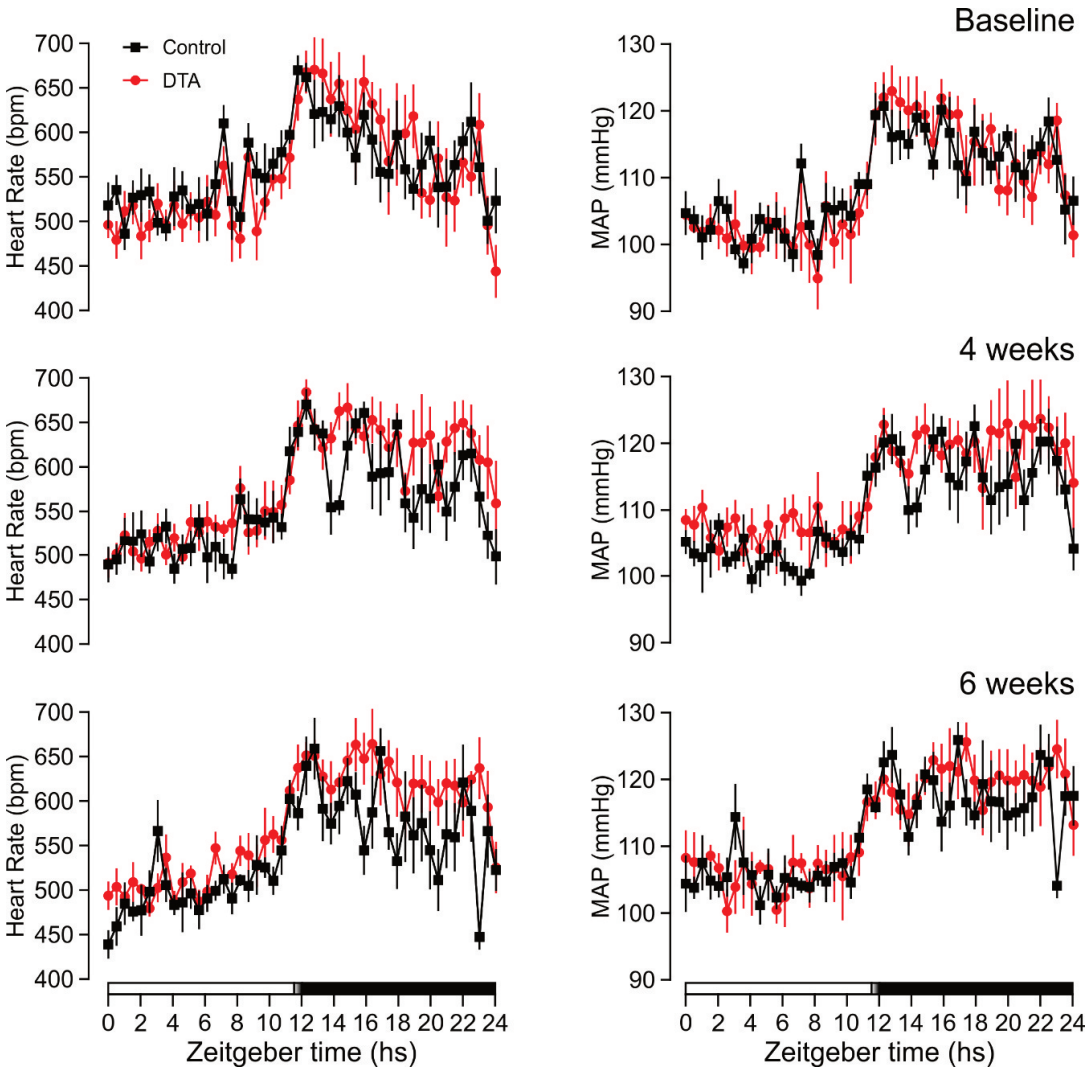

Fig 5.12 Ablation of PPG neurons has no effect on 24-hour heart rate and blood pressure. Heart rate (panels on left) and mean arterial blood pressure (MAP, panels on right) were recorded before DTA ablation of NTS PPG neurons (Baseline, top panel) and at four (middle panel) and six weeks (bottom panel) after surgery. Traces display average±SEM heart rate and blood pressure every 30 mins for control (black squares) and DTA mice (red circles). Light (white bar), twilight (gradient bar) and dark phase (black bar) are indicated at the bottom along with Zeitgeber time.

Because GLP-1R activation was found to increase heart rate at times of rest, I investigated whether PPG ablation affected resting heart rate in these mice. To explore this possibility, I extracted heart rate and MAP from periods of inactivity of at least 10 mins. Values were taken from across the 24-hour recording period. Heart rate and blood pressure do not return to baseline immediately following activity. To avoid any contamination of heart rate and MAP from recent activity, I ignored the first three minutes of the 10 mins periods of inactivity. Heart rate and MAP values from the last seven minutes of these inactive periods were combined and median heart rate and MAP calculated (Fig 5.13).

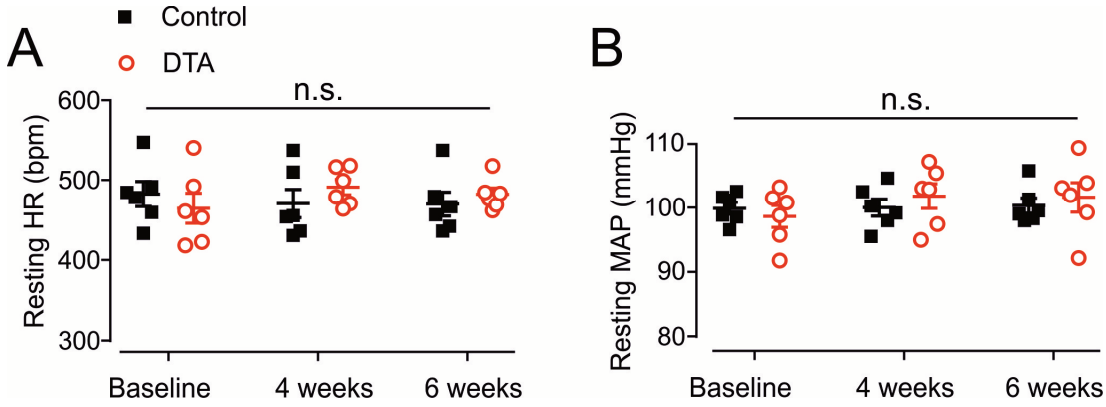

Fig 5.13 Resting heart rate and blood pressure are unaffected by PPG neuron ablation. A) Median resting heart rate (HR) and **B)** MAP of PPG-Cre/GCaMP3 or PPG-Cre/tdRFP transgenic mice transduced with either AAV1/2-FLEX-Perceval (Control, black squares) or AAV8-mCherry-FLEX-DTA (DTA, red circles) at baseline, 4 weeks, and 6 weeks after surgery. n.s.: no significant interaction or main effects according to two-way mixed model ANOVA.

Prior to PPG ablation, there was no difference in resting heart rate between the control (482.5±16 bpm) and DTA cohorts (478.0±22 bpm) (Fig 5.13A, p=0.78, Sidak's multiple comparisons test). Furthermore, there was little change in resting heart rate over time. At six weeks control animals had resting heart rates of 469.8±15 bpm and DTA mice had resting heart rates of 488.6±8 bpm. Two-way mixed model ANOVA yielded no significant interaction between virus and time ($F(2, 20) = 2.178$, $p=0.14$) and no main effects of virus ($p=0.78$) or time ($p=0.74$). Similarly, there was no difference in resting MAP between control (99.9±0.9 mmHg) and DTA cohorts (99.2±1.1 mmHg) prior to surgery (Fig 5.13B, p=0.93, Sidak's multiple comparisons test). PPG ablation had no effect on resting MAP, which did not change substantially in DTA animals from 99.2±1.1 mmHg to 102.1±0.8 mmHg at six weeks. There was no two-way interaction between time and virus ($F(2, 20) = 1.522$, $p=0.2426$) and no main effects of virus ($p=0.77$) or time ($p=0.14$).

These data suggest that control of resting heart rate and MAP does not require NTS PPG neuron activity. To investigate whether *active* heart rate and blood pressure were affected by loss of NTS PPG neurons, I extracted heart rate and MAP values from times of activity, defined as any time when activity was higher than zero. As expected, active heart rate was higher than resting heart rate with control mice having an active heart rate of 665.0±15 bpm as compared to a resting heart rate of 482.5±16 bpm (Fig 5.13A and 5.14A, $p<0.0001$, Student's paired t-test). Two-way mixed model yielded no significant interaction between virus and time ($F(2, 20) = 0.0835$, $p=0.9202$) and no main effects of virus ($p=0.36$) or time ($p=0.37$). Active heart rate remained similar from baseline to six weeks and there was no difference between control (661.1±11 bpm) and DTA animals (681.8±21 bpm) at six weeks after surgery ($p=0.76$, Sidak's multiple comparisons test).

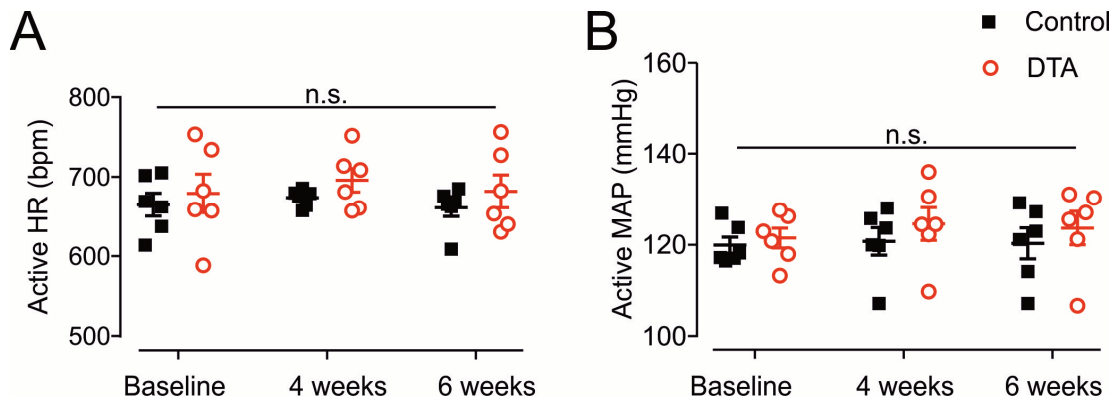

Fig 5.14 Active heart rate and blood pressure are unaffected by ablation of PPG. A) Median active heart rates and **B)** MAP of PPG-Cre/GCaMP3 or PPG-Cre/tdRFP transgenic mice transduced with either AAV1/2-FLEX-Perceval (Control, black squares) or AAV8-mCherry-FLEX-DTA (DTA, red circles) at baseline, 4 weeks, and 6 weeks after surgery. n.s.: no significant interaction or main effects according to two-way mixed model ANOVA.

Similarly, there was no effect of DTA ablation on active MAP (Fig 5.14). As with heart rate, MAP was significantly higher during activity than during rest ($p<0.0001$, Student's paired t-test). Two-way mixed model ANOVA yielded no significant interaction between time and virus ($F(2, 20) = 0.1653$, $p=0.85$) and no main effect of virus ($p=0.43$) or time ($p=0.65$), suggesting NTS PPG neuron activity is not required for regulation of resting and active heart rate and blood pressure.

Next, I explored if loss of NTS PPG neurons affects locomotor activity. Fig 5.15 shows plots of activity over 24 hours for two control and two DTA mice at baseline and six weeks post-surgery. There was no clear difference between control and DTA animals at baseline or at six weeks, and no discernible change in the level or pattern of locomotor activity between baseline and six weeks in either group.

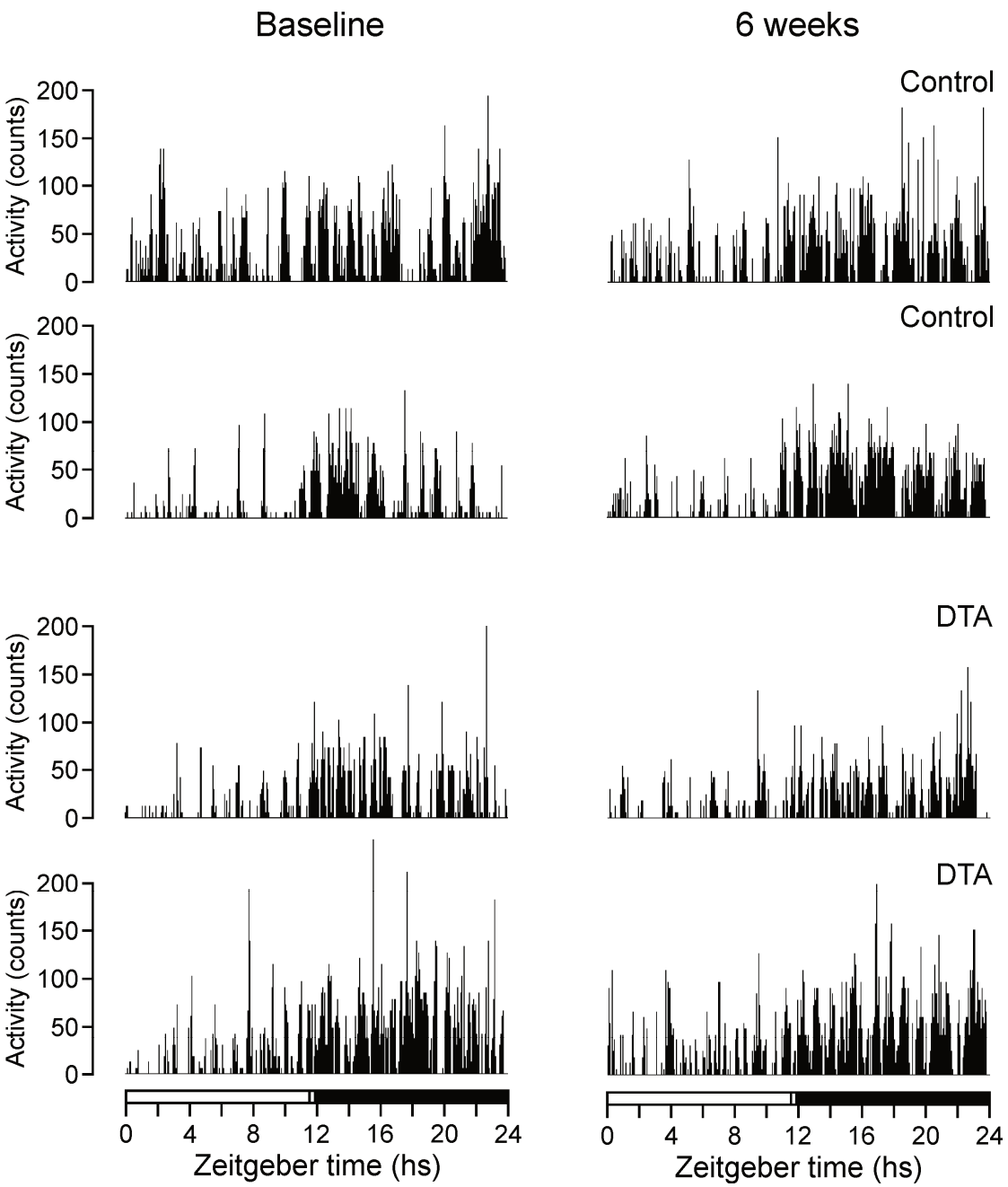

Fig 5.15 Ablation of NTS PPG neurons does not affect locomotor activity. Activity levels were monitored over 24 hours at Baseline and six weeks after stereotaxic injection of either AAV1/2-FLEX-Perceval (Control, two top panels) or AAV8-mCherry-FLEX-DTA (DTA, two bottom panels). Here are shown plots from four representative mice. Light (white bars), twilight (gradient bar), dark phase (black bar) are indicated at the bottom along with Zeitgeber time.

I quantified this by calculating the time spent inactive during light phase and dark phase, respectively (Fig 5.16). PPG ablation did not affect activity levels and six weeks post-surgery, there was no difference between the time control (88.3±1%) and DTA mice (89.1±1%) spent inactive during light phase (Fig 5.16A, p=0.98, Sidak's multiple comparisons test).

During dark phase, mice spent less time inactive with control mice spending only 65±3% of their time inactive in comparison with 85.9±2% during light phase (Fig 5.16B). This pattern was similar at all timepoints for both control and DTA mice (Fig 5.16B). At six weeks, control mice spent 64.3±3% of their time inactive during dark phase, similar to DTA mice, which spent 62.9±4% of their time inactive (p=0.99, Sidak's multiple comparisons test). These data suggest that loss of NTS PPG neurons does not affect locomotor activity, although future studies should address this in more detail.

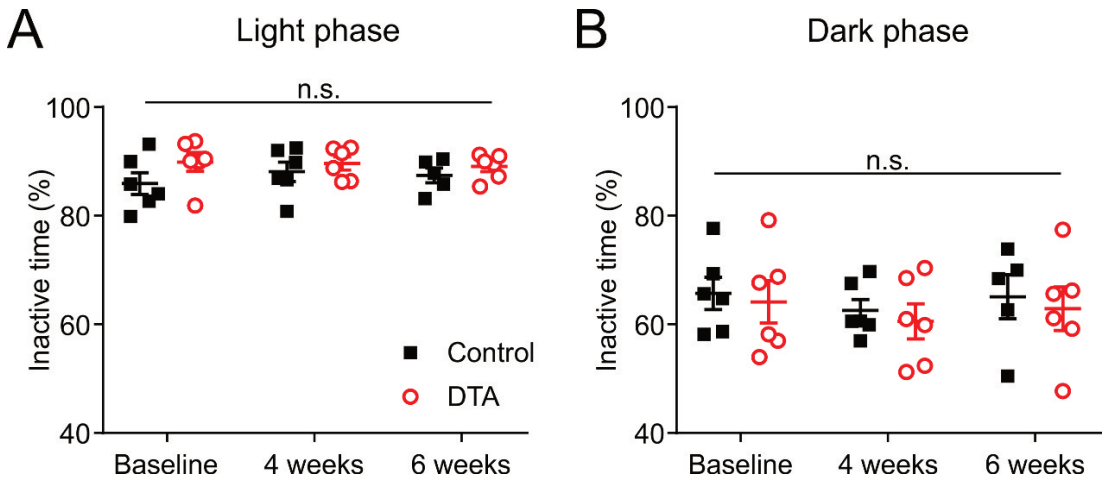

Fig 5.16 Ablation of PPG neurons has no effect on locomotor activity. Percentage of time spent inactive during light phase **(A)** and dark phase **(B).** Activity of PPG-Cre/GCaMP3 or PPG-Cre/tdRFP transgenic mice transduced with either AAV1/2-FLEX-Perceval (Control, black squares) or AAV8-mCherry-FLEX-DTA (DTA, red circles) at baseline, 4 weeks, and 6 weeks after surgery. n.s.: no significant interaction or main effects according to two-way mixed model ANOVA. Light phase: Two-way mixed model ANOVA: No significant interaction time x virus ($F(2, 20) = 0.9748$, $p=0.39$) and no main effect of virus ($p=0.25$) or time ($p=0.71$). Dark phase: No significant interaction time x virus ($F(2, 20) = 0.006161$, $p=0.9939$) and no main effects of virus ($p=0.65$) or time ($p=0.44$).

As demonstrated previously (Fig 5.2) heart rate and activity are positively correlated. To assess whether this correlation is affected by PPG neuron ablation, I analysed heart rate change in response to increasing activity. This confirmed a clear correlation between activity and heart rate for both control and DTA mice (Fig 5.17A and B). At low activity levels heart rate increased rapidly, whereas at higher activity levels increases in heart rate followed a linear regression. This correlation did not change with PPG ablation. At six weeks, linear regression slopes were similar for control and DTA mice (Fig 5.17C).

Furthermore, when inspecting the longitudinal data, no effect was found of PPG ablation (Fig 5.17D). In control mice, heart rate increased by 2.0±0.2 bpm per activity count at baseline. This was unchanged at six weeks when the slope was found to be 2.3±0.4 bpm per activity count (p=0.67, Sidak's multiple comparisons test). DTA mice had marginally attenuated increases in

heart rate in response to activity at six weeks (1.8±0.3 bpm per activity count) compared to baseline (2.6±0.4 bpm per activity count). However, this did not reach significance (p=0.20, Sidak's multiple comparisons test) and there was no two-way interaction between virus and time although it did approach statistical significance (F(2, 20) = 2.872, p=0.08).

Taken together these data suggest that NTS PPG neurons have no physiological role in cardiovascular control or regulation of locomotor activity. Furthermore, NTS PPG neurons were not important for increasing heart rate during rising activity.

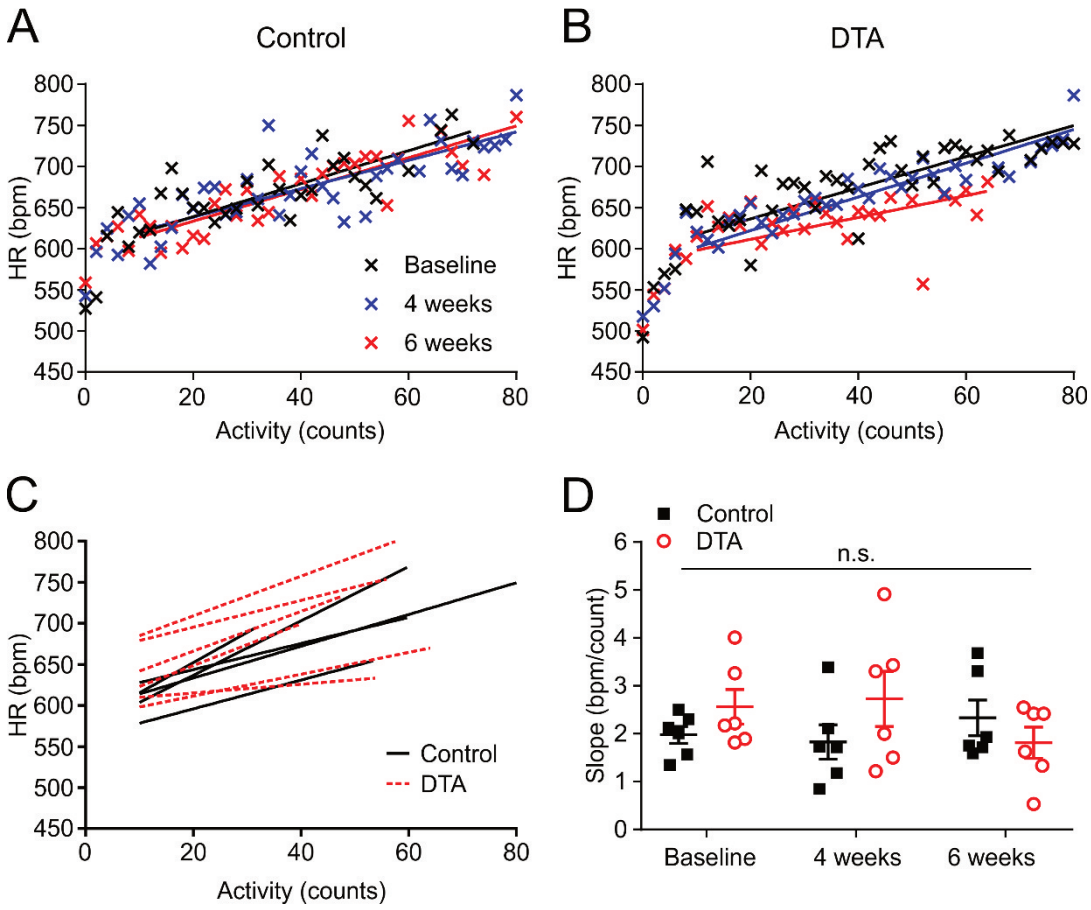

Fig 5.17 Ablation of PPG neurons has no effect on heart rate changes in response to increase in activity. Heart rate at increasing levels of activity at Baseline (black), four weeks (blue), and six weeks (red) from a representative control mouse **(A)** and DTA mouse **(B)**. Linear regressions were fitted for activity levels higher than 10. **C)** Plot of fitted linear regressions at six weeks after surgery from Control (black solid lines) and DTA mice (red dotted lines). **D)** Slopes from fitted linear regressions at Baseline, four weeks, and six weeks after surgery from Control (black squares) and DTA mice (red circles). n.s.: no significant interaction or main effects according to two-way mixed model ANOVA.

5.2.4 Ex4-induced tachycardia is independent of NTS PPG neuron activity

Having found no evidence for a physiological role of NTS PPG neurons in cardiovascular control, I next investigated whether Ex4-induced tachycardia is altered following loss of the central

source of GLP-1. To investigate this, I injected control and DTA animals with 10 µg/kg Ex4 i.p. nine weeks post-surgery.

As seen previously, i.p. injection with 10 µg/kg Ex4 led to an increase in heart rate with an initial stress-induced peak followed by a gradually declining elevated heart rate (Fig 5.18A). The response was similar in control and DTA animals. Indeed, analysis of the change in resting heart rate in response to saline and 10 µg/kg Ex4 revealed no significant difference between control and DTA mice in the response to both (Fig 5.18B and C). Two-way mixed model ANOVA yielded no significant interaction between treatment and virus ($F(1, 7) = 0.3287$, $p=0.5844$). There was no main effect of virus ($p=0.7610$), while there was a significant main effect of treatment ($p=0.0008$) suggesting NTS PPG neurons are not required for Ex4-induced tachycardia.

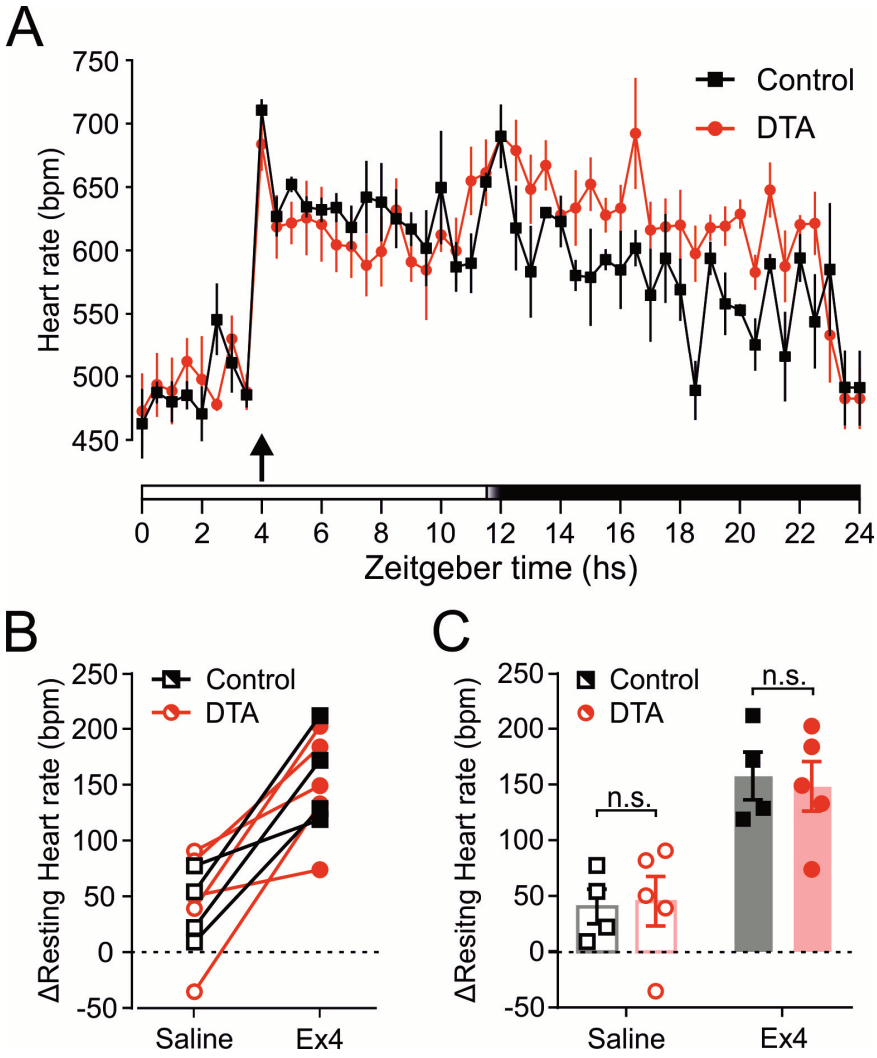

Fig 5.18 Ex4 increases heart rate independently of PPG neuron activity. A) Heart rate of control (black squares) and DTA mice (red circles) injected i.p. with 10 µg/kg Ex4 four hours into light phase. Shown here are mean±SEM of control (n=4, black) and DTA mice (n=5, red) mice taken every 30 mins over 24 hours as indicated by Zeitgeber time on the x-axis. The arrow indicates time of injection and the bars at the bottom indicate light (white bar) and dark (black bar) phases with a brief period of half-light indicated by a white to black gradient. **B)** and **C)** two different graphs showing the change in resting heart rate of control (black squares) and DTA mice (red circles) in response to saline (open symbols) and 10 µg/kg Ex4 (filled symbols). n.s.: not significant according to Sidak's multiple comparisons test.

5.2.5 High-fat diet for eight weeks induces weight gain, glucose intolerance, and tachycardia in C57BL/6 mice

In the next two sections, I investigate whether giving mice a metabolic challenge in the form of diet-induced obesity could unveil a physiological role for NTS PPG neurons in cardiovascular control. Previous studies have shown that HFD reduces the sensitivity of rats to the food intake-suppressive effects of Ex4 and GLP-1 (Williams et al. 2011; Duca et al. 2013; Mul et al. 2013),

suggesting a link between diet and the GLP-1 system. Furthermore, HFD has been shown to increase the levels of GLP-1 in the bloodstream (Wu et al. 2015).

To establish a model for diet-induced obesity in our laboratory, I fed a cohort of naïve, male C57BL/6 mice either normal chow or HFD for eight weeks (60% caloric content from fat). Mice kept on normal chow maintained their body weight over a period of 57 days with only a small increase in body weight at the end of the experiment (Fig 5.19). Two-way mixed model ANOVA revealed a significant interaction between diet and time ($F(16, 128) = 9.072$, $p<0.0001$). At 57 days, mice fed a HFD weighed significantly more than control mice ($p=0.001$, Fig 5.19A). Similarly, the percentage increase in bodyweight of HFD fed mice was significantly larger than that of mice fed normal chow with HFD fed mice gaining up to 44% of their initial bodyweight (Fig 5.19B, $p=0.0067$, Student's t-test).

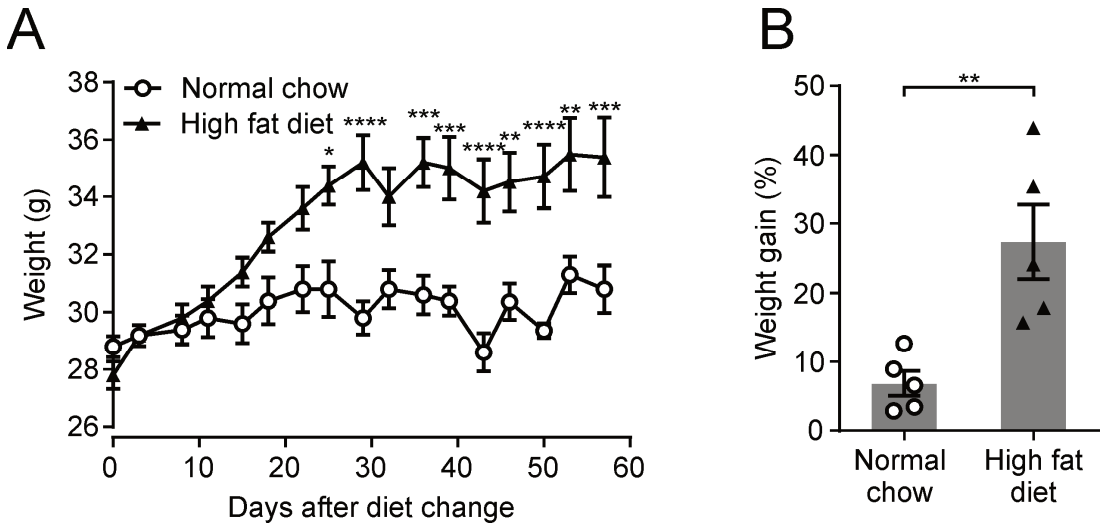

Fig 5.19 High-fat diet induces obesity in naïve C57BL/6 mice. A) Bodyweights of ten mice fed either normal chow (open circles, N=5) or HFD (filled triangles, N=5) were monitored over 57 days. *p<0.05, **p<0.01, ***p<0.001, ****p<0.0001, Sidak's multiple comparisons test. **B)** Percentage change in bodyweight from day 0 after 57 days for mice kept on normal chow (open circles) and mice fed a high-fat diet (filled triangles). **p<0.01, Student's t-test.

I next explored whether eight weeks of HFD was sufficient to induce glucose intolerance in these mice. Mice were given i.p. glucose tolerance tests (1 g/kg glucose load) at baseline and after eight weeks of HFD or normal chow (Fig 5.20A). There was a significant three-way interaction between timepoint, diet and time ($F(5, 5) = 2.398$, $p=0.0428$). I followed up with two separate two-way ANOVAs comparing data from normal chow and high-fat fed mice at baseline and 8 weeks. At baseline, there was no significant two-way interaction between time and diet, as expected ($F(5, 40) = 0.5283$, $p=0.7535$), and no main effect of diet ($p=0.12$). However, at eight weeks, two-way ANOVA revealed a significant interaction between time and diet ($F(5, 40) = 5.41$,

p=0.0007). Mice fed a HFD had significantly higher blood glucose levels after 15 mins (p<0.0001). This elevated blood glucose concentration failed to return to baseline over two hours (Fig 5.20A, p=0.02).

Two-way ANOVA of the AUCs revealed a significant interaction between timepoint and diet (F(1, 8) = 18.64, p=0.0026). At baseline, before mice had been given HFD or normal chow, there was no significant difference between the two groups (Fig 5.20B, p=0.41). In contrast, after eight weeks of HFD the AUC of the blood glucose response was significantly larger as compared to the AUC of mice kept on normal chow (p=0.0006). This demonstrates that eight weeks of HFD is sufficient to induce glucose intolerance in male C57BL/6 mice.

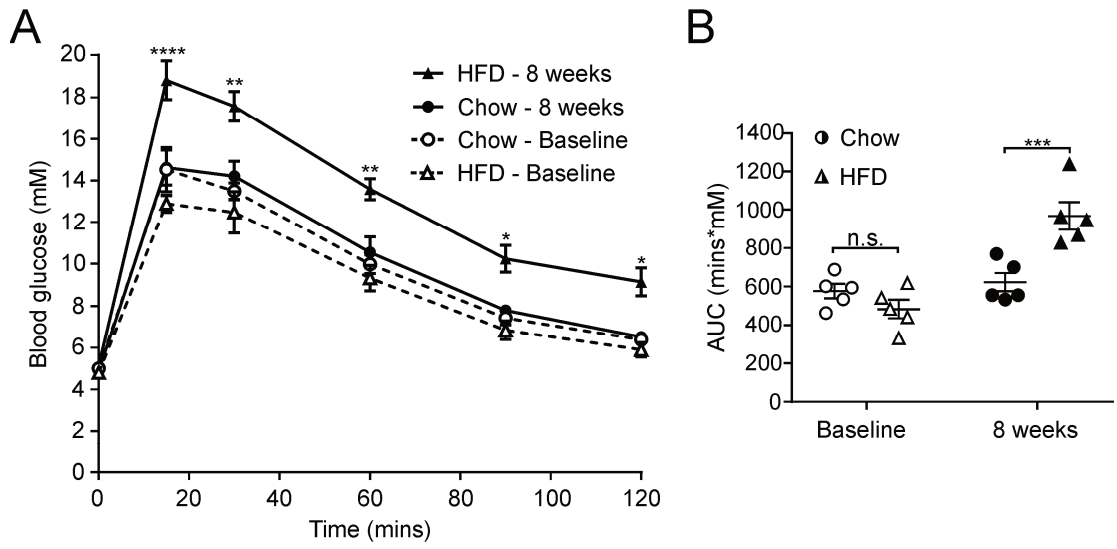

Fig 5.20 Diet-induced obesity leads to glucose intolerance in naïve C57BL/6 mice. A) Blood glucose concentrations following i.p. glucose tolerance test. Mice were tested before (Baseline, open symbols) and after (closed symbols) 8 weeks of HFD (triangles) or normal chow (circles). *p<0.05, **p<0.01, ****p<0.0001 as compared to Chow – 8 weeks, Sidak's multiple comparisons test. **B)** Quantification of A). Area under the curve (AUC) of glucose curves in A) for mice kept on normal chow (circles) and mice fed a high-fat diet (triangles) at Baseline and 8 weeks. n.s.: not significant. ***p<0.001, Sidak's multiple comparisons test.

Next, I investigated whether maintenance on HFD for eight weeks resulted in increased heart rate and blood pressure. Both were measured non-invasively using the tail-cuff system described previously. MAP, systolic, and diastolic pressure were unaffected by HFD (Fig 5.21A, p=0.77, p=0.84, and p=0.59, respectively). In contrast, heart rate was significantly elevated in mice fed a HFD for eight weeks as compared to mice on normal chow (Fig 5.21B, p=0.032).

In summary, eight weeks of HFD is sufficient to induce significant weight gain and glucose intolerance in male C57BL/6 mice. In addition, diet-induced obesity resulted in tachycardia without affecting blood pressure.

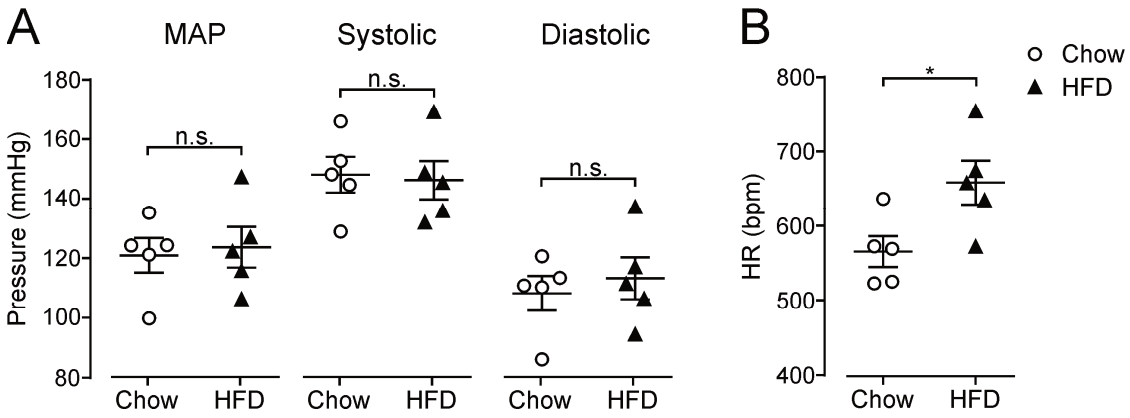

Fig 5.21 High-fat diet induces tachycardia, without affecting blood pressure, in naïve C57BL/6 mice. **A)** Mean arterial (MAP), systolic, and diastolic blood pressure, and **B)** mean heart rate (HR) of mice kept on normal chow (Chow, open circles) or fed a high-fat diet for 8 weeks (HFD, filled triangles). Mean±SEM are indicated. *p<0.05, n.s.: not significant, Student's t-test.

5.2.6 Diet-induced obesity leads to tachycardia and high blood pressure independently of PPG neuron activity

In the previous section, I demonstrated how switching to a HFD for two months induces obesity, glucose intolerance and tachycardia in male C57BL/6 mice. Having established a model for obesity-related cardiovascular pathology, I asked if tachycardia was dependent on the activity of NTS PPG neurons. To answer this, I transferred four control and five PPG-ablated mice from normal chow to HFD. After one month, control animals had gained 37±4% bodyweight and DTA mice had gained 49±9% bodyweight. This difference in bodyweight gain did not reach statistical significance (p=0.15).

Following one month of HFD, mice were significantly less active during dark phase as seen from two representative plots in Fig 5.22A. There was no obvious difference between control and DTA animals. Light phase activity was unaffected by HFD with mice spending between 85% and 92% of their time inactive after one month of HFD (Fig 5.22B). There was no two-way interaction between diet and virus ($F(1, 15) = 0.001386$, $p=0.9708$) and no main effect of HFD ($p=0.58$). In contrast, HFD decreased locomotor activity during dark phase (Fig 5.22B). Control mice spent 76±2% of their time inactive after HFD compared to 65±4% before diet-induced obesity. HFD decreased dark phase locomotor activity similarly in both groups (Fig 5.22B, $p=0.018$, main effect of diet in two-way ANOVA). There was no significant two-way interaction between diet and virus ($F(1, 15) = 0.04044$, $p=0.84$) and no main effect of virus ($p=0.45$), suggesting the decrease in dark phase locomotor activity is independent of PPG neuron activity.

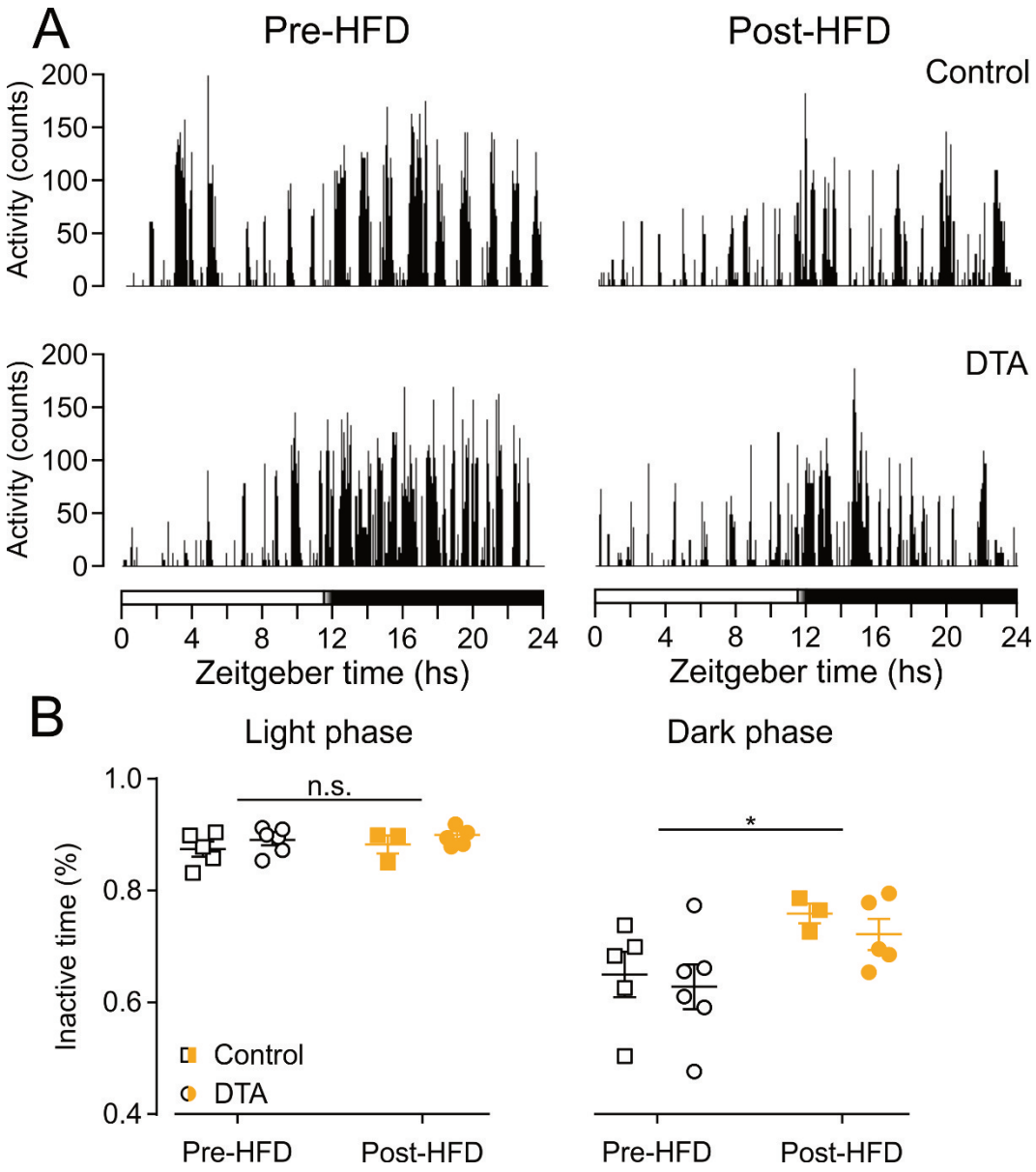

Fig 5.22 High-fat diet increases the time mice spend inactive independently of NTS PPG neuron activity. A) Activity plotted over 24 hours in a representative control (top panel) and DTA mouse (bottom panel) before (Pre-HFD, left panels) and after one month of HFD (Post-HFD, right panels). Light (white bar), twilight (gradient bar) and dark phase (black bar) are indicated at the bottom along with Zeitgeber time. **B)** Percentage of time spent inactive in control (squares) and DTA mice (circles) before (Pre-HFD, black open symbols) and after high-fat diet (Post-HFD, orange filled symbols). *p<0.05, main effect of diet in two-way ANOVA.

After only one month of HFD, both control and DTA mice had significantly elevated heart rate (Fig 5.23). In particular, heart rates were higher during light phase (Fig 5.23A). This difference in light phase and dark phase was hypothesised to be due to lower activity during light phase, which unmasks effects on resting heart rate. Indeed, when resting heart rate values were computed and their distributions plotted, it became clear that diet-induced obesity induced a

shift in the distributions towards higher resting heart rate values (Fig 5.23B) and resting heart rate was significantly increased in both control and DTA mice (Fig 5.23C). There was no two-way interaction between virus and diet ($F(1, 15) = 2.349$, $p=0.15$) and no main effect of virus ($p=0.28$). There was, however, a main effect of diet ($p<0.0001$), suggesting HFD induces tachycardia similarly in both control and DTA mice.

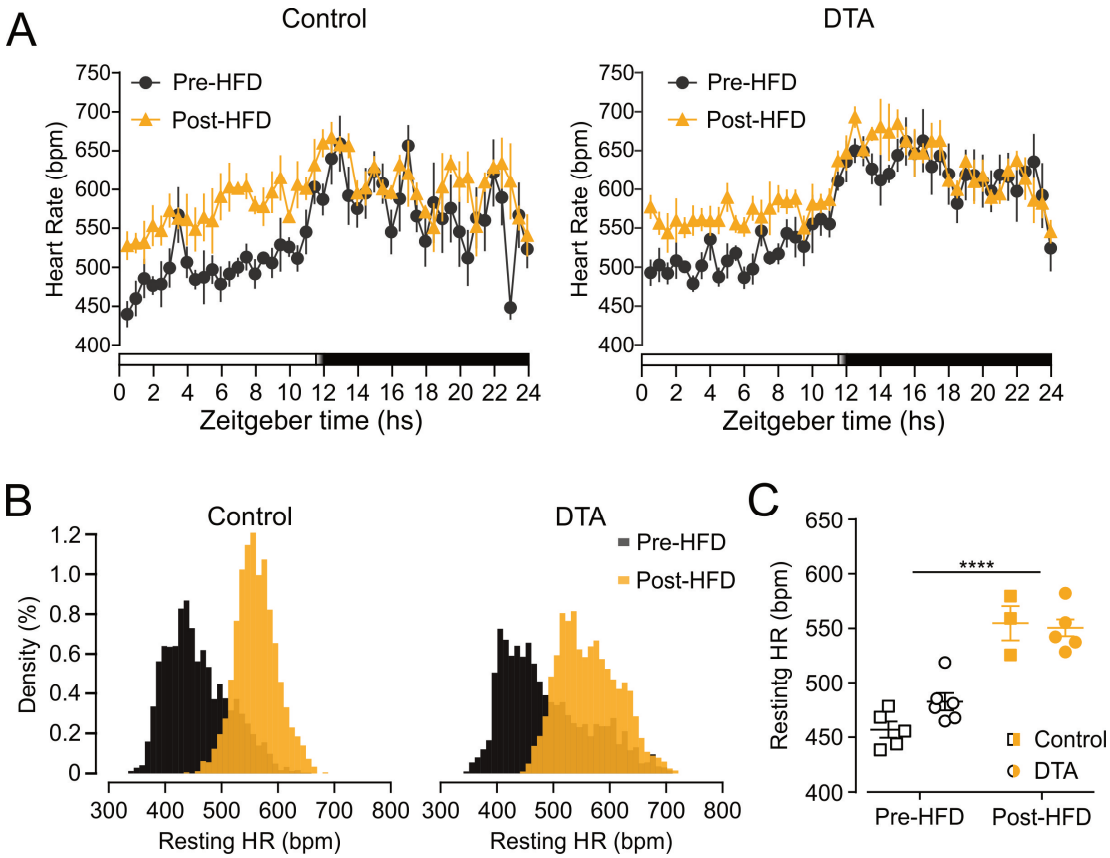

Fig 5.23 HFD induces tachycardia independently of PPG neuron activity. A) Mean heart rate taken every 30 mins over 24 hours in control (left panel) and DTA mice (right panel) before (Pre-HFD, black circles) and after one month of HFD (Post-HFD, orange triangles). Traces display average±SEM. Light (white bar), twilight (gradient bar) and dark phase (black bar) are indicated at the bottom along with Zeitgeber time. N=5 and 3 (Control, Pre-HFD and Post-HFD); N=6 and 5 (DTA, Pre-HFD and Post-HFD) **B)** Representative densities of resting heart rate (HR) from one control (left panel) and one DTA mouse (right panel) before (Pre-HFD, black) and after high-fat diet (Post-HFD, orange). Total density areas of individual histograms are 100. **C)** Resting HR of control (squares) and DTA mice (circles) Pre-HFD (empty black symbols) and after one month of high-fat diet (Post-HFD, orange symbols). ****$p<0.0001$, main effect of diet in two-way ANOVA.

Similarly, HFD led to an increase in resting MAP (Fig 5.24C). This was not detected with VPR tail-cuff measurements even after two months of HFD (Fig 5.21), suggesting the biotelemetry system is more sensitive than the tail-cuff system. The elevated MAP was most pronounced in control mice (Fig 5.24A). However, closer inspection of the distributions of resting MAP values revealed no obvious differences in the shift in the distributions after one month of HFD (Fig 5.24B). Both control and DTA mice displayed a shift towards higher resting MAP values. Indeed, analysis of

the resting median MAP yielded no significant two-way interaction between virus and diet ($F(1, 15) = 0.9044$, $p=0.3567$) and no main effect of virus (Fig 5.24C, $p=0.47$), whereas there was a main effect of HFD ($p=0.0018$).

Taken together, these results suggest that one month of HFD is sufficient to induce elevations in both resting heart rate and MAP, but that NTS PPG neurons play no physiological role in these changes.

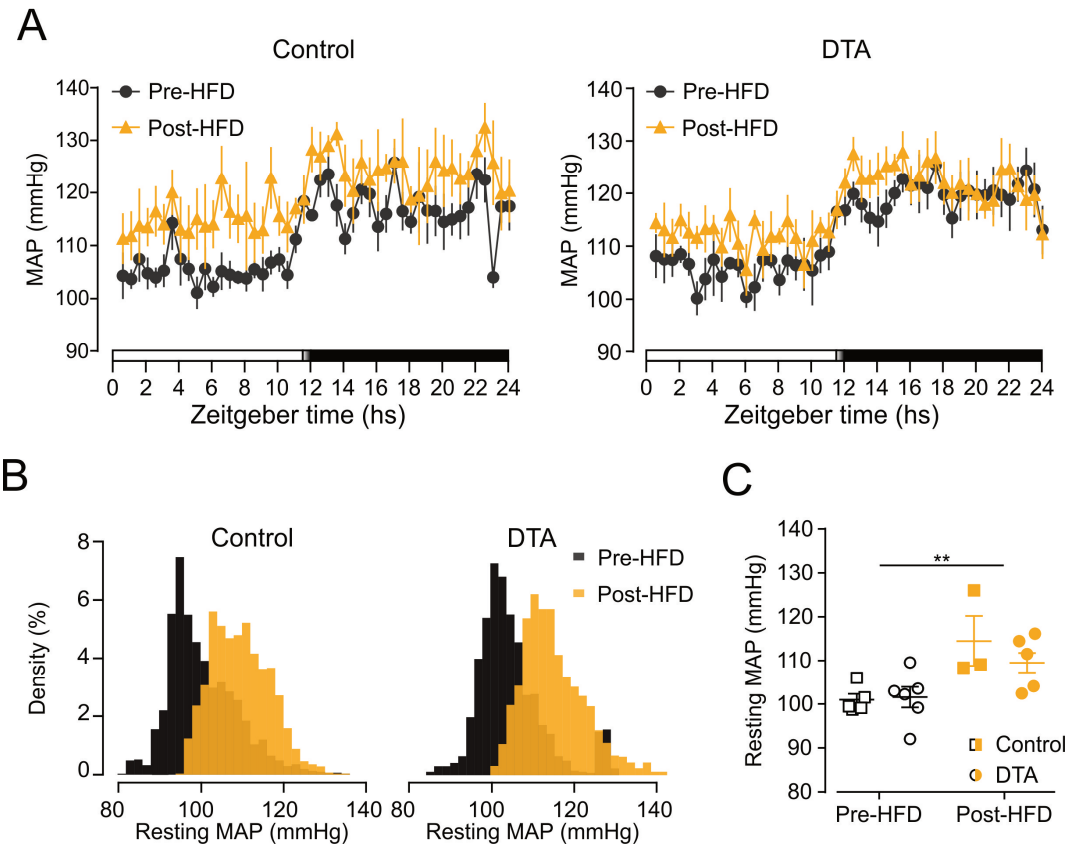

Fig 5.24 Diet-induced obesity increases MAP independently of PPG neuron activity. A) Mean MAP over 24 hours in control (left panel) and DTA mice (right panel) before (Pre-HFD, black circles) and after one month of HFD (Post-HFD, orange triangles). Traces display mean±SEM taken every 30 mins. Light (white bar), twilight (gradient bar) and dark phase (black bar) are indicated at the bottom along with Zeitgeber time. N=5 and 3 (Control, Pre-HFD and Post-HFD); N=6 and 5 (DTA, Pre-HFD and Post-HFD). **B)** Representative histograms showing densities of resting MAP values from one control (left panel) and one DTA mouse (right panel) before (Pre-HFD, black) and after one month of high-fat diet (Post-HFD, orange). Total density areas of individual histograms are 100. **C)** Resting MAP of control (squares) and DTA mice (circles) Pre-HFD (empty black symbols) and after one month of high-fat diet (Post-HFD, orange symbols). ***p<0.001, main effect of diet in two-way ANOVA.

5.2.7 Ex4 increases heart rate following high-fat diet

Having found no evidence for recruitment of NTS PPG neurons in response to diet-induced obesity, I next investigated if HFD affects the tachycardic response to systemic GLP-1R

activation. Previous studies has suggested that maintenance on HFD desensitises rats to the food intake-suppressive effects of GLP-1R stimulation (Williams et al. 2011; Mul et al. 2013).

Ex4 (10 μg/kg), injected i.p. four hours into light phase, increased heart rate in both control and DTA animals after HFD to a similar level as seen before HFD (Fig 5.25A). The change in resting heart rate from baseline in response to Ex4 was significantly reduced in both control and DTA animals following one month of HFD (Fig 5.25B, p=0.001, main effect of diet). There was no two-way interaction between diet and virus ($F(1, 7) = 1.519$, p=0.26) and no main effect of virus (p=0.86).

These data appear to suggest that diet-induced obesity attenuates the tachycardic effect of Ex4. However, the difference in the Ex4 responses could be due to an increase in baseline resting heart rate after one month of HFD as described in the previous section. Therefore, I also analysed the absolute heart rate in response to Ex4 and found that Ex4 increased resting heart rate to a similar level before and after diet-induced obesity (Fig 5.25C). In support of this, two-way repeated measures ANOVA revealed no interaction between diet and virus ($F(1, 6) = 0.2924$, p=0.61) and no main effects of diet (p=0.38) or virus (p=0.81).

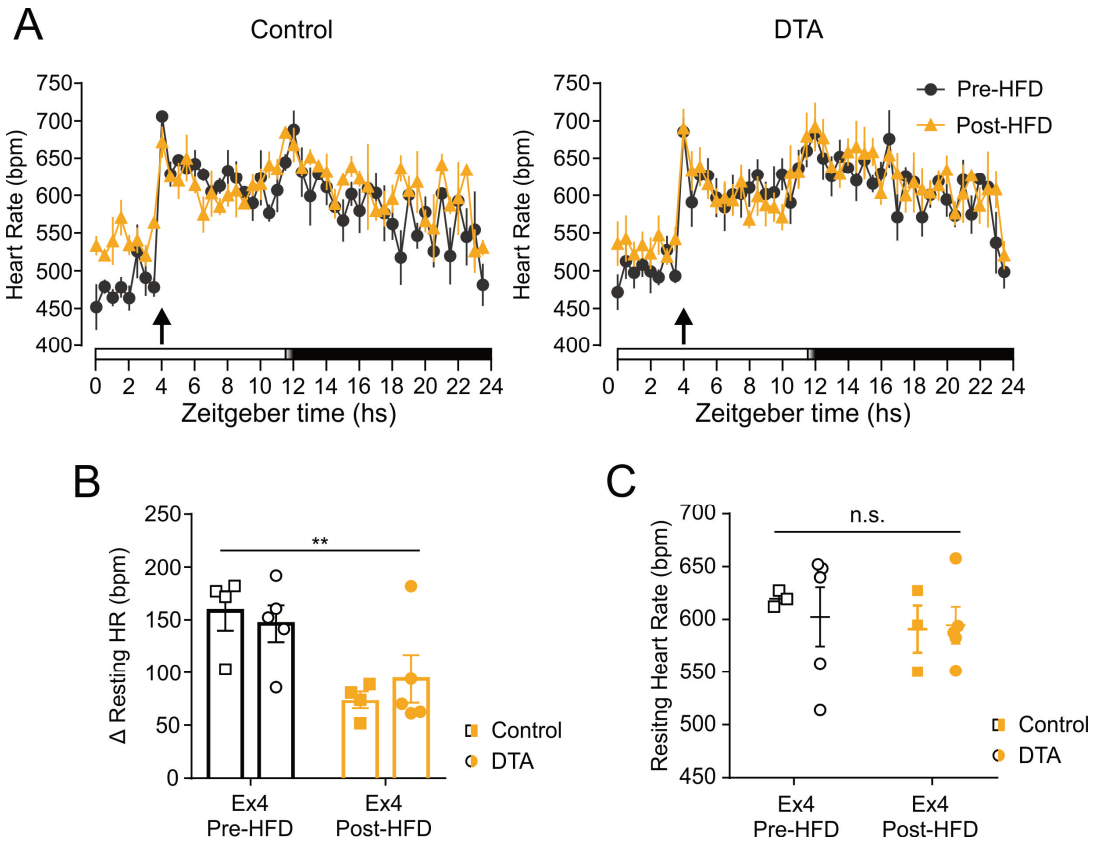

Fig 5.25 High-fat diet does not alter the tachycardic effect of systemic GLP-1R activation. A) Mean heart rate over 24 hours in control (left panel) and DTA mice (right panel) in response to 10 µg/kg Ex4 before (Pre-HFD, black circles) and after one month of HFD (Post-HFD, orange triangles). Traces display mean±SEM taken every 30 mins. Light (white bar), twilight (gradient bar), and dark phase (black bar) are indicated at the bottom along with Zeitgeber time. N=4 and 3 (Control, Pre-HFD and Post-HFD); N=6 and 5 (DTA, Pre-HFD and Post-HFD). Change in **(B)** and absolute **(C)** resting heart rate in response to 10 µg/kg Ex4 in control (squares) and DTA mice (circles) before (Pre-HFD, black empty symbols) and after one month of high-fat diet (Post-HFD, filled orange symbols). **p<0.01, n.s.: not significant, main effect of diet in two-way ANOVA.

5.2.8 Chemogenetic activation of NTS PPG neurons increases heart rate in freely-behaving mice

The data presented here do not support a physiological role for NTS PPG neurons in the regulation of heart rate and blood pressure. However, the sympathetic involvement in the tachycardic response to systemic GLP-1R activation suggests that central GLP-1Rs do have the potential to regulate heart rate. I therefore investigated if selective activation of NTS PPG neurons is sufficient to increase heart rate.

To this end, I injected three PPG-Cre/GCaMP3 transgenic mice with AAV2-FLEX-HM3Dq:mCherry and three PPG-Cre/GCaMP3 mice with AAV2-FLEX-EGFP as control. Two weeks later, I confirmed the effect of PPG activation on feeding. Since food intake is robustly suppressed following PPG activation as demonstrated in chapter 4, hypophagia in response to 2 mg/kg CNO was used as a

positive control for successful transduction of NTS PPG neurons with HM3Dq:mCherry. Indeed, control mice ate 1.6±0.09 g of chow in the first four hours, whereas HM3Dq-expressing mice ate only 0.7±0.15 g of chow (p=0.0006, Sidak's multiple comparisons test, Fig 5.26). Two-way mixed model ANOVA yielded no significant interaction between time and virus ($F(3, 12) = 2.821$, $p=0.0839$), but did reveal a significant main effect of both time ($p<0.0001$) and virus ($p=0.0092$), confirming that chemogenetic activation of NTS PPG neurons reduces food intake over several hours.

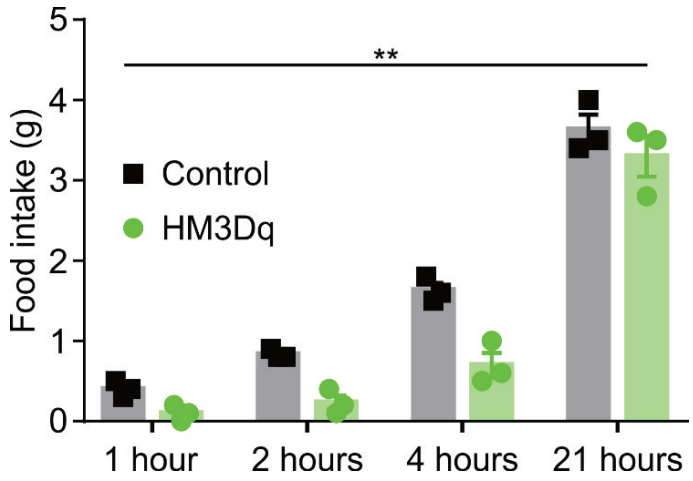

Fig 5.26 Selective activation of NTS PPG neurons induces hypophagia. Cumulative food intake measured over 21 hours following NTS PPG activation. Both control (black squares, N=3) and HM3Dq-expressing mice (green circles, N=3) were injected i.p. with 2 mg/kg CNO 30 mins prior to dark onset. **p<0.01, main effect of virus on food intake according to two-way mixed model ANOVA.

Having confirmed successful transduction of NTS PPG neurons in these mice, I implanted biotelemetry probes in the three control and three HM3Dq-expressing mice. After the recovery period, two of the biotelemetry probes implanted into control mice were blocked and therefore no longer detected meaningful blood pressure changes. I continued with one control mouse and three HM3Dq mice.

Mice were injected i.p. with 2 mg/kg CNO or saline 7.5 hours into light phase. As shown previously, injection of saline led to a transient increase in heart rate (Fig 5.27). At dark onset, heart rate rose as activity increased. When the same HM3Dq-expressing mouse was injected i.p. with 2 mg/kg CNO heart rate rose as with saline injection. However, heart rate did not return to baseline and remained elevated until onset of dark phase, suggesting activation of NTS PPG neurons increases heart rate (Fig 5.27). Locomotor activity was reduced in this animal following

2 mg/kg CNO compared to saline injection, demonstrating that the elevated heart rate cannot be explained by increased activity.

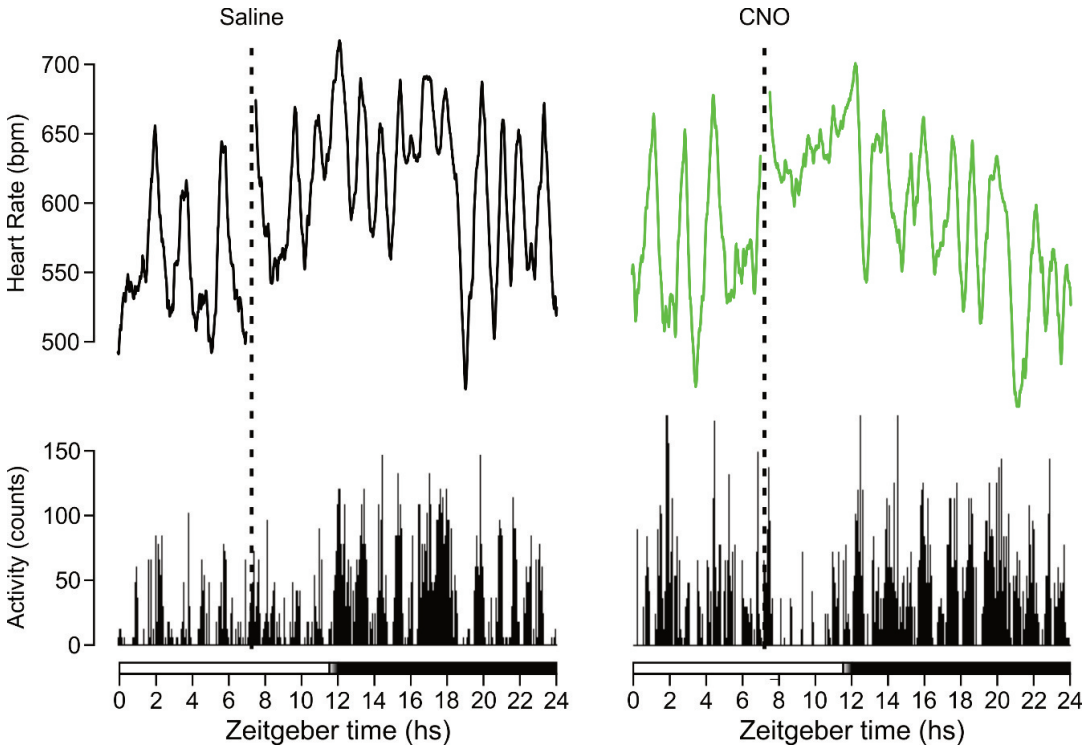

Fig 5.27 Chemogenetic activation of NTS PPG neurons increases heart rate in awake, behaving mice. Heart rate (top) and locomotor activity (bottom) of one mouse injected i.p. with either saline (black, left) or 2 mg/kg CNO (green, right) recorded over 24 hours as indicated by zeitgeber time at the bottom. Dotted lines indicate times of injection and the bar at the bottom indicates light (white bar) and dark (black bar) phases with a brief period of half-light indicated by a white to black gradient. Traces are running averages over 30 mins.

I quantified this tachycardia in three HM3Dq-expressing mice by extracting resting heart rates after saline and CNO, respectively. These values were taken from hours 8.5-10.5 to avoid contamination of resting heart rates with heart rate values during handling stress. As seen from the histogram in Fig 5.28A, the distribution of heart rate values following saline was skewed to the right with a median resting heart rate of 550 bpm. Chemogenetic activation of NTS PPG neurons resulted in a shift in the histogram towards higher heart rate values and a median resting heart rate of 631 bpm (Fig 5.28A).

To further compare the responses to saline and CNO, I calculated median resting heart rate at baseline and after i.p. injections of either saline or 2 mg/kg CNO. Baseline values were taken two hours prior to i.p. injection (hours 5-7) and response heart rates were taken from hours 8.5-10.5 as above. Resting heart rate was increased following saline by 41±11 bpm in HM3Dq-expressing mice (Fig 5.28B). However, injection of 2 mg/kg CNO increased heart rate by 108±10 bpm, which

was significantly more than that observed following saline (p=0.02, Student's pair t-test). In comparison, heart rate was slightly decreased following 2 mg/kg CNO in the control mouse (Fig 5.28B). Although I observed a reduction in locomotor activity in two HM3Dq-expressing mice following 2 mg/kg CNO as compared to saline, this decrease did not occur in the third HM3Dq-expressing mouse and in fact a decrease in locomotor activity was also observed in the one control mouse following 2 mg/kg CNO (Fig 5.28C).

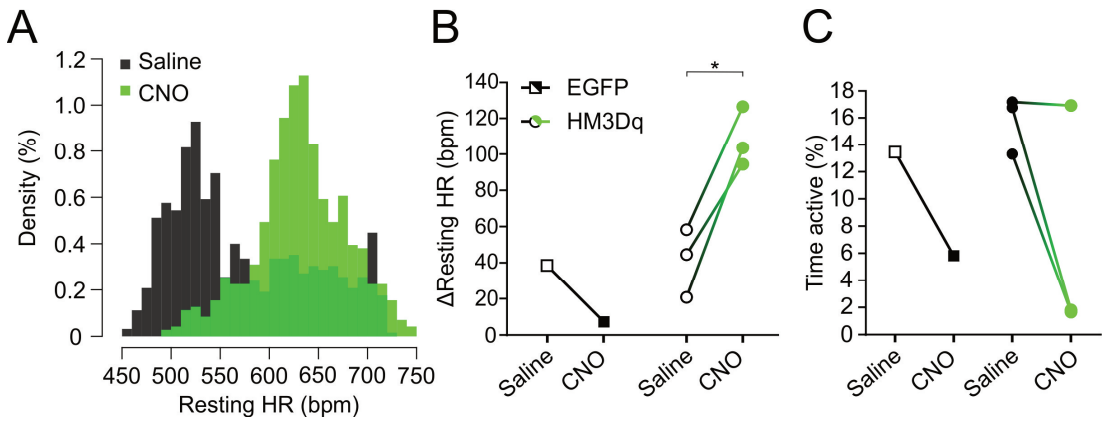

Fig 5.28 Activation of PPG neurons *in vivo* induces tachycardia. A) Representative histogram showing densities of resting heart rate (HR) values following i.p. injections of either saline (black) or 2 mg/kg CNO (green). Total density areas of individual histograms are 100. Change in resting HR **(B)** and time spent active **(C)** of control (squares, N=1) and HM3Dq-expressing mice (circles, N=3) in response to saline (empty black symbols) and 2 mg/ kg CNO (filled symbols). *p<0.05, paired t-test.

These data indicate that chemogenetic activation of PPG neurons is sufficient to increase resting heart rate. However, a future study with increased numbers of mice is needed to verify these effects. Furthermore, I did not obtain any data on blood pressure changes in response to PPG neuron activation, because the biotelemetry probes were partially blocked giving blunted blood pressure measurements. This only allowed accurate extraction of heart rate values from the frequency of the peaks of blood pressure trace. However, in collaboration with Dan R. Cook, another PhD student in our group, we have confirmed that heart rate is significantly increased following chemogenetic activation of NTS PPG neurons in anaesthetised mice (N=5). For this study, I performed the stereotaxic injections of the viruses and Dan R. Cook measured heart rate in the anaesthetised mice three weeks later. Taken together these data suggest that PPG neuron activation is sufficient to increase heart rate in mice.

5.3 Discussion

The mechanisms underlying GLP-1R mediated tachycardia are controversial and the implications for the use of GLP-1 analogues in the treatment of both diabetes and obesity are unknown. This chapter gives new insight into the role of GLP-1 in cardiovascular control. I first identified implantable biotelemetry as the optimal approach to investigate this and confirmed previous findings that Ex4-induced tachycardia is mediated by sympathetic activation (Yamamoto et al. 2002, 2003; Baggio et al. 2017) (Fig 5.9-5.10), but also demonstrated that it does not require PPG neuron engagement (Fig 5.18). Expanding on this, I found that ablation of NTS PPG neurons had little impact on heart rate and blood pressure, suggesting that central GLP-1 is not necessary for cardiovascular control (Fig 5.12-5.14). Tachycardia and hypertension following diet-induced obesity developed independently of PPG neuron activity (Fig 5.23-5.24). Finally, I found that selective activation of NTS PPG neurons was sufficient to increase heart rate (Fig. 5.28), suggesting that the central GLP-1 system does have the potential to modulate cardiovascular parameters.

5.3.1 Choosing and understanding a method for measuring blood pressure and heart rate in conscious mice

Accurate recordings of heart rate and blood pressure can be obtained using VPR tail-cuff systems (Feng et al. 2008). However, tail-cuff recordings require restraint, which causes stress and affects heart rate and blood pressure (Wilde et al. 2017). Importantly, the acute stress associated with handling and restraint does not disappear with training (Gross and Luft 2003). In comparison, biotelemetry does not require handling of the animal beyond the initial surgical intervention. Indeed, measurements of resting heart rate and MAP were consistently lower when measured using the biotelemetry system in comparison with the VPR tail-cuff system (Fig 5.3). Since these measurements were not done in the same mice or in the same environment, I cannot exclude that other factors contributed to the higher heart rate and MAP in tail-cuff measurements. However, similar results have been demonstrated previously with even larger effects of restraint and tail-cuff measurements (Wilde et al. 2017). Indeed, Gross & Luft (2003) argued that the tail-cuff method should only be used when large differences in blood pressure and heart rate are expected from the experiment. Considering the putative role of central GLP-1 in stress (Kinzig et al. 2003; Maniscalco et al. 2012; Ghosal et al. 2013, 2017; Holt and Trapp 2016), I concluded that the relatively stress-free biotelemetry method was the most appropriate.

Most studies using biotelemetry recordings of cardiovascular output simply report mean heart rate and blood pressure (Yamamoto et al. 2002, 2003; Griffioen et al. 2011). I demonstrate here

that the mean is not a meaningful measure of these parameters (Fig 5.2). Heart rate and MAP measurements did not follow a normal distribution and were dependent on activity levels as reported previously (Sheward et al. 2010). In fact, when I plotted heart rate values against activity (no activity versus any level of activity), I found that the bimodal distribution was made up of two unimodal distributions. Importantly, these distributions were not normal. Although Sheward et al. (2010) did investigate the distributions of heart rate and blood pressure values, they only reported mean values. As mentioned, most studies fail to acknowledge the non-normal distribution of their measurements (Yamamoto et al. 2002; Griffioen et al. 2011). Based on the skewed distributions, I concluded that the mean values would not be meaningful and I instead calculated the medians.

5.3.2 The tachycardic effect of Ex4 – peripheral and central contributions

GLP-1R activation is well-known to induce robust tachycardia, whether the agonist is injected systemically (Barragán et al. 1994, 1996; Yamamoto et al. 2002; Hayes et al. 2008) or directly into the brain (Barragán et al. 1999; Yamamoto et al. 2002; Griffioen et al. 2011). Here, I confirmed those findings in mice implanted with biotelemetry probes (Fig 5.4-5.6). Peripheral injection of 10 µg/kg Ex4 dramatically increased heart rate without affecting locomotor activity, suggesting the tachycardic effects was not secondary to a change in activity, in accordance with previously published studies (Hayes et al. 2008; Griffioen et al. 2011). Interestingly, I found no effect of i.p. injections of GLP-1 on heart rate (Fig 5.4 and 5.6). However, this is most likely due to the short half-life of GLP-1 in the bloodstream. The stress-induced peak in heart rate and blood pressure observed with both saline and Ex4 injections would mask any effects of GLP-1 on heart rate. Indeed, Barragan et al. (1994, 1996) demonstrated potent tachycardic effects of intravenous GLP-1 in anaesthetised rats, but found that the effect was shorter lived than that of Ex4, although their recordings did not go beyond 30 mins after injection. In support of this, Dan R. Cook, another PhD student in our group, found that in the anaesthetised mouse, in the absence of stress-induced tachycardia, 100 µg/kg GLP-1 significantly elevated heart rate (N=5, unpublished).

In the experiments presented here, Ex4 was injected i.p. and could work to increase heart rate via both peripheral and central GLP-1Rs. Literature on the mechanisms underlying Ex4's tachycardic effects is controversial, with the most commonly proposed scenario involving both peripheral and central mechanisms (Barragán et al. 1999; Yamamoto et al. 2002; Baggio et al. 2017). Current evidence is conflicting and fails to paint a clear picture.

A direct chronotropic effect of GLP-1R agonism on the heart has been proposed, but the evidence is sparse. GLP-1Rs are found on the heart of mice (Richards et al. 2014) and Baggio et al. (2017) recently demonstrated that mice lacking cardiac GLP-1Rs have reduced heart rate responses to treatment with liraglutide. However, this appeared to be mainly due to an increase in heart rate in response to vehicle injections in mice lacking cardiomyocyte GLP-1Rs. Furthermore, it was the opposite of what was found by the same group a few years earlier in an experiment where sensitivity to liraglutide was unaffected by genetic disruption of cardiac GLP-1Rs (Ussher et al. 2014). In addition, they failed to show any direct effects of GLP-1R agonism on isolated hearts (Baggio et al. 2017), leaving the role of cardiac GLP-1R in GLP-1-mediated tachycardia elusive.

In 1999, Barragan et al. investigated the relative contributions of peripheral and central GLP-1Rs to GLP-1-induced tachycardia. They found that the tachycardic effects of peripheral GLP-1R stimulation could be blocked with central infusions of the selective antagonist Ex9, suggesting central GLP-1Rs are responsible for the cardiovascular effects of GLP-1. In contrast, the effects of central GLP-1 could not be blocked by peripheral Ex9. Interestingly, however, peripheral GLP-1 did increase heart rate and that effect was blocked by peripheral Ex9, suggesting some contribution by peripheral receptors. These data suggest a mechanism in which peripheral GLP-1 activates peripheral GLP-1Rs leading to engagement of the central GLP-1 system. However, there is at present no other evidence for such a link and in fact one study found that central Ex9 was not able to block the food intake-suppressive effects of peripheral GLP-1 (Williams et al. 2009). As such, the contributions of peripheral GLP-1Rs to the effects of systemic GLP-1 remain unknown.

There is some evidence for a neural link between peripheral GLP-1 and central pathways. Peripherally administered GLP-1 activates vagal afferents and GLP-1Rs are expressed in the nodose ganglion (Kakei et al. 2002; Nakagawa et al. 2004; Bucinskaite et al. 2009; Gaisano et al. 2010; Richards et al. 2014). However, the physiological role of these GLP-1Rs remains uncertain with some reports suggesting no necessity for vagal afferents in the response to GLP-1 (Hayes et al. 2011b; Zhang and Ritter 2012; Reidelberger et al. 2014; Sisley et al. 2014), whereas other studies have found clear involvement of the vagus-brain communication (Abbott et al. 2005; Fujiwara et al. 2012; Krieger et al. 2015). However, none of these studies were performed in the context of cardiovascular control. This highlights the need for further research into the importance of vagal afferents in peripheral GLP-1's effects and the downstream targets of GLP-1-mediated vagal stimulation.

It is likely that peripherally administered Ex4 acts directly on central GLP-1Rs, diminishing the importance of the potential vagal pathways involved. This notion is supported by several pieces of evidence described in the introduction. It is likely that Ex4 crosses the blood brain barrier to reach receptors in the brain (Kastin and Akerstrom 2003; Secher et al. 2014). Furthermore, peripheral Ex9 has no impact on the cardiovascular and food intake-suppressive effects of peripheral Ex4 (Barragán et al. 1996; Kanoski et al. 2011), suggesting the effects are mediated by central GLP-1Rs, although it is unclear why Ex9, which is structurally similar to Ex4, should have no access to central GLP-1Rs. The question then remains why peripheral GLP-1, assuming it does not reach receptors in the brain due to its rapid degradation, is able to increase heart rate (Barragán et al. 1999). Peripheral injection of a GLP-1 analogue, albugon (Baggio et al. 2004a), which cannot cross the blood-brain barrier, would partly address the question of a contribution of peripheral GLP-1Rs to tachycardia.

5.3.3 Ex4-induced tachycardia is mediated by the sympathetic nervous system

The involvement of the autonomic nervous system in GLP-1R-mediated tachycardia is a much-disputed point. Although most data from rats have suggested a role of the sympathetic nervous system in GLP-1R-mediated tachycardia (Barragán et al. 1994; Yamamoto et al. 2002), a study in mice concluded that depression of the parasympathetic nervous system was in fact the cause of increased heart rate (Griffioen et al. 2011). The data presented in this chapter clearly demonstrated that i.p. Ex4 does not increase heart rate in the absence of sympathetic input to the heart (Fig 5.9 and 5.10). This finding corresponds with a recent publication by Baggio et al. (2017), in which propranolol, a non-selective β-blocker, abolished the heart rate response to liraglutide in mice.

I did not find any evidence for an effect of i.p. 10 µg/kg Ex4 on locomotor activity in accordance with other studies in mice (Griffioen et al. 2011; Baggio et al. 2017), although there have been reports of decreased activity following i.p. injection of 2.4 µg/kg Ex4 in rats (Hayes et al. 2008). Importantly, the decrease observed in the latter study was only obvious when activity was elevated due to chronic decerebration. Similarly, Ex4 has been found to reduce locomotor activity in response to amphetamine (Erreger et al. 2012). Taken together, this suggests that Ex4 has no effect when activity is otherwise low, but at times of high activity it may work to reduce locomotion. Whether this is a direct effect on activity or indirectly affects activity by suppressing food-seeking behaviour remains unclear.

Additionally, I did not observe any difference in MAP after i.p. injection of Ex4. This is in contrast to what has been observed in rats (Barragán et al. 1994; Yamamoto et al. 2002) and could be

the result of regulatory mechanisms preventing potentially detrimental increases in blood pressure. Previous studies in mice did not measure blood pressure in response to GLP-1R activation, although one study did find antihypertensive effects of liraglutide in mice with pharmacologically elevated blood pressure (Kim et al. 2013).

The involvement of the sympathetic nervous system in Ex4-induced tachycardia and the evidence described above suggest that GLP-1R activation leads to increased heart rate, at least in part, through engagement of the central nervous system. Yamamoto et al. (2003) proposed that activation of catecholaminergic neurons in the AP, possibly via other areas in the brainstem, the PBN, VLM, and NTS, ultimately leads to increased sympathetic outflow. In support of a mechanism relying on the brainstem, a study by Hayes et al. (2008) using decerebrate rats concluded that no brainstem → forebrain communication was necessary for tachycardia induced by fourth ventricle infusions of Ex4, suggesting that brainstem → spinal cord circuits culminating in sympathetic activation are responsible for the increase in heart rate. Importantly, the findings by Hayes et al. (2008) can also be explained by direct activation of GLP-1Rs in the spinal cord, which would be accessible to fourth ventricle Ex4 in decerebrate rats. Interestingly, I show here that tachycardia induced by systemic Ex4 is not dependent on NTS PPG neurons (Fig 5.18), suggesting a potential brainstem → spinal cord circuit does not include PPG neurons. This is most likely due to circumvention of these cells by Ex4, which acts directly on downstream central GLP-1Rs. Importantly, these findings do not exclude the possibility that NTS PPG neurons are essential regulators of heart rate and blood pressure in mice or that brainstem → forebrain circuits contribute to the impact of these neurons on cardiovascular control.

5.3.4 NTS PPG neurons are not involved in normal cardiovascular control

These pharmacological studies provide insight into the mechanisms by which GLP-1 analogues used in the treatment of diabetes and obesity lead to cardiovascular pathology (Robinson et al. 2013). However, in normal physiology, GLP-1 from the periphery is unlikely to reach GLP-1Rs in the brain as discussed in the Introduction. I was therefore interested in the potential involvement of NTS PPG neurons in cardiovascular control. As in Chapter 4, I ablated PPG neurons in the NTS. Unpublished data from our laboratory show that PPG ablation results in 80% reduction in GLP-1 in the hypothalamus and spinal cord (James E. Richards and S. Trapp, unpublished). However, this loss of central GLP-1 did not affect heart rate and blood pressure at rest or during activity (Fig 5.12-5.14). Similarly, genetic disruption of GLP-1Rs has no effect on baseline cardiovascular parameters and lack of hypothalamic GLP-1Rs does not affect baseline heart rate (Gros et al. 2003; Ghosal et al. 2017). Notably, these studies failed to report how

baseline values were calculated and did not appear to acknowledge the strong correlation between activity and heart rate observed here. In this chapter, I report for the first time that NTS PPG neurons are not necessary for control of resting and active heart rate and blood pressure (Fig 5.13). More in-depth analysis of the relationship between heart rate and activity in control and PPG ablated mice revealed no difference in the heart rate response to increased activity although these findings should be substantiated by repeating the study with a larger cohort of mice (Fig 5.17).

Ghosal et al. (2017) recently demonstrated that tachycardia induced by acute restraint stress is mediated by GLP-1Rs in Sim1-positive neurons in the hypothalamus. Although I did not specifically design an experiment to investigate the effect of lack of NTS PPG neurons on cardiovascular responses to stress, I did expose the mice to brief handling stress when injecting them. Both control and PPG ablated mice responded to i.p. injection of saline with a similar increase in resting heart rate (Fig 5.18). This suggests that PPG neurons are not necessary for the tachycardic response to acute stress. However, handling during i.p. injections is usually shorter than 1 min, which could be too brief to detect differences. In future experiments using PPG-ablated mice it would be interesting to expose them to acute restraint stress for 30 mins, as I did in Chapter 4. Based on the reports by Ghosal et al. (2017), I would expect PPG ablated mice to have blunted tachycardia in response to acute stress.

5.3.5 NTS PPG neurons are not necessary for tachycardia and hypertension following diet-induced obesity

Metabolic syndrome is the medical term for a combination of obesity, diabetes and hypertension. It can be caused by intake of HFD and puts humans at greater risk of coronary heart disease and stroke. Here, mice became obese, glucose intolerant, and tachycardic after only eight weeks of HFD as reported previously (Winzell and Ahren 2004). Blood pressure did not appear to be affected by HFD when measured using the VPR tail-cuff system. However, implantable biotelemetry revealed a clear, overall effect on both heart rate and blood pressure after only four weeks of HFD. This discrepancy could have several causes. Firstly, the increased sensitivity of the implantable biotelemetry system may allow me to calculate more accurate resting heart rate and blood pressure from undisturbed mice. Alternatively, these mice developed more severe metabolic syndromes after just one month of HFD. Although I can make no certain conclusions based on these data, I did observe that biotelemetry mice gained weight faster than mice in the preliminary HFD experiment. Notably, mice implanted with biotelemetry

probes were housed individually, which could lead to overeating and lower activity than mice group-housed as in the preliminary experiment (Bartolomucci et al. 2009).

Alongside metabolic syndrome, PPG-ablated and control mice appeared to be less active during dark phase, when activity normally increases due to food-seeking behaviour, indicating a level of lethargy as a result of diet-induced obesity (Fig 5.22 and 5.8). My findings do not support a role for NTS PPG neurons in the hypertension and tachycardia following diet-induced obesity. Interestingly, our laboratory has data demonstrating maintenance on HFD approximately doubles brain GLP-1 levels (James E. Richards, S. Trapp, unpublished). It is curious that the increased expression levels did not affect cardiovascular control, since PPG-ablated and control mice developed tachycardia and hypertension to a similar degree. This could indicate that although expression is increased, GLP-1 is not released in significant amounts from PPG neurons during development of metabolic syndrome. Alternatively, downstream GLP-1Rs are desensitised to GLP-1 in diet-induced obesity.

There is some evidence for reduced sensitivity to GLP-1 analogue treatment after HFD (Williams et al. 2011; Mul et al. 2013). This appeared to be partly due to reduced vagal sensitivity to GLP-1 at the level of the nodose ganglion (Duca et al. 2013). In contrast, I did not observe any change in the tachycardic response to Ex4 following HFD in both control and PPG-ablated mice, suggesting the sensitivity of the downstream pathways is not compromised by the development of metabolic syndrome (Fig 5.25). If the effect of diet-induced obesity on GLP-1 sensitivity is partly due to decreased sensitivity of vagal afferents, it is likely that Ex4 would circumvent this by acting directly on brain GLP-1Rs. It is worth noting that in previous studies, the food intake-suppressive effects of Ex4 have persisted after HFD and diet-induced obesity has mainly affected the temporal profile of the response to Ex4 (Williams et al. 2011; Mul et al. 2013). Considering the finding that HFD suppresses the expression of GLP-1R in the nodose ganglion, it is possible that only peripheral GLP-1 signalling is perturbed by HFD (Duca et al. 2013).

5.3.6 NTS PPG neurons are sufficient to increase heart rate in mice

It is surprising that Ex4 induces such a robust increase in heart rate when the central source of GLP-1 has no impact on normal heart rate and blood pressure. I reject the explanation that Ex4 in fact increases heart rate via peripheral GLP-1Rs independent of the central GLP-1 system. There is substantial evidence for a role of central GLP-1Rs in the response to peripheral Ex4 (Barragán et al. 1999; Yamamoto et al. 2002; Hayes et al. 2008; Griffioen et al. 2011), and in contrast little convincing data supporting a role of cardiac GLP-1Rs (Ussher et al. 2014; Baggio et al. 2017). In line with my observations, Gros et al. (2003) found no effect of genetic disruption

of the GLP-1R, suggesting the central GLP-1 system is not engaged in normal cardiovascular control. Is the tachycardia following i.p. Ex4 then simply a result of overactivation of GLP-1Rs, which does not occur in normal physiology? Acute stress appeared to reveal a role for hypothalamic GLP-1Rs in cardiovascular control, suggesting the central GLP-1 system needs a physiological push to become engaged, similar to what I observed in Chapter 4 in the context of food intake (Ghosal et al. 2017).

My results from chemogenetic activation suggest that NTS PPG neurons do have the ability to increase heart rate (Figs 5.27-5.28). This corresponds with what we have observed in anaesthetised mice (Dan R Cook, unpublished), where chemogenetic activation of PPG neurons led to an increase in heart rate. Taken together, the evidence presented here demonstrates that NTS PPG neurons do have the ability to regulate heart rate, but do not affect cardiovascular parameters under normal conditions, nor do they contribute to the development of tachycardia and hypertension as a result of diet-induced obesity. The exact physiological context in which PPG neurons are relevant for cardiovascular control will need to be examined. The chemogenetic manipulation of PPG neurons is an important tool in this endeavour. Of particular interest is refeeding-induced tachycardia as described by Ussher et al. (2014) in mice lacking cardiomyocyte GLP-1Rs, as well as acute stress paradigms as described in Chapter 4 and in mice lacking hypothalamic GLP-1Rs (Ghosal et al. 2017). Considering the effects of PPG inactivation on food intake in those paradigms, this could unveil a physiological role for PPG neurons in cardiovascular control.

6. Summary and Perspectives

This thesis provides new insight into the physiological role of the central GLP-1 system. Whilst most studies have used pharmacological overactivation of GLP-1Rs to study the actions of GLP-1 in the brain, here I addressed for the first time the physiological role of the source of endogenous GLP-1, PPG neurons. Although activation of GLP-1Rs in the CNS induces hypophagia and tachycardia, no studies have addressed the physiological role of PPG neurons in the regulation of food intake and heart rate. In the experiments presented here, I selectively manipulated the activity of PPG neurons and observed the impact on feeding and cardiovascular control. My findings clarify the role of PPG neurons in satiety and investigate for the first time the requirement for these cells in the regulation of heart rate and blood pressure.

The data presented in **Chapter 3** elucidated the signals detected by NTS PPG neurons and dissected the mechanisms underlying serotonergic modulation of these cells, which involved 5-HT_{2c} receptor-mediated dendritic activation and 5-HT_{1A} receptor-mediated electrical inhibition. Experiments in **Chapter 4** used selective manipulation of PPG neurons to demonstrate a role for PPG neurons in food intake. Interestingly, PPG neurons were not important in the control of normal feeding or bodyweight, but rather prevented overeating. I showed for the first time the importance of NTS PPG neuron activity in the hypophagic response to acute stress, highlighting the need for further studies into the role of central GLP-1 in stress. Finally, I established in **Chapter 5** that although there is no requirement for endogenous GLP-1 signalling in normal cardiovascular control, PPG neurons do have the ability to increase heart rate.

The data presented here support a role for PPG neurons in food intake and cardiovascular control. In the next sections, I propose how the evidence presented collectively indicates a crucial role for the central GLP-1 system in the physiological response to eating, illness, and stress, ultimately leading to decreased food intake and increased sympathetic outflow.

6.1 NTS PPG neurons – integration of neural and humoral signals

Experiments in **Chapter 3** were designed to elucidate modulation of PPG neuron activity *in vitro* using a genetically encoded Ca^{2+} indicator. The results obtained have significantly expanded our knowledge of the regulation of PPG neuron activity and have revealed new potential links between satiety-regulatory systems. Notably, these data highlight the variety of inputs, which modulate PPG activity, including signals not traditionally associated with meal termination. Based on the widespread projections of PPG neurons, the diverse inputs regulating PPG activity, as well as the many effects of central GLP-1, I propose that PPG neurons integrate signals of both

long-term energy balance and short-term disruptions to homeostasis, including feeding, illness, and stress.

Food intake is regulated by changes in caloric need (homeostatic feeding), the pleasure and reward associated with food intake (hedonic feeding), and by the presence of immediate or perceived threats to the well-being of the animal. For example, immediate danger or illness, may suppress feeding. I suggest that PPG neurons integrate signals of all of the above and relay this information to regulate food intake and sympathetic activity.

6.1.1 PPG neurons integrate signals of satiety and energy homeostasis

NTS PPG neurons were activated by peripheral signals of energy homeostasis and satiety, including leptin and CCK-8 (Hisadome et al. 2010, 2011; Holt et al. 2017). In addition, PPG neuron activity was modulated by 5-HT, a well-established central regulator of food intake (Holt et al. 2017). Finally, AChR-mediated activation of PPG neurons may contribute to satiety as was shown for POMC neurons in the Arc (Mineur et al. 2011). Future experiments should investigate whether muscarinic or nicotine AChRs are involved in the carbachol-mediated increase in PPG neuron [Ca^{2+}]. Considering the evidence for a role of central GLP-1 in nicotine reward and intake (Tuesta et al. 2017), it is also possible that the nicotinic AChR-mediated activation of PPG neurons reduces drug reward.

In addition to detecting peripheral and central satiety signals, PPG neurons were activated by the cytokine IL-6 (Anesten et al. 2016). Keeping in mind the ability of interoceptive stressors LiCl, CCK-8, and LPS to activate rat GLP-1-producing neurons (Rinaman 1999b), these data suggest a role for PPG neurons in detecting visceral illness. Where CCK-8, LiCl, and LPS induce general discomfort and nausea, IL-6 signals inflammation. In healthy animals, IL-6 levels are low in both brain and blood. During disease, IL-6 acts via receptors in the brain to decrease food intake (Molotkov et al. 1998). It is uncertain whether low levels of IL-6 in healthy animals are sufficient to activate PPG neurons, or whether high levels, occurring at times of inflammation, are needed.

6.2 PPG neurons in satiety

The evidence presented above indicates a comprehensive role for PPG neurons in integrating signals of energy balance and well-being. Similarly, POMC and AgRP neurons in the Arc detect leptin, insulin, glucose, and nicotine (Belgardt et al. 2009) and have profound effects on homeostatic feeding. In fact, loss of AgRP neurons completely abolishes feeding leading to fatal starvation (Luquet et al. 2005). Whether PPG neurons play a similarly critical part in energy intake has been elusive until now.

As such, experiments in **Chapter 4** were designed to test the hypothesis that PPG neurons are sufficient and essential for satiety. Chemogenetic activation of PPG neurons dramatically reduced feeding at dark onset, when mice are most likely to eat. Despite this strong hypophagic potential, two methods of PPG inactivation had no effect on daily food intake and body weight. Only when mice were refed after a long fast or were encouraged to eat a large meal did PPG activity become necessary for satiety.

The finding that PPG neurons are necessary for the intake-suppressive response to a large meal suggests that these cells could be part of the counter-regulatory response to overeating. This is further supported by the finding that gastric distension activates PPG neurons (Vrang et al. 2003) and that the ensuing decrease in food intake is mediated by central GLP-1 signalling (Hayes et al. 2009).

The large meals eaten by mice in this study were voluntary and can therefore not be considered supraphysiological. However, food intake in itself is a significant challenge to homeostasis (Woods 1991) and the neuroendocrine responses to feeding resemble that of stress (Al-Damluji et al. 1987). Notably, the neuronal response to overconsumption of chow is remarkably similar to that of aversive stimuli (Yamamoto et al. 1992; Rinaman et al. 1998; Zittel et al. 1999). The organism must rapidly deal with the post-prandial surge in nutrients to ensure maintenance of homeostasis. Because of this, stringent physiological processes are initiated in response to food intake. It was recently shown that overconsumption in rats results in a specific form of conditioned taste aversion leading to moderation of future intake (Tracy et al. 2016). Whether NTS PPG neurons are necessary for this adaptive response to overeating should be addressed. Specifically, future experiments could investigate the ability of PPG-ablated mice to develop aversion to large meals.

6.2.1 GLP-1 in stress-induced hypophagia

Further experiments presented in **Chapter 4** were designed to investigate the physiological role of PPG neurons and central GLP-1 in stress-induced hypophagia. As well as physical stress in the form of a visceral illness or injury, the organism experiences psychogenic stress. The body has a remarkable ability to initiate anticipatory responses to a perceived threat (Ulrich-Lai and Herman 2009). Part of this response is to limit attention given to behavioural processes, such as food intake, which are not needed to cope with the immediate danger.

I found that 30 mins restraint stress significantly reduced food intake, and that this stress-induced hypophagia was dependent on PPG neuron activity. Considering the evidence that

stress activates rat GLP-1-producing neurons, these data suggest that NTS PPG neurons mediate anticipatory responses to perceived challenges by limiting food intake following a stressful stimulus. Stress-induced hypophagia was partly mediated by GLP-1 release into the dLS, a site known for its involvement in stress and anxiety (Singewald et al. 2011). Future experiments should investigate the role of this NTS^{PPG} → dLS circuit in food intake and stress regulation by targeting expression of excitatory and inhibitory DREADDs to the specific NTS^{PPG} → dLS projections.

6.2.2 Metabolic tuning of PPG neurons

One avenue for future investigations is the impact of energy balance on PPG neuron recruitment. Interestingly, the ability of psychogenic stress or homeostatic stress to activate PPG neurons is dependent on nutritional status (Maniscalco and Rinaman 2013, 2017; Maniscalco et al. 2015). At times of negative energy balance hypophagia is a potentially detrimental phenomenon. Indeed, central GLP-1R blockade is only effective at times of plentiful energy, when rats are sated (Turton et al. 1996), but not in rats fasted for 24 hours, suggesting GLP-1 release does not occur when energy is low. These data indicate that recruitment of the central GLP-1 system is metabolically tuned. When energy stores are low, PPG activity is kerbed. During these periods, anorexic responses to interoceptive or psychogenic stress are counterproductive and potentially harmful (Youngblood et al. 1997). The intake of a large meal following a prolonged fast then releases the brake on PPG neurons as demonstrated here, by Kreisler et al. (2016), and by Hayes et al. (2009). In future *in vitro* experiments, brainstem sections should be obtained from both food-deprived and *ad libitum* fed mice to investigate the responsiveness of PPG neurons at times of low and high energy availability.

6.3 PPG neurons in cardiovascular control

Evidence presented here and by others collectively suggests that PPG neurons sense changes in signals relating to appetite regulation, visceral illness, and stress. Furthermore, I have demonstrated that PPG neurons drive hypophagia in response to psychogenic stress. Acute stress elicits in the animal a concerted, physiological effort to cope with potential threats. Ultimately this relies on activation of the sympathetic nervous system. Following on from central GLP-1's role in stress-induced hypophagia, I hypothesised that NTS PPG neurons are involved in broader responses to stress, including sympathetic activation. In particular, experiments in **Chapter 5** were designed to elucidate the role of PPG neurons in cardiovascular control. This was based on numerous studies demonstrating a robust tachycardic response to GLP-1R activation.

I confirmed those findings and presented evidence that the tachycardic effect of systemic GLP-1R activation is dependent on activation of the sympathetic nervous system. Additionally, I presented novel data demonstrating the ability of PPG neurons to increase heart rate in freely-behaving mice. PPG neurons are unusual NTS cells in that they project directly to the spinal cord (Llewellyn-Smith et al. 2015) and future experiments should investigate the role of this recently discovered $NTS^{PPG} \rightarrow IML/CAA^{ChAT}$ circuit in cardiovascular control.

Despite the clear sympathoexcitation by Ex4 and the tachycardic effect of chemogenetic activation of PPG neurons, there was no obvious effect of loss of central GLP-1 on heart rate and blood pressure, suggesting these neurons do not contribute to normal cardiovascular control. However, I did not address the importance of PPG neurons in the tachycardic response to acute stress. This is a key experiment for elucidating the role of PPG neurons in stress and I expect it will reveal a dependency of stress-induced tachycardia on PPG neuron activity, since GLP-1Rs in the PVN were recently found to be essential for this response (Ghosal et al. 2017).

6.4 Does central GLP-1 need a push?

The conclusions from Chapter 4 and Chapter 5 are somewhat analogous. PPG neurons have the ability to induce significant hypophagia and tachycardia when chemogenetically activated, but they are not necessary for maintenance of daily satiety or heart rate. Based on food intake experiments it appears that these neurons need a physiological 'push' to be recruited, be it a large meal or restraint stress.

It is unclear how this model fits with data obtained in rats, in which GLP-1R inhibition in several brain regions increases food intake, indicating release of GLP-1 in the absence of a physiological stimulus. Notably, food intake experiments are often conducted with varying lengths of fast and at different times of the day. Furthermore, different environments and handling protocols may induce varying levels of stress in the animals leading to activation of PPG neurons and release of GLP-1. The ablation model, in which no handling is needed and minimal stress elicited, is therefore an important tool in investigations of the central GLP-1 system.

It is worth mentioning that, although PPG-ablation led to an 80% reduction in hypothalamic and spinal cord GLP-1, I did not ablate all brainstem PPG neurons. The IRT population was left intact, and it is therefore possible that the lack of effects was due to insufficient knockdown of central GLP-1 signalling. In view of this, future studies should include viral targeting of IRT PPG neurons. Importantly, my findings align with other studies in mice, in which genetic knockout of GLP-1R

has no impact on feeding, bodyweight, or cardiovascular control (Scrocchi et al. 1996; Gros et al. 2003; Sisley et al. 2014).

6.5 Delineating circuits

In this thesis, I took the first steps towards delineating a NTS^{PPG} → dLS circuit regulating stress-induced hypophagia. Similar efforts should be made to understand other circuits involved in PPG function. We can base these investigations on several pieces of evidence: 1) The inputs the cells receive; 2) their known projection pattern; 3) the expression of GLP-1Rs in known brain nuclei; and 4) the behavioural and physiological effects of GLP-1 microinjections into distinct brain regions.

For example, projections to the LH and BNST may be important in reward, whereas an NTS^{PPG} → CAA/IML^{ChAT} circuit may be the main driver of sympathoexcitatory effects of central GLP-1. Similarly, an NTS^{PPG} → PVN^{CRH} circuit may mediate neuroendocrine responses to acute stress. These questions can be investigated by virally targeting DREADDs or Channelrhodopsin-2 to specific projections. Furthermore, it is currently unclear whether the co-transmitters released from PPG neurons contribute to the hypophagic and tachycardic effects observed in response to chemogenetic activation. This question should be answered by pharmacologically blocking GLP-1 release in CNS and seeing the effect on the PPG-elicited hypophagia or tachycardia.

6.6 Central GLP-1 regulates diverse processes relating to food intake, stress, and reward

Collectively, evidence presented in this thesis and by others demonstrates the diverse impact of central GLP-1 on homeostasis, including potent effects on feeding, stress, and reward (Fig 6.1). These proposed roles of central GLP-1 have several areas of overlap. Homeostatic feeding is initiated by the lack of sufficient calories. Satiation follows when the organism senses sufficient energy intake to maintain energy homeostasis. Hedonic food intake, on the other hand is driven by the activation of reward centres in the brain, a process not dissimilar to the reinforcement experienced following intake of psychostimulant drugs such as cocaine and amphetamine. PPG neurons may induce anorexia by both attenuating food reward and by relaying signals of sufficient caloric intake. Similarly, feeding is potently inhibited by stress and visceral illness and PPG neurons may be part of a general response to homeostatic and psychogenic stress leading to decreased food intake as well as activation of neuroendocrine responses to stress.

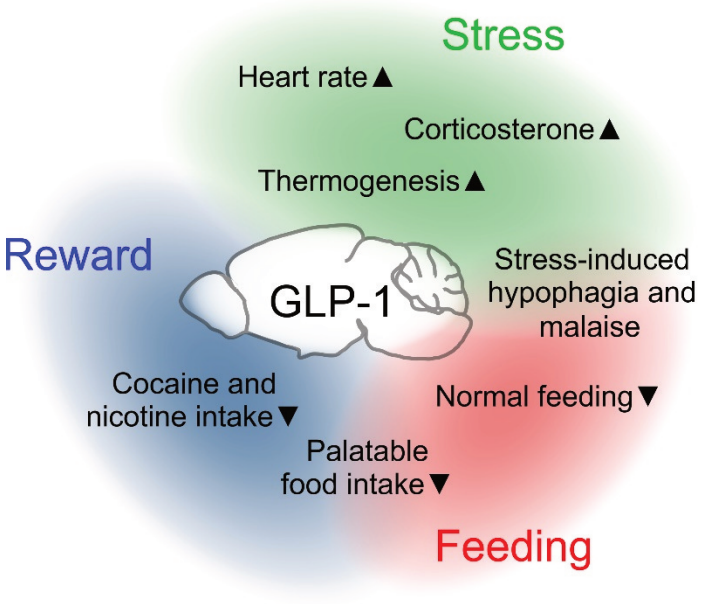

Fig. 6.1 The diverse roles of central GLP-1. Three physiological phenomena are affected by central GLP-1 signalling: Stress, reward, and feeding. Normal feeding is regulated by the availability of nutrients and is decreased in response to central GLP-1. However, food intake is also affected by reward and stress and GLP-1 plays a key role in regulating processes, which fall into these categories. GLP-1 increases heart rate, thermogenesis, and blood corticosterone, and central GLP-1 mediates the hypophagic response to psychogenic and interoceptive stress. Brain GLP-1 also reduces the rewarding value of psychostimulant drugs and palatable food.

6.6 Summary and conclusions

This thesis presents the first evidence that PPG neurons are crucial mediators of satiety by specifically preventing overeating. I also demonstrated that NTS PPG neurons and endogenous GLP-1 within the dLS are crucial for hypophagia in response to acute restraint stress. Furthermore, these studies provided the first evidence that PPG neurons are able to increase heart rate, but that they are not involved in the normal regulation of heart rate and blood pressure. Finally, I have expanded our knowledge of the regulation of PPG neuron activity by a range of compounds, highlighting potential avenues for future research. These findings shed new light on the importance of NTS PPG neurons and encourage further investigations into the specific physiological context in which central GLP-1 plays its part. Collectively, data presented here and by others suggest that PPG neurons integrate signals of satiety and stress to reduce food intake and increase sympathetic outflow. Future studies should focus on interoceptive and psychogenic stress as the 'push' needed to recruit the central GLP-1 system.

Bibliography

Abbas, T., Faivre, E. and Hölscher, C. (2009) 'Impairment of synaptic plasticity and memory formation in GLP-1 receptor KO mice: Interaction between type 2 diabetes and Alzheimer's disease', *Behavioural Brain Research*, 205(1), pp. 265–271.

Abbott, C. R. et al. (2005) 'The inhibitory effects of peripheral administration of peptide YY(3-36) and glucagon-like peptide-1 on food intake are attenuated by ablation of the vagal-brainstem-hypothalamic pathway.', *Brain research*, 1044(1), pp. 127–31.

Accorsi-Mendonça, D., Zoccal, D. B., Bonagamba, L. G. H. and Machado, B. H. (2013) 'Glial cells modulate the synaptic transmission of NTS neurons sending projections to ventral medulla of Wistar rats.', *Physiological reports*, 1(4), p. e00080.

Al-Damluji, S. et al. (1987) 'Food-induced cortisol secretion is mediated by central alpha-1 adrenoceptor modulation of pituitary ACTH secretion.', *Clinical endocrinology*, 26(5), pp. 629–36.

Alcántara, A. I. et al. (1997) 'Exendin-4 agonist and exendin(9-39)amide antagonist of the GLP-1(7-36)amide effects in liver and muscle.', *Archives of biochemistry and biophysics*, 341(1), pp. 1–7.

Alexander, G. M. et al. (2009) 'Remote Control of Neuronal Activity in Transgenic Mice Expressing Evolved G Protein-Coupled Receptors', *Neuron*, 63(1), pp. 27–39.

Alhadeff, A. L. et al. (2014) 'Glucagon-like Peptide-1 receptor signaling in the lateral parabrachial nucleus contributes to the control of food intake and motivation to feed', *Neuropsychopharmacology*. 2014/04/01, 39(9), pp. 2233–2243.

Alhadeff, A. L. and Grill, H. J. (2014) 'Hindbrain nucleus tractus solitarius glucagon-like peptide-1 receptor signaling reduces appetitive and motivational aspects of feeding', *AJP: Regulatory, Integrative and Comparative Physiology*, 307(4), pp. R465–R470.

Alhadeff, A. L., Rupprecht, L. E. and Hayes, M. R. (2012) 'GLP-1 neurons in the nucleus of the solitary tract project directly to the ventral tegmental area and nucleus accumbens to control for food intake.', *Endocrinology*, 153(2), pp. 647–58.

Anesten, F. et al. (2016) 'Preproglucagon neurons in the hindbrain have IL-6 receptor-alpha and show Ca2+ influx in response to IL-6', *Am J Physiol Regul Integr Comp Physiol*. 2016/04/22, 311(1), pp. R115-23.

Anthony, T. E. et al. (2014) 'Control of stress-induced persistent anxiety by an extra-amygdala septohypothalamic circuit.', *Cell*, 156(3), pp. 522–36.

Armbruster, B. N. et al. (2007) 'Evolving the lock to fit the key to create a family of G protein-coupled receptors potently activated by an inert ligand', *Proceedings of the National Academy of Sciences*, 104(12), pp. 5163–5168.

Armstrong, D. M., Rotler, A., Hersh, L. B. and Pickel, V. M. (1988) 'Localization of choline acetyltransferase in perikarya and dendrites within the nuclei of the solitary tracts', *Journal of Neuroscience Research*, 20(3), pp. 279–290.

Asarian, L. (2009) 'Loss of cholecystokinin and glucagon-like peptide-1-induced satiation in mice lacking serotonin 2C receptors', *Am J Physiol Regul Integr Comp Physiol*. 2008/11/14, 296(1), pp. R51-6.

Asin, K. E. et al. (1992) 'Effects of selective CCK receptor agonists on food intake after central or peripheral administration in rats.', *Brain research*, 571(1), pp. 169–74.

Astrup, A. et al. (2009) 'Effects of liraglutide in the treatment of obesity: a randomised, double-blind, placebo-controlled study.', *Lancet*, 374(9701), pp. 1606–1616.

Atasoy, D., Aponte, Y., Su, H. H. and Sternson, S. M. (2008) 'A FLEX switch targets Channelrhodopsin-2 to multiple cell types for imaging and long-range circuit mapping', *The Journal of neuroscience : the official journal of the Society for Neuroscience*. 2008/07/11, 28(28), pp. 7025–7030.

Attele, A. S., Shi, Z. Q. and Yuan, C. S. (2002) 'Leptin, gut, and food intake.', *Biochemical pharmacology*, 63(9), pp. 1579–83.

Baggio, L. L. et al. (2017) 'The autonomic nervous system and cardiac GLP-1 receptors control heart rate in mice', *Molecular Metabolism*.

Baggio, L. L., Huang, Q., Brown, T. J. and Drucker, D. J. (2004a) 'A recombinant human glucagon-like peptide (GLP)-1-albumin protein (albugon) mimics peptidergic activation of GLP-1 receptor-dependent pathways coupled with satiety, gastrointestinal motility, and glucose homeostasis.', *Diabetes*, 53(9), pp. 2492–2500.

Baggio, L. L., Huang, Q., Brown, T. J. and Drucker, D. J. (2004b) 'Oxyntomodulin and glucagon-like peptide-1 differentially regulate murine food intake and energy expenditure.', *Gastroenterology*, 127(2), pp. 546–58.

Balfour, R. H., Hansen, A. M. K. and Trapp, S. (2006) 'Neuronal responses to transient hypoglycaemia in the dorsal vagal complex of the rat brainstem', *J Physiol*. 2005/11/15, 570(Pt 3), pp. 469–484.

Balfour, R. H. and Trapp, S. (2007) 'Ionic currents underlying the response of rat dorsal vagal neurones to hypoglycaemia and chemical anoxia', *J Physiol*. 2007/01/16, 579(Pt 3), pp. 691–702.

Balkenius, A. et al. (2015) 'Comparing Analysis Methods in Functional Calcium Imaging of the Insect Brain', *PLOS ONE*. Edited by W. Gronenberg, 10(6), p. e0129614.

Ban, K. et al. (2008) 'Cardioprotective and vasodilatory actions of glucagon-like peptide 1 receptor are mediated through both glucagon-like peptide 1 receptor-dependent and -independent pathways.', *Circulation*, 117(18), pp. 2340–50.

Barragán, J. M., Eng, J., Rodríguez, R. and Blázquez, E. (1999) 'Neural contribution to the effect of glucagon-like peptide-1-(7-36) amide on arterial blood pressure in rats.', *The American journal of physiology*, 277(5 Pt 1), pp. E784-91.

Barragán, J. M., Rodríguez, R. E. and Blázquez, E. (1994) 'Changes in arterial blood pressure and heart rate induced by glucagon-like peptide-1-(7-36) amide in rats.', *The American journal of physiology*, 266(3 Pt 1), pp. E459-66.

Barragán, J. M., Rodríguez, R. E., Eng, J. and Blázquez, E. (1996) 'Interactions of exendin-(9-39) with the effects of glucagon-like peptide-1-(7-36) amide and of exendin-4 on arterial blood pressure and heart rate in rats.', *Regulatory peptides*, 67(1), pp. 63–8.

Barrera, J. G. et al. (2009) 'Differences in the central anorectic effects of glucagon-like peptide-1 and exendin-4 in rats.', *Diabetes*, 58(12), pp. 2820–7.

Barrera, J. G. et al. (2011) 'Hyperphagia and increased fat accumulation in two models of chronic CNS glucagon-like peptide-1 loss of function', *J Neurosci*. 2011/03/11, 31(10), pp. 3904–3913.

Bartolomucci, A. et al. (2009) 'Metabolic consequences and vulnerability to diet-induced obesity in male mice under chronic social stress.', *PloS one*, 4(1), p. e4331.

Basalay, M. V. et al. (2016) 'Glucagon-like peptide-1 (GLP-1) mediates cardioprotection by remote ischaemic conditioning', *Cardiovascular Research*, 112(3), pp. 669–676.

Baumgartner, I. et al. (2010) 'Hepatic-portal vein infusions of glucagon-like peptide-1 reduce meal size and increase c-Fos expression in the nucleus tractus solitarii, area postrema and central nucleus of the amygdala in rats', *J Neuroendocrinol*. 2010/03/20, 22(6), pp. 557–563.

Beiroa, D. et al. (2014) 'GLP-1 Agonism Stimulates Brown Adipose Tissue Thermogenesis and Browning Through Hypothalamic AMPK', *Diabetes*, 63(10), pp. 3346–3358.

Belgardt, B. F., Okamura, T. and Brüning, J. C. (2009) 'Hormone and glucose signalling in POMC and AgRP neurons', *The Journal of Physiology*, 587(22), pp. 5305–5314.

Berg, J., Hung, Y. P. and Yellen, G. (2009) 'A genetically encoded fluorescent reporter of ATP:ADP ratio.', *Nature methods*, 6(2), pp. 161–6.

Berk, M. L.; Finkelstein, J. A. (1981) 'Afferent projections to the preoptic area and hypothalamic regions in the rat brain', *Neuroscience*, 6(8), pp. 1601–1624.

Bose, A. K. et al. (2005) 'Glucagon-like peptide 1 can directly protect the heart against ischemia/reperfusion injury.', *Diabetes*, 54(1), pp. 146–51.

Bremholm, L. et al. (2017) 'Acute effects of glucagon-like peptide-1, GLP-1 $_{9–36\ \text{amide}}$, and exenatide on mesenteric blood flow, cardiovascular parameters, and biomarkers in healthy volunteers', *Physiological Reports*, 5(4), p. e13102.

Bucinskaite, V. et al. (2009) 'Receptor-mediated activation of gastric vagal afferents by glucagon-like peptide-1 in the rat', *Neurogastroenterology & Motility*, 21(9), pp. 978-e78.

Burdakov, D. et al. (2006) 'Tandem-Pore K+ Channels Mediate Inhibition of Orexin Neurons by Glucose', *Neuron*, 50(5), pp. 711–722.

Burmeister, M. A. et al. (2017) 'The Hypothalamic Glucagon-Like Peptide 1 Receptor Is Sufficient but Not Necessary for the Regulation of Energy Balance and Glucose Homeostasis in Mice', *Diabetes*, 66(2), pp. 372–384.

Cabou, C. et al. (2008) 'Brain glucagon-like peptide-1 regulates arterial blood flow, heart rate, and insulin sensitivity', *Diabetes*, 57(10), pp. 2577–2587.

Cahlin, C. et al. (2000) 'Experimental cancer cachexia: the role of host-derived cytokines interleukin (IL)-6, IL-12, interferon-gamma, and tumor necrosis factor alpha evaluated in gene knockout, tumor-bearing mice on C57 Bl background and eicosanoid-dependent cachexia.', *Cancer research*, 60(19), pp. 5488–93.

Campfield, L. A. et al. (1995) 'Recombinant mouse OB protein: evidence for a peripheral signal linking adiposity and central neural networks.', *Science (New York, N.Y.)*, 269(5223), pp. 546–9.

Campos, C. A., Bowen, A. J., Schwartz, M. W. and Palmiter, R. D. (2016) 'Parabrachial CGRP Neurons Control Meal Termination.', *Cell metabolism*, 23(5), pp. 811–20.

Carreras-Torres, R. et al. (2017) 'The Role of Obesity, Type 2 Diabetes, and Metabolic Factors in Pancreatic Cancer: A Mendelian Randomization Study', *JNCI: Journal of the National Cancer Institute*, 109(9).

Carter, M. E., Soden, M. E., Zweifel, L. S. and Palmiter, R. D. (2013) 'Genetic identification of a neural circuit that suppresses appetite', *Nature*. 2013/10/15, 503(7474), pp. 111–114.

Chen, J. P., van Praag, H. M. and Gardner, E. L. (1991) 'Activation of 5-HT3 receptor by 1-phenylbiguanide increases dopamine release in the rat nucleus accumbens.', *Brain research*, 543(2), pp. 354–7.

Chimerel, C. et al. (2014) 'Bacterial Metabolite Indole Modulates Incretin Secretion from Intestinal Enteroendocrine L Cells', *Cell Rep*, 9(4), pp. 1202–1208.

Cork, S. C. et al. (2015) 'Distribution and characterisation of Glucagon-like peptide-1 receptor expressing cells in the mouse brain', *Molecular Metabolism*, 4(10), pp. 718–731.

Cowley, M. A. et al. (2001) 'Leptin activates anorexigenic POMC neurons through a neural network in the arcuate nucleus.', *Nature*, 411(6836), pp. 480–4.

Cui, R. J. et al. (2012) 'Serotonin Activates Catecholamine Neurons in the Solitary Tract Nucleus by Increasing Spontaneous Glutamate Inputs', *Journal of Neuroscience*, 32(46), pp. 16530–16538.

D'Agostino, G. et al. (2016) 'Appetite controlled by a cholecystokinin nucleus of the solitary tract to hypothalamus neurocircuit', *eLife*, 5.

Dakin, C. L. et al. (2001) 'Oxyntomodulin Inhibits Food Intake in the Rat', *Endocrinology*, 142(10), pp. 4244–4250.

Dayas, C. V et al. (2001) 'Stressor categorization: acute physical and psychological stressors elicit distinctive recruitment patterns in the amygdala and in medullary noradrenergic cell groups', *Eur J Neurosci*. 2001/10/31, 14(7), pp. 1143–1152.

Dickson, S. L. et al. (2012) 'The glucagon-like peptide 1 (GLP-1) analogue, exendin-4, decreases the rewarding value of food: a new role for mesolimbic GLP-1 receptors', *J Neurosci*. 2012/04/12, 32(14), pp. 4812–4820.

Dill, M. J., Shaw, J., Cramer, J. and Sindelar, D. K. (2013) '5-HT1A receptor antagonists reduce food intake and body weight by reducing total meals with no conditioned taste aversion', *Pharmacology Biochemistry and Behavior*, 112, pp. 1–8.

Dombeck, D. A. et al. (2010) 'Functional imaging of hippocampal place cells at cellular resolution during virtual navigation', *Nature Neuroscience*, 13(11), pp. 1433–1440.

Dossat, A. M. et al. (2013) 'Nucleus accumbens GLP-1 receptors influence meal size and palatability', *Am J Physiol Endocrinol Metab*. 2013/04/25, 304(12), pp. E1314-20.

Dossat, A. M., Lilly, N., Kay, K. and Williams, D. L. (2011) 'Glucagon-like peptide 1 receptors in nucleus accumbens affect food intake', *J Neurosci*. 2011/10/14, 31(41), pp. 14453–14457.

Drucker, D. J. et al. (1987) 'Glucagon-like peptide I stimulates insulin gene expression and increases cyclic AMP levels in a rat islet cell line.', *Proceedings of the National Academy of*

Sciences of the United States of America, 84(10), pp. 3434–8.

Duca, F. A., Sakar, Y. and Covasa, M. (2013) 'Combination of obesity and high-fat feeding diminishes sensitivity to GLP-1R agonist exendin-4', *Diabetes*. 2013/02/21, 62(7), pp. 2410–2415.

Dunn-Meynell, A. A. et al. (2002) 'Glucokinase is the likely mediator of glucosensing in both glucose-excited and glucose-inhibited central neurons', *Diabetes*. 2002/06/28, 51(7), pp. 2056–2065.

During, M. J. et al. (2003) 'Glucagon-like peptide-1 receptor is involved in learning and neuroprotection', *Nature Medicine*, 9(9), pp. 1173–1179.

Edelstein, A. D. et al. (2014) 'Advanced methods of microscope control using μManager software.', *Journal of biological methods*, 1(2), p. 10.

Edwards, C. M., Edwards, A. V and Bloom, S. R. (1997) 'Cardiovascular and pancreatic endocrine responses to glucagon-like peptide-1(7-36) amide in the conscious calf.', *Experimental physiology*, 82(4), pp. 709–16.

Egecioglu, E. et al. (2013a) 'The glucagon-like peptide 1 analogue Exendin-4 attenuates the nicotine-induced locomotor stimulation, accumbal dopamine release, conditioned place preference as well as the expression of locomotor sensitization in mice'. Edited by E. Bezard, 8(10), p. e77284.

Egecioglu, E., Engel, J. and Jerlhag, E. (2013b) 'The glucagon-like peptide 1 analogue, exendin-4, attenuates the rewarding properties of psychostimulant drugs in mice', *PLoS ONE*. 2013/07/23, 8(7), p. e69010.

Ellacott, K. L. J. et al. (2010) 'Assessment of feeding behavior in laboratory mice.', *Cell metabolism*, 12(1), pp. 10–7.

Erreger, K. et al. (2012) 'Exendin-4 decreases amphetamine-induced locomotor activity', *Physiology & Behavior*, 106(4), pp. 574–578.

Ervin, G. N., Mosher, J. T., Birkemo, L. S. and Johnson, M. F. (1995) 'Multiple, small doses of cholecystokinin octapeptide are more efficacious at inducing taste aversion conditioning than single, large doses.', *Peptides*, 16(3), pp. 539–45.

Feng, L. and Uteshev, V. V. (2014) 'Projection target-specific action of nicotine in the caudal nucleus of the solitary tract', *Journal of Neuroscience Research*, 92(11), pp. 1560–1572.

Feng, M. et al. (2008) 'Validation of Volume-Pressure Recording Tail-Cuff Blood Pressure Measurements', *American Journal of Hypertension*, 21(12), pp. 1288–1291.

Fioramonti, X. et al. (2007) 'Characterization of Glucosensing Neuron Subpopulations in the Arcuate Nucleus: Integration in Neuropeptide Y and Pro-Opio Melanocortin Networks?', *Diabetes*, 56(5), pp. 1219–1227.

Flint, A., Raben, A., Astrup, A. and Holst, J. J. (1998) 'Glucagon-like peptide 1 promotes satiety and suppresses energy intake in humans', *J Clin Invest*. 1998/03/21, 101(3), pp. 515–520.

Forster, E. A. et al. (1995) 'A pharmacological profile of the selective silent 5-HT1A receptor antagonist, WAY-100635', *European Journal of Pharmacology*, 281(1), pp. 81–88.

Franklin, K. B. J. and Paxinos, G. (2008) *The mouse brain in stereotaxic coordinates*.

Frühbeck, G. (2006) 'Intracellular signalling pathways activated by leptin.', *The Biochemical journal*, 393(Pt 1), pp. 7–20.

Fujiwara, K. et al. (2012) 'Intraportal administration of DPP-IV inhibitor regulates insulin secretion and food intake mediated by the hepatic vagal afferent nerve in rats', *J Neurochem*. 2011/11/01, 121(1), pp. 66–76.

Furuya, W. I. et al. (2014) 'Differential modulation of sympathetic and respiratory activities by cholinergic mechanisms in the nucleus of the solitary tract in rats', *Experimental Physiology*, 99(5), pp. 743–758.

Gaisano, G. G., Park, S. J., Daly, D. M. and Beyak, M. J. (2010) 'Glucagon-like peptide-1 inhibits voltage-gated potassium currents in mouse nodose ganglion neurons', *Neurogastroenterol Motil*. 2009/12/17, 22(4), pp. 470–9, e111.

Garfield, A. S. et al. (2012) 'Neurochemical Characterization of Body Weight-Regulating Leptin Receptor Neurons in the Nucleus of the Solitary Tract', *Endocrinology*, 153(10), pp. 4600–4607.

Gaykema, R. et al. (2017) 'Activation of murine pre-proglucagon–producing neurons reduces food intake and body weight', *Front Neuroanat*, 8(2), p.

Gaykema, R. P. et al. (2009) 'Immune challenge and satiety-related activation of both distinct and overlapping neuronal populations in the brainstem indicate parallel pathways for viscerosensory signaling', *Brain Research*, 1294, pp. 61–79.

Ghosal, S. et al. (2017) 'Disruption of Glucagon-Like Peptide 1 Signaling in Sim1 Neurons Reduces Physiological and Behavioral Reactivity to Acute and Chronic Stress', *The Journal of Neuroscience*, 37(1), pp. 184–193.

Ghosal, S., Myers, B. and Herman, J. P. (2013) 'Role of central glucagon-like peptide-1 in stress regulation', *Physiol Behav*. 2013/04/30, 122, pp. 201–207.

Giel-Moloney, M. et al. (2007) 'Ubiquitous and uniform in vivo fluorescence in ROSA26-EGFP BAC transgenic mice.', *Genesis (New York, N.Y. : 2000)*, 45(2), pp. 83–9.

Gil-Lozano, M. et al. (2010) 'GLP-1(7-36)-amide and Exendin-4 stimulate the HPA axis in rodents and humans', *Endocrinology*. 2010/04/07, 151(6), pp. 2629–2640.

Gil-Lozano, M. et al. (2014) 'Circadian secretion of the intestinal hormone GLP-1 by the rodent L cell.', *Diabetes*, 63(11), pp. 3674–85.

Goke, R., Larsen, P. J., Mikkelsen, J. D. and Sheikh, S. P. (1995) 'Distribution of GLP-1 binding sites in the rat brain: evidence that exendin-4 is a ligand of brain GLP-1 binding sites', *Eur J Neurosci*. 1995/11/01, 7(11), pp. 2294–2300.

Goldstone, A. P. et al. (1997) 'Leptin interacts with glucagon-like peptide-1 neurons to reduce food intake and body weight in rodents', *FEBS Lett*. 1997/11/14, 415(2), pp. 134–138.

Goldstone, A. P. et al. (2000) 'Effect of leptin on hypothalamic GLP-1 peptide and brain-stem pre-proglucagon mRNA.', *Biochemical and biophysical research communications*, 269(2), pp. 331–5.

Gomez, J. L. et al. (2017) 'Chemogenetics revealed: DREADD occupancy and activation via converted clozapine', *Science*, 357(6350).

Gourine, A. V. et al. (2010) 'Astrocytes Control Breathing Through pH-Dependent Release of

ATP', *Science*, 329(5991).

Graham, D. L., Erreger, K., Galli, A. and Stanwood, G. D. (2013) 'GLP-1 analog attenuates cocaine reward', *Molecular Psychiatry*, 18(9), pp. 961–962.

Gribble, F. M., Williams, L., Simpson, A. K. and Reimann, F. (2003) 'A novel glucose-sensing mechanism contributing to glucagon-like peptide-1 secretion from the GLUTag cell line', *Diabetes*. 2003/04/30, 52(5), pp. 1147–1154.

Griffioen, K. J. et al. (2011) 'GLP-1 receptor stimulation depresses heart rate variability and inhibits neurotransmission to cardiac vagal neurons', *Cardiovasc Res*. 2010/08/26, 89(1), pp. 72–78.

Grill, H. J. et al. (2002) 'Evidence that the caudal brainstem is a target for the inhibitory effect of leptin on food intake.', *Endocrinology*, 143(1), pp. 239–46.

Grill, H. J. and Hayes, M. R. (2012) 'Hindbrain Neurons as an Essential Hub in the Neuroanatomically Distributed Control of Energy Balance', *Cell Metabolism*, 16(3), pp. 296–309.

Gros, R. et al. (2003) 'Cardiac function in mice lacking the glucagon-like peptide-1 receptor.', *Endocrinology*, 144(6), pp. 2242–52.

Gross, V. and Luft, F. C. (2003) 'Exercising Restraint in Measuring Blood Pressure in Conscious Mice', *Hypertension*, 41(4), pp. 879–881.

Guettier, J.-M. et al. (2009) 'A chemical-genetic approach to study G protein regulation of cell function in vivo', *Proceedings of the National Academy of Sciences*, 106(45), pp. 19197–19202.

Gutzwiller, J. P. et al. (1999) 'Glucagon-like peptide-1 promotes satiety and reduces food intake in patients with diabetes mellitus type 2.', *The American journal of physiology*, 276(5 Pt 2), pp. R1541-4.

Hansen, H. H. et al. (2015) 'The GLP-1 Receptor Agonist Liraglutide Improves Memory Function and Increases Hippocampal CA1 Neuronal Numbers in a Senescence-Accelerated Mouse Model of Alzheimer's Disease', *Journal of Alzheimer's Disease*, 46(4), pp. 877–888.

Hayes, M. R. et al. (2011a) 'Intracellular signals mediating the food intake-suppressive effects of hindbrain glucagon-like peptide-1 receptor activation', *Cell metabolism*, 13(3), pp. 320–330.

Hayes, M. R. et al. (2011b) 'The common hepatic branch of the vagus is not required to mediate the glycemic and food intake suppressive effects of glucagon-like-peptide-1', *Am J Physiol Regul Integr Comp Physiol*. 2011/08/19, 301(5), pp. R1479-85.

Hayes, M. R., Bradley, L. and Grill, H. J. (2009) 'Endogenous hindbrain glucagon-like peptide-1 receptor activation contributes to the control of food intake by mediating gastric satiation signaling', *Endocrinology*, 150(6), pp. 2654–2659.

Hayes, M. R. and Covasa, M. (2005) 'CCK and 5-HT act synergistically to suppress food intake through simultaneous activation of CCK-1 and 5-HT3 receptors', *Peptides*, 26(11), pp. 2322–2330.

Hayes, M. R. and Covasa, M. (2006) 'Dorsal hindbrain 5-HT3 receptors participate in control of meal size and mediate CCK-induced satiation.', *Brain research*, 1103(1), pp. 99–107.

Hayes, M. R., Skibicka, K. P. and Grill, H. J. (2008) 'Caudal brainstem processing is sufficient for behavioral, sympathetic, and parasympathetic responses driven by peripheral and hindbrain

glucagon-like-peptide-1 receptor stimulation', *Endocrinology*, 149(8), pp. 4059–4068.

Heisler, L. K. et al. (1998) 'Elevated anxiety and antidepressant-like responses in serotonin 5-HT1A receptor mutant mice.', *Proceedings of the National Academy of Sciences of the United States of America*, 95(25), pp. 15049–54.

Heisler, L. K. et al. (2003) 'Central serotonin and melanocortin pathways regulating energy homeostasis.', *Annals of the New York Academy of Sciences*, 994, pp. 169–74.

Heisler, L. K. et al. (2007) 'Serotonin 5-HT $_{2C}$ receptors regulate anxiety-like behavior', *Genes, Brain and Behavior*, 6(5), pp. 491–496.

Higley, M. J. and Sabatini, B. L. (2012) 'Calcium signaling in dendritic spines.', *Cold Spring Harbor perspectives in biology*, 4(4), p. a005686.

Hisadome, K., Reimann, F., Gribble, F. M. and Trapp, S. (2010) 'Leptin directly depolarizes preproglucagon neurons in the nucleus tractus solitarius: electrical properties of glucagon-like Peptide 1 neurons', *Diabetes*, 59(8), pp. 1890–1898.

Hisadome, K., Reimann, F., Gribble, F. M. and Trapp, S. (2011) 'CCK stimulation of GLP-1 neurons involves α1-adrenoceptor-mediated increase in glutamatergic synaptic inputs.', *Diabetes*, 60(11), pp. 2701–2709.

Hoess, R. H. and Abremski, K. (1985) 'Mechanism of strand cleavage and exchange in the Cre-lox site-specific recombination system.', *Journal of molecular biology*, 181(3), pp. 351–62.

Hoess, R. H., Ziese, M. and Sternberg, N. (1982) 'P1 site-specific recombination: nucleotide sequence of the recombining sites.', *Proceedings of the National Academy of Sciences of the United States of America*, 79(11), pp. 3398–402.

Holmes, G. M. et al. (2009) 'Vagally mediated effects of glucagon-like peptide 1: in vitro and in vivo gastric actions.', *The Journal of physiology*, 587(Pt 19), pp. 4749–59.

Holscher, C. (2013) 'Central effects of GLP-1: new opportunities for treatments of neurodegenerative diseases', *J Endocrinol*. 2013/09/04.

Holst, J. J. (2007) 'The physiology of glucagon-like peptide 1', *Physiol Rev*, 87(4), pp. 1409–1439.

Holst, J. J. and Deacon, C. F. (2005) 'Glucagon-like peptide-1 mediates the therapeutic actions of DPP-IV inhibitors', *Diabetologia*. 2005/03/11, 48(4), pp. 612–615.

Holst, J. J., Orskov, C., Nielsen, O. V and Schwartz, T. W. (1987) 'Truncated glucagon-like peptide I, an insulin-releasing hormone from the distal gut.', *FEBS letters*, 211(2), pp. 169–74.

Holt, M. K. et al. (2017) 'Serotonergic modulation of the activity of GLP-1 producing neurons in the nucleus of the solitary tract in mouse.', *Molecular metabolism*, 6(8), pp. 909–921.

Holt, M. K. and Trapp, S. (2016) 'The physiological role of the brain GLP-1 system in stress', *Cogent Biol*, 2(1).

Hosoi, T. et al. (2002) 'Brain stem is a direct target for leptin's action in the central nervous system.', *Endocrinology*, 143(9), pp. 3498–504.

Hsu, T. M. et al. (2015) 'Hippocampal GLP-1 Receptors Influence Food Intake, Meal Size, and Effort-Based Responding for Food through Volume Transmission', *Neuropsychopharmacology*, 40(2), pp. 327–337.

Huber, D. et al. (2012) ‘Multiple dynamic representations in the motor cortex during sensorimotor learning’, *Nature*, 484(7395), pp. 473–478.

Huo, L., Gamber, K. M., Grill, H. J. and Bjørbaek, C. (2008) ‘Divergent leptin signaling in proglucagon neurons of the nucleus of the solitary tract in mice and rats.’, *Endocrinology*, 149(2), pp. 492–7.

Huo, L., Maeng, L., Bjorbaek, C. and Grill, H. J. (2007) ‘Leptin and the control of food intake: neurons in the nucleus of the solitary tract are activated by both gastric distension and leptin’, *Endocrinology*. 2007/02/24, 148(5), pp. 2189–2197.

Ibrahim, N. et al. (2003) ‘Hypothalamic proopiomelanocortin neurons are glucose responsive and express K(ATP) channels’, *Endocrinology*. 2003/03/18, 144(4), pp. 1331–1340.

Iglewicz, B. and Hoaglin, D. (1993) *Volume 16: How to Detect and Handle Outliers*, *The ASQC Basic References in Quality Control: Statistical Techniques*. Edited by E. F. Mykytka.

Ireland, S. J. and Tyers, M. B. (1987) ‘Pharmacological characterization of 5-hydroxytryptamine-induced depolarization of the rat isolated vagus nerve.’, *British journal of pharmacology*, 90(1), pp. 229–38.

Iwasaki, Y., Goswami, C. and Yada, T. (2017) ‘Glucagon-like peptide-1 and insulin synergistically activate vagal afferent neurons’, *Neuropeptides*.

Jansson, J. O. and Palsdottir, V. (2015) ‘Brain IL-6-Where Amylin and GLP-1 Antiobesity Signaling Congregate’, *Diabetes*. 2015/04/25, 64(5), pp. 1498–1499.

Jarsky, T., Roxin, A., Kath, W. L. and Spruston, N. (2005) ‘Conditional dendritic spike propagation following distal synaptic activation of hippocampal CA1 pyramidal neurons’, *Nature Neuroscience*, 8(12), pp. 1667–1676.

Jensen, T., Kiersgaard, M., Sørensen, D. and Mikkelsen, L. (2013) ‘Fasting of mice: a review’, *Laboratory Animals*, 47(4), pp. 225–240.

Jessen, L. et al. (2012) ‘Suppression of food intake by glucagon-like peptide-1 receptor agonists: relative potencies and role of dipeptidyl peptidase-4’, *Endocrinology*. 2012/10/04, 153(12), pp. 5735–5745.

Jin, S. L. et al. (1988) ‘Distribution of glucagonlike peptide I (GLP-I), glucagon, and glicentin in the rat brain: an immunocytochemical study’, *J Comp Neurol*. 1988/05/22, 271(4), pp. 519–532.

Jo, Y.-H., Talmage, D. A. and Role, L. W. (2002) ‘Nicotinic receptor-mediated effects on appetite and food intake.’, *Journal of neurobiology*, 53(4), pp. 618–32.

Jordan, D. (2005) ‘Vagal control of the heart: central serotonergic (5-HT) mechanisms’, *Experimental Physiology*, 90(2), pp. 175–181.

Just, A., Faulhaber, J. and Ehmke, H. (2000) ‘Autonomic cardiovascular control in conscious mice.’, *American journal of physiology. Regulatory, integrative and comparative physiology*, 279(6), pp. R2214-21.

Kahles, F. et al. (2014) ‘GLP-1 Secretion Is Increased by Inflammatory Stimuli in an IL-6-Dependent Manner, Leading to Hyperinsulinemia and Blood Glucose Lowering’, *Diabetes*, 63(10), pp. 3221–3229.

Kakei, M., Yada, T., Nakagawa, A. and Nakabayashi, H. (2002) ‘Glucagon-like peptide-1 evokes

action potentials and increases cytosolic Ca2+ in rat nodose ganglion neurons.', *Autonomic neuroscience : basic & clinical*, 102(1–2), pp. 39–44.

Kalappa, B. I. et al. (2011) 'Mechanisms of facilitation of synaptic glutamate release by nicotinic agonists in the nucleus of the solitary tract.', *American journal of physiology. Cell physiology*, 301(2), pp. C347-61.

Kang, L. et al. (2006) 'Glucokinase Is a Critical Regulator of Ventromedial Hypothalamic Neuronal Glucosensing', *Diabetes*, 55(2), pp. 412–420.

Kanoski, S. E. et al. (2011) 'Peripheral and central GLP-1 receptor populations mediate the anorectic effects of peripherally administered GLP-1 receptor agonists, liraglutide and exendin-4.', *Endocrinology*, 152(8), pp. 3103–12.

Kastin, A. J. and Akerstrom, V. (2003) 'Entry of exendin-4 into brain is rapid but may be limited at high doses', *International Journal of Obesity*, 27(3), pp. 313–318.

Kastin, A. J., Akerstrom, V. and Pan, W. (2002) 'Interactions of glucagon-like peptide-1 (GLP-1) with the blood-brain barrier', *J Mol Neurosci*. 2002/04/05, 18(1–2), pp. 7–14.

Katsurada, K. et al. (2014) 'Endogenous GLP-1 acts on paraventricular nucleus to suppress feeding: Projection from nucleus tractus solitarius and activation of corticotropin-releasing hormone, nesfatin-1 and oxytocin neurons', *Biochemical and Biophysical Research Communications*, 451(2), pp. 276–281.

Khor, K. H. et al. (2016) 'A Potential Link between the C5a Receptor 1 and the β1-Adrenoreceptor in the Mouse Heart', *PLOS ONE*. Edited by S. Koutsopoulos, 11(1), p. e0146022.

Kieffer, T. J., McIntosh, C. H. and Pederson, R. A. (1995) 'Degradation of glucose-dependent insulinotropic polypeptide and truncated glucagon-like peptide 1 in vitro and in vivo by dipeptidyl peptidase IV', *Endocrinology*, 136(8), pp. 3585–3596.

Kim, M. et al. (2013) 'GLP-1 receptor activation and Epac2 link atrial natriuretic peptide secretion to control of blood pressure', *Nature Medicine*, 19(5), pp. 567–575.

Kinzig, K. P. et al. (2003) 'CNS glucagon-like peptide-1 receptors mediate endocrine and anxiety responses to interoceptive and psychogenic stressors', *J Neurosci*. 2003/07/18, 23(15), pp. 6163–6170.

Kinzig, K. P., D'Alessio, D. A. and Seeley, R. J. (2002) 'The diverse roles of specific GLP-1 receptors in the control of food intake and the response to visceral illness.', *The Journal of neuroscience : the official journal of the Society for Neuroscience*, 22(23), pp. 10470–6.

Klok, M. D., Jakobsdottir, S. and Drent, M. L. (2007) 'The role of leptin and ghrelin in the regulation of food intake and body weight in humans: a review.', *Obesity reviews : an official journal of the International Association for the Study of Obesity*, 8(1), pp. 21–34.

Kosse, C., Schöne, C., Bracey, E. and Burdakov, D. (2017) 'Orexin-driven GAD65 network of the lateral hypothalamus sets physical activity in mice', *Proceedings of the National Academy of Sciences*, 114(17), pp. 4525–4530.

Krahn, D. D. et al. (1990) 'The anorectic effects of CRH and restraint stress decrease with repeated exposures', *Biological Psychiatry*, 27(10), pp. 1094–1102.

Krashes, M. J. et al. (2011) 'Rapid, reversible activation of AgRP neurons drives feeding behavior

in mice.', *The Journal of clinical investigation*, 121(4), pp. 1424–8.

Kreisler, A. D., Davis, E. A. and Rinaman, L. (2014) 'Differential activation of chemically identified neurons in the caudal nucleus of the solitary tract in non-entrained rats after intake of satiating vs. non-satiating meals', *Physiol Behav*. 2014/02/11.

Kreisler, A. D. and Rinaman, L. (2016) 'Hindbrain glucagon-like peptide-1 neurons track intake volume and contribute to injection stress-induced hypophagia in meal-entrained rats', *Am J Physiol Regul Integr Comp Physiol*. 2016/03/05, 310(10), pp. R906-16.

Kreymann, B., Williams, G., Ghatei, M. A. and Bloom, S. R. (1987) 'Glucagon-like peptide-1 7-36: a physiological incretin in man', *Lancet*. 1987/12/05, 2(8571), pp. 1300–1304.

Krieger, J.-P. et al. (2015) 'Knockdown of GLP-1 receptors in vagal afferents affects normal food intake and glycemia.', *Diabetes*.

Labiner, D. M. et al. (1993) 'Induction of c-fos mRNA by kindled seizures: complex relationship with neuronal burst firing.', *The Journal of neuroscience : the official journal of the Society for Neuroscience*, 13(2), pp. 744–51.

Lachey, J. L. et al. (2005) 'The Role of Central Glucagon-Like Peptide-1 in Mediating the Effects of Visceral Illness: Differential Effects in Rats and Mice', *Endocrinology*, 146(1), pp. 458–462.

Lam, D. D. et al. (2008) 'Serotonin 5-HT $_{2C}$ Receptor Agonist Promotes Hypophagia via Downstream Activation of Melanocortin 4 Receptors', *Endocrinology*, 149(3), pp. 1323–1328.

Lamy, C. M. et al. (2014) 'Hypoglycemia-activated GLUT2 neurons of the nucleus tractus solitarius stimulate vagal activity and glucagon secretion', *Cell Metab*. 2014/03/13, 19(3), pp. 527–538.

Larsen, P. J., Fledelius, C., Knudsen, L. B. and Tang-Christensen, M. (2001) 'Systemic administration of the long-acting GLP-1 derivative NN2211 induces lasting and reversible weight loss in both normal and obese rats.', *Diabetes*, 50(11), pp. 2530–9.

Larsen, P. J., Tang-Christensen, M., Holst, J. J. and Orskov, C. (1997a) 'Distribution of glucagon-like peptide-1 and other preproglucagon-derived peptides in the rat hypothalamus and brainstem', *Neuroscience*, 77(1), pp. 257–270.

Larsen, P. J., Tang-Christensen, M. and Jessop, D. S. (1997b) 'Central administration of glucagon-like peptide-1 activates hypothalamic neuroendocrine neurons in the rat.', *Endocrinology*, 138(10), pp. 4445–4455.

Larsson, H., Elmståhl, S., Berglund, G. and Ahrén, B. (1998) 'Evidence for leptin regulation of food intake in humans.', *The Journal of clinical endocrinology and metabolism*, 83(12), pp. 4382–5.

Li, B. et al. (2015) 'Role of 5-HT3 Receptor on Food Intake in Fed and Fasted Mice'. Edited by J. A. Chowen, 10(3), p. e0121473.

Llewellyn-Smith, I. J. et al. (2013) 'Preproglucagon (PPG) neurons innervate neurochemically identified autonomic neurons in the mouse brainstem', *Neuroscience*, 229, pp. 130–143.

Llewellyn-Smith, I. J. et al. (2015) 'Spinally projecting preproglucagon axons preferentially innervate sympathetic preganglionic neurons.', *Neuroscience*, 284, pp. 872–87.

Llewellyn-Smith, I. J., Reimann, F., Gribble, F. M. and Trapp, S. (2011) 'Preproglucagon neurons project widely to autonomic control areas in the mouse brain', *Neuroscience*, 180, pp. 111–121.

Lockie, S. H. et al. (2012) 'Direct control of brown adipose tissue thermogenesis by central nervous system glucagon-like peptide-1 receptor signaling', *Diabetes*. 2012/08/31, 61(11), pp. 2753–2762.

López-Ferreras, L. et al. (2017) 'Lateral hypothalamic GLP-1 receptors are critical for the control of food reinforcement, ingestive behavior and body weight.', *Molecular psychiatry*.

Lovshin, J. A. and Drucker, D. J. (2013) 'Metabolic disease puts up a fight: are diet and exercise helpful for the heart?', *Nat Med*. 2013/10/09, 19(10), pp. 1216–1217.

Luche, H. et al. (2007) 'Faithful activation of an extra-bright red fluorescent protein in "knock-in" Cre-reporter mice ideally suited for lineage tracing studies.', *European journal of immunology*, 37(1), pp. 43–53.

Luquet, S., Perez, F. A., Hnasko, T. S. and Palmiter, R. D. (2005) 'NPY/AgRP Neurons Are Essential for Feeding in Adult Mice but Can Be Ablated in Neonates', *Science*, 310(5748), pp. 683–685.

Mack, C. M. et al. (2006) 'Antiobesity action of peripheral exenatide (exendin-4) in rodents: effects on food intake, body weight, metabolic status and side-effect measures', *International Journal of Obesity*, 30(9), pp. 1332–1340.

MacLaren, D. A. A. et al. (2016) 'Clozapine N-Oxide Administration Produces Behavioral Effects in Long-Evans Rats: Implications for Designing DREADD Experiments', *eNeuro*, 3(5).

Maniscalco, J. W., Kreisler, A. D. and Rinaman, L. (2012) 'Satiation and stress-induced hypophagia: examining the role of hindbrain neurons expressing prolactin-releasing Peptide or glucagon-like Peptide 1', *Frontiers in neuroscience*, 6, p. 199.

Maniscalco, J. W. and Rinaman, L. (2013) 'Overnight food deprivation markedly attenuates hindbrain noradrenergic, glucagon-like peptide-1, and hypothalamic neural responses to exogenous cholecystokinin in male rats', *Physiology & Behavior*, 121, pp. 35–42.

Maniscalco, J. W. and Rinaman, L. (2017) 'Interoceptive modulation of neuroendocrine, emotional, and hypophagic responses to stress', *Physiology & Behavior*, 176, pp. 195–206.

Maniscalco, J. W., Zheng, H., Gordon, P. J. and Rinaman, L. (2015) 'Negative Energy Balance Blocks Neural and Behavioral Responses to Acute Stress by "Silencing" Central Glucagon-Like Peptide 1 Signaling in Rats', *J Neurosci*. 2015/08/01, 35(30), pp. 10701–10714.

Marcinkiewcz, C. A. et al. (2016) 'Serotonin engages an anxiety and fear-promoting circuit in the extended amygdala', *Nature*, 537(7618), pp. 97–101.

Marina, N. et al. (2016) 'Astrocytes and Brain Hypoxia.', *Advances in experimental medicine and biology*, 903, pp. 201–7.

Mark, C. et al. (1998) 'Subcutaneous glucagon-like peptide-1 (7-36) amide is insulinotropic and can cause hypoglycaemia in fasted healthy subjects', *Clinical Science*, 96, pp. 719–724.

Marston, O. J. et al. (2011) 'Neuropeptide Y Cells Represent a Distinct Glucose-Sensing Population in the Lateral Hypothalamus', *Endocrinology*, 152(11), pp. 4046–4052.

McCann, M. J., Verbalis, J. G. and Stricker, E. M. (1989) 'LiCl and CCK inhibit gastric emptying and feeding and stimulate OT secretion in rats', *Am J Physiol*. 1989/02/01, 256(2 Pt 2), pp. R463-8.

McClure, C. et al. (2011) 'Production and titering of recombinant adeno-associated viral vectors.', *Journal of visualized experiments : JoVE*, (57), p. e3348.

McCorvy, J. D. and Roth, B. L. (2015) 'Structure and function of serotonin G protein-coupled receptors', *Pharmacology & Therapeutics*, 150, pp. 129–142.

McDougal, D. H., Hermann, G. E. and Rogers, R. C. (2011) 'Vagal afferent stimulation activates astrocytes in the nucleus of the solitary tract via AMPA receptors: evidence of an atypical neural-glial interaction in the brainstem', *J Neurosci*. 2011/10/01, 31(39), pp. 14037–14045.

McDougal, D. H., Hermann, G. E. and Rogers, R. C. (2013) 'Astrocytes in the nucleus of the solitary tract are activated by low glucose or glucoprivation: evidence for glial involvement in glucose homeostasis', *Front Neurosci*. 2014/01/07, 7, p. 249.

McMahon, L. R. and Wellman, P. J. (1998) 'PVN infusion of GLP-1-(7-36) amide suppresses feeding but does not induce aversion or alter locomotion in rats', *The American Journal of Physiology*, 274(1 Pt 2), pp. R23-9.

Meeran, K. et al. (1999) 'Repeated intracerebroventricular administration of glucagon-like peptide-1-(7-36) amide or exendin-(9-39) alters body weight in the rat', *Endocrinology*, 140(1), pp. 244–250.

Meibach, R. C. and Siegel, A. (1977) 'Efferent connections of the septal area in the rat: an analysis utilizing retrograde and anterograde transport methods.', *Brain research*, 119(1), pp. 1–20.

Melhorn, S. J. et al. (2014) 'Initial evidence that GLP-1 receptor blockade fails to suppress postprandial satiety or promote food intake in humans.', *Appetite*, 82, pp. 85–90.

Merchenthaler, I., Lane, M. and Shughrue, P. (1999) 'Distribution of pre-pro-glucagon and glucagon-like peptide-1 receptor messenger RNAs in the rat central nervous system', *The Journal of comparative neurology*, 403(2), pp. 261–280.

Mietlicki-Baase, E. G. et al. (2013) 'The food intake-suppressive effects of glucagon-like peptide-1 receptor signaling in the ventral tegmental area are mediated by AMPA/kainate receptors', *Am J Physiol Endocrinol Metab*. 2013/10/10.

Mietlicki-Baase, E. G. et al. (2014) 'Glucagon-Like Peptide-1 Receptor Activation in the Nucleus Accumbens Core Suppresses Feeding by Increasing Glutamatergic AMPA/Kainate Signaling', *J Neurosci*. 2014/05/16, 34(20), pp. 6985–6992.

Mojsov, S. et al. (1986) 'Preproglucagon gene expression in pancreas and intestine diversifies at the level of post-translational processing.', *The Journal of biological chemistry*, 261(25), pp. 11880–9.

Mojsov, S., Weir, G. C. and Habener, J. F. (1987) 'Insulinotropin: glucagon-like peptide I (7-37) co-encoded in the glucagon gene is a potent stimulator of insulin release in the perfused rat pancreas', *J Clin Invest*. 1987/02/01, 79(2), pp. 616–619.

Mokdad, A. H. et al. (2003) 'Prevalence of obesity, diabetes, and obesity-related health risk factors, 2001.', *JAMA*, 289(1), pp. 76–9.

Molotkov, A., Satoh, M. and Tohyama, C. (1998) 'Tumor growth and food intake in interleukin-6 gene knock-out mice.', *Cancer letters*, 132(1–2), pp. 187–92.

Mul, J. D. et al. (2013) 'High-fat diet changes the temporal profile of GLP-1 receptor-mediated hypophagia in rats', *Am J Physiol Regul Integr Comp Physiol*. 2013/04/26, 305(1), pp. R68-77.

Muroya, S., Yada, T., Shioda, S. and Takigawa, M. (1999) 'Glucose-sensitive neurons in the rat

arcuate nucleus contain neuropeptide Y.', *Neuroscience letters*, 264(1–3), pp. 113–6.

Murray, A. J. et al. (2011) 'Parvalbumin-positive CA1 interneurons are required for spatial working but not for reference memory', *Nature neuroscience*, 14(3), pp. 297–299.

Nakagawa, A. et al. (2004) 'Receptor gene expression of glucagon-like peptide-1, but not glucose-dependent insulinotropic polypeptide, in rat nodose ganglion cells', *Autonomic Neuroscience : Basic & Clinical*, 110(1), pp. 36–43.

Nakai, J., Ohkura, M. and Imoto, K. (2001) 'A high signal-to-noise Ca(2+) probe composed of a single green fluorescent protein.', *Nature biotechnology*, 19(2), pp. 137–41.

Ng, M. et al. (2014) 'Global, regional, and national prevalence of overweight and obesity in children and adults during 1980-2013: a systematic analysis for the Global Burden of Disease Study 2013.', *Lancet (London, England)*, 384(9945), pp. 766–81.

Nonogaki, K. et al. (2011) 'The contribution of serotonin 5-HT2C and melanocortin-4 receptors to the satiety signaling of glucagon-like peptide 1 and liraglutide, a glucagon-like peptide 1 receptor agonist, in mice', *Biochem Biophys Res Commun*. 2011/07/16, 411(2), pp. 445–448.

Nonogaki, K., Strack, A. M., Dallman, M. F. and Tecott, L. H. (1998) 'Leptin-independent hyperphagia and type 2 diabetes in mice with a mutated serotonin 5-HT2C receptor gene', *Nat Med*. 1998/10/15, 4(10), pp. 1152–1156.

O'Connor, D. H., Peron, S. P., Huber, D. and Svoboda, K. (2010) 'Neural Activity in Barrel Cortex Underlying Vibrissa-Based Object Localization in Mice', *Neuron*, 67(6), pp. 1048–1061.

Oka, J., Suzuki, E. and Kondo, Y. (2000) 'Endogenous GLP-1 is involved in beta-amyloid protein-induced memory impairment and hippocampal neuronal death in rats', *Brain Res*. 2000/09/21, 878(1–2), pp. 194–198.

Ong, Z. Y., Liu, J.-J., Pang, Z. P. and Grill, H. J. (2017) 'Paraventricular Thalamic Control of Food Intake and Reward: Role of Glucagon-Like Peptide-1 Receptor Signaling', *Neuropsychopharmacology*.

Orskov, C. et al. (1996) 'Glucagon-like peptide I receptors in the subfornical organ and the area postrema are accessible to circulating glucagon-like peptide I', *Diabetes*, 45(6), pp. 832–835.

Ørskov, C. et al. (1986) 'Glucagon-Like Peptides GLP-1 and GLP-2, Predicted Products of the Glucagon Gene, Are Secreted Separately from Pig Small Intestine but Not Pancreas*', *Endocrinology*, 119(4), pp. 1467–1475.

Orskov, C., Holst, J. J. and Nielsen, O. V (1988) 'Effect of truncated glucagon-like peptide-1 [proglucagon-(78-107) amide] on endocrine secretion from pig pancreas, antrum, and nonantral stomach', *Endocrinology*. 1988/10/01, 123(4), pp. 2009–2013.

Parker, H. E. et al. (2012) 'Predominant role of active versus facilitative glucose transport for glucagon-like peptide-1 secretion.', *Diabetologia*, 55(9), pp. 2445–55.

Parton, L. E. et al. (2007) 'Glucose sensing by POMC neurons regulates glucose homeostasis and is impaired in obesity', *Nature*. 2007/08/31, 449(7159), pp. 228–232.

Patel, J. D. and Ebenezer, I. S. (2008) 'The effect of intraperitoneal administration of leptin on short-term food intake in rats.', *European journal of pharmacology*, 580(1–2), pp. 143–52.

Pelleymounter, M. A. et al. (1995) 'Effects of the obese gene product on body weight regulation

in ob/ob mice.', *Science (New York, N.Y.)*, 269(5223), pp. 540–3.

Pinto, S. et al. (2004) 'Rapid rewiring of arcuate nucleus feeding circuits by leptin.', *Science (New York, N.Y.)*, 304(5667), pp. 110–5.

Punjabi, M. et al. (2014) 'Circulating glucagon-like peptide-1 (GLP-1) inhibits eating in male rats by acting in the hindbrain and without inducing avoidance.', *Endocrinology*, 155(5), pp. 1690–9.

R Core Team (2016) 'R: A language and environment for statistical computing', *R Foundation for Statistical Computing, Vienna, Austria. ISBN 3-900051-07-0*.

Reidelberger, R., Haver, A., Anders, K. and Apenteng, B. (2014) 'Role of capsaicin-sensitive peripheral sensory neurons in anorexic responses to intravenous infusions of cholecystokinin, peptide YY-(3-36), and glucagon-like peptide-1 in rats', *AJP: Endocrinology and Metabolism*, 307(8), pp. E619–E629.

Reimann, F. et al. (2008) 'Glucose sensing in L cells: a primary cell study.', *Cell Metab*, 8(6), pp. 532–539.

Reiner, D. J. et al. (2016) 'Astrocytes Regulate GLP-1 Receptor-Mediated Effects on Energy Balance', *Journal of Neuroscience*, 36(12), pp. 3531–3540.

Reiner, D. J. et al. (2017) 'Glucagon-like peptide-1 receptor signaling in the lateral dorsal tegmental nucleus regulates energy balance', *Neuropsychopharmacology*.

Reis, D. G. et al. (2010) 'Involvement of the lateral septal area in the expression of fear conditioning to context.', *Learning & memory (Cold Spring Harbor, N.Y.)*, 17(3), pp. 134–8.

Richard, J. E. et al. (2014) 'GLP-1 receptor stimulation of the lateral parabrachial nucleus reduces food intake: neuroanatomical, electrophysiological, and behavioral evidence', *Endocrinology*. 2014/08/15, 155(11), pp. 4356–4367.

Richards, P. et al. (2014) 'Identification and characterization of GLP-1 receptor-expressing cells using a new transgenic mouse model.', *Diabetes*, 63(4), pp. 1224–33.

Rinaman, L. et al. (1998) 'Medullary c-Fos activation in rats after ingestion of a satiating meal.', *The American journal of physiology*, 275(1 Pt 2), pp. R262-8.

Rinaman, L. (1999a) 'A functional role for central glucagon-like peptide-1 receptors in lithium chloride-induced anorexia', *American Journal of Physiology - Regulatory, Integrative and Comparative Physiology*, 277(5).

Rinaman, L. (1999b) 'Interoceptive stress activates glucagon-like peptide-1 neurons that project to the hypothalamus.', *The American journal of physiology*, 277(2 Pt 2), pp. R582-90.

Robinson, L. E. et al. (2013) 'Effects of exenatide and liraglutide on heart rate, blood pressure and body weight: systematic review and meta-analysis', *BMJ Open*. 2013/01/29, 3(1).

Roman, C. W., Derkach, V. A. and Palmiter, R. D. (2016) 'Genetically and functionally defined NTS to PBN brain circuits mediating anorexia', *Nature Communications*, 7, p. 11905.

Roman, C. W., Sloat, S. R. and Palmiter, R. D. (2017) 'A tale of two circuits: CCK NTS neuron stimulation controls appetite and induces opposing motivational states by projections to distinct brain regions', *Neuroscience*, 358, pp. 316–324.

Ronveaux, C. C., de Lartigue, G. and Raybould, H. E. (2014) 'Ability of GLP-1 to decrease food

intake is dependent on nutritional status.', *Physiology & behavior*, 135, pp. 222–9.

RStudio Team (2015) 'RStudio: Integrated Development for R'.

Rüttimann, E. B. et al. (2009) 'Intrameal Hepatic Portal and Intraperitoneal Infusions of Glucagon-Like Peptide-1 Reduce Spontaneous Meal Size in the Rat via Different Mechanisms', *Endocrinology*, 150(3), pp. 1174–1181.

Sagar, S. M., Sharp, F. R. and Curran, T. (1988) 'Expression of c-fos protein in brain: metabolic mapping at the cellular level.', *Science (New York, N.Y.)*, 240(4857), pp. 1328–31.

Saito, R. et al. (2016) 'Activation of Nesfatin-1-Containing Neurones in the Hypothalamus and Brainstem by Peripheral Administration of Anorectic Hormones and Suppression of Feeding via Central Nesfatin-1 in Rats', *Journal of Neuroendocrinology*, 28(9).

Sandoval, D. A. et al. (2008) 'Arcuate glucagon-like peptide 1 receptors regulate glucose homeostasis but not food intake.', *Diabetes*, 57(8), pp. 2046–54.

Sarkar, S., Fekete, C., Legradi, G. and Lechan, R. M. (2003) 'Glucagon like peptide-1 (7-36) amide (GLP-1) nerve terminals densely innervate corticotropin-releasing hormone neurons in the hypothalamic paraventricular nucleus', *Brain Res*. 2003/09/12, 985(2), pp. 163–168.

Sawchenko, P. E., Li, H. Y. and Ericsson, A. (2000) 'Circuits and mechanisms governing hypothalamic responses to stress: a tale of two paradigms', *Prog Brain Res*. 2000/03/29, 122, pp. 61–78.

Schick, R. R., Zimmermann, J. P., vorm Walde, T. and Schusdziarra, V. (2003) 'Peptides that regulate food intake: glucagon-like peptide 1-(7-36) amide acts at lateral and medial hypothalamic sites to suppress feeding in rats', *American journal of physiology.Regulatory, integrative and comparative physiology*, 284(6), pp. R1427-35.

Schindelin, J. et al. (2012) 'Fiji: an open-source platform for biological-image analysis', *Nat Meth*, 9(7), pp. 676–682.

Schmidt, H. D. et al. (2016) 'Glucagon-Like Peptide-1 Receptor Activation in the Ventral Tegmental Area Decreases the Reinforcing Efficacy of Cocaine', *Neuropsychopharmacology*. 2015/12/18, 41(7), pp. 1917–1928.

Schnutgen, F. et al. (2003) 'A directional strategy for monitoring Cre-mediated recombination at the cellular level in the mouse', *Nature biotechnology*, 21(5), pp. 562–565.

Schuhler, S. et al. (2005) 'Involvement of 5-HT2C Receptors in the Regulation of Food Intake in Siberian Hamsters', *Journal of Neuroendocrinology*, 17(5), pp. 276–285.

Schwartz, M. W. et al. (1996) 'Cerebrospinal fluid leptin levels: Relationship to plasma levels and to adiposity in humans', *Nature Medicine, Published online: 01 May 1996; | doi:10.1038/nm0596-589*, 2(5), p. 589.

Scrocchi, L. A. et al. (1996) 'Glucose intolerance but normal satiety in mice with a null mutation in the glucagon-like peptide 1 receptor gene.', *Nature medicine*, 2(11), pp. 1254–8.

Secher, A. et al. (2014) 'The arcuate nucleus mediates GLP-1 receptor agonist liraglutide-dependent weight loss.', *The Journal of clinical investigation*, 124(10), pp. 4473–88.

Sévoz-Couche, C. et al. (2000) 'In vivo modulation of nucleus tractus solitarius (NTS) neurones by activation of 5-hydroxytryptamine(2) receptors in rats.', *Neuropharmacology*, 39(11), pp.

2006–16.

Sheward, W. J. et al. (2010) ‘Circadian Control of Mouse Heart Rate and Blood Pressure by the Suprachiasmatic Nuclei: Behavioral Effects Are More Significant than Direct Outputs’, *PLoS ONE*. Edited by S. Yamazaki, 5(3), p. e9783.

Shihara, M. et al. (1999) ‘Cholinergic systems in the nucleus of the solitary tract of rats.’, *The American journal of physiology*, 276(4 Pt 2), pp. R1141-8.

Shillabeer, G. and Davison, J. S. (1987) ‘Endogenous and exogenous cholecystokinin may reduce food intake by different mechanisms.’, *The American journal of physiology*, 253(2 Pt 2), pp. R379-82.

Shirazi, R. et al. (2013) ‘Glucagon-like peptide 1 receptor induced suppression of food intake, and body weight is mediated by central IL-1 and IL-6’, *Proceedings of the National Academy of Sciences*.

Singewald, G. M., Rjabokon, A., Singewald, N. and Ebner, K. (2011) ‘The modulatory role of the lateral septum on neuroendocrine and behavioral stress responses.’, *Neuropsychopharmacology*, 36(4), pp. 793–804.

Sisley, S. et al. (2014) ‘Neuronal GLP1R mediates liraglutide’s anorectic but not glucose-lowering effect.’, *The Journal of clinical investigation*, 124(6), pp. 2456–63.

Sjostrom, P. J., Rancz, E. A., Roth, A. and Hausser, M. (2008) ‘Dendritic Excitability and Synaptic Plasticity’, *Physiological Reviews*, 88(2), pp. 769–840.

Skibicka, K. P. (2013) ‘The central GLP-1: implications for food and drug reward’, *Frontiers in Neuroscience*, 7.

Smits, M. M. et al. (2016) ‘Exenatide acutely increases heart rate in parallel with augmented sympathetic nervous system activation in healthy overweight males’, *Br J Clin Pharmacol*. 2015/11/27, 81(4), pp. 613–620.

Sørensen, G. et al. (2015) ‘The glucagon-like peptide 1 (GLP-1) receptor agonist exendin-4 reduces cocaine self-administration in mice’, *Physiology & Behavior*, 149, pp. 262–268.

Steinert, R. E. et al. (2014) ‘Effect of glucagon-like peptide-1 receptor antagonism on appetite and food intake in healthy men.’, *The American journal of clinical nutrition*, 100(2), pp. 514–23.

Sutherland, E. W. and De Duve, C. (1948) ‘Origin and distribution of the hyperglycemic-glycogenolytic factor of the pancreas.’, *The Journal of biological chemistry*, 175(2), pp. 663–74.

Suzuki, K., Jayasena, C. N. and Bloom, S. R. (2012) ‘Obesity and Appetite Control’, *Experimental Diabetes Research*, 2012, pp. 1–19.

Swanson, L. W. and Cowan, W. M. (1979) ‘The connections of the septal region in the rat’, *The Journal of Comparative Neurology*, 186(4), pp. 621–655.

Tabuchi, S. et al. (2014) ‘Conditional Ablation of Orexin/Hypocretin Neurons: A New Mouse Model for the Study of Narcolepsy and Orexin System Function’, *Journal of Neuroscience*, 34(19).

Takagi, H. et al. (1984) ‘Fine structural studies of cholecystokinin-8-like immunoreactive neurons and axon terminals in the nucleus of tractus solitarius of the rat’, *The Journal of Comparative Neurology*, 227(3), pp. 369–379.

Takahashi, K. A. and Cone, R. D. (2005) 'Fasting induces a large, leptin-dependent increase in the intrinsic action potential frequency of orexigenic arcuate nucleus neuropeptide Y/Agouti-related protein neurons.', *Endocrinology*, 146(3), pp. 1043–7.

Tang-Christensen, M. et al. (1996) 'Central administration of GLP-1-(7-36) amide inhibits food and water intake in rats', *Am J Physiol*, 271(4 Pt 2), pp. R848-56.

Tang-Christensen, M. et al. (2000) 'The proglucagon-derived peptide, glucagon-like peptide-2, is a neurotransmitter involved in the regulation of food intake.', *Nature Medicine*, 6(7), pp. 802–807.

Tantama, M., Martínez-François, J. R., Mongeon, R. and Yellen, G. (2013) 'Imaging energy status in live cells with a fluorescent biosensor of the intracellular ATP-to-ADP ratio', *Nature Communications*, 4, p. 2550.

Tartaglia, L. A. et al. (1995) 'Identification and expression cloning of a leptin receptor, OB-R.', *Cell*, 83(7), pp. 1263–71.

Tecott, L. H. et al. (1995) 'Eating disorder and epilepsy in mice lacking 5-HT2C serotonin receptors', *Nature*, 374(6522), pp. 542–546.

Terrill, S. J. et al. (2016) 'Role of lateral septum glucagon-like peptide 1 receptors in food intake', *American Journal of Physiology - Regulatory, Integrative and Comparative Physiology*, 311(1), pp. R124–R132.

Teschemacher, A. G., Gourine, A. V and Kasparov, S. (2015) 'A Role for Astrocytes in Sensing the Brain Microenvironment and Neuro-Metabolic Integration.', *Neurochemical research*, 40(12), pp. 2386–93.

Thevenaz, P. et al. (1998) 'A pyramid approach to subpixel registration based on intensity', *IEEE Trans Image Process*. 2008/02/13, 7(1), pp. 27–41.

Thiebaud, N. et al. (2016) 'The incretin hormone glucagon-like peptide 1 increases mitral cell excitability by decreasing conductance of a voltage-dependent potassium channel', *J Physiol*. 2016/03/05, 594(10), pp. 2607–2628.

Thiele, T. E. et al. (1997) 'Central infusion of GLP-1, but not leptin, produces conditioned taste aversions in rats.', *The American journal of physiology*, 272(2 Pt 2), pp. R726-30.

Thorens, B. (1992) 'Expression cloning of the pancreatic beta cell receptor for the gluco-incretin hormone glucagon-like peptide 1.', *Proceedings of the National Academy of Sciences of the United States of America*, 89(18), pp. 8641–5.

Thorens, B. et al. (1993) 'Cloning and functional expression of the human islet GLP-1 receptor. Demonstration that exendin-4 is an agonist and exendin-(9-39) an antagonist of the receptor.', *Diabetes*, 42(11), pp. 1678–82.

Thorens, B. (2012) 'Sensing of glucose in the brain', *Handb Exp Pharmacol*. 2012/01/18, (209), pp. 277–294.

Tian, L. et al. (2009) 'Imaging neural activity in worms, flies and mice with improved GCaMP calcium indicators', *Nat Methods*. 2009/11/10, 6(12), pp. 875–881.

Toft-Nielsen, M. B., Madsbad, S. and Holst, J. J. (1999) 'Continuous subcutaneous infusion of glucagon-like peptide 1 lowers plasma glucose and reduces appetite in type 2 diabetic patients.',

Diabetes care, 22(7), pp. 1137–43.

Tracy, A. L., Schurdak, J. D., Chambers, J. B. and Benoit, S. C. (2016) 'Aversion learning can reduce meal size without taste avoidance in rats', *Obesity*, 24(3), pp. 606–614.

Trapp, S. and Cork, S. C. (2015) 'PPG neurons of the lower brain stem and their role in brain GLP-1 receptor activation.', *American journal of physiology. Regulatory, integrative and comparative physiology*, 309(8), pp. R795-804.

Tuesta, L. M. et al. (2017) 'GLP-1 acts on habenular avoidance circuits to control nicotine intake', *Nature Neuroscience*, 20(5), pp. 708–716.

Turton, M. D. et al. (1996) 'A role for glucagon-like peptide-1 in the central regulation of feeding', *Nature*, 379(6560), pp. 69–72.

Ulrich-Lai, Y. M. and Herman, J. P. (2009) 'Neural regulation of endocrine and autonomic stress responses', *Nat Rev Neurosci*, 10(6), pp. 397–409.

Ussher, J. R. et al. (2014) 'Inactivation of the cardiomyocyte glucagon-like peptide-1 receptor (GLP-1R) unmasks cardiomyocyte-independent GLP-1R-mediated cardioprotection', *Molecular Metabolism*, 3(5), pp. 507–517.

Ussher, J. R. and Drucker, D. J. (2012) 'Cardiovascular Biology of the Incretin System', *Endocrine Reviews*, 33(2), pp. 187–215.

Vahl, T. P. et al. (2007) 'Glucagon-like peptide-1 (GLP-1) receptors expressed on nerve terminals in the portal vein mediate the effects of endogenous GLP-1 on glucose tolerance in rats', *Endocrinology*. 2007/06/23, 148(10), pp. 4965–4973.

Vallöf, D. et al. (2016) 'The glucagon-like peptide 1 receptor agonist liraglutide attenuates the reinforcing properties of alcohol in rodents', *Addiction Biology*, 21(2), pp. 422–437.

Verbalis, J. G., McCann, M. J., McHale, C. M. and Stricker, E. M. (1986) 'Oxytocin secretion in response to cholecystokinin and food: differentiation of nausea from satiety.', *Science (New York, N.Y.)*, 232(4756), pp. 1417–9.

Vickers, S. P., Clifton, P. G., Dourish, C. T. and Tecott, L. H. (1999) 'Reduced satiating effect of d-fenfluramine in serotonin 5-HT(2C) receptor mutant mice.', *Psychopharmacology*, 143(3), pp. 309–14.

Vickers, S. P., Dourish, C. T. and Kennett, G. A. (2001) 'Evidence that hypophagia induced by d-fenfluramine and d-norfenfluramine in the rat is mediated by 5-HT2C receptors.', *Neuropharmacology*, 41(2), pp. 200–9.

Vilsboll, T., Krarup, T., Madsbad, S. and Holst, J. J. (2003) 'Both GLP-1 and GIP are insulinotropic at basal and postprandial glucose levels and contribute nearly equally to the incretin effect of a meal in healthy subjects', *Regul Pept*. 2003/07/02, 114(2–3), pp. 115–121.

Vrang, N. and Grove, K. (2011) 'The brainstem preproglucagon system in a non-human primate (Macaca mulatta)', *Brain Res*, 1397, pp. 28–37.

Vrang, N., Hansen, M., Larsen, P. J. and Tang-Christensen, M. (2007) 'Characterization of brainstem preproglucagon projections to the paraventricular and dorsomedial hypothalamic nuclei.', *Brain Res*, 1149, pp. 118–126.

Vrang, N., Phifer, C. B., Corkern, M. M. and Berthoud, H. R. (2003) 'Gastric distension induces c-

Fos in medullary GLP-1/2-containing neurons', *American journal of physiology.Regulatory, integrative and comparative physiology*, 285(2), pp. R470-8.

Wallenius, V. et al. (2002) 'Interleukin-6-deficient mice develop mature-onset obesity', *Nature Medicine*, 8(1), pp. 75–79.

Wang, Z. et al. (1995) 'Glucagon-like peptide-1 is a physiological incretin in rat', *J Clin Invest*, 95(1), pp. 417–421.

Weber, J. T., Rzigalinski, B. A. and Ellis, E. F. (2001) 'Traumatic injury of cortical neurons causes changes in intracellular calcium stores and capacitative calcium influx.', *The Journal of biological chemistry*, 276(3), pp. 1800–7.

Wettergren, A. et al. (1993) 'Truncated GLP-1 (proglucagon 78-107-amide) inhibits gastric and pancreatic functions in man', *Digestive Diseases and Sciences*, 38(4), pp. 665–673.

WHO (2016) *WHO: Obesity and overweight*, *WHO*.

Wilde, E. et al. (2017) 'Tail-Cuff Technique and Its Influence on Central Blood Pressure in the Mouse', *Journal of the American Heart Association*, 6(6).

Williams, D. L. et al. (2011) 'Maintenance on a high-fat diet impairs the anorexic response to glucagon-like-peptide-1 receptor activation', *Physiol Behav*. 2011/04/26, 103(5), pp. 557–564.

Williams, D. L., Baskin, D. G. and Schwartz, M. W. (2006) 'Leptin Regulation of the Anorexic Response to Glucagon-Like Peptide-1 Receptor Stimulation', *Diabetes*, 55(12), pp. 3387–3393.

Williams, D. L., Baskin, D. G. and Schwartz, M. W. (2009) 'Evidence that intestinal glucagon-like peptide-1 plays a physiological role in satiety.', *Endocrinology*, 150(4), pp. 1680–1687.

Williams, M. R., Riach, R. A., Collison, D. J. and Duncan, G. (1977) *Role of the Endoplasmic Reticulum in Shaping Calcium Dynamics in Human Lens Cells*, *Prog Retina Eye Res*.

Winzell, M. S. and Ahren, B. (2004) 'The high-fat diet-fed mouse: a model for studying mechanisms and treatment of impaired glucose tolerance and type 2 diabetes', *Diabetes*. 2004/11/25, 53 Suppl 3, pp. S215-9.

Woods, S. C. (1991) 'The eating paradox: how we tolerate food.', *Psychological review*, 98(4), pp. 488–505.

Wu, Q., Clark, M. S. and Palmiter, R. D. (2012) 'Deciphering a neuronal circuit that mediates appetite', *Nature*. 2012/03/16, 483(7391), pp. 594–597.

Wu, S.-C. et al. (2015) 'Effect of Weight-Reduction in Obese Mice Lacking Toll-Like Receptor 5 and C57BL/6 Mice Fed a Low-Fat Diet', *Mediators of Inflammation*, 2015, pp. 1–12.

Wu, Z. et al. (2014) 'Galanin neurons in the medial preoptic area govern parental behaviour', *Nature*. 2014/05/16, 509(7500), pp. 325–330.

Yamamoto, H. et al. (2002) 'Glucagon-like peptide-1 receptor stimulation increases blood pressure and heart rate and activates autonomic regulatory neurons', *J Clin Invest*. 2002/07/03, 110(1), pp. 43–52.

Yamamoto, H. et al. (2003) 'Glucagon-like peptide-1-responsive catecholamine neurons in the area postrema link peripheral glucagon-like peptide-1 with central autonomic control sites', *J Neurosci*. 2003/04/10, 23(7), pp. 2939–2946.

Yamamoto, T. et al. (1992) 'C-fos expression in the rat brain after intraperitoneal injection of lithium chloride.', *Neuroreport*, 3(12), pp. 1049–52.

Yang, L., Qi, Y. and Yang, Y. (2015) 'Astrocytes control food intake by inhibiting AGRP neuron activity via adenosine A1 receptors.', *Cell reports*, 11(5), pp. 798–807.

Yettefti, K., Orsini, J. C. and Perrin, J. (1997) 'Neuronal responses to systemic nicotine in the solitary tract nucleus: origin and possible relation with nutritional effects of nicotine.', *Pharmacology, biochemistry, and behavior*, 58(2), pp. 529–35.

Youngblood, B. D., Ryan, D. H. and Harris, R. B. (1997) 'Appetitive operant behavior and free-feeding in rats exposed to acute stress.', *Physiology & behavior*, 62(4), pp. 827–30.

Zambrowicz, B. P. et al. (1997) 'Disruption of overlapping transcripts in the ROSA beta geo 26 gene trap strain leads to widespread expression of beta-galactosidase in mouse embryos and hematopoietic cells.', *Proceedings of the National Academy of Sciences of the United States of America*, 94(8), pp. 3789–94.

Zariwala, H. A. et al. (2012) 'A Cre-dependent GCaMP3 reporter mouse for neuronal imaging in vivo', *J Neurosci*. 2012/03/02, 32(9), pp. 3131–3141.

Zhang, J. and Ritter, R. C. (2012) 'Circulating GLP-1 and CCK-8 reduce food intake by capsaicin-insensitive, nonvagal mechanisms', *Am J Physiol Regul Integr Comp Physiol*. 2011/10/28, 302(2), pp. R264-73.

Zhang, Y. et al. (1994) 'Positional cloning of the mouse obese gene and its human homologue.', *Nature*, 372(6505), pp. 425–32.

Zhang, Y. et al. (2017) 'Cryo-EM structure of the activated GLP-1 receptor in complex with a G protein.', *Nature*, 546(7657), pp. 248–253.

Zhao, C., Eisinger, B. and Gammie, S. C. (2013) 'Characterization of GABAergic Neurons in the Mouse Lateral Septum: A Double Fluorescence In Situ Hybridization and Immunohistochemical Study Using Tyramide Signal Amplification', *PLoS ONE*. Edited by H. Fatemi, 8(8), p. e73750.

Zhao, S. et al. (2012) 'Hindbrain leptin and glucagon-like-peptide-1 receptor signaling interact to suppress food intake in an additive manner.', *International journal of obesity (2005)*, 36(12), pp. 1522–8.

Zheng, H., Cai, L. and Rinaman, L. (2015a) 'Distribution of glucagon-like peptide 1-immunopositive neurons in human caudal medulla', *Brain Struct Funct*. 2014/02/11, 220(2), pp. 1213–1219.

Zheng, H., Stornetta, R. L., Agassandian, K. and Rinaman, L. (2015b) 'Glutamatergic phenotype of glucagon-like peptide 1 neurons in the caudal nucleus of the solitary tract in rats.', *Brain structure & function*, 220(5), pp. 3011–22.

Zhou, L. et al. (2011) 'Glucokinase inhibitor glucosamine stimulates feeding and activates hypothalamic neuropeptide Y and orexin neurons.', *Behavioural brain research*, 222(1), pp. 274–8.

Zittel, T. T. et al. (1999) 'C-fos protein expression in the nucleus of the solitary tract correlates with cholecystokinin dose injected and food intake in rats.', *Brain research*, 846(1), pp. 1–11.

Zoccal, D. B. et al. (2014) 'The nucleus of the solitary tract and the coordination of respiratory

and sympathetic activities.', *Frontiers in physiology*, 5, p. 238.